

# CYCLIC PERFORMANCE OF RUBBER-SOIL MIXTURES TO ENHANCE SEISMIC PROTECTION

by

JUAN BERNAL SANCHEZ



A thesis submitted in partial fulfilment of the requirements of  
Edinburgh Napier University, for the award of  
*Doctor of Philosophy*

School of Engineering and the Built Environment

Edinburgh Napier University

January 2020

# *Declaration*

---

I hereby declare that this thesis is my own work and that, to the best of my knowledge and belief, is my work that I solely carried out at Edinburgh Napier University, except where due acknowledgement is made, and that neither the thesis nor the original work contained therein has been submitted to this or any other institution for a degree.

SIGNED: ..... DATE: .....

# *Acknowledgements*

---

It would be impossible to thank each and every one of those relatives, friends, colleagues, acquaintances, teachers, or students who have supported me throughout my life, but do not worry, that is why I have you all in my mind. This thesis is also yours.

Firstly, I would like to recognise the enormous effort provided by my two supervisors, Dr. John McDougall and Dr. Daniel Barreto. I feel privileged to have been supervised by such dedicated and caring human beings. I have learnt so many things in these four years but, without any doubt, I will always remember being part of your team. Thanks for not giving up on me.

I would like to acknowledge the help received from my colleagues, Dr. Marina Miranda, Dr. Aikaterini Marinelli and Dr. Aamir Khokhar, who were always there to offer guidance and comfort me in the difficult days. I also need to acknowledge the invaluable assistance offered by Willie Laing, who had the patience to spend weeks repeating relentlessly each one of tests included in this document.

To Dr. Kenny Leitch, who has been a model and who did not doubt in trusting me since the moment I moved into E52. I cannot express with words how grateful I feel to be part of the Graduate Apprenticeship programme with you. I wish I had met you before then, but I am sure this is just the beginning of a beautiful friendship.

This thesis is specially dedicated to the Bernal Sanchez family, including my parents, Maria Del Carmen Sanchez Caballero and Jose Maria Bernal Martinez, and to my

brothers, Jose Maria Bernal Sanchez and David Alcaraz Garcia. You gave me everything and I am here today is because of you, so the least I can do is make you be parte of all my success. I hope I make you proud.

I would like to give a special mention to the E21 gang. We spent many years suffering together so that we could eventually achieve the final and desired goal: becoming doctors. This is a long and winding road, with its highlights and lowlights, that not many are capable of imagining. I would also like to take this opportunity to thank Edinburgh Napier University for placing their trust in me and offering me this PhD.

Last but not least, I have to express all my gratitude to Dr. Clare McTigue, who has completely changed my life. You are everything I could ask for, so please, never change. I met you the same day I initiated this adventure and here you are at the end of the same journey. However, this is not the end of our thesis. Many chapters are still to be written.

*Yet with all its difficulties, and if I went back in time,  
I would not regret travelling this path again*



# *Abstract*

---

The disposal of scrap tyres has become a major environmental problem around the world. For its recovery, a geomaterial has been used as part of civil constructions, commonly known as Rubber-Soil mixture (RSm). The use of RSm has the potential to be used as geotechnical seismic isolation system and hence provide protection against earthquakes. However, the static and dynamic behaviour of RSm is not well understood. Various bulk (macro), particle (micro) properties, and the test conditions affect its characterisation. Whilst addressing this knowledge gap, the aim of this study was to understand the response of RSm under cyclic loading and evaluate its effectiveness in attenuating accelerations when used to retrofit a soil foundation.

An experimental programme was chosen for this research and is divided into three scales; particle, element and 1g model scales. Plain strain visualisations, oedometer, and x-ray tomographic tests were performed to elucidate RSm particulate behaviour. To understand RSm dynamic behaviour, the evolution in stiffness and damping of the mixture was analysed from small-to-large deformations whilst altering rubber content and number of cycles. A sweep analysis was also performed via 1g shaking table tests to evaluate the cyclic performance of a scaled foundation-modified soil with RSm.

The findings in this thesis revealed that the macro behaviour of RSm is highly influenced by the particle properties, including rubber mass, size, shape, stiffness and its interaction with sand particles. Tests showed a greater change in void ratio of mixtures containing shredded rubber compared to crumb rubber. 3D x-ray tomographic images revealed an increase in contact and a decrease in rubber volume of RSm under loading.

This demonstrated that the high RSm compressibility is the result of both particle re-arrangement and rubber distortion. At an element scale, liquefaction resistance increased and mixtures did not liquefy by adding 20% rubber. The addition of rubber led to a reduction in soil stiffness whilst it increased the mixture resilience against cyclic loading, ameliorating the cyclic effect on stiffness and damping degradation. Material damping increased with rubber content at small-to-medium strains, whereas an upper value was revealed by adding 10% rubber at larger deformations. Test results supported the basis that energy dissipation in RSm is generated through particle sliding and rubber deformation, which takes over the dissipation mode after several cycles. Altering a host soil system by adding vertical discrete zones with RSm showed a lower amplification ratio and as a result mitigated part of the incident vibrations. The increase in damping capacity at a model scale was postulated to be the result of combining geometrical and material damping. The vertical disposition of the soft zone herein proposed could allow its application to both existing and new infrastructure.

**To those who have believed in me**

*"As you set out for Ithaka  
hope your road is a long one,  
full of adventure, full of discovery.  
And if you find her poor, Ithaka won't have fooled you.  
Wise as you will have become, so full of experience,  
you'll have understood by then what these Ithakas mean"*

# *Table of contents*

---

<b>Declaration</b>	<b>i</b>
<b>Acknowledgements</b>	<b>ii</b>
<b>Abstract</b>	<b>iv</b>
<b>Table of contents</b>	<b>vi</b>
<b>List of Tables</b>	<b>x</b>
<b>List of Figures</b>	<b>xiii</b>
<b>1 Introduction</b>	<b>1</b>
1.1 Background . . . . .	1
1.2 Scope of this thesis . . . . .	2
1.3 Aim, objectives and research questions . . . . .	3
1.4 Structure of the thesis . . . . .	4
<b>2 Background information</b>	<b>6</b>
2.1 Introduction . . . . .	6
2.2 Variable-parameter-property scheme . . . . .	7
2.3 Phase relationships . . . . .	10
2.4 Stress and strain analysis . . . . .	12
2.4.1 One-dimensional vertical loading . . . . .	13

---

2.4.2	Triaxial loading . . . . .	16
2.4.3	Torsional resonant loading . . . . .	21
2.5	Evaluation of damping . . . . .	24
2.5.1	Material damping . . . . .	24
2.5.2	Geometrical damping . . . . .	30
2.5.3	Energy dissipation at a lab scale . . . . .	34
2.6	Summary . . . . .	38
<b>3</b>	<b>Literature review</b>	<b>39</b>
3.1	Introduction . . . . .	39
3.2	Mechanics of RSm . . . . .	39
3.3	Response of RSm under static loading . . . . .	41
3.3.1	Shear strength . . . . .	46
3.3.2	Compressibility . . . . .	53
3.3.3	Micro-mechanics of RSm . . . . .	54
3.4	Response of RSm under dynamic loading . . . . .	57
3.4.1	Dynamic properties at medium-to-large strains . . . . .	58
3.4.2	Dynamic properties at small-to-medium strains . . . . .	68
3.5	Geotechnical seismic isolation systems . . . . .	71
3.5.1	Wave barriers . . . . .	75
3.5.2	RSm for seismic isolation . . . . .	80
3.6	Summary . . . . .	88
<b>4</b>	<b>Micro to macro behaviour of RSm</b>	<b>89</b>
4.1	Introduction . . . . .	89
4.2	Plain strain visualisations . . . . .	90
4.2.1	Equipment, materials and methods . . . . .	90
4.2.2	Results and discussion . . . . .	91
4.3	Materials . . . . .	94
4.3.1	Sand . . . . .	94
4.3.2	Rubber . . . . .	96

---

---

4.3.3	Rubber-soil mixtures . . . . .	98
4.4	Oedometer tests . . . . .	105
4.4.1	Equipment, sample preparation and methods . . . . .	105
4.4.2	Results and discussion . . . . .	108
4.5	X-ray tomography on RSm . . . . .	119
4.5.1	Equipment, materials and methods . . . . .	119
4.5.2	Results and discussion . . . . .	120
4.5.3	Energy dissipation at a particle scale . . . . .	123
4.6	RSm compressive behaviour . . . . .	124
4.7	Summary . . . . .	128
<b>5</b>	<b>Cyclic behaviour of RSm - Element test</b>	<b>129</b>
5.1	Introduction . . . . .	129
5.2	Cyclic triaxial equipment . . . . .	130
5.2.1	Equipment, materials and methods . . . . .	130
5.2.2	Cyclic behaviour at medium-to-large strains . . . . .	138
5.2.3	Liquefaction potential . . . . .	145
5.2.4	Shear modulus at medium-to-large strains . . . . .	148
5.2.5	Damping ratio at medium-to-large strains . . . . .	153
5.3	Torsional resonant column equipment . . . . .	158
5.3.1	Equipment, materials and methods . . . . .	158
5.3.2	Shear modulus at small-to-medium strains . . . . .	164
5.3.3	Damping ratio at small-to-medium strains . . . . .	166
5.4	Summary . . . . .	168
<b>6</b>	<b>Cyclic behaviour of a small scale RSm foundation</b>	<b>169</b>
6.1	Introduction . . . . .	169
6.2	Equipment, materials and methods . . . . .	170
6.3	Results and discussion . . . . .	179
6.3.1	Acceleration response . . . . .	179
6.3.2	Amplification ratio . . . . .	181

---

6.4	Analysis . . . . .	184
6.4.1	Energy dissipation at lab scale . . . . .	184
6.4.2	Vibration isolation efficacy . . . . .	186
6.4.3	Comparison with literature review . . . . .	187
6.5	Summary . . . . .	190
<b>7</b>	<b>Characterisation of dynamic properties in RSm</b>	<b>191</b>
7.1	Introduction . . . . .	191
7.2	Dynamic behaviour of RSm . . . . .	192
7.2.1	Effect of particle properties . . . . .	192
7.2.2	Cyclic effect on dynamic behaviour . . . . .	196
7.2.3	Energy dissipation mechanisms in RSm . . . . .	201
7.3	Determination of $G_0$ and $\xi_0$ for RSm . . . . .	205
7.3.1	Sand . . . . .	205
7.3.2	Rubber-soil mixtures . . . . .	206
7.4	Stiffness relationship of RSm . . . . .	210
7.4.1	Reference strain . . . . .	211
7.4.2	Normalised shear modulus curve based on Darendeli (2001) . . . . .	212
7.4.3	Normalised shear modulus curve based on MMF model . . . . .	212
7.5	Damping ratio relationship of RSm . . . . .	214
7.5.1	Damping ratio curve based on Senetakis et al. (2012a) . . . . .	217
7.5.2	Damping ratio curve based on Phillips and Hashash (2009) . . . . .	220
7.6	Summary . . . . .	223
<b>8</b>	<b>Conclusions</b>	<b>224</b>
8.1	Introduction . . . . .	224
8.2	Summary of findings . . . . .	225
8.3	Limitations and recommendations for future work . . . . .	232
	<b>References</b>	<b>234</b>

# *List of Tables*

---

<b>TABLES</b>	<b>Page</b>
2.1 Relative density descriptors ( <a href="#">Lambe and Whitman, 2010</a> ) . . . . .	12
3.1 Studies on response of RSm under static loading . . . . .	42
3.1 Studies on response of RSm under static loading . . . . .	43
3.1 Studies on response of RSm under static loading . . . . .	44
3.2 Classification of scrap tyres in civil engineering projects according to <a href="#">ASTM D6270 (2017)</a> . . . . .	45
3.3 Studies on shear strength of RSm . . . . .	50
3.3 Studies on shear strength of RSm . . . . .	51
3.3 Studies on shear strength of RSm . . . . .	52
3.4 Studies on response of RSm under dynamic loading . . . . .	65
3.4 Studies on response of RSm under dynamic loading . . . . .	66
3.4 Studies on response of RSm under dynamic loading . . . . .	67
3.5 Comparison of structural isolation systems . . . . .	73
3.6 Comparison of geotechnical seismic isolation systems . . . . .	74
3.7 Efficiency of seismic isolation systems with RSm . . . . .	83
3.8 Studies on seismic performance of RSm . . . . .	84
3.8 Studies on seismic performance of RSm . . . . .	85
4.1 Material properties of sand and rubber particles . . . . .	95
4.2 Composition of scrap tyres used in this study ( <a href="#">South et al., 2001</a> ) . . . . .	96



---

4.3	Composition of rubber-soil mixtures . . . . .	100
4.4	Minimum density of RSm . . . . .	101
4.5	Maximum density of RSm . . . . .	103
4.6	Classification of specimens for oedometer tests . . . . .	107
4.7	Measurements of sample height and global void ratio of sample at the three stages, obtained from the 3D images . . . . .	121
4.8	Conceptual framework to explain the particle shear and compressive behaviour of mineral (sand) and rubber particles . . . . .	125
5.1	Resolution and range for transducers of cyclic triaxial experiments . . . . .	132
5.2	Relative density obtained for cyclic triaxial tests . . . . .	134
5.3	Classification of cyclic triaxial experiments . . . . .	137
5.4	Resolution and range for transducers of resonant column experiments . . . . .	159
5.5	Relative density obtained for resonant column experiments . . . . .	161
5.6	Classification of resonant column experiments . . . . .	163
6.1	Resolution and range for transducers of EMC . . . . .	172
6.2	Scaling laws for dynamic centrifuge tests and 1g shake table test ( <a href="#">Park and Kim, 2013</a> ) . . . . .	173
6.3	Mass solids, volume solids, voids and void ratio per bag . . . . .	175
6.4	Determination of velocity, displacement and acceleration for experimental programme . . . . .	177
7.1	Effect of particle properties and test conditions on the dynamic behaviour of RSm . . . . .	200
7.2	Calculation of $G_0$ for sand . . . . .	204
7.3	Calculation of $G_0$ for RSm . . . . .	207
7.4	Calculation of $\xi_0$ for RSm . . . . .	208
7.5	Calculation of reference strain $\gamma_{RSm}$ for RSm . . . . .	210
7.6	Function parameters of MMF (Equation 7.23) for RSm . . . . .	213
7.7	Function parameters to adjust damping based on <a href="#">Senetakis et al. (2012a)</a> . . . . .	218

---

7.8 Function parameters to adjust damping based on [Phillips and Hashash \(2009\)](#) 220

# *List of Figures*

---

<b>FIGURES</b>	<b>Page</b>
2.1 Framework defining variable-parameter-property scheme . . . . .	8
2.2 Mohr circles for CU triaxial test ( <a href="#">Craig and Knappett, 2012</a> ) . . . . .	17
2.3 Evaluation of cyclic behaviour from hysteresis loop . . . . .	19
2.4 Effective stress path of a soil under cyclic loading . . . . .	20
2.5 Determination of maximum shear strain versus frequency with resonant column test . . . . .	22
2.6 Evaluation of stored and dissipated energy ( <a href="#">Shamy and Denissen, 2012</a> ) . .	25
2.7 Representation of a) maximum stored energy, and b) energy released under dynamic loading according to <a href="#">Shamy and Denissen (2012)</a> . . . . .	27
2.8 Half power bandwidth based on ( <a href="#">Papagiannopoulos and Hatzigeorgiou, 2011</a> )	29
2.9 Distribution of elastic waves ( <a href="#">Towhata, 2014</a> ) . . . . .	31
2.10 Incident and refraction angle at a soil boundary ( <a href="#">Yoshida, 2015</a> ) . . . . .	32
2.11 Attenuation of a) displacement and b) stress amplitude of shear waves through medium ( <a href="#">Yoshida, 2015</a> ) . . . . .	34
2.12 Time domain analysis on horizontal accelerations of a single degree of free- dom system . . . . .	36
2.13 Structural response of a system to harmonic excitations ( <a href="#">Chopra, 2011</a> ) . .	37
3.1 Studies on a) calculation of friction angle and b) maximum deviator stress by adding tyre derived aggregates . . . . .	48

3.2	Studies on a) calculation of friction angle and b) maximum deviator stress by adding particulate rubber . . . . .	49
3.3	Vertical strain versus vertical stress by adding a) tyre chips (Rao and Dutta, 2006) and b) particulate rubber (Lee et al., 2010) . . . . .	54
3.4	Small strain shear modulus with size ratio of RSm (Lee et al., 2010) . . . . .	56
3.5	a) Normalised shear modulus and b) damping ratio of rubber soil mixtures at $\chi = 10\%$ and $\sigma_m = 100$ kPa . . . . .	61
3.6	a) Normalised shear modulus and b) damping ratio of rubber soil mixtures at $\chi = 10\%$ and $\sigma_m = 200$ kPa . . . . .	61
3.7	a) Normalised shear modulus and b) damping ratio of rubber soil mixtures at $\chi = 30\%$ and $\sigma_m = 100$ kPa . . . . .	62
3.8	a) Normalised shear modulus, and b) damping ratio, with N of RSm in dry (Madhusudhan et al., 2019) and saturated (Mashiri et al., 2016) conditions .	64
3.9	Maximum shear modulus and minimum damping ratio at a,c) $\sigma_m = 100$ kPa, and b,d) $\sigma_m = 200$ kPa . . . . .	70
3.10	a) Active and b) passive isolators using wave barriers (Mahdavisefat et al., 2017) . . . . .	76
3.11	Geometrical configurations of isolating layers a) Kirtas et al. (2009) b) Nappa (2014) . . . . .	78
4.1	Plain strain test on sand with a) shredded rubber particles and b) crumb rubber particle . . . . .	91
4.2	Plain strain test with shredded rubber a) before and b) during loading . . .	92
4.3	Plain strain test with crumb rubber particles a) before and b) during loading	93
4.4	Microscopic image of Leighton Buzzard sand . . . . .	94
4.5	Particle size distribution of Leighton Buzzard sand, crumb and shredded rubber . . . . .	95
4.6	Microscopic images of a) shredded rubber and b) crumb rubber particles .	97
4.7	Maximum and minimum density of RSm . . . . .	102
4.8	Maximum, minimum void ratio of RSm . . . . .	104

4.9	Conventional oedometer apparatus set-up . . . . .	106
4.10	Sample void ratio for oedometer tests in relation to maximum and minimum void ratio . . . . .	107
4.11	Change in void ratio with effective vertical stress of RSm with a) crumb rubber particles and (b) shredded rubber particles . . . . .	110
4.12	Plastic strain after each cycle of unloading . . . . .	111
4.13	Compression index versus vertical effective stress of RSm with a) crumb rubber particles and b) shredded rubber particles . . . . .	112
4.14	Swelling index versus vertical effective stress of RSm with a) crumb rubber particles and b) shredded rubber particles . . . . .	113
4.15	Constrained modulus with applied vertical stress of RSm . . . . .	115
4.16	Shear stress - shear strain of bulk rubber and 30% ShRm . . . . .	116
4.17	Shear stress - shear strain curve of RSm with a) crumb rubber particles and b) shredded rubber particles . . . . .	117
4.18	Tomographic image of the sample prior to loading: a) cross sectional view and b) vertical section . . . . .	120
4.19	Cross sectional views through the segmented images with the three phases differentiated: a) Stage 0, b) Stage 1 and c) Stage 2 . . . . .	121
4.20	Evolution in void ratio with a) rubber volume and b) contact area of 30% ShRm from mini oedometer tests . . . . .	123
4.21	Microscopic image showing high porosity together with fissures and cracks found on surface of recycled rubber particle . . . . .	126
5.1	Cyclic triaxial equipment and set up . . . . .	131
5.2	Sample preparation for cyclic triaxial tests of (a)sand and (b) 30%RSm . . .	134
5.3	Maximum, minimum and sample a)density b) void ratio . . . . .	134
5.4	Membrane after consolidation during cyclic triaxial test . . . . .	136
5.5	Cyclic behaviour of 0RSm at (a) $\gamma_{cyc} = 0.05\%$ N = 400 (b) $\gamma_{cyc} = 0.1\%$ N = 84 (c) $\gamma_{cyc} = 0.2\%$ N = 41 and (d) $\gamma_{cyc} = 1\%$ N = 14 . . . . .	140

5.6	Stress path of 0RSm at (a) $\gamma_{cyc} = 0.05\%$ N = 400 (b) $\gamma_{cyc} = 0.1\%$ N = 84 (c) $\gamma_{cyc} = 0.2\%$ N = 41 and (d) $\gamma_{cyc} = 1\%$ N = 14 . . . . .	140
5.7	Cyclic behaviour of 10RSm at (a) $\gamma_{cyc} = 0.05\%$ N = 400 (b) $\gamma_{cyc} = 0.1\%$ N = 400 (c) $\gamma_{cyc} = 0.2\%$ N = 240 and (d) $\gamma_{cyc} = 1\%$ N = 50 . . . . .	141
5.8	Stress path of 10RSm at (a) $\gamma_{cyc} = 0.05\%$ N = 400 (b) $\gamma_{cyc} = 0.1\%$ N = 400 (c) $\gamma_{cyc} = 0.2\%$ N = 240 and (d) $\gamma_{cyc} = 1\%$ N = 50 . . . . .	141
5.9	Cyclic behaviour of 20RSm at (a) $\gamma_{cyc} = 0.05\%$ N = 400 (b) $\gamma_{cyc} = 0.1\%$ N = 400 (c) $\gamma_{cyc} = 0.2\%$ N = 400 and (d) $\gamma_{cyc} = 1\%$ N = 400 . . . . .	143
5.10	Stress path of 20RSm at (a) $\gamma_{cyc} = 0.05\%$ N = 400 (b) $\gamma_{cyc} = 0.1\%$ N = 400 (c) $\gamma_{cyc} = 0.2\%$ N = 400 and (d) $\gamma_{cyc} = 1\%$ N = 400 . . . . .	143
5.11	Cyclic behaviour of 30RSm at (a) $\gamma_{cyc} = 0.05\%$ N = 400 (b) $\gamma_{cyc} = 0.1\%$ N = 400 (c) $\gamma_{cyc} = 0.2\%$ N = 400 and (d) $\gamma_{cyc} = 1\%$ N = 400 . . . . .	144
5.12	Stress path of 30RSm at (a) $\gamma_{cyc} = 0.05\%$ N = 400 (b) $\gamma_{cyc} = 0.1\%$ N = 400 (c) $\gamma_{cyc} = 0.2\%$ N = 400 and (d) $\gamma_{cyc} = 1\%$ N = 400 . . . . .	144
5.13	Liquefaction potential of RSm at (a) $\gamma_{cyc} = 0.1\%$ (b) $\gamma_{cyc} = 0.2\%$ and (c) $\gamma_{cyc} = 1\%$ . . . . .	147
5.14	Shear modulus - shear strain at N = 2 from a) this study, and b) <a href="#">Mashiri (2014)</a>	150
5.15	Shear modulus - number of cycles up to N = 400, at (a) $\gamma_{cyc} = 0.1\%$ , (b) $\gamma_{cyc} = 0.2\%$ and (c) $\gamma_{cyc} = 1\%$ . . . . .	153
5.16	Damping ratio - shear strain curve at N = 2 from a) this study, and b) <a href="#">Mashiri (2014)</a> . . . . .	155
5.17	Damping ratio - number of cycles up to N = 400 at (a) $\gamma_{cyc} = 0.1\%$ , (b) $\gamma_{cyc} = 0.2\%$ and (c) $\gamma_{cyc} = 1\%$ . . . . .	157
5.18	Resonant column equipment and set-up . . . . .	159
5.19	Maximum, minimum and sample void ratio . . . . .	161
5.20	Shear modulus - shear strain from a) this study, and b) <a href="#">Senetakis et al. (2012a)</a>	165
5.21	Damping ratio - shear strain curve from a) this study, and b) <a href="#">Senetakis et al., 2012a</a> . . . . .	167
6.1	Experimental set-up for shaking table test . . . . .	171

6.2	Electromechanical Cylinder . . . . .	172
6.3	Front view of the rigid box . . . . .	173
6.4	Mixture bags with RSm at $\chi = 0-40\%$ . . . . .	176
6.5	Plan view of rigid box . . . . .	177
6.6	Transmitted accelerations on building and box at a) $f = 3$ Hz b) $f = 5.5$ Hz and c) $f = 9$ Hz . . . . .	180
6.7	Transmitted accelerations on building and box at a) $f = 5.5$ Hz and b) $f = 5$ Hz	181
6.8	Amplification ratio versus input frequency during a) stage 1 and b) stage 2-3	182
6.9	a) Frequency, and b) amplification ratio at resonant frequency and $f = 5.5$ Hz, with rubber content . . . . .	184
6.10	Half power bandwidth for the foundation-soil system at $\chi = 0$ and $40\%$ . . .	185
6.11	Damping ratio at lab scale with RSm varying rubber content . . . . .	186
6.12	Change in amplification ratio with rubber content versus sand only config- uration . . . . .	187
7.1	a) Shear modulus and b) normalised shear modulus versus shear strain . .	193
7.2	Normalised shear modulus versus shear strain of RSm at a) $\chi = 10\%$ , and b) $\chi = 30\%$ . . . . .	194
7.3	Damping ratio - shear strain of RSm . . . . .	195
7.4	Damping ratio - shear strain of RSm at a) $\chi = 10\%$ , and b) $\chi = 30\%$ . . . . .	196
7.5	a) stiffness degradation and b) liquefaction potential versus shear strain, rubber percentage and cycles to liquefaction . . . . .	198
7.6	Damping degradation versus shear strain, rubber percentage and cycles to liquefaction . . . . .	199
7.7	a) Peak frequency, and b) damping ratio at lab scale . . . . .	203
7.8	Maximum shear modulus and minimum damping ratio of RSm . . . . .	210
7.9	Normalised shear modulus - shear strain of RSm based on <a href="#">Darendeli (2001)</a>	212
7.10	Normalised shear modulus - shear strain using MMF model . . . . .	214
7.11	Normalised damping ratio - shear strain based on <a href="#">Darendeli (2001)</a> . . . . .	216
7.12	Correlation between $\xi - \xi_0$ and $G/G_0$ of RSm based on <a href="#">Senetakis et al. (2012a)</a>	218

7.13	Correlation between $\xi - \xi_0$ and $G/G_0$ of a) 0RSm and b) 10RSm . . . . .	218
7.14	Correlation between $\xi - \xi_0$ and $G/G_0$ of a) 20RSm and d) 30RSm . . . . .	219
7.15	Normalised damping ratio - shear strain based on <a href="#">Senetakis et al. (2012a)</a> .	220
7.16	Normalised damping ratio - shear strain based on <a href="#">Phillips and Hashash (2009)</a>	222



# *Introduction*

---

## **1.1 Background**

The disposal of scrap tyres has become a major environmental problem in many countries around the world. The high durability in addition to the strength of the vulcanised rubber has made the recovery of the material difficult, hence used tyres typically end up in landfills or stockpiles (ETRMA, 2015). However, a new landfill directive was approved in 2006 in Europe prohibiting both whole and shredded tyres in landfills which led to achieve a 96% recovery rate by 2013 (European Communities, 2006).

Preferred routes for used End Life Tyres (ELT) are energy and material recovery. As a consequence of their high organic component, energy recovery has gained importance in the past twenty years for heating purposes in cement kilns, commonly known as tyre derived fuel. There is the risk that it becomes the single solution to deal with ELT due to being considered the cheapest as well as the quickest processing option.

As for the material recovery, recycled whole scrap tyres have been used as drainage layer material in solid waste landfills, for constructing roads, admixture in bituminous concrete, bridge abutments, light rail, and septic systems. A geomaterial has been alternatively produced since the early 90's by combining a proportion of rubber particles with a mineral, typically sandy soil or gravels, commonly known as a Rubber-Soil mixture (RSm). RSm has been used in lightweight material applications due to its low unit weight, high shear strength, high hydraulic conductivity and very high resilience.

However, its implementation in civil engineering applications is relatively new and the use of such a complex material in permanent long-term constructions is still questioned.

The mechanics of soil have always presented difficulties of observation and interpretation primarily because of their particulate nature. However, whilst conventional soils are assumed to be incompressible, RSm have the complexity of containing particulate rubber that are compressible and distort under loading. In addition to this, the behaviour of RSm is affected by the large range of tyre derived aggregates. Hence, particle properties such as stiffness, content, shape or size of rubber make understanding the behaviour of RSm a significant challenge. A conceptual framework is therefore required to understand the role of system variables, bulk, particle (micro) properties and test conditions, and their influence on the bulk parameters which characterise the macro-behaviour of the mixture.

Major previous earthquakes have evidenced that soil deposits can be subjected to larger strain amplitudes with the appearance of prolonged aftershock conditions. Under large deformations, saturated soils have been shown to undergo a significant stiffness and damping degradation. RSm have been proposed to modify the ground soil and thus partially mitigate the seismic hazard. However, most existing research has studied the cyclic response of RSm at relatively small deformations. Additional experimental testing is required to assess the evolution in the dynamic behaviour of RSm from small-to-large strain amplitudes and elucidate its effect on the soil response under cyclic loading.

## **1.2 Scope of this thesis**

Earthquakes are one of the deadliest natural disasters, accounting for just 7.5 % of such events between 1994 and 2013 but causing 37 % of deaths. As with other natural disasters, it is not the countries that suffer the most earthquakes that see the biggest losses. Instead, the number of people who die in an earthquake is inversely related to the wealth of the country (Guha-Sapir et al., 2016). More generally, low quality buildings and inadequate town planning are held to be the two main reasons why seismic events are more destructive in developing countries. A problem with conventional solutions

such as base isolation systems is their high cost as well as the inability to be retrofitted in existing infrastructure.

Geotechnical seismic isolations systems (GIS) have shown to successfully mitigate part of the horizontal and vertical accelerations at the surface level by introducing sliding systems or wave barriers. The literature highlights, however, that two major issues still need to be addressed when using this approach; a limiting maximum vertical load due to the excessive static settlement, and the preclusion of the system from existing buildings, which currently occurs with typical structural base isolation systems.

This work seeks to investigate the viability of a low-cost, easy deployment GIS capable of mitigating the seismic vibrations and thus protect both new and existing structures from collapsing during an earthquake. The key aspect of the system herein investigated relies on the addition of particulate rubber, obtained from scrap tyres, to give the soil a higher level of deformability.

Within the theme of this investigation, one objective is to explore the feasibility of using retrofitted vertical soft zones consisting of rubber-sand mixtures that introduced in the ground might alter the cyclic response of the foundation and the superstructure. Introducing rubber-soil mixtures offers the opportunity to control natural ground frequencies in such a way that offset the vibrations so that the resonance phenomenon does not occur. To prove its effectiveness, the modified soil needs to be tested using scaled models where particle, element and field scale aspects need to be considered.

### **1.3 Aim, objectives and research questions**

The aim of this research is to understand the response of RSm under cyclic loading, identifying those factors that influence its dynamic behaviour, and evaluate its effectiveness in improving the structural response when used to retrofit the soil. This will be achieved through the completion of the following objectives:

- i) Define the mechanics of RSm to establish the relationship between bulk parameters with its micro and macro-structure.

ii) Characterise the compressibility of RSm whilst assessing the effect of rubber particle shape.

iii) Study the evolution of the bulk parameters that define the dynamic behaviour of RSm whilst assessing the effect of particle properties as well as test conditions.

iv) Understand the dynamic response of a lumped mass-foundation system laterally modified by adding vertical installations of RSm.

v) Elucidate the energy dissipation mechanisms developed in RSm from a particulate, to an element and a lab scale level.

The following research questions will facilitate in addressing the aim and objectives of the study:

1. What is the relationship between the micro and macro-structure of RSm and how does this correlate to the mechanics of RSm during particle shear and compression?

2. How do the particle properties and test conditions influence the cyclic performance and energy dissipation mechanisms of rubber-soil mixtures under cyclic loading?

3. Can the introduction of vertical soft zones, comprising of particulate rubber, to the ground enhance the resistance of soil foundations against cyclic loading?

## **1.4 Structure of the thesis**

Chapter 1 explains the contextual background. It outlines the core issues related to the research topic and the motivation for undertaking this study. It sets out the aims and objectives of this research, as well as the research questions to achieve these outcomes.

Chapter 2 introduces a description of the technical information to underpin the understanding of the following chapters. It includes a review of the concepts to analyse the response of soils under static and dynamic loading through stress-strain analysis.

Chapter 3 provides a review of the literature. It establishes a conceptual framework which will set out the main aspects considered in the study of the mechanics of RSm. It includes the recent developments in the investigation of the response of RSm under both static (monotonic) and dynamic loading. It explores the interaction between rigid and deformable soils at a particulate level and its effect on the macrostructure.

Chapter 4 discusses the particle compression and re-arrangement in RSm under one-dimensional conditions and plain strain visualisations. It describes the material properties of Leighton Buzzard sand and particulate rubber tested in this thesis. It covers the particle scale interaction at a microscopic level using mini-oedometer samples in x-ray tomographic tests. A conceptual framework is introduced to explain the evolution in one-dimensional compressive behaviour of RSm. Findings and conclusions from this chapter have been peer reviewed and published in [Fonseca et al. \(2019\)](#).

Chapter 5 provides the results from undrained consolidated strain controlled cyclic triaxial tests at medium-to-large strain amplitudes. It includes experimental data obtained from resonant column tests at very small-to-medium strains. It analyses the stress-strain behaviour and liquefaction potential of RSm varying material properties and test conditions.

Chapter 6 discusses the feasibility of using retrofitted RSm modified soil for isolating vibrations and analyses the experimental data obtained using the shaking table apparatus. It includes a brief description of the structural and geotechnical seismic isolation systems and the potential use of RSm in soil foundations for vibration isolation. It assesses the energy dissipation mechanisms found in a foundation-soil system from the lab scale perspective. It provides the results on the horizontal acceleration at the surface level by modifying material properties and test conditions.

Chapter 7 covers the stiffness and damping degradation strain curves which are studied from very small to large strain amplitudes. It discusses the resilience of shredded rubber - sand mixtures by analysing the stiffness and damping degradation in relation to the number of cycles. The energy dissipation mechanisms in RSm are discussed by comparing the results from a particulate to a 1g scale model level. It characterises the dynamic behaviour of RSm by adjusting analytical expressions provided in the literature to the experimental results from this study.

Chapter 8 consists of conclusions, contribution to the knowledge, recommendations and provides a summary of the main findings. It highlights the limitations of the research and identifies areas for further research.

## *Background information*

---

### **2.1 Introduction**

This chapter presents the engineering and scientific basis on which this thesis is founded. A conceptual framework is proposed to elucidate the interaction between variable-parameter-property of soils and its interdependencies. Soils studied in this thesis are classified in accordance with the phase relationships as established in the field of Soil Mechanics. The typical response of soils under static (monotonic) and dynamic loading is examined within the context of oedometer tests, cyclic triaxial and resonant column tests. Expressions adopted for the evaluation of cyclic behaviour, liquefaction potential and soil stiffness are reviewed.

Stress wave attenuation is examined through evaluation of the different forms of damping. This includes viscous and non-linear hysteretic damping, as material damping, and geometrical damping, accounting for radiation damping and wave scattering. The evaluation of the energy dissipation and the dynamic response of a scaled foundation-modified soil system is also discussed. For that, both time and frequency domain analyses are adopted to study the evolution of sinusoidal harmonic motions transmitted by means of shaking table testing.

## 2.2 Variable-parameter-property scheme

The mechanics of soil have always presented difficulties of observation and interpretation primarily because of the particulate nature of the material and the disturbance experienced by those particles under loading. In dry soil particles, testing assemblies are subject to external or boundary stresses while displacements are monitored. In a saturated soil, the stress state is complicated by the presence of a water phase, the 'seat' of which is the internal (or pore) structure of the soil. The role of the pore water and its intrinsic pressure have been well-known since 1930s (Craig and Knappett, 2012).

It is important to understand the role of system variables and material properties by which soil behaviour can be interpreted. Indeed, such conceptual framework is essential to the development of soil models. In this thesis, a rubber-soil mixture (RSm) is the object of study, which introduces an additional complexity to the conceptual framework; the presence of an amount of rubber particles that are measurably compressible and distort under the action of loading. Soil particles are, on the other hand, as usual, assumed to be incompressible.

For this reason, it is essential to understand the conceptual framework within which the mechanics of RSm and this thesis exist. In other words, to define explicitly the distinction between i) system variables, ii) test conditions, iii) material (micro) properties and iv) bulk (macro) properties and their interdependencies. This is important when considering RSm under static (monotonic) loading regimes and more so under dynamic (cyclic) loads when additional test and material property conditions, including frequency and material damping, have to be considered.

The variable-parameter-property scheme presented in Figure 2.1 has been devised to make clear the context and focus of previous studies on RSm behaviour:

- A variable represents the evolving state of the system and is usually an intensive quantity, i.e. its dimensions are normalised.
- A parameter defines a relationship between variables; it cannot be measured directly but needs to be deduced by experiment, e.g. stiffness or strength. Its value may

change during the test.

- A property describes a characteristic; may be influential in the evolution of system variables but its value remains fixed during the course of a test. May be measured directly from the macro-scale, e.g. mass, volume, density, particle size distribution (PSD). Or at a particle level: shape ( $A_R$ ), size ratio ( $S_R$ ), coefficient of friction, rubber/mineral stiffness.

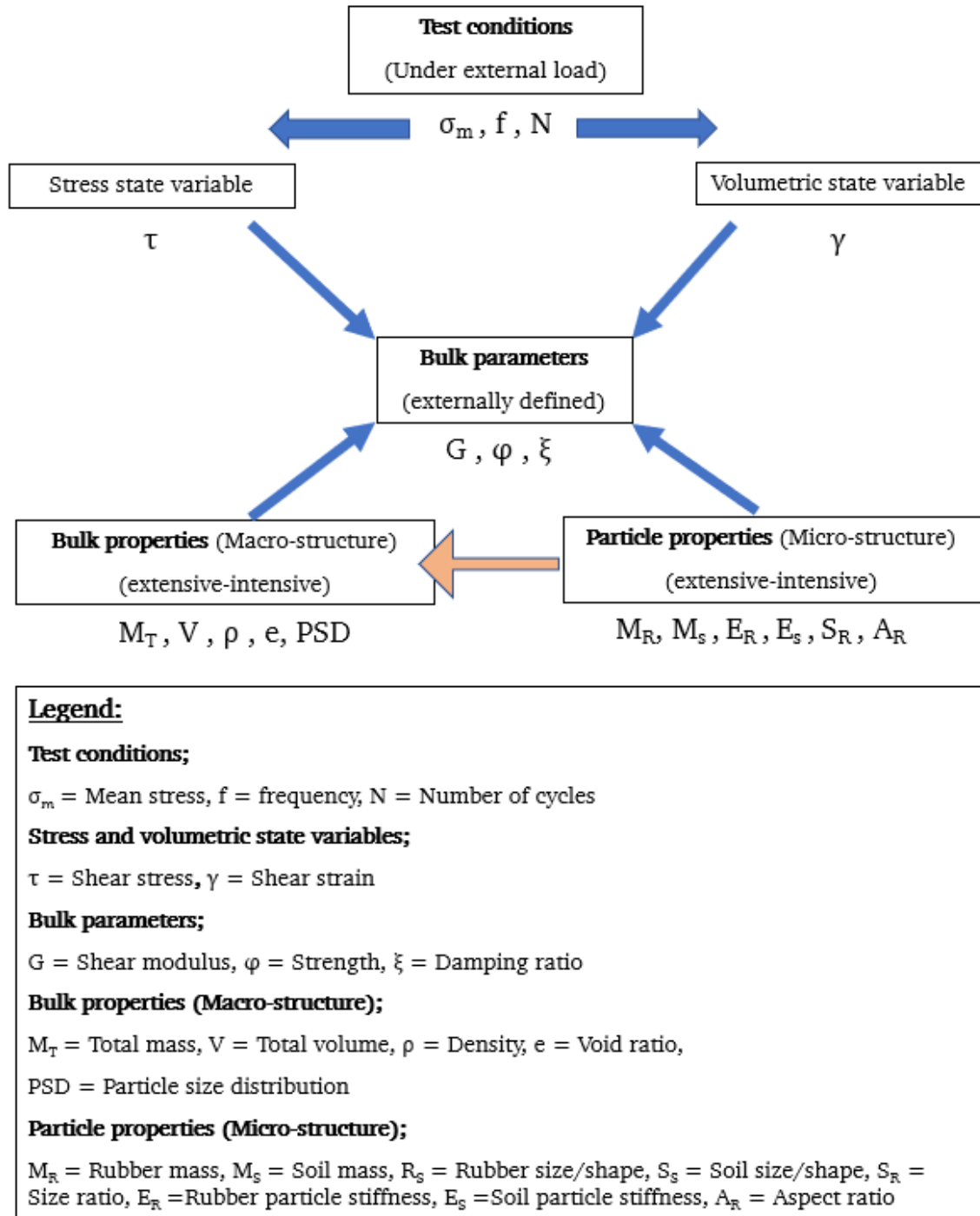


Figure 2.1: Framework defining variable-parameter-property scheme



This variable-parameter-property scheme can then be applied to any conventional soil in order to elucidate the factors influencing the response of the material under loading. The bulk parameters, focus of this study, are for instance the shearing resistance and shear modulus; which define the soil static (monotonic) behaviour, and damping ratio; that characterises the soil dynamic behaviour. These bulk parameters then represent the soil behaviour at an element scale level and they vary with both stress ( $\tau$ ) and volumetric ( $\gamma$ ) state variables.

In accordance with Figure 2.1, the bulk parameters can be influenced by the macro-structure of the soil, characterised by the bulk properties, i.e. volume, mass or density, and respectively, by the particle properties. The latter would account for the micro-structure of the soil, considered in this study as the particulate scale level, which includes properties such as coefficient of friction, fabric and particle stiffness. A review of the literature on the bulk parameters that characterise the static and dynamic behaviour of RSm is undertaken in Chapter 3. This includes the study of the bulk (macro) and particle (micro) properties as well as the test conditions which may have an influence in the externally defined bulk parameters.

This Chapter provides the scientific basis on which this thesis is found. In Section 2.3, the phase relationships are described to classify the soils and thus allow the comparison between different mixtures. The stress-strain analysis, result of the response of soils under loading, is covered in Section 2.4. It presents the main parameters and equations used for the study of soil compressibility, via oedometer tests, and dynamic behaviour of RSm, using cyclic triaxial and resonant column testing. The evaluation of damping in soils and the expressions adopted for its determination are discussed in Section 2.5.

## 2.3 Phase relationships

The classification of sand and RSm has been undertaken based on their mass and volume, the relation between those properties (specific gravity, soil density and unit weight), the volumetric state of the samples (void ratio) and the normalisation of this volumetric state (relative density). A soil consists of solid particles and voids filled with air and/or other fluids. That is why a soil is commonly classified as a three-phase material (Craig, 2013).

### *Intrinsic properties of material - Mass and volume*

The mass of soil ( $m$ ) is a measure which accounts for the amount of matter of that soil. Based on the three-phase soil model, the mass of a wet soil is divided into mass of soil particles ( $m_s$ ) and mass of water ( $m_w$ ); the air does not possess any mass.

The volume of a soil ( $V$ ) corresponds to the amount of space occupied by the soil. The total volume of soil comprises the volume of soil particles ( $V_s$ ), volume of water ( $V_w$ ) and the volume of air ( $V_a$ ). Hence, the volume of voids ( $V_v$ ) consists of combining the volume of water ( $V_w$ ) and the volume of air ( $V_a$ ).

### *Mass/volume relationship - Density, specific gravity and unit weight*

The ratio of the total mass of soil in a given volume determines the soil bulk density ( $\rho$ ):

$$\rho = \frac{m}{V} \quad (2.1)$$

If only the dry mass of the soil is considered, the relationship between the mass of soil particles  $m_s$  and the total volume  $V$  is denoted as the dry density of soil  $\rho_d$ :

$$\rho_d = \frac{m_s}{V} \quad (2.2)$$

Minimum dry density of a soil  $\rho_{dmin}$  is obtained from the loosest state of packing in which dry particles can be found in a granular soil. On the other hand, maximum dry density  $\rho_{dmax}$  corresponds to the densest state of packing of a granular soil.

Particle density ( $\rho_s$ ) is obtained from the ratio between mass of soil particles ( $m_s$ ) and volume occupied by those particles ( $V_s$ ):

$$\rho_s = \frac{m_s}{V_s} \quad (2.3)$$

Specific gravity ( $G_s$ ) represents the ratio between particle density ( $\rho_s$ ) and density of water ( $\rho_w$ ):

$$G_s = \frac{\rho_s}{\rho_w} \quad (2.4)$$

Dry unit weight of a soil ( $\gamma_d$ ) is obtained from the product of dry density of soil ( $\rho_d$ ) and gravity ( $g = 9.81\text{m/s}^2$ ) as follows:

$$\gamma_d = \rho_d g \quad (2.5)$$

#### ***Volumetric state - Void ratio ( $e$ )***

Void ratio  $e$  defines a volumetric state of a soil as the ratio of the volume occupied by voids  $V_v$  to the volume of soil particles  $V_s$ .

$$e = \frac{V_v}{V_s} \quad (2.6)$$

Void ratio is not an intrinsic soil property but it varies depending on how packed the particles are within the soil. Void ratio can also be expressed as a function of soil specific gravity  $G_s$ , dry density of soil  $\rho_d$  and density of water ( $\rho_w$ ):

$$e = \frac{G_s \rho_w}{\rho_d} - 1 \quad (2.7)$$

#### ***Normalised volumetric state - Relative density ( $D_r$ )***

The relative density defines the degree of compaction of a soil specimen. This is determined by comparing the current value of the soil void ratio with the minimum and maximum void ratio as follows:

$$D_r(\%) = \frac{e_{max} - e}{e_{max} - e_{min}} 100 \quad (2.8)$$

Table 2.1 shows the relative density descriptors of soil materials depending on the degree of packing. It ranges from very loose to very dense in accordance with the classification created by (Lambe and Whitman, 2010).

**Table 2.1:** Relative density descriptors (Lambe and Whitman, 2010)

Description	Relative density (%)
Very loose	0-15
Loose	15-35
Medium	36-65
Dense	65-85
Very dense	85-100

## 2.4 Stress and strain analysis

This section reviews the stress and strain analysis of soils under the action of vertical, cyclic triaxial and torsional resonant loading. Due to the wide range of experimental testing covered in this investigation, a summary is herein added to set out the main features of each set of experiments, which will be individually developed:

- Vertical loading (Chapter 4); the one dimensional compressive behaviour is analysed, via oedometer tests, and discussed by comparing the evolution in vertical strain versus the vertical stress of RSm. Other stress-strain parameters, including compression/swelling index, plastic strain or constrained modulus are also covered.
- Triaxial loading (Chapter 5); the stress-strain response of soils under cyclic triaxial loading is discussed for specimens tested under saturated, undrained conditions. This analysis is adopted to evaluate the cyclic behaviour and the liquefaction potential of RSm from medium-to-large shear strain amplitudes.
- Torsional resonant loading (Chapter 5); the dynamic behaviour is studied in the small-to-medium range by vibrating the top of soil specimens using a resonant shear column apparatus. The maximum shear strain and shear modulus are also determined, enabling the creation of stiffness and damping degradation curves (Chapter 7).

### 2.4.1 One-dimensional vertical loading

One-dimensional compressive behaviour of RSm specimens is studied in Chapter 4 through the performance of conventional oedometer tests. In this test, the sample is held in a rigid confining ring which prevents the lateral displacement but allows to compress or swell vertically in response to vertically applied loading. Main stress and strain variables for oedometer tests are herein discussed. Vertical stress ( $\sigma_v$ ) is obtained from the ratio between applied vertical load ( $F$ ) and area of oedometer plate ( $A$ ).

$$\sigma_v = \frac{F}{A} \quad (2.9)$$

Effective vertical stress ( $\sigma'_v$ ) is then determined by subtracting pore water pressure  $u$  to the total value of vertical stress ( $\sigma_v$ ).

$$\sigma'_v = \sigma_v - u \quad (2.10)$$

In this study, oedometer tests were conducted under dry conditions therefore the effective vertical stress was equal to the vertical stress, i.e.  $\sigma'_v = \sigma_v$ .

Axial strain ( $\varepsilon_a$ ) is obtained from the relationship between vertical displacement developed in the soil ( $\delta h$ ) and sample initial height ( $H_0$ ):

$$\varepsilon_a = \frac{\delta h}{H_0} \quad (2.11)$$

With the change in height due to the vertical load, the volume of voids ( $V_v$ ) decreases whilst the volume of soil particles ( $V_s$ ) remains the same. This results in a change in void ratio ( $\Delta e$ ). Due to the variable initial void ratio with rubber content, the compressibility is evaluated in this study by calculating the normalised change in void ratio, i.e.  $\Delta e/e_0$ . The plastic strain ( $\varepsilon_p$ ) refers to the irrecoverable plastic deformation experienced by a soil after unloading.  $\varepsilon_p$  has been calculated by reporting the maximum value of axial strain, with respect to the initial height, recorded for every cycle.

The change in one dimensional compression and swelling is evaluated in this study through the determination of compression ( $C_c$ ) and swelling indices ( $C_s$ ). These two

values describe the slope of the load and unload line, respectively, and it gives an indication of the rate of compression under applied vertical stress and swelling after unloading the soil.  $C_c$  and  $C_s$  can be calculated as follows:

$$C_c = \frac{\Delta e_1}{\log \frac{\sigma'_{v1}}{\sigma'_{v0}}} \quad (2.12)$$

$$C_s = -\frac{\Delta e_2}{\log \frac{\sigma'_{v2}}{\sigma'_{v1}}} \quad (2.13)$$

where  $\Delta e_1$  is the change in the void ratio with the first loading,  $\Delta e_2$  is the change in void ratio when unloading soil,  $\sigma'_{v0}$  is the initial vertical stress,  $\sigma'_{v1}$  is the vertical stress after loading, and  $\sigma'_{v2}$  is the vertical stress after unloading.

One dimensional compression and swelling behaviour is non-linear under the application of high vertical stresses. Thus, the change in the apparent stiffness of a soil in one-dimensional compression is also studied by using the constrained modulus ( $M$ ) which depends on stress state, i.e. stress history and load increase. Constrained modulus is given by:

$$M = \frac{\Delta \sigma'_v}{\Delta \varepsilon_a} \quad (2.14)$$

where  $\Delta \sigma'_v$  is change in effective vertical stress and  $\varepsilon_a$  is change in axial strain.

### ***Shear stress - shear strain***

The assessment of the shear strength of a particular soil involves the determination of both shear stress ( $\tau$ ) and shear strain ( $\gamma$ ), which cannot be obtained by means of the oedometer due to not allowing lateral deformation. This study has, however, calculated shear stress and strain with the change in vertical strain obtained through the oedometric tests. This was done to enable the comparison in stress-strain behaviour between mixtures containing different rubber shape, i.e. crumbs or shreds, and rubber in its bulk state, via unconfined compression tests. Whilst not pretending to be a rigorous quantitative analysis, this approach was preliminary undertaken to understand the

hysteretic behaviour of bulk and particulate rubber under cyclic loading. For that, a series of assumptions have been made:

Due to the type of loading in oedometer tests, i.e. one-dimensional vertical, soils cannot fail due to shearing as it occurs in triaxial testing. Moreover, only the vertical stress can be recorded, hence it cannot be distinguished between principal major ( $\sigma_1$ ) and principal minor ( $\sigma_3$ ) stresses. However, this study has assumed that the principal major effective stress  $\sigma'_1$  is equal to the vertical effective stress, which stays as:

$$\sigma'_1 = \sigma_v = \frac{F}{A} \quad (2.15)$$

To estimate the magnitude of the shear stress and shear strain of soils, an assumption of the earth pressure at rest ( $K_0$ ) would be required. For that, the value corresponding to the angle of internal friction ( $\phi$ ), which refers to the angle at which the shear failure occurs, is needed. However, the angle of internal friction is commonly determined by means of shear box and triaxial tests. The graphs created in Chapter 4 on shear stress against shear strain do not intend to show the absolute magnitude of the hysteresis in RSm. Instead, the nature of the energy dissipation in RSm and a comparison between the effect of the rubber particle shape are presented. Thus, the shear stress has been determined in Chapter 4 by assuming a value of internal friction for the different contents as:

$$\tau = \frac{\sigma'_1}{2} \sin \phi' \quad (2.16)$$

When testing the one-dimensional compression via oedometer tests, only the axial strain ( $\varepsilon_a$ ) is recorded. As a result of the lateral constraints in oedometric tests, the radial strain  $\varepsilon_r$  is equal to zero due to not allowing the lateral deformation of the soil, i.e.  $\varepsilon_r = 0$ . The shear strain ( $\gamma$ ) is then assumed to be the difference between the axial and the radial strain. Since  $\varepsilon_r = 0$ , the value of the shear strain has been assumed to be calculated from:

$$\gamma = \frac{2}{3}(\varepsilon_a - \varepsilon_r) = \frac{2}{3}\varepsilon_a \quad (2.17)$$

## 2.4.2 Triaxial loading

The response of soils under triaxial loading is discussed by presenting the stress-strain analysis of samples subjected to cyclic triaxial tests. This is then used as the basis to explain the response of soils under the action of cyclic loading from medium-to-large strains, using cyclic triaxial equipment. A triaxial test involves testing a soil specimen with the application of stresses in different axes, one being perpendicular to the vertical direction. Due to the axial symmetry found in triaxial tests,  $\sigma_2 = \sigma_3 = \sigma_r$ . Consequently, from these experiments two principal stresses, axial (vertical), i.e.  $\sigma_1$ , and radial (horizontal), i.e.  $\sigma_3$ , have been considered in accordance with the assumption that the specimen deforms uniformly as a circular cylinder.

Principal major stress ( $\sigma_1$ ) is obtained from combining the principal minor stress ( $\sigma_3$ ) and the applied vertical force ( $D$ ) divided by the radial area ( $A$ ):

$$\sigma_1 = \frac{D}{A} + \sigma_3 \quad (2.18)$$

Principal major effective stress ( $\sigma'_1$ ) and principal minor effective stress ( $\sigma'_3$ ) are determined by subtracting pore water pressure ( $u$ ) from  $\sigma_1$  and  $\sigma_3$ , respectively.

The deviatoric stress invariant ( $q$ ) recorded due to the triaxial loading causes shearing within the sample and its magnitude is independent of pore water pressure. Due to the axial symmetry, i.e.  $\sigma_2 = \sigma_3$ , the equation for the deviatoric stress reduces to:

$$q = \sigma'_1 - \sigma'_3 = \sigma_1 - \sigma_3 \quad (2.19)$$

The mean stress invariant ( $p'$ ) is the result of combining the three principal stress components, and it only induces volumetric change, it does not induce shear change as it occurs with the deviatoric stress. Since  $\sigma_2 = \sigma_3$ ,  $p'$  is calculated by obtaining an average value between principal major effective and principal minor effective stress as:

$$p' = \frac{\sigma'_1 + 2\sigma'_3}{3} \quad (2.20)$$



***Consolidated Undrained (CU) conditions***

Saturated specimens of RSm were tested under consolidated undrained conditions in Chapter 5. The specimen drainage is permitted with a specified confining pressure before the consolidation is complete. Then, the principal stress difference is applied and drainage is not longer permitted. The pore water pressure measurements are recorded whilst loading the soil and thus, the strength parameters are determined in terms of effective stresses. A graph representing typical total and effective stress failure envelopes, i.e. Mohr circles, is shown in Figure 2.2. Under undrained conditions, total stress are translated in the stress state representation due to the presence of pore water pressure, i.e.  $\sigma = \sigma' + u$ , whilst the magnitude of the diameter of both total and effective Mohr circles is the same. Hence,  $\sigma_1 - \sigma_3 = \sigma'_1 - \sigma'_3$ .

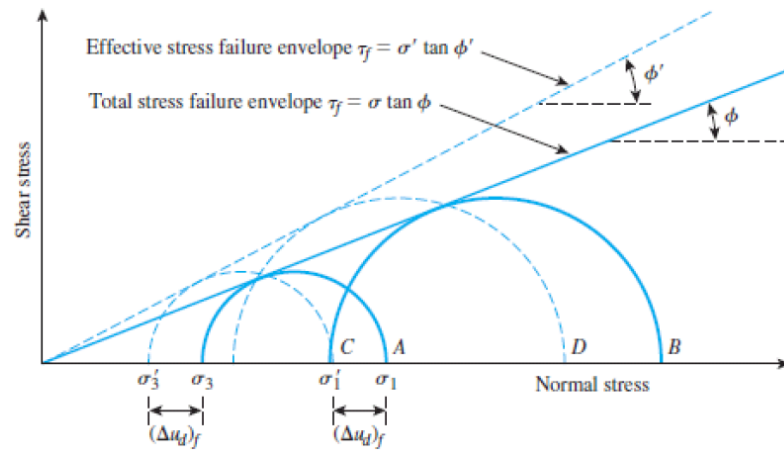


**Figure 2.2:** Mohr circles for CU triaxial test (Craig and Knappett, 2012)

Based on Figure 2.2, the shear stress ( $\tau$ ) is obtained from the effective internal friction angle ( $\phi'$ ), which represents the angle where the effective stress failure envelope lies, and the effective normal stress as:

$$\tau = \sigma' \tan \phi' \quad (2.21)$$

Under undrained consolidated conditions, the maximum shear stress is obtained from the diameter of the total or effective Mohr circle. In practice, this is calculated as the difference between principal stresses, and equal to the deviatoric invariant stress as:

$$\tau_{max} = (\sigma'_1 - \sigma'_3)/2 = (\sigma_1 - \sigma_3)/2 = q/2 \quad (2.22)$$

With regards to Mohr circle of strain, volumetric strain is considered to be zero in undrained conditions due to not allowing the change in soil volume:

$$\epsilon_v = \epsilon_1 + \epsilon_2 + \epsilon_3 = \epsilon_a + 2\epsilon_r = 0 \quad (2.23)$$

Radial strain ( $\epsilon_r$ ) is the result of the change in the volumetric strain and the axial strain:

$$\epsilon_r = \frac{-\frac{\delta v}{V_0} + \frac{\delta h}{H_0}}{2} \quad (2.24)$$

where  $\delta v$  is the change in volume,  $V_0$  is the initial soil volume, and  $\frac{\delta h}{H_0}$  is the axial strain. In undrained case, the change in volumetric strain is zero and the radial strain remains as equal to half the value of the axial strain:

$$\epsilon_r = -\frac{1}{2}\epsilon_a \quad (2.25)$$

The application of deviatoric stress ( $q$ ) to the specimen induces strain in the soil which is known as triaxial shear strain ( $\epsilon_q$ ). Given that the test is conducted under undrained conditions, i.e. no volume change, the deviatoric shear strain stays as:

$$\epsilon_q = \frac{2}{3}(\epsilon_a - \epsilon_r) = \epsilon_a \quad (2.26)$$

This is useful to determine the value of shear modulus, given that the ratio between the deviatoric stress and the deviatoric shear strain describes a slope equal to three times the shear modulus of a soil. Instead, the shear modulus can be directly obtained from the slope between the shear modulus ( $\tau$ ) and shear strain ( $\gamma$ ). Under undrained conditions,  $\epsilon_q = \gamma = \epsilon_a$ . The relationships to determine the soil shear modulus are:

$$3G = \frac{q}{\epsilon_q} \quad (2.27)$$

$$G = \frac{\tau}{\gamma} \quad (2.28)$$

### *Cyclic behaviour*

The response of soils under the action of cyclic triaxial loading results in a series of hysteretic loops which represent the cyclic stress-strain behaviour. The dynamic behaviour of RSm has been studied in the medium-to-large strain range, i.e. 0.05-1%, by determining the change in deviatoric stress ( $q$ ) or shear stress ( $\tau$ ) versus shear strain ( $\gamma$ ) when subjecting the specimen to cycling regimes. Stress-strain analysis of every specimen has been calculated and plotted as observed in Figure 2.3. The ratio stress/strain represents the soil stiffness or, in other words, the resistance of the soil to deform under shear forces increases as the slope of the ratio increases. As observed in Figure 2.3, the evolution in the soil stiffness is non-linear and this is expected to vary with the level of deformation and the properties of the soil tested.

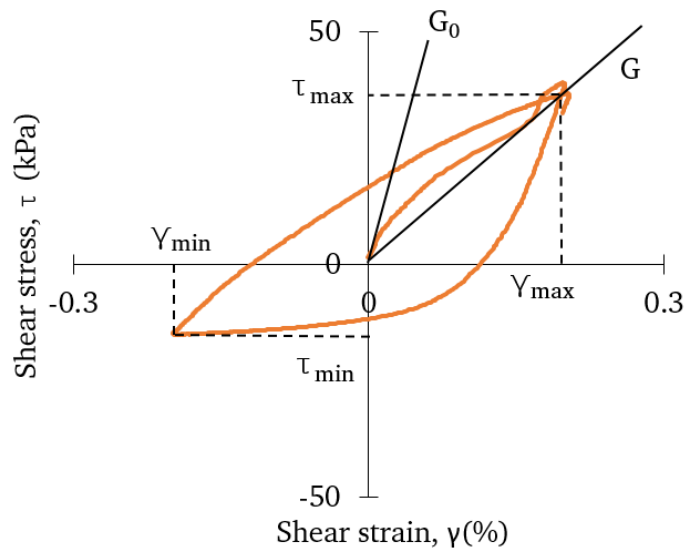


**Figure 2.3:** Evaluation of cyclic behaviour from hysteresis loop

Another form to analyse the cyclic behaviour of a soil is via stress paths. As observed in Figure 2.4, these lines describe the evolution in deviatoric stress ( $q$ ), i.e. induces shear, against the effective mean stress ( $p'$ ), i.e. induces volume change. As deviatoric stress is independent of  $u$ , any excess in pore water pressure may induce a change in the mean stress. The stress path represents the successive states of stress, and it is considered to be an easier representation than Mohr circles under cyclic loading. In this study, the effective mean stress is calculated, hence the effective stress path is described.

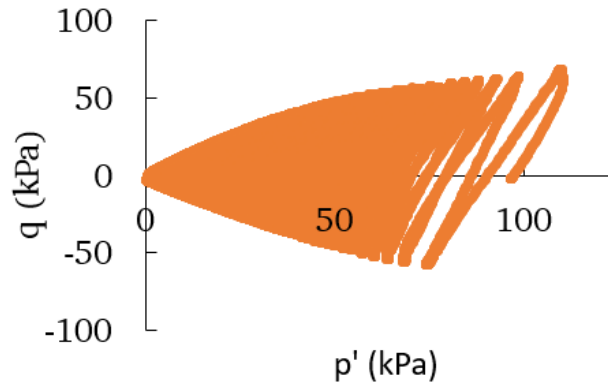


**Figure 2.4:** Effective stress path of a soil under cyclic loading

### ***Liquefaction potential***

Liquefaction potential of soils is evaluated by measuring the change in the pore water pressure ( $\Delta u$ ), as pore pressure ratio ( $r_u$ ), with number of cycles ( $N$ ). A soil specimen liquefies when the value of pore pressure ratio is equal to 1. This occurs when there is an increase in the value of the change in pore water pressure and the effective confining pressure drops to 0. Pore pressure ratio is defined as:

$$r_u = \frac{\Delta u}{\sigma'_3} \quad (2.29)$$

Where,  $\Delta u$  = change in pore water pressure,  $\sigma'_3$  = principal minor effective stress

Change in pore water pressure ( $\Delta u$ ) is obtained from recorded pore water pressure during the cyclic triaxial test and it is defined as:

$$\Delta u = u_i - u_0 \quad (2.30)$$

Due to the fluctuation in  $\Delta u$ , liquefaction potential of RSm is evaluated by taking the average value of 1000 data points, i.e. one value per second or per loading cycle. The cyclic effect on RSm liquefaction potential is studied in Chapter 5 by applying a constant amplitude through strain controlled cycles. The liquefaction potential is then analysed by plotting the value of pore pressure ratio against number of cycles ( $N$ ).

### ***Shear modulus***

Shear modulus ( $G$ ) describes the soil stiffness or the resistance of a material to deformation under cyclic loading regimes. It can be defined as initial tangent shear modulus; also known as  $G_{max}$  or  $G_0$  which represents the maximum soil stiffness, and secant shear modulus; that indicates the soil stiffness at certain strain amplitude (Figure 2.3). The latter is adopted to determine shear modulus at deformations in the medium-to-large strain range. As the hysteretic loops are not always centred,  $G$  is calculated for each hysteretic loop when plotting shear stress ( $\tau$ ) against shear strain ( $\gamma$ ) as follows:

$$G = \frac{\tau_{max} - \tau_{min}}{\gamma_{max} - \gamma_{min}} \quad (2.31)$$

Where  $\gamma_{max}$  and  $\gamma_{min}$  are maximum and minimum shear strain and  $\tau_{max}$  and  $\tau_{min}$  are maximum and minimum shear stress.

### **2.4.3 Torsional resonant loading**

Dynamic behaviour of soils is evaluated at very small-to-medium strains ( $\gamma = 0.0001 - 0.05\%$ ) by means of resonant column experiments. The principle of this experiment is to excite one end of a cylindrical confined soil specimen under the action of a torsional single-degree of freedom oscillation. Once the resonance condition is established, then measurements are taken to establish the maximum strain amplitudes. Shear modulus and damping capacity determined at very small strains correspond to the elastic dynamic properties of a given soil. Thus, these are commonly denoted as maximum shear modulus ( $G_0$ ) and minimum damping ratio ( $\xi_0$ ), which are determined for every RSm in Chapter 5 and used to establish stiffness and damping degradation curves in Chapter 7.

The low level of deformation undergone by the specimen implies different procedures to determine the variation in soil shear modulus with the level of strain amplitude. To proceed with the determination of shear stiffness and damping, a sinusoidal torsional motion is applied on top of the soil specimen with a constant amplitude, whilst varying the range of frequencies between 10 Hz and 1 kHz. Then, the soil response is measured and plotted against the frequency to elucidate the peak deformation of the

specimen with a given torque force (Figure 2.5). The torque is then increased in order to calculate the soil stiffness at higher strain amplitudes.

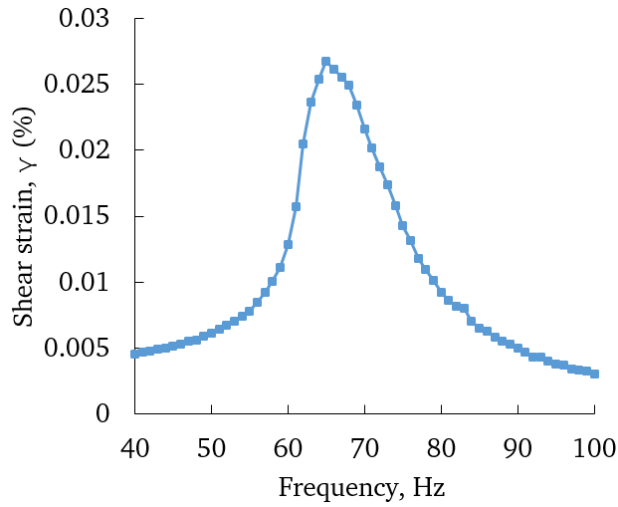


**Figure 2.5:** Determination of maximum shear strain versus frequency with resonant column test

Shear modulus is determined from the value of shear wave velocity, measured in the first-mode of resonant frequency, and soil density. The expressions adopted to calculate shear strain and shear modulus are described here:

### ***Shear strain***

When subjected to resonant torsional tests, shear strain ( $\gamma$ ) reached by a soil cylindrical specimen varies from zero, at the center of the specimen, to maximum deformation, at the outer edge of the same. Hence, maximum shear strain for a given torque force is determined as follows:

$$\gamma_{max} = \frac{r_{max}\theta_{max}}{L} \quad (2.32)$$

Where,  $r_{max}$  is the maximum radial distance from the soil column axis,  $\theta_{max}$  is maximum angle of rotation from center line and  $L$  is specimen length.

### ***Shear modulus***

A fixed-free resonant column test is undertaken to determine the maximum shear modulus of RSm. In this case, the base of the specimen is fixed whilst the drive system is

idealised to be a lumped mass. A sinusoidal torsional motion is applied on top of the soil cylinder which induces the propagation of shear waves and the twist of the specimen. The solution corresponding to the wave equation for the first mode of vibration stays as:

$$\frac{I}{I_0} = \frac{w_n L}{V_s} \tan\left(\frac{w_n L}{V_s}\right) \quad (2.33)$$

Where,  $I_0$  = mass of polar moment inertia of the system including the top cap,  $I$  = mass polar moment of inertia of the soil column,  $w_n$  = is the circular frequency of the torsional model of vibration,  $L$  = specimen length and  $V_s$  = shear wave velocity.

If the linear isotropic elasticity is assumed, shear modulus of a soil tested can be calculated from the shear wave velocity ( $V_s$ ) and soil density ( $\rho$ ) as:

$$G = \rho V_s^2 \quad (2.34)$$

According to [ASTM D4015 \(2015\)](#), this equation is broken down into sub-expressions which depend on a dimensionless modulus factor ( $F_a$ ):

$$G = \rho(wL)^2 F_a \quad (2.35)$$

Where  $\rho$  is density of soil specimen,  $L$  is specimen length,  $w$  is system resonant circular frequency and  $F_a$  is a dimensionless modulus factor.

The only unknown variables in the expression are  $w$  and  $F_a$ .  $w$  is obtained by finding the minimum frequency at which the applied torque is 90 degrees out of phase with respect to rotational displacement. On the other hand,  $F_a$  has to be obtained from the active-end inertia factor ( $T_a$ ), calculated with Equation 2.36, which is directly related to the moment of inertia recorded in the soil cylinder ( $J$ ):

$$T_a = \frac{J_a}{J} \left[1 - \frac{f_a^2}{f_r^2}\right] \quad (2.36)$$

Where  $J_a$  is rotational inertia of active-end platen system,  $J$  is specimen rotational inertia,  $f_a$  is apparatus resonant frequency and  $f_r$  is system resonant frequency.

Dimensionless factor ( $F_a$ ) and, in last instance, shear modulus were determined when knowing  $T_a$ , using the table of equivalences provided by [ASTM D4015 \(2015\)](#).

## 2.5 Evaluation of damping

This section reviews the different forms of damping which are of interest for understanding the dynamic behaviour of RSm when subjected to cyclic loading regimes.

The scope of this study focuses on the vibration waves generated as a result of the application of cyclic loading such as the ones generated in seismic events. From the moment the rupture of a fault occurs and a seismic event is triggered, vibration waves propagate through the soil until they reach the surface. Within the seismic waves there are two types, body and surface waves. From the point of view of the seismic structural design, the body waves are the most important attributed to the damage occasioned when striking structural elements (Towhata, 2014).

It has been proven that energy and, in turn, stress of body waves can be amplified or attenuated when they move through the soil deposit until they reach the surface. When attenuation occurs, the dissipation of energy associated with the transmission of body waves through the ground soil is attributed to two main causes; (i) mechanical properties of the soil in which the wave is transmitted and (ii) geometrical characteristics of the medium (Kramer, 1996). Within the first group, two types of damping or energy dissipation mechanisms are distinguished: material viscous and non-linear hysteretic damping. The latter is associated with wave scattering and radiation damping, which has been denoted as geometrical damping.

### 2.5.1 Material damping

Linear viscous and hysteretic non-linear damping correspond to the most common forms of material damping:

#### *Non-linear hysteretic damping*

Hysteretic damping is commonly related to the soil non-linear behaviour. This is defined as the mechanical energy lost due to dry friction and sliding at inter-particle contacts, which is represented by the area within the stress-strain loop (Fig. 2.6) of



a viscoelastic material (Ashmawy et al., 1995; Thorby, 2008). Hysteretic damping is typically calculated from stress-strain loops obtained during cyclic triaxial tests.

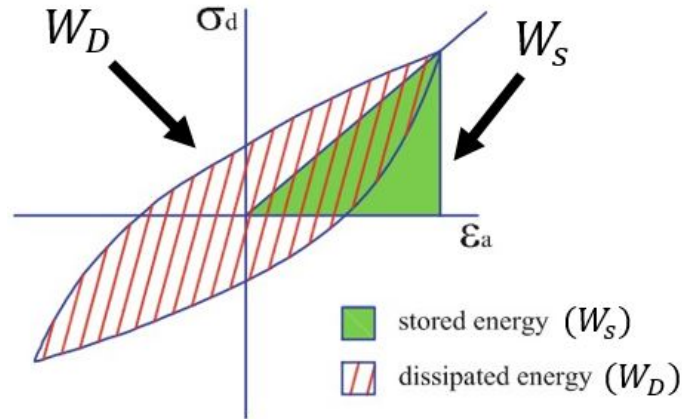


**Figure 2.6:** Evaluation of stored and dissipated energy (Shamy and Denissen, 2012)

A common metric of energy loss is the specific damping capacity ( $\psi$ ) which represents the lag between soil response, i.e. displacement or strain, and input, i.e. force or stress, when subjected to dynamic loading. Loss coefficient ( $\delta$ ) represents the loss/phase angle by which strain lags stress under loading, in other words, it represents the delay in the response of the soil with respect to the applied stress. The tangent of the loss coefficient ( $\delta$ ) coincides with the value of hysteretic damping and it is estimated to be equal to two times the viscous damping under resonant conditions.

The expression of specific damping capacity was initially expressed by Read and Dean (1998) in terms of time domain analysis. Thus,  $\psi$  is equal to  $2\pi$  the tangent of the phase angle. However, for simplicity purposes,  $\psi$  is commonly calculated in terms of work/energy done. This is obtained from the relationship between energy dissipated during a loading cycle ( $W_D$ ) and maximum elastic energy stored during that cycle ( $W_S$ ):

$$\psi = \frac{W_D}{W_S} = 2\pi \tan \delta \quad (2.37)$$

Another common way of defining dissipation of energy in a soil material, which includes energy dissipation capacity expression, is damping ratio  $\xi$ . This is defined by Brennan et al. (2005) as the average damping capacity of a soil per radian during a loading cycle at medium-to-large strains:

$$\xi = \frac{\psi}{4\pi} = \frac{W_D}{4\pi W_S} \quad (2.38)$$

To determine both specific damping capacity  $\psi$  and damping ratio  $\xi$ , dissipated energy  $W_D$  and absorbed energy  $W_S$  in a loading cycle need to be defined.

Maximum stored energy is also known as the total work done on the material  $W^+$  (Figure 2.7a) comprising of energy dissipated by the material in the form of heat and energy stored in the material (Shamy and Denissen, 2012). It can be determined from the area under the loading branch of a stress-strain loop when passing from zero to the maximum stress as seen in Figure 2.7a. However, for simplicity, the maximum elastic energy stored  $W_D$  is commonly calculated as the bounded triangular area under the secant stiffness at the maximum stress-strain amplitude (Fig. 2.6).

During the unloading branch, the released energy  $W^-$  is identified as work done by the material. This is calculated as the area under the stress-strain loop during the unloading sequence when passing from maximum to zero shear stress (Fig. 2.6).

The energy dissipated  $W_D$  is commonly determined as the area enclosed within the loading-unloading branch by means of stress-strain behaviour resulting from the inter-particle friction at a macroscopic level (Thorby, 2008; Verruijt, 2010), as observed in Figure 2.6. Following the previous assumptions, energy dissipated  $W_D$  can then be defined as the difference between the work done on the material ( $W^+$ ) and the work released or done by the material ( $W^-$ ).

Equation 2.38 has been used to evaluate the hysteretic (non-linear) material damping of RSm from medium-to-large deformations. For that, the values of maximum elastic energy stored and energy dissipated have been determined for each one of the stress-strain loops obtained from the response of the mixtures under cyclic loading. The evolution in material damping capacity has then been analysed in Chapter 7 from small-to-large deformations as a function of particle properties and test conditions, in order to understand the dynamic behaviour of RSm.

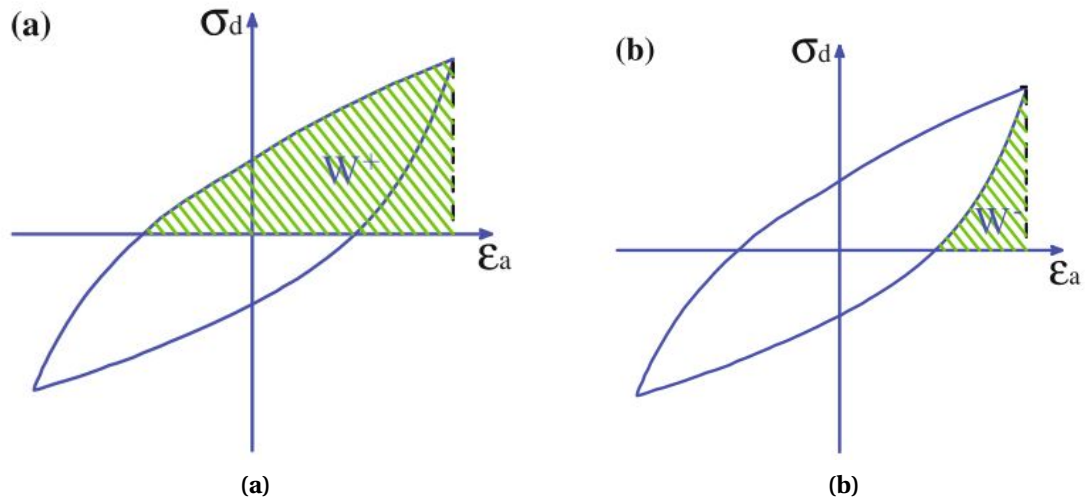


**Figure 2.7:** Representation of a) maximum stored energy, and b) energy released under dynamic loading according to [Shamy and Denissen \(2012\)](#)

### *Viscous damping*

The value corresponding to hysteretic damping developed by a soil is almost negligible at small strains. This underestimates the overall material damping evaluated experimentally, as established in the literature ([Ashmawy et al., 1995](#)). A different material damping is therefore introduced in linear analysis, or materials that experience a linear behaviour, which is known as material viscous damping.

Viscous damping is originated in a soil through the vibration of a material which posses viscosity. Unlike it occurs with the hysteretic damping, the viscous damping is a velocity and, consequently, frequency proportional damping. Rayleigh damping is the most common form used to represent viscous damping of a soil given that it is easy to measure. Thus, Rayleigh damping is dependent on both soil mass and stiffness as well as loading frequency ([Yoshida, 2015](#)).

The usual practice to define material damping of a soil in the range from very small to medium strains comes by adopting an equivalent material viscous damping, i.e.  $\xi$ . Equivalent viscous damping accounts for the amount of damping that provides the same bandwidth in the frequency-response curve as it would be experimentally obtained. Thus, this procedure is commonly known as half-power bandwidth method, i.e. frequency domain, for calculating damping ratio using a torsional resonant column.

Viscous damping ratio is calculated considering as if the soil cylinder was equal to a single degree of freedom and it is subject to a harmonic force applied by the rotor (Papagiannopoulos and Hatzigeorgiou, 2011). For that, a transfer function  $X(w)$  needs to be calculated, obtained then from the non-dimensional frequency response as:

$$X(w) = \frac{1}{1 - (\frac{w}{w_n})^2 + 2\xi(\frac{w}{w_n})i} \quad (2.39)$$

Where,  $w_n$  = is natural frequency of the system,  $w$  = is current loading frequency, and  $X(w)$  is amplitude of the transfer function and  $i = \sqrt{-1}$ .

From Equation 2.39, the modulus of the maximum value of the transfer function, i.e. at resonant frequency ( $X_r(w)$ ), is calculated as:

$$|X_r(w)| = \frac{1}{2\xi\sqrt{1-\xi^2}} \quad (2.40)$$

For small values of  $\xi$ ,  $w_r \cong w_n$ , i.e.,  $\frac{w}{w_n} = 1$ . In other words, when small values of damping ratio are considered, natural frequency  $w_n$  and resonant frequency  $w_r$  can be considered to have approximately the same value. Thus, it is obtained from Equation 2.39 that the modulus of the transfer function at the natural frequency is  $|X_n(w)| = \frac{1}{2\xi}$ , similar the transfer function calculated at resonant frequency (Equation 2.40). However, even when the value of  $\xi$  is very close to zero, the values of  $|X_n(w)|$  and  $|X_r(w)|$  are not exactly the same. This is even more evident at greater values of damping ratio, reason why the alternative method for determining  $\xi$ , i.e. free vibration procedure, is only used at very small strains (Papagiannopoulos and Hatzigeorgiou, 2011). Two frequency points  $X_1$  and  $X_2$  are used instead on either side of  $|X_n(w)|$  (See Figure 2.8):

$$|X_{(w1)}| = |X_{(w2)}| = \frac{1}{\sqrt{2}}|X_n(w)| = \frac{1}{\sqrt{2}}(\frac{1}{2\xi}) \quad (2.41)$$

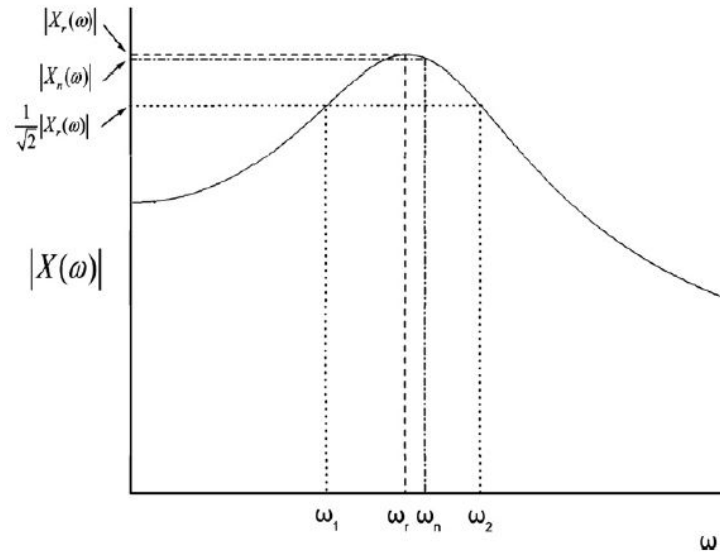


**Figure 2.8:** Half power bandwidth based on (Papagiannopoulos and Hatzigeorgiou, 2011)

The two frequency points are commonly denoted as half-power frequency points and the bandwidth comprised between them is known as half-power bandwidth. By substituting the modulus of the transfer function  $|X_n(\omega)|$  with the final value obtained in Equation 2.41, the Equation 2.39 becomes:

$$\left(\frac{\omega}{\omega_n}\right)^4 - 2(1 - 2\xi^2)\left(\frac{\omega}{\omega_n}\right)^2 + (1 - 8\xi^2) = 0 \quad (2.42)$$

Solution for Equation 2.42 leads to:

$$\left(\frac{\omega}{\omega_n}\right)^2 = 1 - 2\xi^2 \pm 2\xi\sqrt{1 + \xi^2} \quad (2.43)$$

Finally, the value of  $\xi$  can be determined by introducing a binomial expansion of  $\sqrt{1 + \xi^2}$  and maintaining the first two terms. This expression is accurate when  $\xi \leq 0.353$  and states as:

$$\left(\frac{\omega_2 - \omega_1}{\omega_n}\right) \cong 2\xi \quad (2.44)$$

Equation 2.44 is used in this study to calculate the viscous (linear) material damping of RSm from small-to-medium deformations.

## 2.5.2 Geometrical damping

Geometrical damping includes those form of stress wave attenuation due to the interaction between incident vibration waves with either the geometry of the area (radiation damping) or change in properties of the medium (wave scattering):

### *Radiation damping*

Radiation damping accounts for dissipation of energy over a large volume of material. Although energy conservation states that energy should remain the same over time, energy released from the fault rupture propagates in all directions and results in a subsequent reduction of the earthquake waves. This is observed in both body and surface, i.e. Rayleigh, waves and it can be clearly observed in Figure 2.9, where the cyclic loading is applied on top of the ground surface.

The geometric attenuation will cause body waves to decay with distance at a rate  $1/r$  within the soil medium. This attenuation is much larger if the body waves travel along the surface. On the other hand, the Rayleigh waves are attenuated at a lower rate ( $1/r^{0.5}$ ), reason why more surface wave motions are detected in comparison with body motions (Woods, 1968). If the attenuation of the incident wave energy is considered in conjunction with the dissipative properties of the material, the amplitude stays as:

$$A_1 = A \frac{r}{r_1} \exp^{-\frac{w}{2Q_f V_s}(r_1 - r)} \quad (2.45)$$

where  $V_s$  is shear wave velocity,  $w$  is the input circular angular frequency,  $Q_f$  is the quality factor influenced by the damping ratio and  $r_1 - r$  is the considered distance.

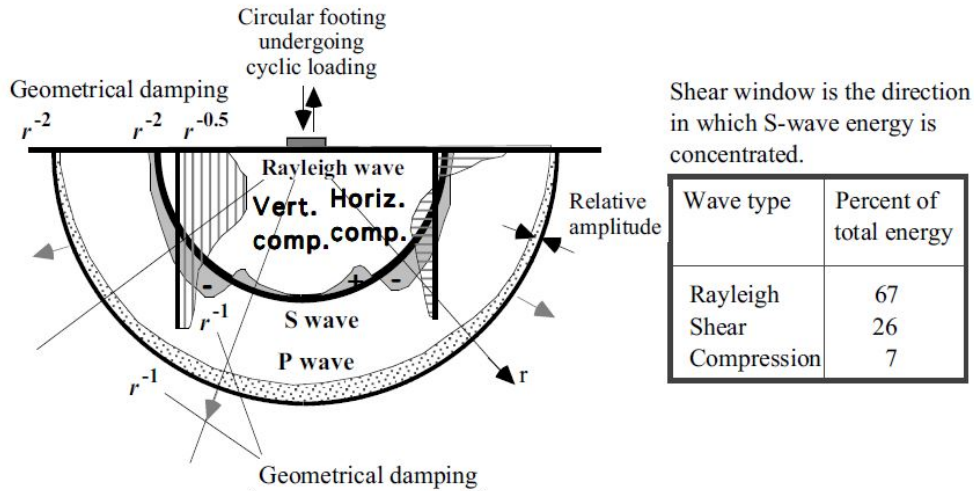


**Figure 2.9:** Distribution of elastic waves (Towhata, 2014)

The geometrical damping can be of great importance when the distance between the fault rupture or the different stratum and soil foundation are large enough, being in occasions more relevant than soil non-linear damping. Radiation damping is, however, complex to estimate and it is commonly added to the boundary conditions as additional dashpots. In other investigations, additional internal damping is added so as to include the possible geometrical damping (Kramer, 1996). Due to the small size of the scaled model tested in this investigation, radiation damping has not been accounted to prove the stress wave attenuation.

### ***Attenuation by wave scattering***

Wave scattering refers to the wave reflection and diffraction as a result of the difference in the mechanical properties of two elastic media. This concept was adopted by previous studies to design wave screening barriers and thus reduce ground-borne vibrations (Woods, 1968; Gao et al., 2006; Mahdavisefat et al., 2017) and it has been lately proposed for seismic protection (Kirtas et al., 2009; Brennan et al., 2019).

It is important to stress that the travel path of body waves through the soil deposit is not straight but curved as a consequence of soil stratification. This phenomenon is described in Snell's law (Figure 2.10), which establishes that when a body wave reaches an interface with another elastic medium, it will be partially reflected into the

first medium and partially transmitted into the second medium (Yoshida, 2015). The relationship between incident  $\theta_1$  and refracted angle  $\theta_2$  is:

$$\frac{\sin(\theta_2)}{\sin(\theta_1)} = \frac{V_2}{V_1} \quad (2.46)$$

Where  $V_1$  = shear wave velocity of stratum 1, and  $V_2$  = shear wave velocity of stratum 2. As observed in Equation 2.46, the ratio between the refracted and incident wave depends directly on the shear wave velocity ( $V$ ), i.e. soil stiffness, of the two elastic media.

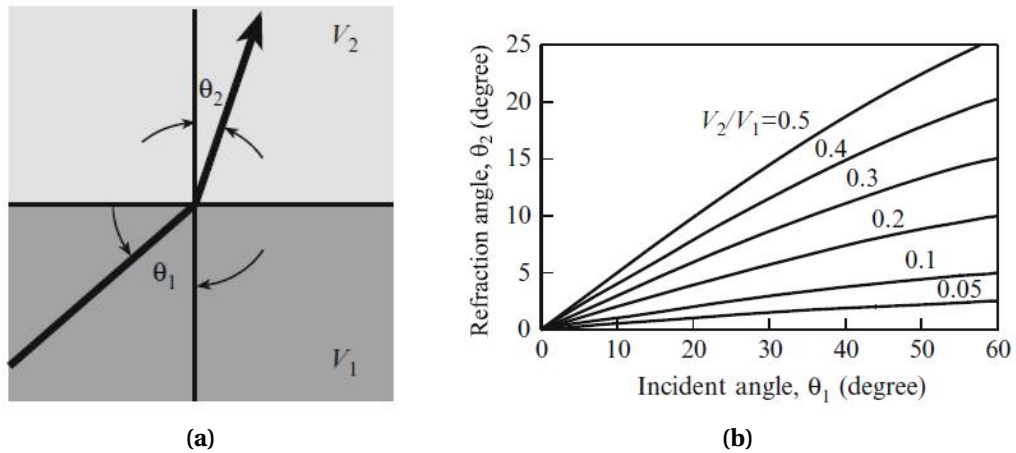


**Figure 2.10:** Incident and refraction angle at a soil boundary (Yoshida, 2015)

In accordance with the theory of elastic energy, it is also established that part of the energy coming from the incident wave is reflected and part of it is refracted. This theory states that at the interface there is not only a change in the direction of propagation, but also in the amplitude of the body wave (Lombardi et al., 2014).

Generally speaking, the disposition of the soil deposit is a combination of numerous layers located at different depths and with variable inclinations. As a consequence, a complex process of reflecting and refracting waves occurs as these pass through the material with different approaching angles (Yoshida, 2015). This study considers that the incident waves travel vertically as they approach the surface based on the assumption that the ground soil is characterised by a lower stiffness when it is closer to the surface. This leads to the calculation of shear wave transmission in a one-dimensional problem in which both reflected and transmitted waves are propagated with the same angle.



The continuity and compatibility of amplitudes and stresses of an incident shear wave approaching an interface must satisfy:

$$A_i + A_r = A_t; \sigma_i + \sigma_r = \sigma_t \quad (2.47)$$

Where  $A_i$ ,  $A_r$ ,  $A_t$  is displacement amplitude of incident, reflected and transmitted waves, and,  $\sigma_i$ ,  $\sigma_r$ ,  $\sigma_t$  is stress amplitude of incident, reflected and transmitted waves. To evaluate the effect that the change in soil stiffness between two soil media has on the stress wave transmission, the dynamic impedance  $\alpha$  is commonly calculated and this is defined as:

$$\alpha = \frac{\rho_2 V_2}{\rho_1 V_1} \quad (2.48)$$

In this case,  $\rho_1 V_1$  are density and shear wave velocity of the soil medium where the wave comes from and  $\rho_2 V_2$  of them medium where it is transmitted. Stress and displacement amplitudes are directly influenced by the dynamic impedance ratio (Figure 2.11). That said, dynamic impedance ratio presents a higher value when the shear wave passes from a soft material into a very hard rock. In this case, the displacement amplitude corresponding to the transmitted wave is nearly zero, and most of the wave is reflected.

On the other hand, when a body wave goes from a very hard rock to a soft upper layer, the transmitted amplitude displacement doubles its value (Figure 2.11a). In terms of stress amplitude, when the dynamic impedance ratio is either very high or very low, the transmitted stress wave tends to zero, and most of the wave energy is reflected. This is, for instance, the case of free end boundaries ( $\alpha = 0$ ), where the totality of the incident wave energy is reflected (Figure 2.11b). This is the reason why some studies have proposed the sub-soil intervention by creating open trenches or introducing soft vertical and horizontal soil layers. Although the stiffening of soil layers might in theory create the same effect on the stress wave transmission, this has been demonstrated not to be as feasible as the former option, given that it would imply the inclusion of rather expensive materials such as glass, steel or iron (Lombardi, 2012).

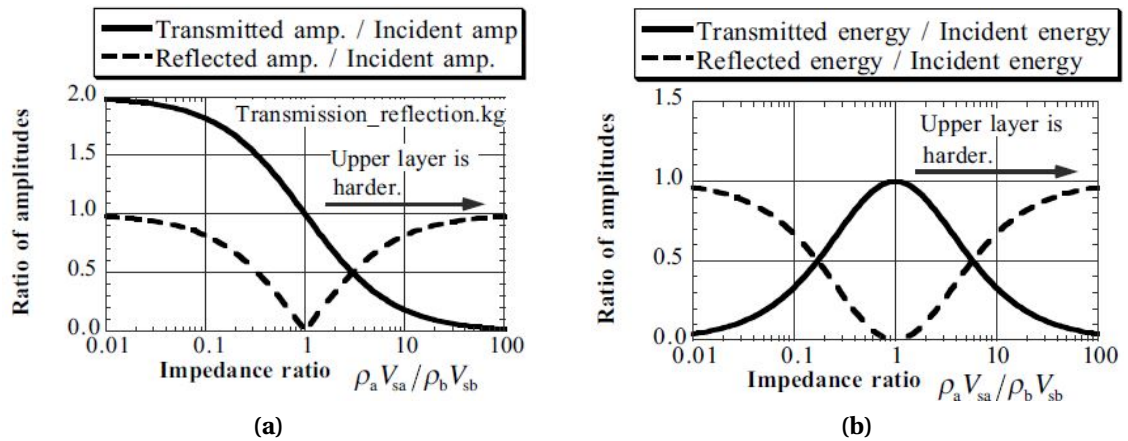


**Figure 2.11:** Attenuation of a) displacement and b) stress amplitude of shear waves through medium (Yoshida, 2015)

### 2.5.3 Energy dissipation at a lab scale

At a particulate and element scale, energy dissipation is measured in soils through the evaluation of material damping, i.e. viscous and hysteretic damping. When it comes to understanding the response of a soil foundation-building, however, this does not provide sufficient information to predict the dynamic response of the entire system. This is due to the fact that such a complex system consists of combining the energy dissipated by various materials, characterised with different dynamic properties. Moreover, there are other factors involved in the stress wave attenuation due to geometrical aspects including wave scattering or radiation damping, difficult to individually quantify. On the other hand, seismic motions are accounted to be non-periodic motions which consist of a broad range of frequencies, making it difficult to evaluate the site response. Numerical simulations have been typically used to evaluate the dynamic response of complex soil deposits adopting the ground response analysis. To undertake this analysis the soil dynamic behaviour needs to be fully understood. Adopting an average stiffness or damping ratio for an entire soil deposit can then become a challenge in order to accurately simulate its response under the action of cyclic vibration waves.

***Harmonic sinusoidal motions***

One way to experimentally study the dynamic response of a structure is by subjecting it to a series of forced harmonic motions with a constant amplitude whilst varying the input frequency (Chopra, 2011). This is the approach followed in Chapter 6 to study the structural response of a small-scale foundation system subject to cyclic loading using a scaled shaking table. For that, both time and frequency domain analysis are considered to assess the correlation between output/input motions.

Time domain analysis is adopted in this study to show the evolution in acceleration histories with the input frequency. This approach can help elucidate when the steady state is reached by supported configurations of the foundation-modified soil. The expressions to calculate peak displacements ( $u$ ), velocities ( $\dot{u}$ ) and accelerations ( $\ddot{u}$ ) are obtained in accordance with evolution of a sinusoidal vibratory motion over time:

$$u(t) = A \sin(\omega t) \quad (2.49)$$

$$\dot{u}(t) = \omega A \cos(\omega t) \quad (2.50)$$

$$\ddot{u}(t) = -\omega^2 A \sin(\omega t) \quad (2.51)$$

Where,  $A$  is the displacement (mm),  $\omega$  is the circular frequency (rad/sec) and  $t$  is the time (sec).

Figure 2.12 represents the evolution in acceleration over time of a single degree of freedom before reaching the steady state. This provides an example of the sinusoidal motions recorded with the accelerometer from 1g shaking table tests. Analytical; based on damped forced vibration expressions, and experimental results; as according to shaking table experiments, are shown in Figure 2.12 at 4.25 Hz frequency. Figure 2.12 reveals similar trends and amplitude in acceleration histories when comparing empirical with analytical results. Hence, the small-scaled box tested in this investigation is assumed to mimic the behaviour of a single-degree of freedom lumped mass system.

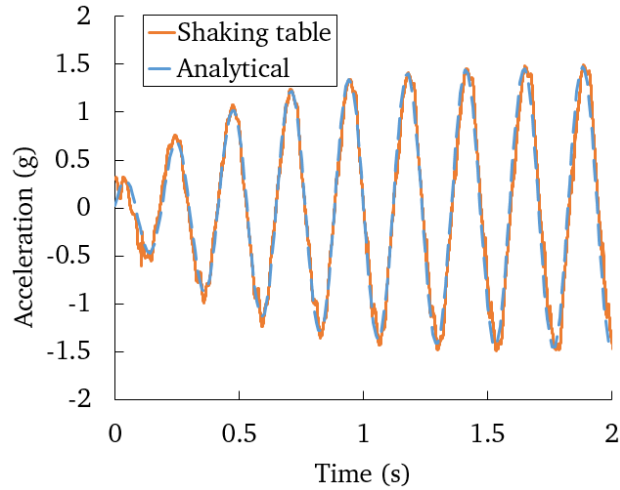


**Figure 2.12:** Time domain analysis on horizontal accelerations of a single degree of freedom system

The acceleration response of the output motion has also been compared to the input motion by determining the phase lag or loss angle between two peaks. As established by [Chopra \(2011\)](#), the maximum response of a system is reached when the loss angle between the output and input is around 90 degrees. This approach has been used to establish when the building-foundation system is under resonance. The phase lag is calculated as follows:

$$\phi = (t/T)360 \quad (2.52)$$

Where,  $\phi$  (deg) is the phase angle,  $t$  (sec) is time difference between the input and output peak and  $T$  (sec) is the period of the sinusoidal wave.

Time domain analysis, using log decay methods, rely on the analysis of a unique signal whilst decreasing strength and, it is postulated ([Signes et al., 2017](#)) more difficult to isolate from other dynamic effects, i.e. boundary reflections. This is not seen as an optimal approach for unbound granular materials, such as the case of RSm, which could introduce additional wave reflections and subsequent high frequency noise due to the change in the soil stiffness with respect to the host soil. This is the reason why test data has been analysed in the frequency domain to provide a steady dynamic state, from which to observe and extract peak acceleration amplitudes as the representative measure of dynamic behaviour.

### ***Amplification ratio***

The key aspect for the estimation of the response of a structural system stems from the determination of the dynamic properties that characterise its cyclic behaviour. Thus, natural frequency, dependent on system stiffness, and damping ratio of the building-foundation have been analysed in this study whilst altering the support conditions.

The maximum response of the studied structure, in terms of acceleration, is compared to the base excitation and this is plotted in a graph in conjunction with the corresponding value of the studied frequency ratio (Figure 2.13). The result accounts for the resultant amplification and it is commonly known as amplification ratio or transmissibility. The damping capacity reported at a lab scale is then determined adopting the half power bandwidth method as determined in Section 2.5.1. The energy dissipation mechanisms in RSm are been evaluated in this study at different levels:

- Particle scale (Chapter 4); using x-ray tomographic images, the particle-to-particle interaction within RSm and its effect on the energy dissipation under loading is discussed.
- Element scale (Chapter 5); the material damping of RSm is evaluated from small-to-large deformations via torsional resonant and cyclic triaxial apparatus.
- 1g scaled model (Chapter 6); a small-scale shaking table is employed to evaluate the energy dissipation mechanisms at a larger scale, with the inclusion of vertical soft zones.

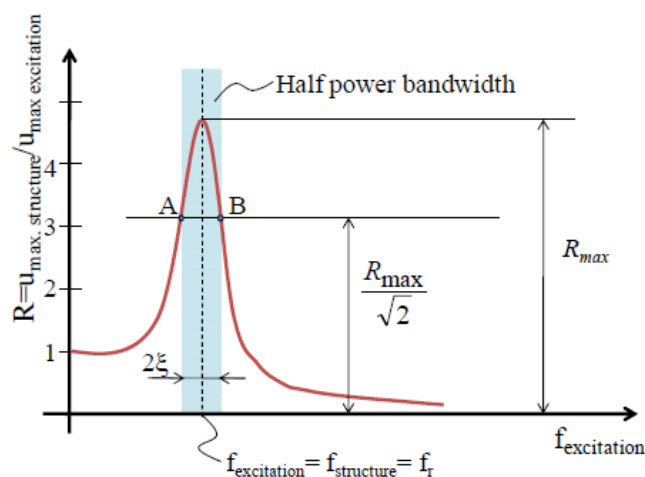


**Figure 2.13:** Structural response of a system to harmonic excitations (Chopra, 2011)

## 2.6 Summary

A review of the engineering and scientific basis required to aid the understanding of the thesis has been discussed:

- A variable-parameter-property scheme is introduced to explicitly define the distinction between system variables, test conditions, material (micro) properties, and bulk (macro), and thus interpret the behaviour of soils.
- The bulk parameters that characterise the behaviour of soils, interest of this study, are stress-dependent. A review of the stress-strain analysis of soils subject to the action of vertical, triaxial and torsional resonant is undertaken.
- The compressibility of soils is evaluated through the performance of one-dimensional vertical loading tests, using oedometer apparatus. The nature of one dimensional compression is studied through the determination of plastic strain, constrained modulus, compression and swelling indices.
- Soil response of soils under cyclic triaxial dynamic loading is covered by describing both stress and strain definitions of saturated specimens under undrained conditions. The cyclic behaviour is represented in the form of hysteretic loops and stress paths.
- The dynamic behaviour of soils is evaluated in the small-to-medium strain range by means of torsional resonant column tests. A fixed-free resonant column has been idealised for the determination of both maximum shear strain and shear modulus.
- Attenuation in transmission of body waves when moving through a soil is attributed to: (i) mechanical properties and (ii) geometrical characteristics of the medium. Material damping is represented by non-linear hysteretic and linear viscous damping, while geometrical damping accounts for both radiation damping and wave scattering.
- Cyclic performance of a small-scale model is examined through the application of sinusoidal harmonic motions via 1g shaking table tests. The amplification ratio is adopted to determine the maximum response of the system and thus calculate the energy dissipation mechanisms at a larger scale.

## *Literature review*

---

### **3.1 Introduction**

Since the early 90's, there has been a growing interest in using recycled tires as geomaterial combined with soil in civil engineering applications. This is due to its mechanical properties including low unit weight, very high resilience and durability, in addition to its hydraulic conductivity. This chapter reviews the work done on the soil mechanics of RSm under both static (monotonic) and dynamic loading on which the current understanding of this thesis rests.

Traditional base isolation systems have successfully mitigated earthquake building damage but their use has been limited to developed regions due to sophisticated design. Based on the concept of soft zone, RSm have emerged as a potential geotechnical seismic isolation system to be used as part of the soil foundation. However, the influence of particle properties and test conditions on the dynamic behaviour of RSm is not well understood. RSm behaviour is reviewed in this chapter from a micro to a macro scale.

### **3.2 Mechanics of RSm**

In accordance with the variable-parameter-property scheme established in Section 2.2 (Chapter 2), the bulk parameters of soils can be influenced by the macro-structure of the soil, characterised by their bulk properties, i.e. volume, mass or density, and respectively, by their particle properties. The latter would account for the micro-structure of the soil,

considered in this study as the particulate scale level, which includes properties such as coefficient of friction, fabric and particle stiffness. The complexity of understanding the response of RSm under loading stems from adding "soft" particulate rubber. This implies the study of additional particle properties such as rubber mass, size, shape, or stiffness and its interaction with stiffer sand particles. The binary skeleton of RSm can then be studied as a combination of rigid-soft particles which interact at a microscopic level and may influence the macroscopic behaviour depending on aspects such as the rubber amount or size ratio between sand/rubber (Kim and Santamarina, 2008).

A broad view of how RSm behaves in comparison with a conventional (incompressible) soil points unambiguously to an increase in compressibility (Lee et al., 2007). With regards to the strength, the picture is less clear: considering only the static case, shearing resistance may increase or decrease due to the addition of rubber depending on the particle properties including particle size, shape, amount and mean stress (Sheikh et al., 2012). The existence of such a vast number of factors leads to a scenario where the evaluation of both static and dynamic behaviour becomes a real challenge. A review of the influence of bulk (macro) and particle (micro) properties on the compressibility and shear strength of RSm is discussed in Section 3.3.

The test conditions to consider, i.e. frequency and number of cycles, added to the non-linearity commonly found in the evaluation of the bulk parameters that characterise the dynamic behaviour of soils complicate their evaluation (Mashiri, 2014). A review of the studies focused on the degree of influence of particle properties and test conditions on the dynamic behaviour of RSm is undertaken in Section 3.4.

At a larger scale, some investigations have proposed the use of "soft" zones, consisting of materials with low stiffness and density, which in contact with geological sediments can attenuate the transmission of body waves through the medium and thus minimise the earthquake building damage (Nappa, 2014). Section 3.5 reviews the literature on the used of geotechnical seismic isolation systems, including the use of RSm, and the influence of macro and micro particle properties on its effectiveness.



### 3.3 Response of RSm under static loading

Static behaviour of RSm has been widely studied by introducing recycled scrap tires as lightweight material in the form of either tyre derived aggregates (TDA), i.e. tire shreds and rubber chips, or particulate rubber, i.e. granulated/ground rubber and rubber fibres. Table 3.1 summarises the current knowledge on the material response of RSm under the action of static (monotonic) loading regimes. Studies are herein reviewed in accordance with aspects including: apparatus or test conducted, rubber content (RC) as gravimetric ( $\chi$ ) or volumetric ( $V$ ) proportion, type and size of sand ( $D_{50s}$ ) and rubber ( $D_{50r}$ ), size ratio between deformable and rigid particles ( $S_R = D_{50r}/D_{50s}$ ), mean stress level ( $\sigma_m$ ), in addition to the main remarks.

Amongst the characteristics that define the static behaviour of RSm, shear strength has been discussed in greater depth based on the experimental results gathered from the existing research (Figures 3.1a-3.3b). A review of the change in the vertical strain of RSm under monotonic loading, i.e. compressibility, has been undertaken. A distinction has been proposed in this thesis between mixtures containing various rubber shapes as a means of classifying the studies dedicated to the static behaviour of RSm, as visualised in Table 3.2 in accordance with ASTM D6270 (2017):

- Tyre derived aggregates are characterised by a basic geometrical shape commonly observed in a rectangular form. Two types of particles can be found within this group. Firstly, tyre shreds, which are found in its crudest form by maintaining the metallic parts and with irregular sizes of between 50 mm and 305 mm. Secondly, rubber chips, which have a smaller size (12-50 mm) and do not contain metallic elements.

- Scrap tyre-sand mixtures have also been tested in the form of small rounded tyre crumbs and, alternatively, elongated rubber fibres obtained from the devulcanisation and shredding after removing the steel belt. Thus, a higher variety in the rubber shape and size was available to investigate when mixed with soil materials. That said, due to the addition of smaller rubber particles, the main characteristic of these mixtures is that they present a lower size compared to TDA.

**Table 3.1:** Studies on response of RSm under static loading

Reference	Apparatus	RC	$D_{50sand}$ (mm)	$D_{50rubber}$ (mm)	SR	$\sigma_m$ (kPa)	Remarks
Edil and Bosscher (1994)	SB	$\chi = 0-25$	WG	TSh; 50-75	NS	0-690	-Shear strength increased for $\chi > 10$
Foose et al. (1996)	SB	$\chi = 0-16$	Uniform 0.58	TSh; 50-150	>20	0-690	-Shear strength raised with $\chi$ and RD
Masad et al. (1996)	T	$\chi = 0, 30, 100$	Uniform 0.23	GR; 3.2	10	150-350	-RD = 90%, Peak strength reduced and $\sigma_v$ became more compressive with $\chi$
Tatlisoiz et al. (1998)	SB	$\chi = 0, 10, 20, 30, 100$	PG 0.85	TCh; 30-110	>20	0-150	-Significant increase in friction angle with rubber content
Wu et al. (2002)	T	$\chi = 100$	-	Various shapes	-	34.5-55.5	-Increase in friction angle found with elongated rubber shapes
Youwai and Bergado (2003)	T	$\chi = 0-100$	PG 0.5	GR; 7 and ShR; 13.7	15-30	50-200	-Peak strength decreased with GR but increased with ShR. Higher compressibility found with ShR
Zornberg et al. (2004)	T	$\chi = 0-100$	Uniform 0.4	TCh; Length = 12.7-25.4, AR = 1-8	NS	50-200	-Optimum peak strength at $\chi = 35\%$ and increased with AR. RD does not have a significant effect on strength
Ghazavi (2004)	SB	$\chi = 0-100$	Uniform 0.62	GR; 3.38	5	23.3-102	-Optimum friction angle reached adding $\chi = 10-20\%$ . Shear strength was not affected with the addition of rubber
Ghazavi and Sakhi (2005)	SB	V = 15-50	Uniform 1.4	TCh; Width = 20-40, AR = 1-7	NS	9.8-100	-Improvement in friction angle and shear strength with addition of tyre shreds. Optimum increased adding $\chi = 50\%$ and tyre shape 40 x 80 mm
Attom (2006)	SB	$\chi = 0-40$	WG 0.8-2	TSh	NS	50-150	Improvement in shear strength with addition of rubber content
Rao and Dutta (2006)	Oed, T	$\chi = 0-100$	Uniform 0.42	TCh; 10x10, 20x20, 20x10	>20	34.5-276	-No significant difference was found in compressibility behaviour with rubber shape. TCh led to a marginal increase in friction angle and shear strength of mixture

**Table 3.1:** Studies on response of RSm under static loading





Reference	Apparatus	RC	$D_{50sand}$ (mm)	$D_{50rubber}$ (mm)	SR	$\sigma_m$ (kPa)	Remarks
Lee et al. (2007)	BE, Oed	V = 0-100	1	GR; 0.25	0.25	0-550	-Peak strength reduced with $\chi$
Kim and Santamarina (2008)	BE, Oed	V = 0-100	0.35	TCh; 3.5	10	0-1100	-Peak strength increased until $\chi = 20\%$ and decreased at higher contents -Large hysteresis loops for load-unload cycles adding rubber. Larger residual strains in simulation than oedometer tests
Valdes and Evans (2008)	Oed	$\chi = 40, 100$	Uniform 0.73	GR; 1.3	2	0-170	-Compressibility increased and G decreased with $\chi$ and rubber size. Transition from SLB to RLB at $\chi = 23\%$
Lee et al. (2010)	BE, Oed	V = 0-100	0.725	GR; 0.25-3.3	0.35-4.7	0-1000	-Peak strength increased with AR and optimum value at $\chi = 20\%$ , then it decreased at higher $\chi$
Edinçliler et al. (2010)	SB	$\chi = 0-100$	Uniform 0.73	GR; 1 and ShR; Length = 3, AR = 1-7	2	NS	-Shear strength decreased with GR. Reduction in strength was minimised using large rubber particles. Plastic deformation was reduced by pre-loading the material
Sheikh et al. (2012)	Oed, T	V = 0-40	PG 0.34	GR = 1.39-2.2	4-6	0-745	-Bearing capacity increased with $\chi$ and thickness of RSm layer. Optimum value in the bearing capacity found at $\chi = 5\%$ . Optimum installation depth at 0.25 times width of the footing and thickness around 0.5 times
Moghaddas and Norouzi (2012)	BLF	$\chi = 0-7.5$	WG 1.65	TCh; 10-50 AR = 3-5	>10	0-500	-Elastic behaviour increased with $\chi$ and transition from SLB to RLB occurred at $\chi = 20\%$
Lee et al. (2014)	Oed, T, BE	$\chi = 0-100$	Uniform 0.73	GR; 0.73	1	0-640	-Shear strength increased and friction angle stayed constant with elongated TCh. Optimum mixing ratio at $\chi = 25\%$
Balunaini et al. (2014)	SB	$\chi = 0-35$	PG 0.5	TCh; L = 76, AR = 1.6 and GR; 9	>20	0-166	

**Table 3.1:** Studies on response of RSm under static loading

Reference	Apparatus	RC	$D_{50sand}$ (mm)	$D_{50rubber}$ (mm)	SR	$\sigma_m$ (kPa)	Remarks
Fu et al. (2014); Fu et al. (2017)	Oed	$\chi = 0-30$	0.8	GR; 0.8 and RF; 10.5	1-10	0-7000	-Soil strength increased with ShR adding $\chi = 30\%$ whereas no effect was found at $\chi = 10\%$ or with GR. The type of rubber influences significantly the stress-strain behaviour of the mixture and only small effects were observed on the compression behaviour
Mashiri et al. (2015b); Mashiri et al. (2015a)	T	$\chi = 0-40$	PG 0.35	TCh; Length = 6, AR = 2.8	20	25-125	-Improvement in shear strength and reduction in dilatancy occurs in the transition SLB to RLB. Optimum shear strength with $\chi = 35\%$ . Initial tangent modulus increased with RD and $\sigma_m$

Note: WG = Well graded; PG = Poorly graded; U = Uniform; L = Length; W = Width;  $\chi$  = Gravimetric proportion;  $V$  = volumetric proportion;  $\sigma_m$  = Confining Pressure;  $\chi$  = Rubber content; RD = Relative density; AR = Aspect ratio; GR = Granulated rubber; TSh = tyre shreds; ShR = Shredded rubber; TCh = Tyre chips; SLB = sand-like behaviour; RLB = Rubber-like behaviour; BE = Bender Element; BLF = Bed Loading Frame; Oed = Oedometer test; T = Triaxial test; SB = Shear Box test; NS = Not specified

**Table 3.2:** Classification of scrap tyres in civil engineering projects according to ASTM D6270 (2017)

Based on ASTM 6270	Terminology	Description	Dimension	Image
Tyre derived aggregate (TDA): pieces of scrap tyres which have a rectangular shape and are generally between 12 and 305 mm	Tyre Shred	Rectangular shape	50 - 305 mm	
	Tyre chip	Rectangular shape and most of the wire removed	12 - 50 mm	
Particulate rubber; raw, uncured, compounded or vulcanised rubber transformed through a mechanical size reduction process into a collection of particles	Granulated rubber	Composed of non-spherical particles that span a broad range of maximum particle dimensions	425 $\mu$ m - 12 mm	
	Ground rubber	Composed of mainly spherical particles that span a broad range of maximum particle dimensions	425 $\mu$ m - 2 mm	
	Buffing rubber	Vulcanised rubber usually obtained from used tyre in the process of removing old tread during retreading	Variable	
	Chopped tyre	Crap tyres cut into relatively large pieces	Variable	
Rubber fibres	Small particles of ground rubber that results from producing shredded rubber particles	Variable		

### 3.3.1 Shear strength

A review of the existing research on shear strength of RSm is presented in Table 3.3. [Humphrey et al. \(1993\)](#), [Edil and Bosscher \(1994\)](#) and [Foose et al. \(1996\)](#) were the first studies to focus on the material response of RSm when subject to monotonic loading. The common feature of all these investigations was combining large tire shreds with small sand particles, i.e.  $D_{50R}/D_{50S} \gg 1$ . These studies evaluated RSm shear strength by using a large shear box apparatus. Tyre shreds with irregular shape, characterised by an aspect ratio ( $A_R$ ) of between 2 and 4, were tested with two different distributions; vertical and random orientation. [Edil and Bosscher \(1994\)](#) performed a series of shear tests using 305 mm diameter shear rings by means of displacing the sample horizontally up to 15 mm. They demonstrated that when the tire shreds are randomly allocated, these can reinforce to a greater degree than the sand specimens at its densest state. On the other hand, [Foose et al. \(1996\)](#) studied the evolution in shear strength of RSm by testing the mixture at three unit weights (14.7, 15.5, 16.8  $kN/m^3$ ) and increasing the mean stress level up to 100 kPa. The study highlighted the improvement in shear strength due to three different factors: addition of up to  $\chi = 30\%$  (Figure 3.1a), application of higher stress levels and increase in unit weight, i.e. denser state. This improvement was attributed to the reinforcing effect due to the length of rubber particles and the way of transmitting loads through the inter-particle contacts.

[Zornberg et al. \(2004\)](#), [Ghazavi and Sakhi \(2005\)](#), and [Mashiri et al. \(2015b\)](#) conducted a series of experiments from oedometer to triaxial tests to evaluate the static behaviour of rubber chips-sand mixtures. Compared to previous investigations, these rubber chips had a smaller size than tire shreds, yet their size ratio was greater than 1 when combined with sand particles. [Zornberg et al. \(2004\)](#) is still today considered one of the most relevant investigations into the static behaviour of RSm. They recognised that RSm of about  $\chi = 20\%$  may not reach a peak within the allowable strain range of a typical triaxial rig. In this case, they chose to report shear resistance values at 15% axial strain. This complicates the comparison of strength parameters obtained from different test programmes since at high aspect ratio, the RSm continues to mobilise shearing

resistance at 15% axial strain.

Zornberg et al. (2004) studied volumetric, stress-strain behaviour and evolution in strength of RSm. Large-scale triaxial tests were performed dry in a 153 mm diameter by 305 mm height specimen, at four mean stress values ranging between 48.7 kPa and 207 kPa. Rubber chips with nominal widths between 12.7 mm and 25.4 mm and aspect ratios from 1 to 8 were prepared. Mixtures of up to  $\chi = 100\%$  were sheared, testing the sample to 20% axial strain. The results showed that the stress-strain and the volumetric strain behaviour of the mixture are highly influenced by the rubber content. On one hand, mixtures with  $\chi < 35\%$  exhibited an initial reduction in the volumetric strain, i.e. contractive behaviour, which resulted in an increase of the specimen volumetric strain, i.e. dilative behaviour, after 2.5% axial strain. At higher rubber contents  $\chi > 35\%$ , a fully contractive behaviour was found as a consequence of the gradual reduction in the specimen volumetric strain. This was argued to be due to the significant capacity of rubber to deform under shearing loading, more prominent with the application of higher mean stress values. The mixture appeared to be, however, less dependent on the relative density of the matrix. In terms of shearing resistance, the friction angle increased with both the rubber content and the aspect ratio, more evident at contents around  $\chi = 35\%$  and  $A_R = 4-8$ . Although these observations were also found at high stresses, this phenomenon was more pronounced at low confining pressures.

To elucidate the effect of the rubber content on the shear strength of RSm, Figure 3.1 shows the evolution in both the friction angle and the maximum deviator stress. These graphs depict the experimental results gathered from previous studies, presented in Table 3.3. In line with other investigations, Rao and Dutta (2006) and Mashiri et al. (2015a) reported an increase in  $\phi$  with rubber chips characterised by an  $A_R = 2$ . For the cases of Ghazavi and Sakhi (2005) and Attom (2006), large shear box tests were conducted on 40 mm x 80 mm tyre chips and tire shreds to evaluate the change in the initial friction angle, resulting in an optimum value in the range  $\chi = 30-50\%$ . As established by Zornberg et al. (2004), the material properties, including rubber content and size ratio, may lead to an improvement of the material shear strength. The aspect ratio arises to be another material property that controls the evolution in soil strength.

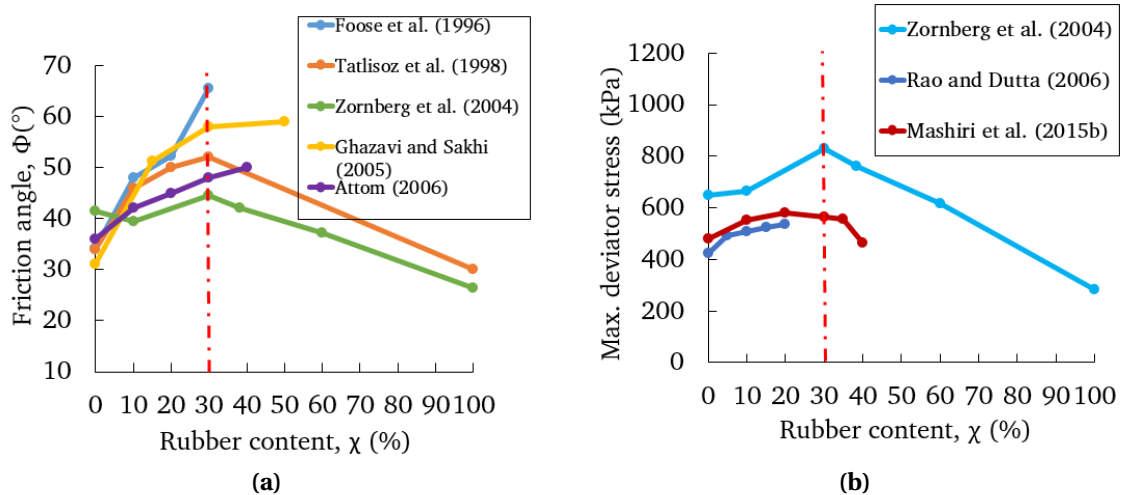


**Figure 3.1:** Studies on a) calculation of friction angle and b) maximum deviator stress by adding tyre derived aggregates

Another group of studies (Masad et al., 1996; Youwai and Bergado, 2003; Sheikh et al., 2012) evaluated stress-strain and volumetric strain behaviour of RSm comprising granulated/ground rubber with relatively similar mean particle sizes, i.e.  $S_R = 1$ .

Youwai and Bergado (2003) was one of the first studies focused on studying the stress-strain behaviour of tyre crumbs-sand mixtures. Eighteen confined drained triaxial tests were performed on a standard 100 x 200 mm triaxial cell. Tyre crumbs were characterised by  $A_R = 1$  and  $D_{50} = 7$  mm. The samples were confined at three different pressures (50 kPa, 100 kPa, and 200 kPa). In line with the results presented by Masad et al. (1996), the application of higher confining pressures resulted in greater deviator stresses at any rubber content. A distinction was observed between low rubber, i.e.  $\chi < 20\%$ , and high rubber contents, i.e.  $\chi > 20\%$ , in relation to the stress-strain behaviour. Whilst sand-like soils reached the peak deviator stress at relatively small axial strains, rubber-like soils reached the peak stress at large strains, similar to the behaviour observed in loose sands. With regards to the volumetric strain behaviour, the sample passed from a fully dilatant behaviour without rubber to a fully contractive behaviour with only tyre crumbs. Unlike the improvement in the shear strength observed when adding TDA (Figure 3.1), Youwai and Bergado (2003) concluded that the shear strength decreases with tyre crumbs.

Sheikh et al. (2012) studied the effect of rubber content, confining pressure and size ratio on the static behaviour of rubber crumbs combined with sand particles. Triaxial



tests in dry conditions were conducted on samples prepared at a constant void ratio ( $e=0.655$ ) at four different rubber percentages ( $\chi = 10, 20, 30, 40\%$ ). The mixtures were prepared at confining pressures ranging between 17 and 483 kPa. The study confirmed the reduction in the peak deviator stress when adding greater rubber contents. The drop in shear strength was, however, minimised when adding bigger rubber crumbs, leading to a higher size ratio ( $S_R = 7$ ), on the basis that there was a higher number of contacts between smaller sand particles.

Within the group of studies that investigated particulate rubber, [Edinçliler et al. \(2010\)](#), [Fu et al. \(2014\)](#) and [Fu et al. \(2017\)](#) compared the use of different rubber shape by introducing tyre crumbs and small elongated rubber fibres. [Edinçliler et al. \(2010\)](#) demonstrated that an increase in the aspect ratio of rubber fibres enhances the shear strength by adding  $\chi = 20\%$ . [Fu et al. \(2017\)](#) showed how tyre crumbs do not contribute to the rise in the peak shear strength and only 30% of rubber fibres can lead to higher values, which was attributed to the reinforcing effect of elongated particles. The development in shear strength when adding particulate rubber, i.e. crumbs or fibres, has been represented in Figure 3.2 based on experimental results gathered from existing research. It can be observed that both friction angle and maximum deviator stress remain nearly similar or decrease when adding small rubber crumbs. According to [Sheikh et al. \(2012\)](#) and [Fu et al. \(2017\)](#), this can be minimised when altering rubber size, either by increasing length, i.e. aspect ratio, or with bigger rubber particles.

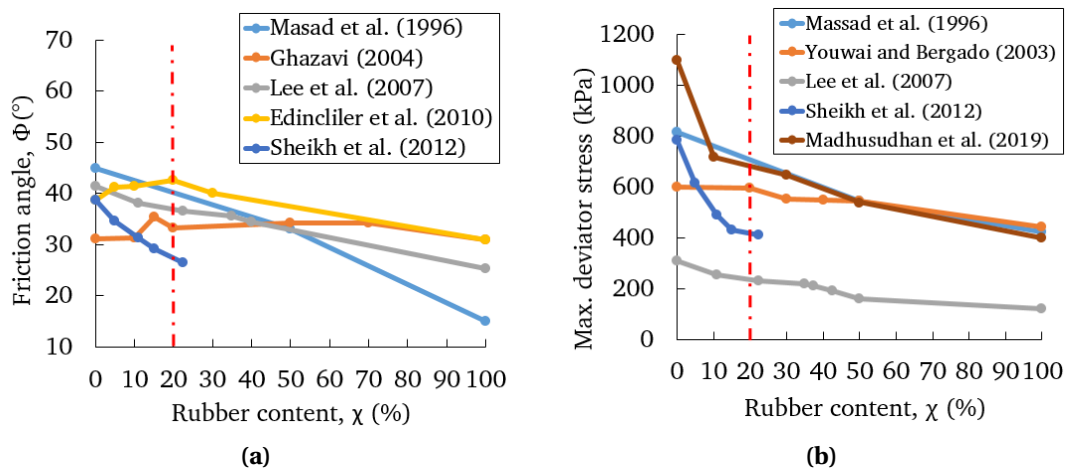


**Figure 3.2:** Studies on a) calculation of friction angle and b) maximum deviator stress by adding particulate rubber

**Table 3.3: Studies on shear strength of RSm**

Reference	Material	RC; $\chi$	Shear strength parameters
Humphrey et al. (1993)	TSh	100	$c = 4.3-11.5$ kPa, $\phi = 19-26^\circ$
Edil and Bosscher (1994)	WG Sand:TSh	0	$\tau = 13.2-54.3$ kPa, $\sigma = 20-80$ kPa
		5	$\tau = 24.3-80$ kPa, $\sigma = 20-80$ kPa
		10	$\tau = 30.1-114$ kPa, $\sigma = 20-100$ kPa
		0	$\phi = 24.8-34.1^\circ$
Foosse et al. (1996)	WG sand:TSh	10	$\phi = 32.6-48^\circ$
		20	$\phi = 38.7-52.3^\circ$
		30	$\phi = 42.7-65.6^\circ$
Masad et al. (1996)	WG sand:GR	0	$c = 0$ kPa, $\phi = 45^\circ$ ; $q_{max}(\sigma_3) = 530(150), 814(200), 992(250), 1120(300), 1389(350)$ kPa
		50	$c = 26$ kPa, $\phi = 33^\circ$ ; $q_{max}(\sigma_3) = 417(150), 545(200), 690(250), 765(300), 894(350)$ kPa
		100	$c = 70-82$ kPa, $\phi = 6-15^\circ$ ; $q_{max}(\sigma_3) = 386(150), 423(200), 452(250), 476(300), 488(350)$ kPa
		0	$c = 2$ kPa, $\phi = 34^\circ$
Tatlisoz et al. (1998)	WG sand:TCh	10	$c = 2$ kPa, $\phi = 46^\circ$
		20	$c = 2$ kPa, $\phi = 50^\circ$
		30	$c = 2$ kPa, $\phi = 52^\circ$
		100	$c = 0$ kPa, $\phi = 30^\circ$
Wu et al. (2002)	TCh-Flat		$c = 0$ kPa, $\phi = 57^\circ$
	TCh-Granular	100	$c = 0$ kPa, $\phi = 54^\circ$
	TCh-Elongated		$c = 0$ kPa, $\phi = 60^\circ$
	TCh-Powder		$c = 0$ kPa, $\phi = 45^\circ$
Youwai and Bergado (2003)	PG sand:ShR	0	$\tau = 428-800$ kPa, $\sigma = 100-200$ kPa; $q_{max}(\sigma_3) = 205(50), 320(100), 598(200)$ kPa
		20	$\tau = 493-793$ kPa, $\sigma = 100-200$ kPa; $q_{max}(\sigma_3) = 191(50), 340(100), 593(200)$ kPa
		30	$\tau = 393-753$ kPa, $\sigma = 100-200$ kPa; $q_{max}(\sigma_3) = 173(50), 333(100), 550(200)$ kPa
		40	$\tau = 374-748$ kPa, $\sigma = 100-200$ kPa; $q_{max}(\sigma_3) = 172(50), 272(100), 549(200)$ kPa
		50	$\tau = 414-743$ kPa, $\sigma = 100-200$ kPa; $q_{max}(\sigma_3) = 135(50), 315(100), 544(200)$ kPa
100	$\tau = 342-650$ kPa, $\sigma = 100-200$ ; $q_{max}(\sigma_3) = 138(50), 240(100), 440(200)$ kPa kPa		

Note: WG = Well graded; PG = Poorly graded;  $\chi$  = Rubber content; GR = Granulated rubber; TSh = tyre shreds; ShR = Shredded rubber; TCh = Tyre chips;  $c$  = cohesion;  $\phi$  = friction angle;  $\tau$  = shear stress;  $\sigma$  = normal stress;  $q_{max}$  = max. deviator stress

**Table 3.3:** Studies on shear strength of RSm

Reference	Material	$\chi$ (%)	Shear strength parameters
Zornberg et al. (2004)	WG sand:TCh	0	$c = 3.8-7.8$ kPa, $\phi = 37.9-41.4^\circ$ ; $q_{max}(\sigma_3) = 180(48.3), 336(103.5), 650(207)$ kPa
		10	$c = 19.8-21.7$ kPa, $\phi = 38.9-39.4^\circ$ ; $q_{max}(\sigma_3) = 220(48.3), 375(103.5), 665(207)$ kPa
		30	$c = 23.7-60$ kPa, $\phi = 38.7-44.5^\circ$ ; $q_{max}(\sigma_3) = 401(48.3), 596(103.5), 828(207)$ kPa
		38.3	$c = 41.2$ kPa, $\phi = 42^\circ$ ; $q_{max}(\sigma_3) = 330(48.3), 460(103.5), 760(207)$ kPa
		60	$c = 18.2$ kPa, $\phi = 37.3^\circ$ ; $q_{max}(\sigma_3) = 183(48.3), 350(103.5), 616(207)$ kPa
		100	$c = 22.8$ kPa, $\phi = 26.5^\circ$ ; $q_{max}(\sigma_3) = 94(48.3), 200(103.5), 284(207)$ kPa
		0	$\phi = 31.2-36.8^\circ$
		10	$\phi = 31.4-37.6^\circ$
		15	$\phi = 35.4-38^\circ$
		20	$\phi = 33.3-34.2^\circ$
Ghazavi (2004)	WG sand:GR	50	$\phi = 34.3-35^\circ$
		70	$\phi = 34.3^\circ$
		100	$\phi = 31^\circ$
		0	$\phi = 31.1-40^\circ$
		15	$\phi = 51.3-55.8^\circ$
		30	$\phi = 58-62^\circ$
Ghazavi and Sakhi (2005)	WG sand:TCh	50	$\phi = 59-64.5^\circ$
		0	$c = 0$ kPa, $\phi = 38^\circ$ ; $q_{max}(\sigma_3) = 424(138)$ kPa
		5	$c = 6.6-15.2$ $\phi = 39.2-39.6^\circ$ ; $q_{max}(\sigma_3) = 490(138)$ kPa
		10	$c = 9.1-15.9$ kPa, $\phi = 39.5-39.7^\circ$ ; $q_{max}(\sigma_3) = 507(138)$
		15	$c = 15.1-17.6$ $\phi = 39.7-39.9^\circ$ ; $q_{max}(\sigma_3) = 523(138)$ kPa
		20	$c = 13.3-18.4, \phi = 39.9-40.1^\circ$ ; $q_{max}(\sigma_3) = 535(138)$
Rao and Dutta (2006)	WG sand:TCh	0	$\phi = 41.5^\circ$ ; $q_{max}(\sigma_3) = 310(80)$ kPa
		20	$\phi = 38.2^\circ$ ; $q_{max}(\sigma_3) = 252(80)$ kPa
		40	$\phi = 36.5^\circ$ ; $q_{max}(\sigma_3) = 232(80)$ kPa
		60	$\phi = 35.7^\circ$ ; $q_{max}(\sigma_3) = 220(80)$ kPa
		70	$\phi = 34.4^\circ$ ; $q_{max}(\sigma_3) = 209(80)$ kPa
		100	$\phi = 25.3^\circ$ ; $q_{max}(\sigma_3) = 120(80)$ kPa
Lee et al. (2007)	WG sand:GR	40	$\phi = 36.5^\circ$ ; $q_{max}(\sigma_3) = 232(80)$ kPa
		60	$\phi = 35.7^\circ$ ; $q_{max}(\sigma_3) = 220(80)$ kPa

**Table 3.3:** Studies on shear strength of RSm

Reference	Material	$\chi$ (%)	Shear strength parameters
		0	$c = 0$ kPa, $\phi = 38.7^\circ$
		5	$c = 1.3$ kPa $\phi = 41.2^\circ$
		10	$c = 0.2$ kPa, $\phi = 41.4^\circ$
		20	$c = 1.1$ kPa, $\phi = 42.6^\circ$
		30	$c = 1.2$ kPa, $\phi = 40^\circ$
		100	$c = 4.6$ kPa, $\phi = 31^\circ$
		0	$\phi = 38.7-55^\circ$ ; $q_{max}(\sigma_3) = 144(17), 316(69), 783(207), 1610(483)$
		10	$\phi = 34.6-52.7^\circ$ ; $q_{max}(\sigma_3) = 124(17), 245(69), 613(207), 1270(483)$
		20	$\phi = 31.3-55.5^\circ$ ; $q_{max}(\sigma_3) = 94(17), 213(69), 490(207), 1050(483)$
		30	$\phi = 29.2-44.8^\circ$ ; $q_{max}(\sigma_3) = 84(17), 180(69), 429(207), 912(483)$
		40	$\phi = 26.5-43.2^\circ$ ; $q_{max}(\sigma_3) = 74(17), 166(69), 409(207), 780(483)$
		20	$\phi = 30^\circ$
		25	$\phi = 33^\circ$
		35	$\phi = 32^\circ$
		0	$\tau = 573$ kPa, $\sigma = 400$ kPa
		10	$\tau = 605$ kPa, $\sigma = 400$ kPa
		30	$\tau = 671$ kPa, $\sigma = 400$ kPa
		0	$q_{max}(\sigma_3) = 170(23), 210(46), 286(69), 480(138)$
		10	$q_{max}(\sigma_3) = 550(138)$
		20	$q_{max}(\sigma_3) = 582(138)$
		30	$q_{max}(\sigma_3) = 565(138)$
		35	$q_{max}(\sigma_3) = 173(23), 245(46), 340(69), 557(138)$
		40	$q_{max}(\sigma_3) = 462(138)$
Edinciler et al. (2010)	WG sand:GR		
Sheikh et al. (2012)	PG sand:GR		
Balunaini et al. (2014)	PG sand:TCh		
Fu et al. (2014)	WG sand:ShR		
Mashiri et al. (2015b)	PG sand:TCh		

### 3.3.2 Compressibility

The study of the evolution in the vertical deformation of RSm under monotonic loading regimes was initially investigated by [Humphrey et al. \(1993\)](#) and [Edil and Bosscher \(1994\)](#). Compression tests were performed in a 6' Proctor mold applying vertical pressures of up to 690 kPa. At the highest vertical stress, [Edil and Bosscher \(1994\)](#) showed a reduction in the initial height of above 35% at high rubber contents ( $\chi > 30\%$ ). They also revealed, through the application of loading-unloading-reloading cycles, that mixtures containing TDA experience an important plastic deformation at rubber contents greater than 10%. They concluded that the high compressible behaviour of tyre chips is attributed to two different mechanisms; the bending and the re-orientation of rubber into a more compact state.

[Rao and Dutta \(2006\)](#) studied the change in vertical strain of RSm containing tyre chips by means of oedometer tests. Tests were conducted in a 15.2 cm x 17.8 cm rigid mould and the samples were prepared at rubber contents ranging at  $\chi = 0 - 100\%$ , considering three different types of rubber chips (Type I; 10 mm x 10 mm, Type II; 20 mm x 20 mm, Type III; 20 mm x 10 mm). Twenty-eight compressibility tests were performed at vertical stresses up to 1300 kPa. The results corresponding to the rubber type I are depicted in [Figure 3.3a](#). Vertical strain is clearly related to rubber content where the addition of rubber leads to a more compressible behaviour. This was also attributed to the higher number of contacts between deformable rubber particles when increasing the rubber content. [Rao and Dutta \(2006\)](#) also demonstrated that the change in the vertical strain is less prominent when increasing the aspect ratio of rubber chips.

Various investigations ([Lee et al., 2007](#); [Kim and Santamarina, 2008](#); [Lee et al., 2010](#); [Fu et al., 2017](#)) have also investigated the one-dimensional compression of RSm containing particulate rubber. [Figure 3.3b](#) shows the results presented by [Lee et al. \(2010\)](#) to compare the influence of rubber content and size ratio by testing two configurations  $S_R = 0.5, 4.8$ . As occurred with the use of bigger rubber particles, i.e. TDA, rubber amount has a significant effect on the compressibility during the loading stage. A larger vertical deformation was also found in specimens containing smaller rubber particles, which

was suggested to be a result of the greater number of contacts between deformable (rubber) particles. This was more evident at  $\chi > 20\%$ , as observed with the decay in strength parameters depicted in Figures 3.2a-3.2b. Interestingly, the effect of the rubber size on the compressive behaviour of RSm can also be elucidated when comparing the evolution in the vertical strain of mixtures containing TDA ( $S_R > 20$ ), which goes up to 23% in vertical strain, and particulate rubber ( $S_R = 0.5$ ), with a reduction of up to 40% of the initial height at similar vertical stress (400 kPa).

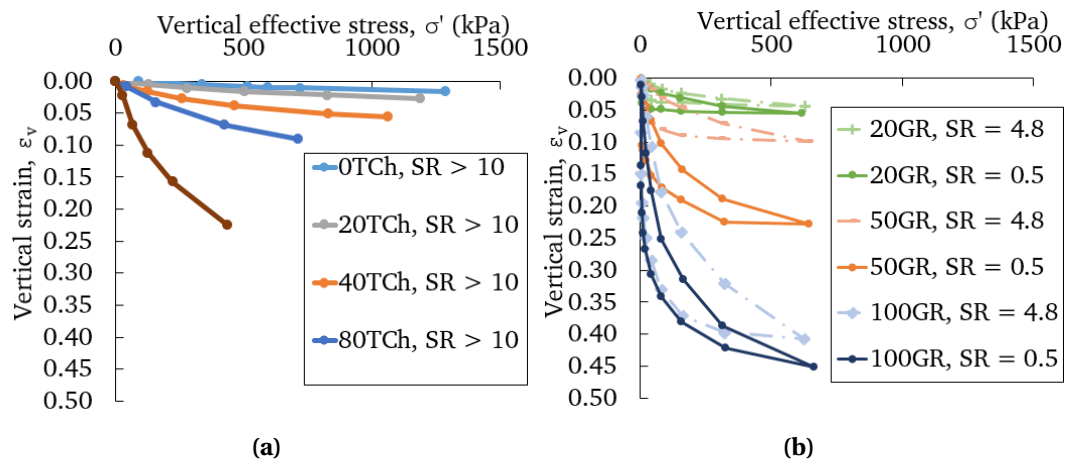


**Figure 3.3:** Vertical strain versus vertical stress by adding a) tyre chips (Rao and Dutta, 2006) and b) particulate rubber (Lee et al., 2010)

### 3.3.3 Micro-mechanics of RSm

The interaction at a particulate scale has been studied between rubber-sand particles at different sizes and contents and its effect on the packing and skeleton.

Lee et al. (2007) was the first study that tried to explain the macroscale small-to-large strain deformation behaviour based on the deformation moduli due to particle-level mechanisms. For that, RSm with granulated rubber particles ( $D_{50R} = 0.09$  mm) and characterised by a  $S_R = 0.25$  were subjected to oedometric tests. The change in vertical strain was monitored whilst applying loading-unloading cycles with a vertical stress moving up from 10 kPa to 556 kPa. The results revealed a change in the compressibility response of the mixture depending on particle properties and test conditions, i.e. rubber content and stress amplitude. The concepts of sand-like behaviour, characterised for

presenting higher small-to-large stiffness, and rubber-like behaviour, defined as a mixture that presents lower shear moduli and deforms more easily under loading, were established to explain the evolution in the macro-scale parameters of RSm. The study postulated that load carrying chains were created along the stiff sand skeleton, whilst the addition of rubber resulted in a reduction of the peak strength. Although the soft rubber particles played a secondary role in the load carrying, it prevented buckling effect, otherwise observed in sands.

Kim and Santamarina (2008) used large rubber chips mixed with sand ( $S_R = 10$ ) to investigate the effect of rubber content and size ratio on small-strain stiffness and the underlying mechanisms. Oedometric tests were conducted at mean stress values between 10 kPa and 1111 kPa with bender elements mounted on top of the oedometer cap and bottom. Sand-like behaviour arose at  $0 < \chi < 30\%$ , then a gradual transition was found with additional rubber until  $\chi = 60\%$ , at when rubber dominated. In contrast with Lee et al. (2007), no transition between sand-like and rubber-like behaviour was found at higher stresses. This was on the basis that rubber particles were highly deformed and behaved as a bulk material at this stage. Both shear wave velocity and constrained modulus increased with the rise in the applied vertical stress as a result of the higher number of contacts between particles. However, this was more predominant in sand-like soils, reaching a peak at  $\chi = 10\text{-}20\%$ , attributed to the friction between sand-to-sand particle contacts, more prominent with the deformation of particulate rubber.

Lee et al. (2010) studied the influence of a variable size ratio between rubber and sand particles ( $S_R = 0.35 - 4.7$ ) on the small and intermediate strain shear modulus by varying rubber content. Tests were performed dry in a 74 mm diameter, 63 mm high, oedometer cell with bender elements attached. The results showed that constrained modulus and small strain shear modulus decrease with the inclusion of rubber or decrease in sand fraction (sf) at any size ratio (Figure 3.4). This was explained on the basis that the mixture stiffness is controlled by load chains created along the sand skeleton. At  $\chi > 60\%$ , there was a predominant rubber-like behaviour, where the stiffness was controlled by the rubber skeleton, and the change in size ratio had no influence. At  $\chi < 60\%$ , load-carrying chains were created between sand particles, as a consequence

of the significant rubber deformation, and there was an increase in small strain shear modulus at size ratios higher and lower than unity. This rise in the soil stiffness was, however, more evident with big rubber particles ( $S_R \gg 1$ ) (Kim and Santamarina, 2008).

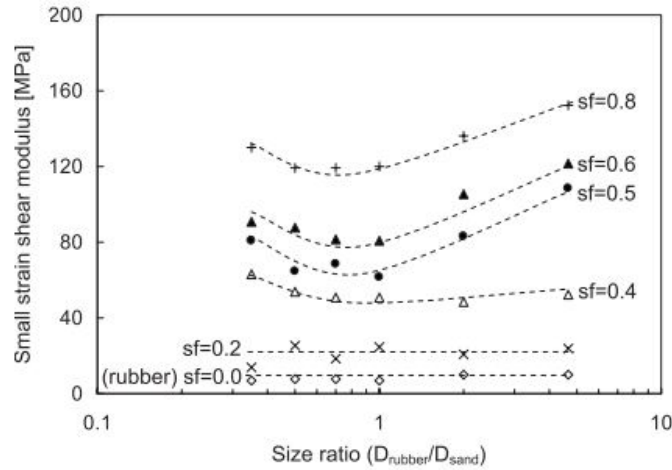


**Figure 3.4:** Small strain shear modulus with size ratio of RSm (Lee et al., 2010)

Platzer et al. (2018) presented a model to predict the evolution in the vertical compression of RSm. The size distributions of both rigid (Leighton Buzzard and Hostun RF sands) and deformable particles (granulated rubber) were similar and the rubber content studied ranged between  $\chi = 0 - 50\%$ . Although the study assumed that both sand and rubber particles are incompressible, it postulated that volumetric changes in RSm are a consequence of particle re-arrangement and rubber deformation, hence a fraction of the porous spaces are filled by the deformed rubber particles under isotropic loading. The model accurately predicted the evolution in void ratio and maximum deformed fraction of rubber undergone by RSm specimens. Some limitations were, however, found at  $\chi = 30\%$  due to not being able to simulate the transitional behaviour in which both the sand re-arrangement and rubber deformation were underestimated. Based on these studies, the interaction between rigid and deformable particles defines the fabric of the binary skeleton, i.e. RSm, and this influences the stiffness of the mixture. It can be stated that sand-like, rubber-like and transitional behaviour are influenced by the soil micro-structure, including rubber content, size, shape, size ratio, and test conditions defined by the stress level.



Although existing research has tried to explain the interaction between rubber and sand at a particulate level, these results are based on macroscopic experiments. No previous studies have assessed the effect of rubber shape on the one-dimensional compression behaviour of RSm from a qualitative or quantitative point of view. For this reason, a series of experiments on RSm have been conducted by means of plain strain models and more accurately with 3D x-ray tomographic experiments on mini-oedometer specimens and compared with macroscopic experiments through the conduction of oedometer tests. The results of these are presented and analysed in Chapter 4 in order to quantitatively evaluate the number of contacts at a particle scale.

### 3.4 Response of RSm under dynamic loading

The dynamic behaviour of soils is characterised by shear modulus ( $G$ ) and damping ratio ( $\xi$ ). As covered in the property-variable-parameter scheme (Sections 2.2, 3.2), the bulk parameters may be influenced by bulk properties, particle properties and test conditions as a function of either stress ( $\tau$ ) and strain ( $\gamma$ ) state variables. Compared to the bulk parameters that define the static (monotonic) behaviour of soils, additional test conditions need to be considered including frequency or cyclic number.

Dynamic bulk parameters of RSm have been typically represented as a function of the deformation undergone by the specimen. That said, two main groups can be found within the existing research; studies focused on small-to-medium deformations through bender element (BE) tests (Lee et al., 2010), and resonant column (RC) tests (Anastasiadis et al., 2012a; Senetakis et al., 2012a) and those focused on medium-to-large strains by means of cyclic triaxial (CT) tests (Nakhaei et al., 2012; Mashiri et al., 2017; Pistolas et al., 2018).

A review of existing literature on the dynamic behaviour of RSm is presented in Table 3.4. These studies have been chronologically ordered and classified by a series of features including: apparatus, rubber content (RC), specimen state, level of state variable (strain ( $\gamma$ ) or stress ( $\tau$ ) controlled),  $D_{50s}$  and  $D_{50r}$ ,  $S_R$ , relative density ( $D_r$ ), number of cycles (N), and mean stress ( $\sigma_m$ ).

The stiffness and damping strain curves are typical representations that show the alteration in the bulk parameters in relation to the deformation experienced by the specimen. Tracing accurately these curves is important to understand the degradation of the bulk parameters and thus, characterise the soil non-linear behaviour so that it can be adopted in numerical simulations. The review undertaken has been split into two groups: i) medium-to-large strains and ii) small-to-medium strains.

### 3.4.1 Dynamic properties at medium-to-large strains

The majority of the recorded seismic events are of a magnitude lower than seven (Kramer, 1996). That said, when an earthquake of this magnitude strikes the ground surface, this suffers from a deformation which may vary within the small-to-medium strain range (i.e.,  $\gamma = 0.0001-0.1\%$ ). Major past earthquakes ( $M > 7$ ) have reflected that the ground soil may be subjected to larger strain amplitudes ( $\gamma > 0.2\%$ ) for durations over ten seconds (Nazari et al., 2014; Towhata, 2014). Moreover, RSm have been proven to be more susceptible to suffer from greater deformations under the action of similar seismic events due to adding highly deformable rubber particles in the mixture. It is consequently important to evaluate the alteration of the dynamic bulk parameters and study the influence of material aspects and test conditions at these strain amplitudes.

Nakhaei et al. (2012) was the first investigation to determine the bulk parameters of fully saturated RSm specimens at medium-to-large strains. A river type granular soil ( $D_{50} = 4.85$  mm) and particulate granulated rubber of smaller size ( $D_{50} = 2$  mm), with  $S_R < 1$ , were used for the preparation of the specimens. The samples composed of eight layers using the undercompaction method whereby a high relative density was reached ( $D_r = 91\%$ ). Up to  $\chi = 14\%$  of granulated rubber was added to the soil and samples were subjected to various confining pressures  $\sigma_m = 50 - 300$  kPa. Forty cycles were applied to the specimens under stress controlled conditions by maintaining a test frequency of 1 Hz. The experimental results showed that stiffness degradation decreases with rubber content and confining pressure. This is also observed in Figures 3.5a, 3.6a and 3.7a where the value of  $\gamma_{ref}$ , which expresses the deformation level at which  $G/G_0 =$

0.5, increases representing a more linear soil behaviour. In terms of damping capacity, the study presented a distinction in the evolution of damping ratio depending on the stress level. At  $\sigma_m < 100$  kPa, damping ratio decreased with rubber content whereas the opposite trend was observed at  $\sigma_m > 100$  kPa.

Ehsani et al. (2015) tested the influence of size ratio on the dynamic behaviour of saturated RSm from small-to-large amplitudes. Firoozkooh sand ( $D_{s50} = 0.22$  mm) and two types of granulated rubber; fine ( $D_{r50} < 1$  mm) and coarse size ( $D_{r50} = 4.75$  mm), were used with a  $S_R = 2.13, 11.07$ . Specimens were subjected to forty cycles under stress controlled conditions by means of a multi-stage procedure until failure was reached. Mixtures were formed by adding rubber contents at  $V = 10 - 30\%$  and consolidated to a unique mean stress value,  $\sigma_m = 300$  kPa. The study established that although a clear reduction in soil stiffness occurs with rubber content, the inclusion of larger rubber particles ( $S_R$ ) results in a lower stiffness degradation when compared to mixtures comprising similar particles' size. On the other hand, although damping capacity increased with content at medium strain amplitudes, 10% RSm presented higher damping capacity values than 30% RSm at large strain amplitudes. The size ratio did not appear to have a significant effect on damping capacity at large deformations.

Li et al. (2016) conducted a similar investigation but a comparison was undertaken between mixtures in two configurations: similar rubber-sand particle size with  $S_R < 1$ . Fujian standard sand ( $D_{s50} = 0.80$  mm) and two sizes of granulated rubber ( $D_{r50} = 0.20, 0.80$  mm) were used. Thirty samples were prepared adding rubber up to  $V = 20\%$  and applying isotropic confinement pressures at  $\sigma_m = 50, 100, \text{ and } 200$  kPa. The experimental programme was performed via stress-controlled cyclic triaxial tests. In accordance with the results obtained by Ehsani et al. (2015), damping was not significantly influenced by size ratio at high stresses ( $\sigma_m > 200$  kPa). The opposite trend was found at lower confining pressures where damping capacity increased by introducing smaller rubber particles. Moreover, greater damping was observed in the medium strain range adding  $V = 10\%$ .

Pistolas et al. (2018) focused on the determination of soil stiffness and damping at medium-to-large strains. The samples contained river sand with rounded-to-

subrounded particles ( $D_{s50} = 0.40$  mm) and granulated rubber of two sizes ( $D_{r50} = 1.50, 3.40$  mm), with a size ratio  $S_R = 3.7 - 8.5$ . The specimens were fully saturated and prepared adding up to  $\chi = 60\%$  and applying isotropic pressures at  $\sigma_m = 25 - 200$  kPa. Twenty-two specimens were tested under undrained conditions applying strain-controlled cycles at  $\gamma = 0.05\%$  to  $2\%$ . In line with previous studies, [Pistolas et al. \(2018\)](#) confirmed that the rubber-like behaviour appears primarily by increasing rubber content and reducing  $D_{50r}/D_{50s}$ . This led to an increase in  $\gamma_{ref}$  and a more linear behaviour of both stiffness and damping strain curves. This study established that sand only specimens present greater damping than RSm at medium strains, whereas introducing 10-20% rubber results in higher damping at large strains ( $\gamma = 1\%$ ). This was explained on the basis that the limiting strain reference ( $\gamma_{lim}$ ), defined as the strain at which higher damping ratio arises, increases with the addition of rubber due to interlocking mechanisms between rigid-deformable particles. As shown in [Li et al. \(2016\)](#), this study found that size ratio has an effect on RSm damping. Thus, mixtures with a  $S_R < 1$  can have a damping ratio higher than sand only specimens at medium-to-large strains. However, this phenomenon is more evident in mixtures with  $\chi < 20\%$  and a  $S_R > 1$ , when there are more contacts between rigid particles.

A comparison has been undertaken between the studies to compare the damping ratio at different stress levels and rubber content (Figures 3.5b, 3.6b and 3.7b). It can be observed that despite the results presented by [Nakhaei et al. \(2012\)](#) showing an increment with the mean stress, in general, damping ratio decreases with confining pressure (Figure 3.6b). Moreover, at relatively similar stress level ( $\sigma_m = 100$  kPa), the addition of rubber ( $\chi > 10\%$ ) results in reduction of damping capacity (Figure 3.7b).

Unlike the review on the static behaviour of RSm, the studies dedicated to the dynamic behaviour of RSm have mainly focused on specimens consisting of rounded granular rubber. [Kaneko et al. \(2013\)](#), [Mashiri et al. \(2016\)](#) and [Mashiri et al. \(2017\)](#) with tyre chips, are the only investigations that have proposed the stiffness and damping characterisation curves by adding elongated rubber. The curves that characterise RSm dynamic behaviour have been included in the graphs presented in Figures 3.5, 3.6 and 3.7. Whilst damping degradation curves of RSm shown in these studies fit into the

existing research (Figures 3.5b-3.6b-3.7b), normalised shear modulus ( $G/G_0$ ) shows a slightly higher stiffness degradation for the case of RSm containing tyre chips (Mashiri et al., 2017), as visualised in Figures 3.5a-3.6a-3.7a.

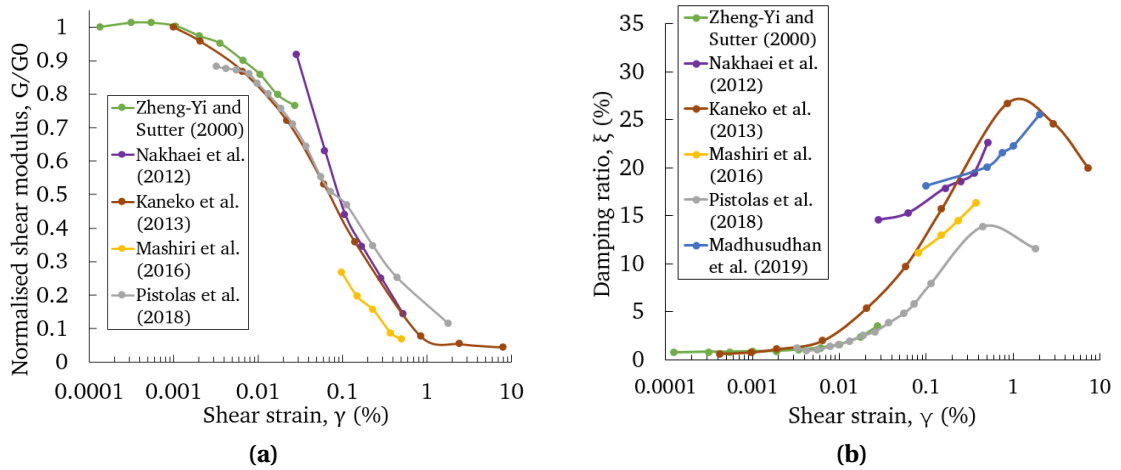


**Figure 3.5:** a) Normalised shear modulus and b) damping ratio of rubber soil mixtures at  $\chi = 10\%$  and  $\sigma_m = 100$  kPa

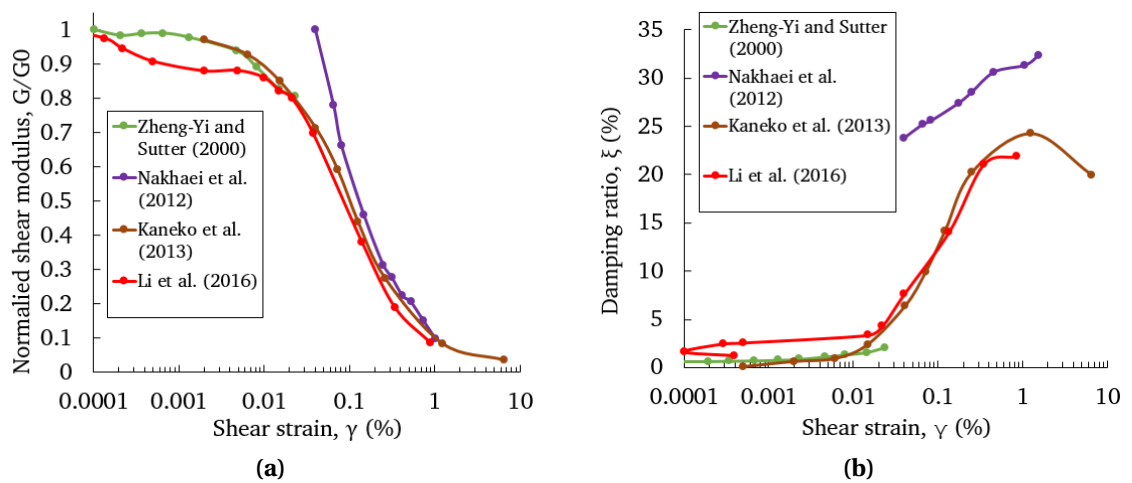


**Figure 3.6:** a) Normalised shear modulus and b) damping ratio of rubber soil mixtures at  $\chi = 10\%$  and  $\sigma_m = 200$  kPa

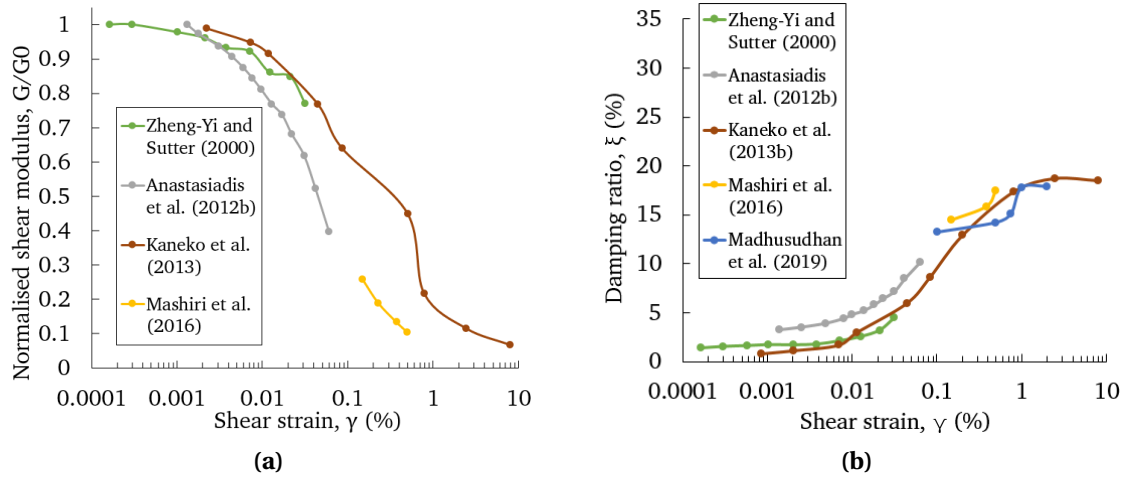


**Figure 3.7:** a) Normalised shear modulus and b) damping ratio of rubber soil mixtures at  $\chi = 30\%$  and  $\sigma_m = 100$  kPa

### *Test conditions*

Amongst the various test conditions which may have an influence on the alteration of soil non-linear bulk parameters in the medium-to-large strain range, only mean stress has been described in the previous section. Excitation frequency, number of cycles or state of the specimen are some other test conditions to consider.

The majority of the specimens tested with cyclic triaxial have been performed at low-frequencies (1-10 Hz). This is the frequency spectrum at which the fundamental frequency of seismic motions is typically found. Within this frequency range, however, the dynamic bulk parameters do not appear to be significantly influenced by excitation frequency (Towhata, 2014; Kumar et al., 2017). On the other hand, torsional resonant column increases the testing frequency to trigger resonance in the soil element with the defined torque and thus, apply a small-to-medium deformation. It is implicit that the frequency needs to be increased so that the maximum shear strain is applied to the sample. This test condition is therefore not included as part of the scope of this study.

Based on the literature review, the number of cycles are not commonly considered for the evaluation of soil stiffness and damping at small-to-medium strains. This is on the basis that soil elements experience a relatively small deformation when predominately tested in the linear elastic zone. As a consequence, there is a small effect on

bulk parameters of conventional soils and RSm when applying multi-cyclic loading. However, the cyclic effect has a bigger influence as the strain amplitude increases ( $\gamma > 0.1\%$ ) given that the soil is subject to greater disturbances. That is why the majority of the studies found in the existing research evaluate the alteration in stiffness and damping up to a maximum of 10 loading cycles, either under stress or strain controlled conditions. This testing procedure is based on the assumption that bulk parameters that define the dynamic behaviour of soils remain nearly constant at  $N > 10$ , as established in the literature (Kokusho, 1980; Ehsani et al., 2015; Kumar et al., 2017).

This assumption has been widely proven to be valid for soils tested under dry conditions where the bulk parameters that define the dynamic behaviour remain nearly constant after ten loading cycles. This is for example the case of Madhusudhan et al. (2019) who studied the response of RSm under cyclic loading in dry and saturated conditions. The samples contained river sand ( $D_{s50} = 0.75$  mm) and granulated rubber ( $D_{s50} = 1.25$  mm), and various specimens were prepared adding up to  $\chi = 50\%$  at a relative density of between 65 and 80 %. Cyclic triaxial tests were then conducted on 50 mm by 100 mm samples under drained conditions by means of strain-controlled cycles, applying up to twenty strain controlled cycles. Shearing strain amplitude increased with the number of cycles ( $\gamma = 0.1 - 2\%$ ) and confining pressure was kept at the same level,  $\sigma_m = 100$  kPa. The results corresponding to the values of  $G$  and  $\xi$  with  $N$  of both sand and 30 % RSm in dry conditions are shown in Figure 3.8. No significant change on the two bulk parameters was found due to the number of cycles, which is in line with results obtained testing mineral soils (Kumar et al., 2017).

Investigations in the literature (Brennan et al., 2005; Okur and Ansal, 2007; Wichtmann and Triantafyllidis, 2016) have demonstrated the increase in stiffness and damping degradation of mineral soils under saturated conditions when subject to several strain controlled cycles. Amongst the various studies on RSm, only Mashiri et al. (2016) has discussed the cyclic effect on the dynamic behaviour of sand-tyre chip mixtures (STCh). Specimens were prepared with poorly graded sand ( $D_{s50} = 0.35$  mm) and 6 x 18 mm rectangular shaped tyre chips at a relative density of 50 %. Various samples were formed adding up to  $\chi = 40\%$  and they were all consolidated to a unique mean

stress level,  $\sigma_m = 69$  kPa. Cyclic triaxial tests were performed on 100 mm by 200 mm specimens under undrained conditions by means of strain controlled cycles ranging at  $\gamma = 0.15, 0.23, 0.38$  and  $0.5$  %. Figure 3.8 shows the variation in stiffness and damping of sand and 30 % STCh with number of cycles. The study established that there is a decay in the damping of the mixtures but, more importantly, there is a significant reduction in soil stiffness up to  $N = 15$ . This was attributed to the build-up in the pore water pressure and the loss of inter-particle contacts. As shown in Figure 3.8, there is a discrepancy in the evolution of RSm dynamic properties in relation to the state of the specimen, i.e. dry or saturated.

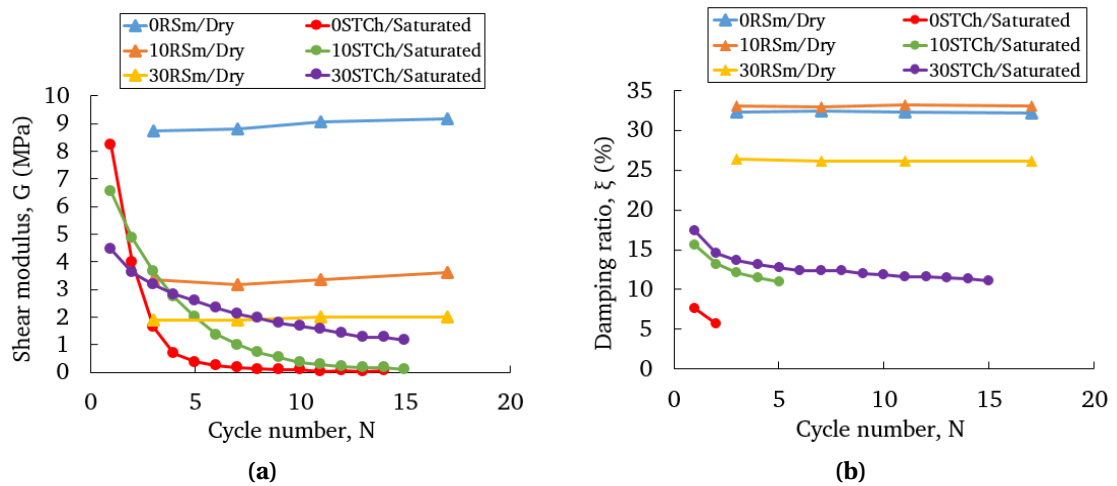


**Figure 3.8:** a) Normalised shear modulus, and b) damping ratio, with N of RSm in dry (Madhusudhan et al., 2019) and saturated (Mashiri et al., 2016) conditions

This study has undertaken a comprehensive experimental testing on the response of RSm comprising shredded rubber particles under undrained saturated conditions. The results of  $G$  and  $\xi$  and its alteration by studying effect of particle properties and test conditions, including cyclic effect, will be analysed and discussed in Chapters 5 and 7.



**Table 3.4:** Studies on response of RSm under dynamic loading

Reference	Apparatus	RC	Specimen	$\gamma_a$ (%) / $q_a$ (kPa)	$D_{50,sand}$ (mm)	$D_{50,rubber}$ (mm)	SR	$D_r$ (%)	N	$\sigma_m$ (kPa)
Zheng-Yi and Sutter (2000)	RC	V = 29-100	Dry	0.0001-0.05	0.6-0.8	RF; 2-4.76	4-6	NS	NT	69-483
Pamukcu and Akbulut (2006)	RC	V = 0-40	Dry	0.0001	0.6-0.85	GR; 0.6-0.92, kaolinite clay	1	NS	NT	34-207
Nakhaei et al. (2012)	CT	$\chi$ = 0-14	SUC	0.01-7	5	GR; 2	0.4	92	11	50-300
Anastasiadis et al. (2012b); Anastasiadis et al. (2012a)	RC	$\chi$ = 0-35	Dry	0.0001-0.02	0.27-7.8	GR; 0.34-2.8	Vr.	NT	<10	50-400
Senetakias et al. (2012a); Sene- takias et al. (2012b)	RC	$\chi$ = 0-35	Dry	0.0001-0.02	0.27-7.8	GR; 0.34-2.8	Vr.	NT	<10	50-400
Mashiri et al. (2013)	CT	$\chi$ = 35	SUC	0.15-0.5	0.35	TCh; 5	15	50	100	23-138
Ehsani et al. (2015)	CT, RC	V = 0-30	SUC	0.0001-4	0.2	RF; 1 and GR; 4.75	5-20	NS	<10	300
Li et al. (2016)	RC, CT	V = 0-20	SDC	CSR = 0.2	PG = 0.8	GR; 0.2, 0.8	1-4	NS	50	50-200
Brara et al. (2016)	BE and CT	V = 0-100	D	0.0001	PG; 0.33	GR; 0.12	0.33	NS	NS	50-500
Mashiri et al. (2016)	CT	$\chi$ = 0-40	SUC	0.15-0.5	0.35	TCh; 6X8	20	50	300	23-138
Mashiri et al. (2017)	CT, BE	$\chi$ = 0-40	SUC	0.15-0.5	0.35	TCh; 6X8	20	50	50	23-138
Pistolas et al. (2018)	CT, RC	$\chi$ = 0-60	S	0.01-2	0.41	GR; 1.55-3.38	4-8	e = 0.7	2	25-200

Note: CT = Cyclic Triaxial, BE = Bender Element; RC = Resonant Column; THC = Torsional hollow cylinder;  $\chi$  = Gravimetric proportion; V = volumetric proportion; SUC = Saturated undrained consolidated; SDU = Saturated drained unconsolidated; D = Dry; S = Saturated; Di = Diameter; GR = granulated rubber; RF = Rubber fibres; TCh = Tyre chips; SS = Sohma sand; Sh = Shredded; RD = Relative density; NS = Not specified; NT = Not tested; Vr = Variable

**Table 3.4:** Studies on response of RSm under dynamic loading

Reference	Apparatus	RC	$D_{50sand}$ (mm)	$D_{50rubber}$ (mm)	Remarks
Zheng-Yi and Sutter (2000)	RC	V = 29-100	0.6-0.8	RF; 2-4.76	- $G_0$ decreased and $\xi_0$ increased at small strains with $\chi$ . Damping is defined as a combination of friction between sand particles and deformation experienced by rubber. The expression proposed by Hardin and Drnevich (1972) revealed a high correlation with the empirical results
Pamukcu and Akbulut (2006)	RC	V = 0-40	0.6-0.85	GR; 0.6-0.92	-Increase in $G_0$ and $\xi_0$ until $\chi = 30\%$ by volume with optimum $\chi = 20\%$ . Explanation for the damping improvement based on the thermoelastic enhancement as a result of the rubber-to-soil contacts which decreased at $\chi > 30\%$
Nakhaei et al. (2012)	CT	$\chi = 0-14$	5	GR; 2	- $\xi$ decreased with $\chi$ at $\sigma_3 = 50-100$ kPa, and increased at $\sigma_3 = 200-300$ kPa. Elastic behaviour was found in $G/G_0$ with addition of rubber
Anastasiadis et al. (2012b), Anastasiadis et al. (2012a)	RC	$\chi = 0-35$	0.27-7.8	GR; 0.34-2.8	-Equivalent void ratio $e_e q$ was proposed due to low contribution of rubber to the stiffness of the mixture. Adding $\chi$ increased $\xi_0$ value at small strains. More pronounced at $D_{50sand} > D_{50rubber}$ where there are more rubber-to-rubber contacts
Senetakis et al. (2012a); Senetakis et al. (2012b)	RC	$\chi = 0-35$	0.27-7.8	GR; 0.34-2.8	-Dynamic properties are influenced by confining pressure, size ratio, strain amplitude and shape of rubber particles. Transition from SLB to RLB occurred at $\chi = 15\%$ . Mixture showed lower stiffness degradation with $\gamma$ . Proposed expressions to determine normalised $G/G_0$ and damping curves with size ratio
Mashiri et al. (2013)	CT	$\chi = 35$	0.35	TCh; 5	-G and $\xi$ were influenced by $\gamma$ and N. Stiffness and damping degradation was more pronounced at N>50
Ehsani et al. (2015)	CT, RC	V = 0-30	0.2	RF; 1 and GR; 4.75	-G was highly influenced by $\chi$ and stiffness degradation was diminished by adding large rubber particles. Type of rubber and size ratio between sand/rubber does not vary $\xi$ value. Optimum $\xi$ found at $\chi = 10\%$

**Table 3.4:** Studies on response of RSm under dynamic loading

Reference	Apparatus	RC	$D_{50sand}$ (mm)	$D_{50rubber}$ (mm)	Remarks
Li et al. (2016)	RC, CT	V = 0-20	PG = 0.8	GR; 0.2, 0.8	- $G_0$ increased with $\chi$ at high confinement pressure due to number of contacts. At $\chi > 20\%$ , $\xi$ was greater than sand specimens. A high liquefaction resistance was found at $D_{50sand}/D_{50rubber} = 1$
Brara et al. (2016)	BE and CT	V = 0-100	PG = 0.33	GR; 0.12	-Sustained increase in damping with addition of $\chi$ , which decays at high rubber contents with $\sigma_m$ . G value reduced at $\chi > 20\%$ which is overcome by applying greater cell pressure. Optimum values found at $\chi = 10\%$ where G maintained constant and $\xi$ increased
Mashiri et al. (2016)	CT	$\chi = 0-40$	0.35	TCh; 6 x 8	-TCh reduced sand liquefaction potential with optimum values at $\chi = 30-33\%$ . G decreased whereas $\xi$ increased with $\gamma$ . Both properties reduced with number of cycles until N = 15
Mashiri et al. (2017)	CT, BE	$\chi = 0-40$	0.35	TCh; 6 X 8	-G decreased with proportion of TCh and shear strain applied. A new expression was proposed to determine $G/G_0$ based on <a href="#">Hardin and Dmievich (1972)</a>
Pistolos et al. (2018)	CT, RC	$\chi = 0-60$	0.41	GR; 1.55-3.38	- $G_0$ decreased with $\chi$ which is more marked when $D_{50sand} < D_{50rubber}$ . $\xi_0$ increased with $\chi$ which is more evident at $D_{50sand} > D_{50rubber}$

### 3.4.2 Dynamic properties at small-to-medium strains

The study of the dynamic behaviour of soil materials start by evaluating  $G$  and  $\xi$  at minimum disturbance or, in other words, when soils experience a very small deformation, i.e.  $\gamma = 0.0001\%$ . At this strain level, dynamic bulk parameters are regarded as maximum shear modulus, or maximum soil stiffness ( $G_0$ ), and minimum damping ratio, or capacity to dissipate energy at very small strains ( $\xi_0$ ). These parameters are required to understand the response of soils under cyclic loading and, more importantly, to elucidate the evolution in the stiffness and damping strain curves.

Zheng-Yi and Sutter (2000) was the first study that proposed expressions to predict stiffness and damping degradation curves for RSm at small-to-medium strains, as depicted in Figures 3.5a-3.5b, by modifying expressions initially postulated by Hardin (1978). Torsional resonant column tests were performed on dry specimens consisting of Ottawa sand and tyre shreds with  $S_R = 4-6$ . Samples were isotropically consolidated at  $\sigma_m = 69, 207, 345, 483$  kPa. The rubber content varied between  $V = 0 - 100\%$  and the initial void ratio at 69 kPa ranged between 0.35 and 0.57, hence, the samples were highly compacted. The results showed an improvement in damping capacity and a gradual reduction in soil shear stiffness with rubber content. Increasing confining pressure led to a development in soil stiffness whilst damping decreased at any rubber percentage, except for rubber only specimens.

Anastasiadis et al. (2012a) evaluated the evolution in  $G$  and  $\xi$  as function of shear strain on samples consisting of gravel-rubber and sand-rubber mixtures in a very dense state ( $D_r = 91 - 100\%$ ). These mixtures were formed combining seven granular soils ( $D_{50} = 0.27 - 7.80$  mm) and four uniform particulate granular rubber ( $D_{50} = 0.35 - 3.00$  mm). Forty-two torsional resonant column tests were conducted on dry soil-rubber mixtures adding rubber up to  $\chi = 35\%$  and at mean confining pressures ranging between 25 and 400 kPa. The study sought to assess the effect of rubber content, size ratio and confining pressure on dynamic bulk parameters at small-to-medium strains. Anastasiadis et al. (2012a) established that small-strain damping increases at any size ratio, lower or higher than unity. However, the greatest improvement is

shown when the rubber-like behaviour arises; more prominent with i) adding more rubber, ii) smaller particle ( $D_{50r}/D_{50s} < 1$ ), and iii) lower confining pressures. In line with [Zheng-Yi and Sutter \(2000\)](#), the addition of rubber led to a reduction in the overall shear modulus of RSm from small-to-medium strains. On the other hand, normalised shear modulus ( $G/G_0$ ) decreased at a lower rate and reference strain ( $\gamma_{ref}$ ) increased, i.e. lower stiffness degradation, when the rubber-like behaviour arose. Whilst the increase in confining pressure resulted in greater values of stiffness, this was less evident on damping, revealing lower damping.

The results presented in [Figures 3.9a-3.9b](#) and [Figures 3.9c-3.9d](#) show a collection of various studies dedicated to the study of  $G_0$  and  $\xi_0$ , respectively, including the results gathered by [Anastasiadis et al. \(2012a\)](#). It is evident that  $G_0$  decreases with rubber content attributed to the capacity of rubber to deform under loading. It can be also observed that  $G_0$  increases with confining pressure at any rubber percentage in the stress level studied, i.e.  $\sigma_m = 69 - 250$  kPa. This increase in stiffness is, however, more prominent during the appearance of sand-like behaviour. As established in [Section 3.3.3](#), sand-like behaviour presents stiffer characteristics and it arises at relatively low rubber contents ( $\chi < 35\%$ ), when size ratio is higher than one and at relatively high stress levels. In line with findings obtained by [Kim and Santamarina \(2008\)](#) and [Anastasiadis et al. \(2012a\)](#), this occurs as a consequence of the higher number of contacts between sand particles and because the response is controlled by soil matrix instead of soil-rubber matrix, otherwise observed at higher rubber contents. Minimum damping ratio also increases when adding more rubber at any stress level, as depicted in [Figures 3.9c-3.9d](#). This is on the basis that material damping generated by RSm is the result of combining friction between sand, and deformation of soft rubber particles under isotropic loading ([Zheng-Yi and Sutter, 2000](#)). By comparing the few studies which have evaluated the minimum damping via torsional resonant column tests, the increasing trend appears to be, however, more marked at  $\sigma_m = 100$  kPa ([Figure 3.9c](#)).

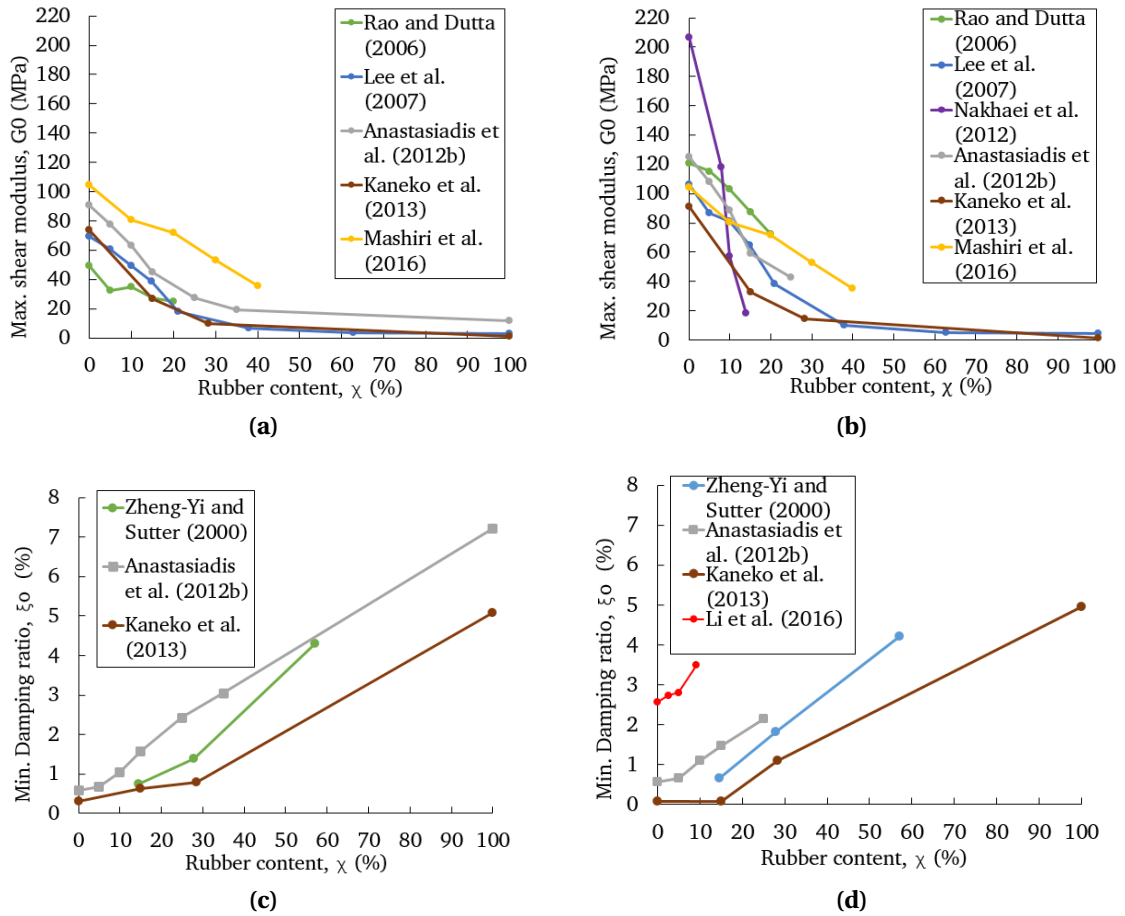


**Figure 3.9:** Maximum shear modulus and minimum damping ratio at a,c)  $\sigma_m = 100$  kPa, and b,d)  $\sigma_m = 200$  kPa

Senetakis et al. (2012a) and Senetakis et al. (2012b) proposed generic normalised shear modulus and damping ratio curves for dry gravel-rubber and sand-rubber mixtures using results gathered by Anastasiadis et al. (2012a). Two soils; a fluvial sand ( $D_{s50} = 0.27 - 1.33$  mm) and quarry sandy gravel ( $D_{s50} = 2.90 - 7.80$  mm), and four uniform granulated rubber materials ( $D_{s50} = 0.34 - 2.80$  mm) were used to form mixtures with a size ratio ranging between 0.1 and 5. Specimens contained different rubber contents, adding up to  $\chi = 35\%$ , in fourteen layers with a high relative density. Torsional column tests were performed in a shearing amplitude going from  $\gamma = 0.0002\%$  to  $\gamma = 0.3\%$ , on samples subject to isotropic pressures at  $\sigma_m = 25 - 400$  kPa. A series of curves were then fitted to the experimental data to predict the evolution in the dynamic bulk parameters. The modified hyperbolic model postulated by Darendeli (2001) was adopted to determine the change in the soil stiffness. Although the results did not show a clear correlation

between material aspects or test conditions and the curvature of coefficient ( $\alpha$ ), reference strain ( $\gamma_{ref}$ ) was altered by rubber content, size ratio, confining pressure and grain size distribution. The expressions showed how rubber-like, sand-like behaviour as well as the transition could be clearly distinguished and correlated to rubber content and size ratio. Expressions proposed by [Senetakis et al. \(2012b\)](#) to predict the variation in minimum stiffness and damping for RSm are covered in Chapter 7 of this investigation. A common trend can be observed in the evolution of shear modulus at various shearing strain amplitudes, i.e. soil stiffness decreases with rubber content and adding smaller rubber particles ( $S_R < 1$ ). Moreover, reference strain increases and normalised shear modulus decreases at a lower rate, which leads to a more linear behaviour and a reduced rate of stiffness degradation. This phenomenon is accentuated with the application of higher confining pressures, as visualised in Figures [3.5a](#), [3.6a](#) and [3.7a](#).

In terms of damping ratio, the evolution in the value changes in relation to the deformation undergone by the specimen. From small-to-medium strains, an improvement in damping was found in the transition from sand-like to rubber-like behaviour, as established by [Anastasiadis et al. \(2012a\)](#) and presented in Figures [3.9](#). The opposite effect was found when increasing confining pressure, which resulted in lower damping. Although many studies have evaluated the minimum damping ratio, no previous study has tried to explain how this dissipation occurs in terms of the interaction between particles at a microscopic level and its correlation to the bulk parameters. This will be further covered in Chapter 4, by means of testing RSm specimens using x-ray tomographic tests, and Chapters 5, through resonant column and cyclic triaxial tests.

### 3.5 Geotechnical seismic isolation systems

The concept of seismic isolation system was first used in the late 60's in New Zealand to enhance the capacity of a structure against seismic motions by increasing its ductility ([Jangid and Datta, 1995](#)). Base isolation is widely recognised as a design approach whereby a flexible or sliding interface is introduced between a structure and its foundation to alleviate potential vibrations coming from an earthquake and thus mitigate

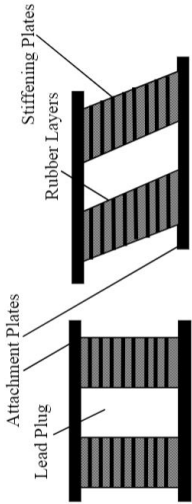
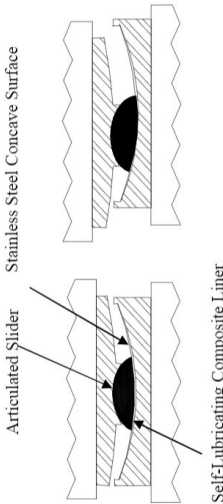
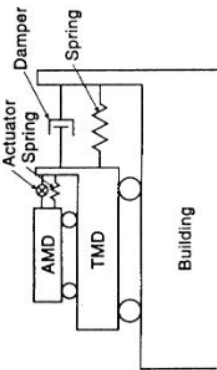
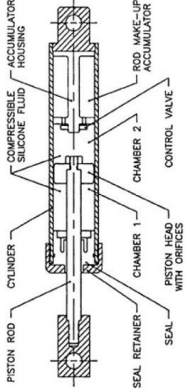
the earthquake building damage (Xu, 2009; Tsang, 2008). The objective is to decouple the horizontal motions of the structure from the ground motions by adding structural elements which enhance the energy dissipation and/or alter the mode of vibration (Naeim and Kelly, 1999). The most typical base isolators are natural rubber bearings, high-damping rubber bearings, friction-pendulum systems and resilient-friction systems. These base isolation systems have been successfully implemented and tested in bridges, nuclear power plants and residential buildings (Yegian and Kadakal, 2004). A description with the main references, advantages/disadvantages, as well as images of most common structural elements employed as isolator systems, including active, semi-active, passive and hybrid devices, is presented in Table 3.5.

The biggest issue found with the use of base isolation systems is that they are best implemented in new constructions. This creates the inconvenience of precluding their installation to those buildings whose capacity cannot be modified or where the integrity of the building needs to be preserved, e.g. historical buildings (Dolce et al., 2000). Most of these devices are also sophisticated systems that require advanced technical knowledge for their design and subsequent installation.

Since the 90's, different approaches have emerged in civil engineering to handle the seismic hazard by attenuating the acceleration or displacement before it reaches the superstructure (Nappa, 2014). These are known as Geotechnical Seismic Isolation (GIS) systems which seek to modify the soil by means of introducing flexible or sliding interfaces directly in contact with geological sediments (Tsang, 2009). These have also been defined by several authors as "soft" zones, which enable the incorporation of a layer that creates a discontinuity within the soil (Brennan et al., 2019). The main difference with typical structural base isolation systems stems from the fact that GIS are physically separated from the superstructure. A comparison of various systems within GIS is given in Table 3.6 including vibration isolation devices using a) wave barriers, and b) rubber-soil mixtures.

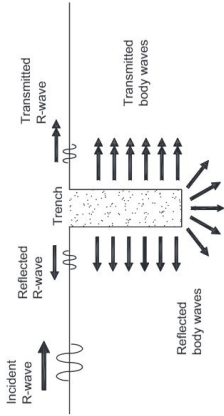
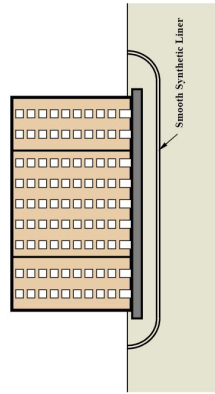
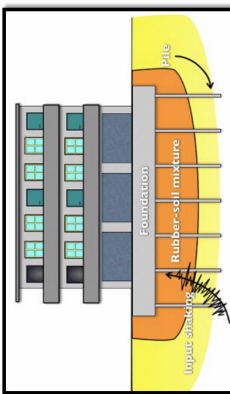


**Table 3.5:** Comparison of structural isolation systems

Reference	Type	System	Advantages	Disadvantages	Image
Skinner et al. (1993); Robinson (2000); Dolce et al. (2000)	STR-P	EB	<ul style="list-style-type: none"> <li>• Relatively low cost</li> <li>• Resistance to moderate loads</li> <li>• Low in-structure accelerations</li> </ul>	<ul style="list-style-type: none"> <li>• Large displacement</li> <li>• No restoring force mechanism</li> <li>• Supplementary devices required to increase energy dissipation</li> <li>• Only applicable to new buildings</li> </ul>	
Jangid and Datta (1995); Matsagar and Jangid (2008)	STR-P	SB	<ul style="list-style-type: none"> <li>• High damping</li> <li>• Relatively easy design</li> <li>• Effective device with restoring force</li> </ul>	<ul style="list-style-type: none"> <li>• Properties are function of pressure, velocity and initial stiffness</li> <li>• High cost</li> <li>• Only applicable to new buildings</li> </ul>	
Soong (1990); Soong and Spencer (2000)	STR-A, H	AMD, HMD	<ul style="list-style-type: none"> <li>• Enhanced effectiveness in response</li> <li>• Insensitivity to site conditions</li> <li>• Selection of specific objectives</li> </ul>	<ul style="list-style-type: none"> <li>• High size thus not practical for low-storey buildings</li> <li>• Required continuous power source</li> </ul>	
Kobori et al. (1993); Kurata et al. (1999)	STR-SA	SAVS, SAD	<ul style="list-style-type: none"> <li>• Can operate on battery power system</li> <li>• Combine benefits of active and passive devices</li> </ul>	<ul style="list-style-type: none"> <li>• Technical difficulties related to design and installation</li> <li>• High cost</li> </ul>	

Note: STR = Structural; P = Passive; A = Active; H = Hybrid; SA = Semi-active; EB = Elastomeric bearing; SB = Sliding bearing; AMD = Active mass damper; HMD = Hybrid mass damper; SAVS = Semi-active variable stiffness; SAD = Semi-active damper

**Table 3.6:** Comparison of geotechnical seismic isolation systems

Reference	Type	System	Advantages	Disadvantages	Image
Gao et al. (2006); Babu et al. (2011); Mahdavisefat et al. (2017)	GEO	WB-A/P	<ul style="list-style-type: none"> <li>• Can be installed for both existing or new buildings</li> <li>• Low-cost, easy deployment technique</li> <li>• Up to 60% attenuation in ground vibration</li> </ul>	<ul style="list-style-type: none"> <li>• Instability of construction</li> <li>• Environmental issues related to run-off waters</li> <li>• Excessive deformation of in-filled material</li> </ul>	
Kim and Konagai (2001); Yegian and Catan (2004); Yegian and Kadakal (2004)	GEO	G-FIS/SIS	<ul style="list-style-type: none"> <li>• Significant reduction in shear forces</li> <li>• Important reduction in transmitted accelerations</li> </ul>	<ul style="list-style-type: none"> <li>• Installation of material</li> <li>• Radioactive attack and oxidation of material</li> <li>• Excessive displacement</li> </ul>	
Tsang (2008); Anastasiadis et al. (2012a); Kaneko et al. (2013)	GEO	RSM	<ul style="list-style-type: none"> <li>• Low cost, easily deployed solution</li> <li>• Re-use of highly contaminant scrap tyres</li> <li>• Reduction in liquefaction potential</li> </ul>	<ul style="list-style-type: none"> <li>• Significant deformation of recycled rubber</li> <li>• Not enough real scale experiments, questioned its use in long term constructions</li> </ul>	

Note: GEO = Geotechnical; WB = Wave barrier; A = Active; P = Passive; G = Geosynthetics; FIS = Foundation Isolation System; SIS = Soil Isolation System; RSM = Rubber-soil mixture

### 3.5.1 Wave barriers

The concept of wave screening accounts for the mitigation of ground-borne vibrations coming from different sources such as blasts, heavy vehicles, or railway traffic by introducing wave barriers (Gao et al., 2006; Babu et al., 2011; Mahdavisefat et al., 2017). This type of vibration isolation system is based on the theory of wave diffraction and can be either active, when located close to the source, or passive, when installed near the protected area. The theory behind the use of this mechanism relies on Snell's law, as explained in Chapter 2, which establishes that when incident body or surface waves reach an interface with another medium, part of this wave will be reflected back into the first medium and part will be transmitted into the second medium. This can be achieved through the installation of open or in-filled trenches, sheet pile walls or tubular piles in the soil (Alzawi, 2011; Mahdavisefat et al., 2017).

Woods (1968) and Woods et al. (1974) are two comprehensive studies on vibration isolation by wave barriers. These studies involved a series of scaled field experiments performed to evaluate the screening effect of open trenches, adopting both active and passive designs. Woods (1968) demonstrated that the energy coming from the traffic is transferred to the ground as surface, i.e. Rayleigh, and body waves. In a homogeneous half space medium, whilst body waves are attenuated due to the geometrical damping ( $1/r$ ), Rayleigh waves are transmitted through the soil surface and thus less influenced by geometrical damping ( $1/r^{0.5}$ ). This is the reason why Rayleigh surface waves become the primary concern, being 67% of the total energy for foundation isolation problems. From the results gathered, the experimental investigation showed that the trench width has little influence on the reduction of the vibration amplitude. On the other hand, it was demonstrated that a trench depth of between 0.6 and 1.3 times the excitation wavelength is required to reduce up to 75% of vertical ground vibrations. By comparing the implementation of different configurations, sheet wall barriers were proven not to be as effective in wave scattering as open trenches. This is based on Snell's law, which states that when an incident wave approaches a free end boundary, i.e. at the surface, the totality of the wave stress and amplitude are reflected and there is no transmission.

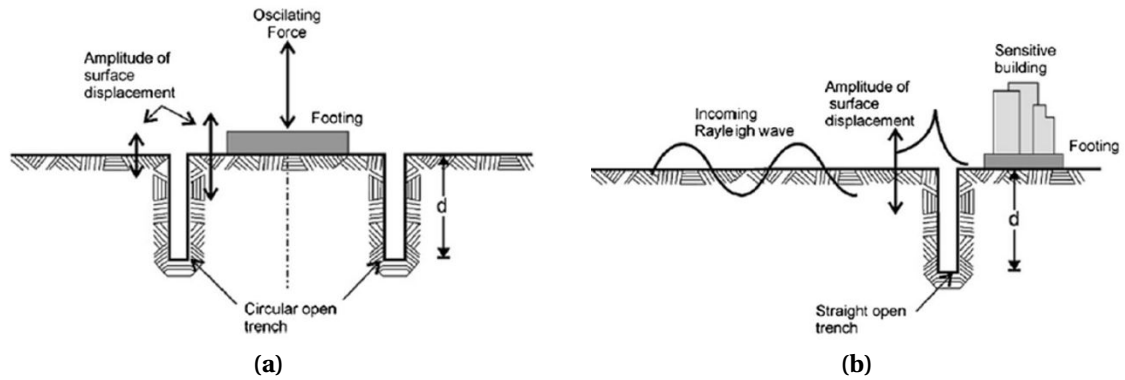


**Figure 3.10:** a) Active and b) passive isolators using wave barriers (Mahdavisefat et al., 2017)

This last conclusion has also been confirmed in the past years by other authors (Bo et al., 2014; Ulgen and Toygar, 2015) who stated that open trenches provide a better performance than in-filled designs. However, these wave barriers are impractical due to the instability of their construction, the safety hazard for people passing over the trench or the environmental issues related to potential run-off waters. To overcome this issue, existing research have considered the use of geofoam materials in trenches to attenuate the magnitude of stress waves propagated based on numerical investigations (Wang et al., 2009) and experimental tests (Murillo et al., 2009; Alzawi, 2011).

Murillo et al. (2009) used a centrifuge model to address the factors influencing a geofoam isolation barrier. The geofoam was an expanded polystyrene (EPS) and this was utilised to construct isolation barriers injected as embedded walls within a container full of Fontainebleau sand ( $D_{s50} = 0.3$  mm). Geometrical aspects including barrier depth, width and distance from the source of excitation were investigated whilst changing excitation input frequency between 50 and 2000 Hz. The results showed amplitude reduction ratios of between 0.2 and 1.8 when changing depth and distance to the source. Half the wavelength of the excitation frequency was adopted as the minimum distance between wave barrier and vibratory origin to mitigate incident surface waves.

Mahdavisefat et al. (2017) was the first study that proposed to fill open trenches with RSm to evaluate its effectiveness in screening incident Rayleigh waves. Nearly similar particle size distributions were prepared for both sand and rubber particles with  $S_R = 1$ . Four different rubber contents were introduced into the barrier. Excitation frequency varied between 10 and 400 Hz and the electric vibrator was placed at various

distances ranging between 2.5 and 10 m. To establish a comparison with previous studies, the results corresponding to barriers containing RSm were compared with previous no-trench and open-trench configurations. Due to the reflection of waves, the study showed that there is magnification of vibrations in front of the wave barrier. The results suggested that adding  $\chi = 30\%$  can attenuate between 60 and 70% of incoming surface waves, similar to the values obtained with open trenches. This supported the idea that alternative materials can have the same impact on wave scattering as open trenches whilst overcoming issues related to installation and maintenance.

The successful attenuation of surface waves together with the feasibility of their installation and maintenance has granted the wave barriers to be a commonly preferred vibration isolation system option. Existing research has proposed over the last decade to transfer the concept behind this system and construct soft or stiff barriers for seismic protection to mitigate body waves transmitted through the soil.

[Kirtas et al. \(2009\)](#) and [Kirtas and Pitilakis \(2009\)](#) studied the seismic performance of soil isolating configurations by means of centrifuge testing and numerical analysis on a single degree of freedom structure (Figure 3.11a). Harmonic and earthquake based excitations were applied to the model whilst varying excitation frequency between 0.6 Hz and 1 Hz as well as amplitude between 0.07 g and 0.37 g. The results revealed that stiffening the subsoil or introducing stiff diaphragm walls does not reduce the seismic hazard. Alternatively, the creation of soft zones, by introducing soil materials which present lower shear modulus than the surrounding soil, resulted in reduction of the structural response. This was undertaken by introducing deformable diaphragm walls as vertical walls or a combination of both horizontal and vertical deformable elements, i.e. soft caisson. The reduction in the horizontal acceleration was also explained on the basis that the fundamental period of the system was elongated. This was demonstrated to be more evident in the case of soft caisson whereby the soil-structure loading and the overall accelerations were significantly reduced at periods lower than the fundamental of the system. The main limitation addressed in the study was related to the displacement at base and top of the superstructure, greater than in the rest of the soil model.

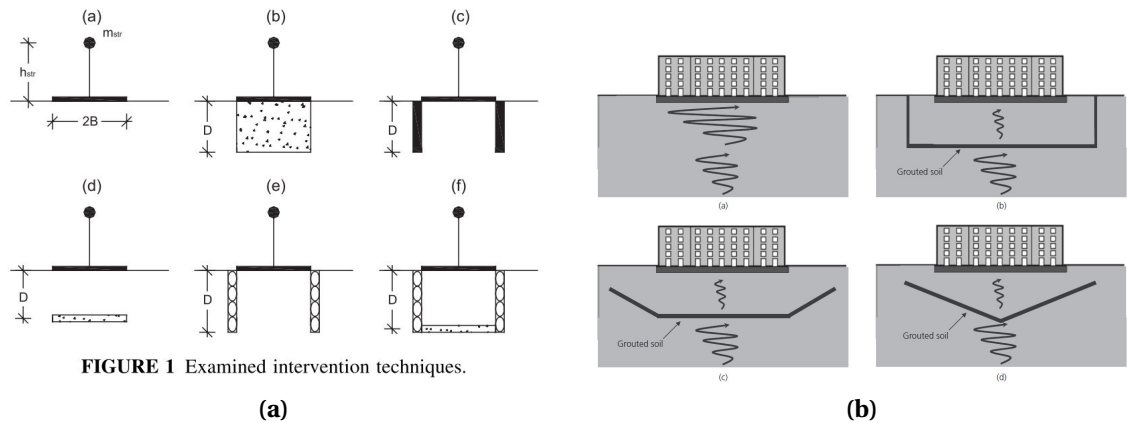


FIGURE 1 Examined intervention techniques.

Figure 3.11: Geometrical configurations of isolating layers a) Kirtas et al. (2009) b) Nappa (2014)

In line with these investigations, Lombardi (2012) and Nappa (2014) proposed to inject grouting to modify the physical properties of the soil to be protected from seismic events. This was possible with super absorbent polymer that would reduce the shear modulus, creating soil layers characterised by low stiffness. Thus, the dynamic impedance was increased to create a "filtering" zone capable of reflecting the incident waves. Nappa (2014) and Nappa et al. (2016) studied the effectiveness of soft barriers to reduce the amplification during seismic events by means of centrifuge testing. The model container, of dimensions 500 mm x 250 mm x 300 mm, was filled with dry Houston sand and compacted to a relative density of 85 %. To create the soft zones, latex balloons were filled up with super absorbent polymer ( $V_S = 20$  m/s) and these were introduced in two different configurations: horizontal and a v-shaped form. Harmonic sinusoidal motions were applied to the container with fundamental frequency excitation ranging between 0.375 and 1 Hz and amplitudes varying between 0.025 g and 0.24 g. The results demonstrated that despite being less practical for its installation, the horizontal barrier is more effective in attenuating incident waves. The study also showed that the reflection caused an amplification of the acceleration in front of the barriers, as established by Mahdavisefat et al. (2017). An important finding was that the system appeared to be more effective in screening body waves and reducing resultant acceleration in stronger events, attributed to the beneficial role of yielding shown by non-linear materials.

Flora et al. (2018) proposed the use of a parametric analysis as benchmark to evaluate soft barriers. In line with the results obtained by Kirtas et al. (2009), this study proposed

two configurations using absorbent polymer: soft caisson and v-shaped. Stiffness and, in consequence, dynamic impedance ratio of absorbent polymers, were modified to assess their influence in transmitted accelerations. The study showed a reduction in natural frequency of the foundation with softer materials contained within the caisson. Although the v-shaped configuration was less effective, both systems screened the incident waves. However, the system appeared to be more effective for "squat" low storey building, characterised by a higher fundamental frequency, in comparison with the "slender" buildings, known for having a lower fundamental frequency.

[Brennan et al. \(2019\)](#) investigated the effect on wave transmission of soft caisson containing dessert jelly by means of centrifuge model testing. A laminar model container was employed wherein Houston S28 silica sand was poured and compacted to a relative density of 80%. A structure was installed on top of the model, with a distributed mass of 65.6 kg, where horizontal accelerations were recorded. Harmonic sinusoidal motions with a fundamental period of 1 s were applied to the container. The results supported evidence from existing research and demonstrated the filtering effect due to the addition of soft zones. Although the amplitude at the fundamental period remained constant, the deformable material attenuated acceleration at frequencies higher than the predominant frequency of the input motion.

### 3.5.2 RSm for seismic isolation

Research to date has demonstrated that artificial barriers can be created within the soil to mitigate potential vibrations either transmitted along the surface, as Rayleigh waves, or transmitted throughout the medium, as body waves. The literature highlights, however, that two major issues need to be addressed; (i) the static stability of the soft material and (ii) the use of a suitable material for which the dynamic response is understood. Rubber-soil mixtures are considered by some studies as a possible candidate to be added in the soft zones given that it has a relatively high damping capacity and low shear modulus. A distinction is herein made between experimental and numerical investigations:

#### *Experimental studies*

A review of the literature on the seismic performance of RSm, via experimental testing, has been undertaken as presented in Table 3.8.

Hazarika et al. (2006), Hazarika et al. (2008a) and Hazarika et al. (2008b) were the first investigations focused on the seismic performance of RSm at modelled field scale. These studies proposed the use of tyre chips as backfill soil at waterfront structures. The main aim was to reduce the action of horizontal loads during strong motions such as earthquakes, whilst adopting a cost-effective design by introducing recycled rubber tyres. Hazarika et al. (2008a) performed large-scale underwater shaking table tests on a steel container of dimensions 4 m x 1.25 m x 1.5 m which included a bedrock layer, a layer of dense compacted sand, foundation rubble and a 0.85 m high backfill. Tests were performed in two configurations; one with only sandy backfill and second with 0.3 m thick layer of tyre chips compacted to a relative density of 46-49 %. A reduction of between 25 and 75% of the earth pressure was revealed attributed to the rubber deformability. An important decay in generated pore water pressure was also found, that in conjunction with the high capacity of rubber to recover the initial shape, resulted in a decay of the permanent horizontal displacement. Rubber ductility contributed thus to the stability of the backfill-soil system.



[Kaneko et al. \(2013\)](#) assessed the seismic response of soil foundations containing tyre chips - sand mixtures by using the online pseudodynamic response test, which consists of performing laboratory element tests and seismic response analysis at the same time. Element experiments were undertaken using a simple shear test apparatus whilst the soil was represented as a lumped-mass system in which seven soil layers are interconnected, with a specific mass and stiffness. Specimens were prepared by adding granulated rubber ( $D_{r50} = 0.7$  mm) and silica sand ( $D_{s50} = 0.4$  mm) at rubber contents ranging between  $\chi = 0 - 100$  %. Various configurations were set by changing the amount of rubber and the depth at which it was introduced, simulated to be 14 m below groundwater level. Effective isolation from wave propagation together with the mitigation of liquefaction potential were achieved when adding greater rubber contents. This was the result of combining high hysteretic damping and filtering effect of long period components obtained with the addition of horizontal soft barriers. The screening effect was more significant when increasing the thickness of RSm layers and introducing it at lower depths. In contrast with [Hazarika et al. \(2008b\)](#), the maximum horizontal displacement increased with rubber, attributed to its low stiffness.

[Xiong and Li \(2013\)](#) studied the acceleration response of a soil-foundation-structure model containing RSm. A soil container of 0.3 m x 1.4 m x 1.3 m was used for the experimental testing in which a horizontal RSm layer was added as the soil foundation. A superstructure was then placed on top simulating a vertical pressure equivalent to 50 and 100 kPa. RSm horizontal layer had a thickness of 100-200 mm and a rubber content  $\chi = 35 - 50$  %. The input motion selected for the test was El Centro with a maximum amplitude of 0.5 g. The outputs from this study were in line with [Kaneko et al. \(2013\)](#) establishing that the efficiency of the system increases as the thickness of the deformable layer increases. A greater isolation of the input motion was achieved at higher stress amplitudes attributed to the non-linear behaviour experienced by RSm. A negligible difference in isolation effectiveness was found at high rubber contents. Hence, an upper limit of  $\chi = 35\%$  was limited to reduce the static settlement.

In the literature, only [Bandyopadhyay et al. \(2015\)](#) evaluated the dynamic response of the mixture by applying harmonic sinusoidal motions using a shaking table. A

model container of 1 m x 1 m x 0.5 m was filled up to 200 mm with Kansai river sand compacted to a relative density of 65 %. A surcharge load was then placed on top of the sand box representing a typical isolated building of 2 to 5 stories. The foundation with a unique RSm horizontal layer, containing  $\chi = 50$  % of shredded rubber tyre, was placed underneath the surcharge load. Input motions applied to the container varied in amplitude between 0.15 and 1 g as well as excitation frequency; 1.5 Hz, 3.5 Hz, 4 Hz and 4.5 Hz. The study established that peak accelerations on top of the footing follow peak base accelerations until an amplitude (0.4 g) from where there is a decay. This phenomenon was more evident at  $\chi > 20$  % and at greater excitation amplitudes.

Table 3.7 shows the ratio between output and input accelerations, also known as system efficiency, of structure-soil foundation modified with the addition of RSm horizontal layers. Although a limited number of studies can be found on this topic, similar trends can be observed in terms of seismic isolation efficiency. That said, the efficiency of the system appears to increase, i.e. the ratio decreases, when adding more rubber as well as altering geometrical aspects such as layer thickness or depth introduced within the soil. Consequently, the increase in deformability of the host soil by adding particulate rubber appears to play an important role in the attenuation of the input motion. Further testing is required to better understand the effect of rubber content on energy dissipation capacity and, subsequently, on the natural frequency of the ground soil and its cyclic performance under cyclic loading.

**Table 3.7:** Efficiency of seismic isolation systems with RSm

Reference	Configuration	Input (g)	Output (g)	Ratio
Kaneko et al. (2013)	SSS		0.26	0.51
	TSS		0.17	0.33
	STS		0.14	0.27
	SST2m	0.51	0.14	0.27
	SST4m		0.11	0.22
	SST6m		0.09	0.18
	TTT		0.09	0.18
Xiong and Li (2013)	35%RSm-100mm		0.32	0.61
	35%RSm-200mm	0.52	0.3	0.58
	50%RSm-100mm		0.35	0.67
	50%RSm-200mm		0.25	0.49
		0.2	0.15	0.75
Bandyopadhyay et al. (2015)	50%RSm-40mm	0.3	0.23	0.76
		0.4	0.32	0.8
		0.5	0.43	0.86
		0.6	0.48	0.8
		0.7	0.52	0.74
		0.8	0.54	0.68
	1	0.56	0.56	

Note: SSS = Sand-sand-sand; TSS = tyres-sand-sand; STS = Sand-tyres-sand; SST2m = sand-sand-2m of tyres; SST4m = sand-sand-4m of tyres; SST6m = sand-sand-6m of tyres; TTT = tyres-tyres-tyres

With regards to the study of the liquefaction potential of mixtures containing rubber, existing research has demonstrated that introducing tyre derived aggregates (Hazarika et al., 2006; Kaneko et al., 2013; Mashiri et al., 2016) leads to a significant reduction in the accumulation of pore water pressure and, as a result, an improvement in the liquefaction resistance of sand specimens. Bahadori and Manafi (2015) and Bahadori and Farzalizadeh (2018) tested the liquefaction resistance of sand and RSm specimens using shaking table tests. Although the addition of tyre shreds showed an improvement in the damping capacity and mitigation of pore water pressure, the study established that the addition of tyre powder is a more effective solution to control the pressure build-up. On the other hand, Promputthangkoon and Hyde (2007), testing mixtures with tyre chips, and Shariatmadari et al. (2018), that performed mixtures with granulated rubber, found that liquefaction resistance of RSm decreases by adding rubber on the basis that specimens were prepared at a very high density ( $D_r = 90\%$ ). Further experimental testing is required to elucidate the effect of particulate rubber on the accumulation of pore water pressure with the number of strain controlled cycles.

**Table 3.8:** Studies on seismic performance of RSm

Reference	Apparatus	RC	Specimen	$\gamma_a$ (%) / $q_a$ (kPa)	$D_{50sand}$ (mm)	$D_{50rubber}$ (mm)	SR	$D_r$ (%)	N	$\sigma_m$ (kPa)
Hazarika et al. (2006); Hazarika et al. (2008b); Hazarika et al. (2008a)	ST	$\chi = 100$	S	EMs	No. 5 SS	TCh; Di = 2	NS	50	Vr.	NT
Hyodo et al. (2007)	CT	V = 0-100	SUC	q = 40	0.4	TCh; 0.655	1.5	50	50	100
Promptthangkoon and Hyde (2007)	CT	V = 0-15	SUC	q = 30	0.7	TCh; 1.2	2	e = 0.6	2	100
Takahashi et al. (2006); Kaneko et al. (2013)	OT	V = 0, 30, 50	S	EMs	PG; 0.4	TCh; 0.7	2	50	Vr.	NT
Bandyopadhyay et al. (2015)	ST	$\chi = 20-50$	D	Acc = 0.1 g	PG; 0.3	TCh; NS	NS	65	42	NS
Otsubo et al. (2016)	ST	V = 0, 30, 50	S	Max = 0.4 g	PG; 0.2	TCh; 10.64	50	30	250	NS
Bahadori and Manafi (2015); Bahadori and Farzalizadeh (2018)	ST	$\chi = 0-30$	S	Max = 0.2 g;	PG; 0.27	Pw, TCh; 30x10	37	NS	60	NS
Shariatmadari et al. (2018)	THC	V = 0-25	SUC	NS	PG; 0.55	GR; 1.79	3	54.5	Vr.	0-400

Note: CT = Cyclic Triaxial, ST = Shaking table; OT = Online test; THC = Torsional hollow cylinder;  $\chi$  = Gravimetric proportion; V = volumetric proportion; CP = Cell pressure; RD = Relative density; SCC = Strain controlled cycles; PWP = Pore water pressure; SUC = Saturated undrained consolidated; SDU = Saturated drained unconsolidated; D = Dry; S = Saturated; EMs = earthquake motions; Di = Diameter; PG = Poorly graded; GR = granulated rubber; RF = Rubber fibres; TCh = Tyre chips; SS = Sohma sand; Sh = Shredded; Pw = Powder NS = Not specified; NT = Not tested; Vr = Variable

**Table 3.8:** Studies on seismic performance of RSm

Reference	Apparatus	RC	$D_{50,sand}$ (mm)	$D_{50,rubber}$ (mm)	Remarks
Hazarika et al. (2006); Hazarika et al. (2008b); Hazarika et al. (2008a)	ST	$\chi = 100$	No. 5 Sohma Sand	TCh; D = 2	-TCh as backfill material resulted in a significant reduction of the dynamic motion and the accumulated PWP compared to sand
Hyodo et al. (2007)	CT	V = 0-100	0.4	TCh; 0.655	-Adding TCh controlled excess of PWP and this behaviour was marked at $\chi > 30\%$ . Liquefaction was not observed in mixtures at $\chi > 50\%$ up to 50 SCC
Promptthangkoon and Hyde (2007)	CT	V = 0-15	0.7	TCh; 1.2	-Liquefaction resistance of sand improved adding only 1% of rubber and then decreased at higher $\chi$
Kaneko et al. (2013)	OT	V = 0, 30, 50	PG; 0.4	TCh; 0.7	-Introducing TCh underneath the soil layer improved the liquefaction resistance of soil and shifted the period of the input motion attenuating the shear waves coming from seismic event. Effectiveness developed by placing the mixture at a deeper location or by increasing the thickness of the RSm layer
Bandyopadhyay et al. (2015)	ST	$\chi = 20-50$	PG; 0.3	TCh; NS	-Base isolation system worked by shifting the natural frequency of the signal and by attenuating the amplitude of the same with 20 mm of RSm layer. System appeared to be ineffective at <0.6g but the opposite occurred at >0.6g
Otsubo et al. (2016)	ST	V = 0, 30, 50	PG; 0.2	TCh; 10.64	-Significant reduction in the accumulated PWP and floating displacement as a consequence of compressibility and interlocking effects between particles. Optimum layer size of 10 cm placed underneath the studied soil
Bahadori and Manafi (2015); Bahadori and Farzalizadeh (2018)	ST	$\chi = 0-30$	PG; 0.27	Pw and TCh; 30 x 10	-Important reduction in accumulated PWP revealed adding 10% of Pw and TCh. G increased adding Pw and the opposite with TCh. $\xi$ value increased with $\chi = 20\%$ Pw and 10% TCh
Shariatmadari et al. (2018)	THC	V = 0-25	PG; 0.55	GR; 1.79	-Shear strength decreased with $\chi$ . Similar liquefaction resistance is found at CP = 110-260 kPa what reveals high liquefaction resistance of RSm. Adding between 10-25% decreases the liquefaction resistance of sand

*Numerical studies on RSm*

Tsang (2008), Xu (2009) and Tsang et al. (2012) focused on the design of soil foundations consisting of recycled scrap tyre/sand to mitigate the action of seismic motions on low-to-medium rise buildings in developing countries. In Tsang et al. (2012), 2D finite element simulations were conducted to calculate the soil-foundation-structure interaction in response to input seismic motions. An equivalent linear approach was adopted to simulate dynamic soil properties adopted from experimental testing undertaken by Zheng-Yi and Sutter (2000) and Xiong and Li (2013). The parameters considered for evaluating the effectiveness of the system were a) thickness of RSm foundation, b) building width, c) number of building storeys and d) type of seismic motion. A typical residential building was used as reference, with 10 stories and 40 m width, whilst the soil foundation was replaced by RSm layers with a minimum thickness of 10 m. On average, a reduction of between 40 and 60% of horizontal accelerations at the roof and floor were attained adding  $\chi = 75\%$ . The horizontal layer thickness was the main factor influencing the wave scattering, as observed in Table 3.7. A correlation between period lengthening and average reduction in horizontal accelerations was established. Hence, the increase in RSm thickness would lead to a rise in the soil natural period, which led to a greater reduction in the horizontal accelerations.

Brunet et al. (2016) studied the response of RSm soil foundations by simulating the inelastic soil behaviour of RSm. Poorly graded dry sand at various sizes were combined with particulate granular rubber. Specimens contained  $\chi = 0 - 35\%$  at a unique confining pressure of 100 kPa and compacted to a high relative density. A two story building with an inter-story height of 2.5 m was simulated on top of the modified soil foundation. The effectiveness of the system did not arise until peak ground accelerations were higher than 0.2 g, from where transmitted accelerations were highly attenuated. The study thus confirmed that it is a combination of rubber deformation and the resultant non-linear behaviour of RSm, under the action of strong ground motions, that mitigates the input motions. A limiting thickness of 2-3 m and 25 % of rubber were suggested to achieve large reductions in the structural response and minimize the settlement of rubber. An

enhancement in cyclic performance was observed with larger sand particles, i.e.  $S_R < 1$ .

[Tsang and Pitilakis \(2019\)](#) is the last known study on RSm to investigate the interaction soil-foundation-structure. A lumped-mass parameter model was adopted to idealise the response of a superstructure embedded within a viscoelastic half-space that represented a shallow foundation. The superstructure was then modelled as a SDOF represented by a mass-spring-dashpot system which accounts for both the horizontal and the rocking stiffness as well as radiation and material damping. The dynamic soil properties of both sand and RSm were simulated based on the results presented by [Senetakis et al. \(2012b\)](#) and a five-story building was built on top of the modified RSm foundation. Following the limiting aspects accounted by [Brunet et al. \(2016\)](#), a 2 m RSm layer was simulated to be placed underneath the structure, adding up to 30 % of rubber and with size ratio greater than 1, subjected to a mean confining pressure of 70 kPa. The novelty of this study stems from combining the experimental testing gathered in the past twenty years with the dynamic soil-structure-foundation interaction and the concept of rocking isolation. An augmented rocking isolation was revealed with reversible effects, attributed to the high elasticity of rubber, that enhanced the overall energy dissipation. An average reduction of 50-60 % of the resultant displacement, total acceleration and base moment were observed. The idea behind the mechanism presented in this study relies fundamentally on the foundation response represented by its translational and rotational displacement.

The only few experimental studies that have studied the seismic hazard at the surface level have demonstrated the successful reduction of both horizontal and vertical accelerations when incorporating RSm. However, a unique design configuration has been proposed in existing research whereby RSm horizontal layers are constructed before the superstructure. This construction design incurs, however, two issues: a) a limiting vertical load on top of the foundation due to the potential static settlement of the highly deformable rubber and b) the nature of the concept precludes its implementation to existing constructions, as occurs with typical base isolation systems. An alternative design is proposed in this investigation as part of Chapter 6 to retrofit the soil foundation and thus, alter its cyclic response.

### 3.6 Summary

The classification of system variables, parameters and material properties has been utilised to clarify the various comparisons of constitutive frameworks through which to more rigorously describe the behaviour of RSm. With the aim of this scheme, these are the main findings:

- Bulk parameters are influenced by bulk properties (macro-structure) and particle properties (micro-structure) of the binary RSm skeleton. The presence of rubber, that deforms and bends under loading, introduces an additional complexity to the conceptual framework to explain the soil behaviour under static and dynamic loading.
- Adding tyre derived aggregates point to an increase in soil strength whereas rounded tyre crumbs do not have a significant effect on its strength. RSm present a higher compressibility with rubber content and addition of smaller particles.
- Particle properties, e.g. rubber content and size ratio, and test conditions, e.g. confining pressure, appear to have a significant effect on the dynamic properties of RSm comprising particulate rubber.
- Although existing research has extensively demonstrated the increase in liquefaction resistance by adding rubber, there are discrepancies in relation to the cyclic effect on the evolution of shear modulus and damping ratio of saturated specimens.
- Ground-borne vibrations can be mitigated with the addition of wave barriers within the soil deposit. The concept of soft zones was proposed to attenuate seismic motions through the creation of low stiffness layers within the soil foundation.
- Existing literature has proposed the use of RSm as a geotechnical isolation system due to its high flexibility and damping capacity. The efficiency of the system is found to improve with rubber amount and increasing thickness or depth of RSm layer.
- The majority of previous investigations rely, however, on the design of horizontal layers placed underneath the structure. This solution precludes its installation to existing buildings and limits the maximum vertical load due to potential settlement.



## *Micro to macro behaviour of RSm*

---

### **4.1 Introduction**

RSm differ from conventional soils due to the presence of deformable particles. An extensive research on the static (monotonic) behaviour and bulk parameters of RSm has been undertaken. However, the micromechanics of RSm is not well understood and the research done on this field is scarce. Whilst not pretending to be a fully-fledged micromechanical analysis, this chapter presents some early and simple experiments devised to reveal in a heuristic way the behaviour of RSm under cyclic loading. The objective is to understand how the micromechanics of a rigid (sand) deformable (rubber) mixtures influences the compressible and stress-strain behaviour.

The properties of both mineral soils, rubber particles and the mixtures are considered. The mixture composition, i.e. gravimetric and volumetric proportion, is also described to establish the common grounds for comparison between specimens with different rubber contents. The testing done includes plain strain visualisations of combined stiff and deformable particles, representing RSm specimens, where the effect of deformable particle shape is studied. One-dimensional compressive behaviour of specimens containing crumb and shred particulate rubber is evaluated through constant and varying amplitude tests performed in the oedometer. 3D x-ray tomographic tests are analysed to quantitatively determine the evolution in contact area and void ratio of RSm to understand the energy dissipation mechanisms at a particle level.

## 4.2 Plain strain visualisations

Plain strain visualisations were carried out in an attempt to understand qualitatively the interaction between a combination of soft versus stiff particulate materials under one-dimensional load and lateral deformation constraint. Rubber particles were shaped into shred and crumb form whereas acrylic discs were used to represent sand particles. A compressive normal load was applied to be the upper boundary. Samples were manually formed before applying the uniaxial compression. Figures 4.1a and 4.1b show two tests: first corresponding to elongated rubber shreds and second to rubber crumbs.

### 4.2.1 Equipment, materials and methods

Rubber crumbs had an aspect ratio between 1.0 and 1.5 while size ratio between rubber and acrylic discs was approximately 1.0. Rubber shreds had an aspect ratio between 5 and 6 while size ratio between shreds and acrylic discs varied between 2 and 3. Both samples were prepared at a rubber percentage equivalent to 30%, in terms of volumetric proportion. The samples were held in plane strain condition by apparatus used for the experiments consisting of an A4-size acrylic sheet with PVC flat bars used as lateral boundaries (Figure 4.1a). Two vertical flat bars made of PVC of 20 mm width and 2 mm thickness were fixed to the sides of the acrylic base. A similar PVC flat bar was fixed horizontally to the bottom to provide a fixed base. Loading in the normal direction was carried out by moving an additional "top" PVC bar attached to a sliding slot along the lateral (fixed) boundaries that enabled accurate control of the specimen's vertical dimension. Due to the geometry of rubber and acrylic particles, any deformations in the out of plane direction were prevented and plane strain conditions were guaranteed.

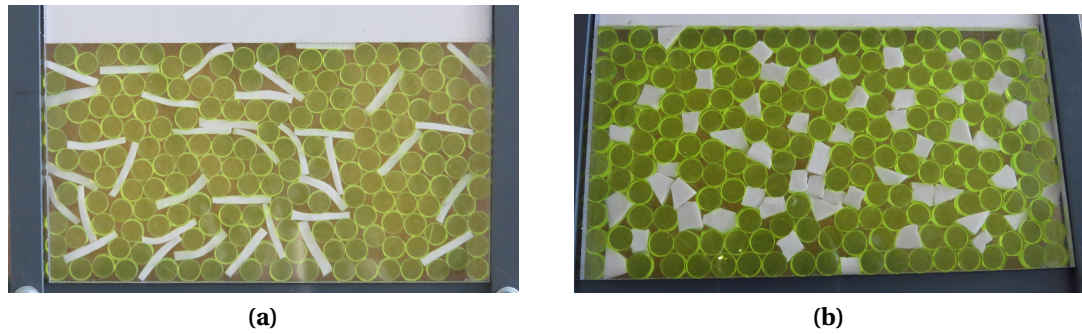


**Figure 4.1:** Plain strain test on sand with a) shredded rubber particles and b) crumb rubber particle

### 4.2.2 Results and discussion

Research to date (Edil and Bosscher, 1994; Sheikh et al., 2012) has demonstrated that the combination of sand particles with tire shreds can lead to a shear strength improvement. This is attributed to an increase in the apparent cohesion due to the interlocking between particles as it occurs in fibre reinforced soils. However, this has only been demonstrated through experimental investigations where particle interaction cannot be visualised (Zornberg et al., 2004). This experiment shows the development in the particle re-arrangement from a visual point of view:

#### *Elongated particles*

Figures 4.2a and 4.2b show one-dimensional compression tests on ShR-acrylic discs before and during loading, respectively. Figure 4.2a illustrates large initial voids between rubber and stiff particles due to the elongated nature of rubber particles and the initial low stress condition. Two main processes can be observed during the sample compression (Figure 4.2b): a) particle rearrangement and b) bending and deformation of rubber particles. In other words, due to high stiffness of acrylic particles, the compression increases the particle interlocking and increases contact surface areas. It is also observed there is more inter-particle sliding on acrylic discs than in rubber particles which leads to a reduction in the size of voids. Under high vertical stress, rubber particles become trapped between rigid sand particles, deform and store energy.

During loading, it can be observed that rubber wraps around acrylic particles in the same way as a tensile reinforcement. This would be consistent with an improvement in the shear strength as well as the reduction in the shear stiffness of RSm when adding more rubber, e.g. [Zheng-Yi and Sutter \(2000\)](#) and [Ehsani et al. \(2015\)](#).

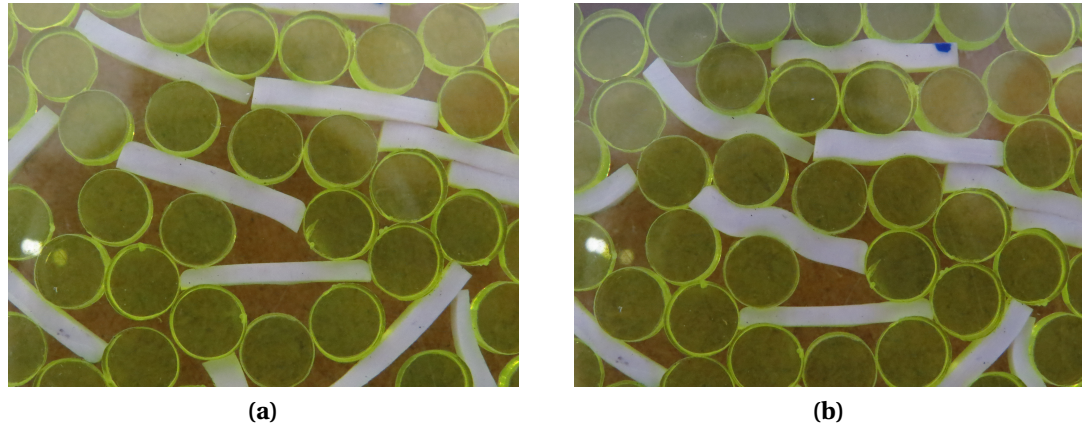


**Figure 4.2:** Plain strain test with shredded rubber a) before and b) during loading

### *Crumb particles*

Figures 4.3a and 4.3b illustrate the plain strain compression of crumb rubber and acrylic discs before and during loading. Initially, loose, the size of voids compared to the shredded rubber test (Figure 4.2a) appears lower which can be attributed to the rounded rubber shape and the relatively similar size ratio between stiff and soft particles (Figure 4.3a). The compression of the sample causes a reduction in voids due to the high deformability of rubber (Fig. 4.3b). Increased contact areas are also observed but to a lesser extent.

The similar particle size ratio restricts the extension of crumb material, in contrast with the shred particles shown in Figure 4.2b, resulting in less deformation of rubber particles. Additional tensile reinforcement is therefore not significant. This would corroborate the statements made by [Masad et al. \(1996\)](#), [Youwai and Bergado \(2003\)](#) and [Sheikh et al. \(2012\)](#) who addressed a reduction in the peak shear strength with the addition of tire crumbs. Elastic stored energy is expected to be lower due to the smaller deformation undergone by rubber crumbs in comparison to shred particles (Fig. 4.2b). In this case, the stored energy under deformation of particulate rubber can be associated with both the bending and the isotropic compression. Due to the simplicity of the test,

it is not possible to quantify which type of compression has a greater contribution to the stored energy. However, and based on the visual observations, it can be said that more bending and thus more energy is expected to be stored in mixtures containing rubber shreds, whilst a higher isotropic compressions should be observed in mixtures containing rubber crumbs.

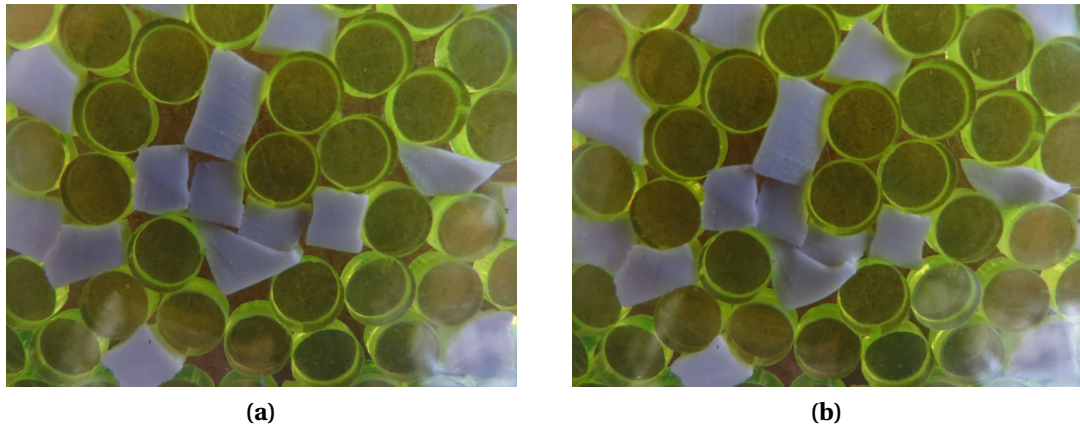


**Figure 4.3:** Plain strain test with crumb rubber particles a) before and b) during loading

Consequently it can be stated that from a visual point of view that rubber shape has an effect on the one-dimensional compression. Compared to crumb rubber particles (Section 4.3b), rubber shreds seem to contribute more towards stress transmission as evidenced by the change in shape of the particles and the increase in the contact area. The compression of the sample is shown through plain strain tests to be a consequence of both the particle rearrangement and deformation of particulate rubber.

On the other hand, the acrylic discs, that represent the incompressible particles, do not suffer from any deformation. Signs of tensile elongation and tensile reinforcement are observed in shredded rubber particles, whereas a lesser deformation and bending is found in crumb particle, possibly as a consequence of the relatively similar mean size. These observations are in line with results from previous studies using oedometer tests, shear tests or triaxial tests which demonstrate the increase in the shear strength when using elongated tyre derived aggregates (Edil and Bosscher, 1994; Zornberg et al., 2004) in contrast to those which showed a reduction in the shear strength when adding rubber crumbs (Youwai and Bergado, 2003; Sheikh et al., 2012).

## 4.3 Materials

The materials used during the experimental programme of this study, which results are analysed in Chapters 4 to 7, are discussed in this section. This includes a description of both Leighton Buzzard sand and the particulate rubber, obtained from recycled scrap tyres, contained within the rubber-soil mixtures. The composition of RSm, showing the determination of both minimum and maximum density, is also reviewed to establish the main methods for comparison and evaluation of the results adopted in every set of experiments.

### 4.3.1 Sand

The rigid incompressible particulate soil used in this study was a coarse rounded to sub-rounded Leighton Buzzard sand (Figure 4.4). The specific gravity of this material,  $G_s = 2.68$ , was determined in accordance with [ASTM D854 \(2014\)](#). Results of a sieve analysis conducted using [ASTM C136 \(2006\)](#) are illustrated in Figure 4.5. The coefficient of uniformity ( $C_u$ ) and coefficient of curvature ( $C_c$ ) have been calculated and presented in Table 4.1. Based on these results, LBS is poorly graded. A coefficient of friction  $\mu = 0.24$  is attributed to LBS as determined in the literature ([Senetakis et al., 2013](#); [Lopera Perez et al., 2016](#)).

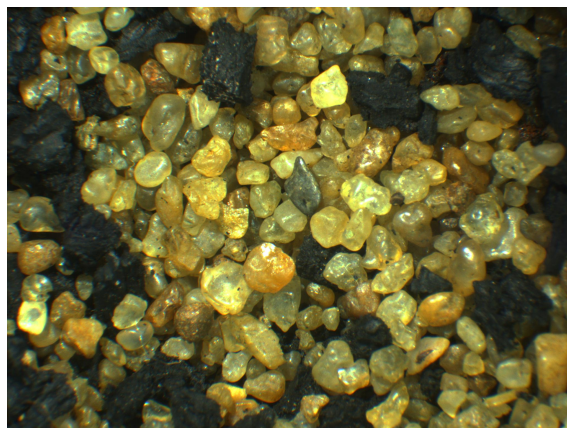
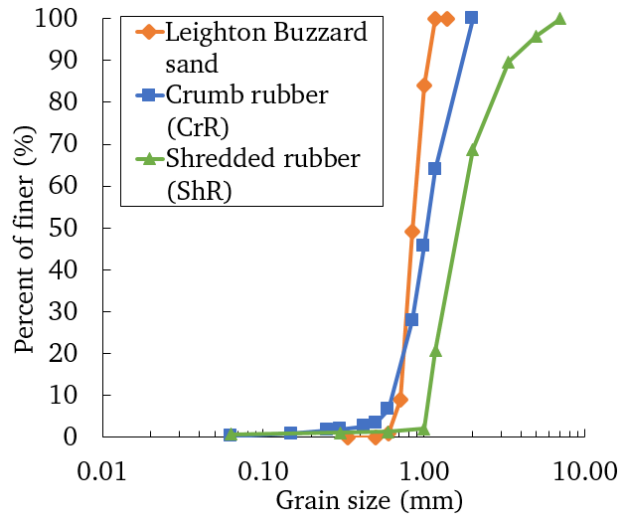


**Figure 4.4:** Microscopic image of Leighton Buzzard sand

Table 4.1 presents a summary of the material properties corresponding to LBS and the particulate rubber used in this investigation. The aspect ratio, equivalent to the ratio



between length and width, is approximately 1. The particle shape, i.e. sphericity and roundness, has been determined in accordance with the expressions adopted by [Cho et al. \(2006\)](#). The diameter of the inscribed and circumscribed spheres was measured using © ImageJ. As a consequence of the uniformity in the particle sizes, a total of ten measurements were sufficient to calculate the sphericity and roundness with an overall variation of  $\pm 5\%$  in the average value.



### 4.3.2 Rubber

Scrap tyres are composed of vulcanised rubber, steel belts and wire-reinforced rubber beads. One of the main elastomers available in a typical rubber tyre, synthetic rubber, commonly known as styrene butadiene, accounts for 55% of the total weight, and other natural rubbers make up the remaining 45 % (Danon and Görgens, 2015).

From the composition of rubber tyres (Table 4.2), an important content comes from the carbon black, used to increase the resistance to abrasion and strengthen the rubber. Acetone extract and other oils are a mixture of aromatic hydrocarbons commonly added to increase the compressibility and thus the workability of the material. Sulphur is the vulcanising agent employed to cross-link the polymer chains within the natural and synthetic rubber in order to reduce the excessive deformation at elevated temperatures. The resulting combination of all these elements gives rise to a highly durable and resistant material ideal for use as a road transport tyre (South et al., 2001).

**Table 4.2:** Composition of scrap tyres used in this study (South et al., 2001)

Ingredient	Minimum Content (%)
Polymer content (natural and synthetic rubbers)	55
Acetone extract	5-20
Carbon black	25-35
Sulphur	1-3
Zinc Oxide	2.5

The recycled rubber used in this thesis was obtained from car tyre sidewalls. Once all steel belts were removed, the rubber was devulcanised and subsequently mechanically shredded to the desired particle size range. Two particle forms, elongated and rounded, have been used in this study to investigate the effect of rubber shape on the particle interaction between rigid (sand) and deformable (rubber) particles. Both rubber shapes have the same specific gravity due to being obtained from the same scrap tyres (Edil and Bosscher, 1994; Sheikh et al., 2012). In terms of coefficient of friction,  $\mu = 1$  is attributed to the two particles (Valdes and Evans, 2008; Lopera Perez et al., 2016), which is around four times higher than the value obtained for LBS.



Elongated particulate rubber presents an average particle size  $D_{50} = 1.62$  mm (Figure 4.5) and an aspect ratio between 2 and 6. Due to the small size of these particles compared to traditional tyre shreds or chips, they are classified as rubber fibres in accordance with ASTM D6270 (2017). These are the resultant particles after producing large tyre shreds, reason why they exhibit the shape of small elongated particles (Figure 4.6a). This is also demonstrated based on the low sphericity presented by these particles, i.e. 0.18. Hence, this study has decided to denote them as shredded rubber (ShR) in order to be differentiated from granular rubber. The ShR thickness has been limited to 1 mm. On the other hand, rounded rubber particles have an average particle size  $D_{50} = 0.83$  mm. Based on the results shown in Table 4.1, crumb particles present a high sphericity and roundness and they are classified as ground rubber (ASTM D6270, 2017). Hence, crumb rubber (CrR) is the name adopted in this study to refer to these rounded particles. CrR is characterised by an aspect ratio of approximately 1.

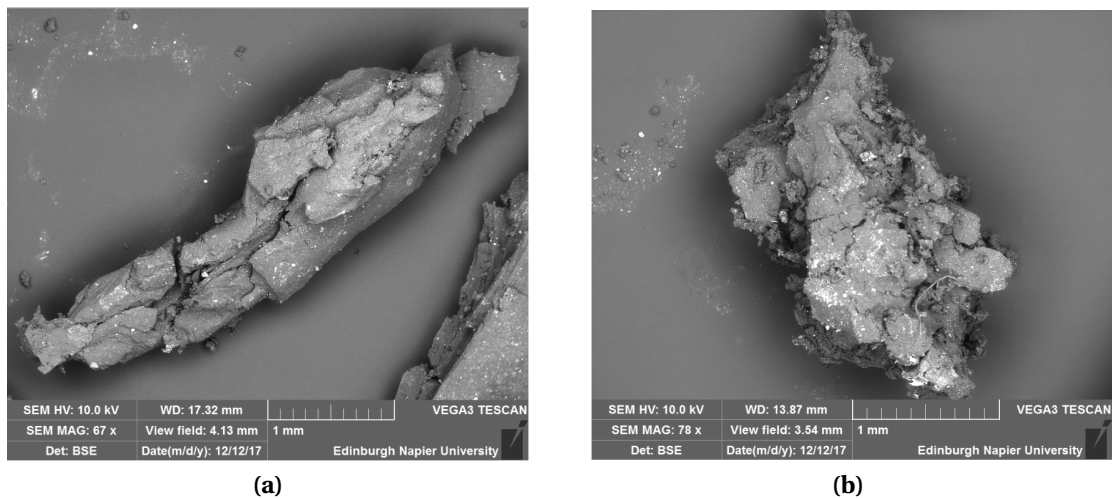


**Figure 4.6:** Microscopic images of a) shredded rubber and b) crumb rubber particles

Rubber soil mixtures differ from more conventional soils in the fact that they are essentially binary mixtures, in which nature and form of the mixture components can exhibit a higher variability. For this reason, it is important to consider and distinguish between size and aspect ratio. The size ratio is commonly calculated as the ratio between the mean size ratio of particulate rubber in relation to the main incompressible soil, in this case sand. This material aspect is commonly adopted in the existing research

on RSm as a conventional method for comparison to evaluate the mechanics of RSm (Kim and Santamarina, 2008). In this study, the size ratio is around 2 for ShR and sand, whereas a size ratio of around 1 is obtained between CrR and sand.

Contrary to the conventionally adopted approach to classify RSm, this study acknowledges that the size ratio presents limitations when considering the incorporation of elongated particles such as ShR. The calculation of particle size distribution using ASTM D854 (2014) does not present a realistic distribution of mixtures containing shredded rubber. Thus, an alternative particle property shall then be considered to account for the different particle shape and the ratio between particles. This study also proposes the adoption of the relative aspect ratio between deformable and rigid particles. Due to the relatively similar size of both CrR and LBS, the aspect ratio of these particles is approximately 1 whilst the aspect ratio of shredded rubber moves between 2 and 6. This approach provides with a more realistic representation of the size of shredded rubber. For comparison purposes, however, this study has also maintained the commonly adopted procedure to determine the particle size distribution and the size ratio of RSm and thus compare the differences in compressibility as well as cyclic behaviour of mixtures containing different rubber size and shape.

### **4.3.3 Rubber-soil mixtures**

Rubber-soil mixture (RSm) is obtained from mixing rigid incompressible soils with deformable particulate rubber (Zornberg et al., 2004). In chapter 4, this investigation distinguishes between shredded rubber-Leighton Buzzard sand mixtures (ShRm) and crumb rubber-LBS mixtures (CrRm) to compare the effect of particle size/shape. From Chapter 5 onwards, the nomenclature RSm is used for simplification referring to mixtures containing ShR. This section describes the composition followed for the classification of RSm in terms of mass, volume and relative density.

**Composition**

The composition of RSm is obtained from the combination of sand and rubber masses for a specific specimen volume. Hence, the composition has been set by defining the gravimetric proportion ( $\chi$ ) of rubber  $R$  in the mixture as:

$$\chi = \frac{m_R}{m_S + m_R} \quad (4.1)$$

Where,  $m_S$  is the mass of sand in the sample  
and  $m_R$  is the mass of rubber.

Volumetric proportion can be also determined based on the value of the specific gravity and the mass of each material. The volume of RSm is obtained from:

$$V_{RSm} = \frac{m_S}{G_{sS}} \left( \frac{1}{\rho_w} \right) + \frac{m_R}{G_{sR}} \left( \frac{1}{\rho_w} \right) \quad (4.2)$$

Where  $G_{sS}$  is the specific gravity of sand,  $G_{sR}$  is rubber specific gravity,  $\rho_w$  is the density of water ( $1g/cm^3$ ).

RSm volume can also be expressed in terms of specific gravity ( $G_{sRSm}$ ):

$$V_{RSm} = \frac{m_t}{G_{sRSm}} \left( \frac{g}{\gamma_w} \right) \quad (4.3)$$

Where  $m_t$  RSm total mass including  $m_S$  and  $m_R$ .

The volumetric proportion of rubber ( $V$ ) with respect to the total amount of volume is adopted by numerous studies in the literature and here is also defined for comparison purposes. The corresponding volumetric proportion is determined from:

$$V = \frac{V_R}{V_R + V_S} = \frac{\frac{m_R}{G_{sR}}}{\frac{m_R}{G_{sR}} + \frac{m_S}{G_{sS}}} = \frac{\frac{m_R}{G_{sR}}}{\frac{m_t}{G_{sRSm}}} \quad (4.4)$$

Where  $V_R$  is the rubber volume and  $V_S$  is the sand volume.

RSm specific gravity ( $G_{sRSm}$ ) can be determined by re-arranging Equations 4.1, 4.2, and 4.3 as follows:

$$G_{sRSm} = \frac{1}{\frac{(1-\chi)}{G_{sS}} + \frac{\chi}{G_{sR}}} \quad (4.5)$$

RSm comprising variable rubber content have been tested throughout this study to understand the micro and macro behaviour of the mixture, varying from sand only to rubber only specimens. The results of the expressions corresponding to gravimetric (Equation 4.1), volumetric proportion (Equation 4.4) and specific gravity (Equation 4.5) of the mixtures tested in this study are presented in Table 4.3. The values of rubber content in this investigation are principally determined as a function of the rubber mass and therefore constitute an objective unit of comparison. Furthermore, most of the existing literature on the behaviour of RSm (Anastasiadis et al., 2012b; Ehsani et al., 2015) presents rubber content by mass and thus it makes sense to follow conventional/standardised methods for evaluation and comparison of the results.

As established in previous studies (Lee et al., 2007), the increase in rubber content leads to a significant increase in the rubber volume, as a consequence of its lower specific gravity when compared to sand (Table 4.3), and subsequently a foreseeable decrease in the mixture density. This is the reason why this investigation has adopted an additional material descriptor, i.e. relative density, to ensure the comparison between mixtures containing different rubber content. In this regard, the relative density is established in the literature (Mashiri, 2014) to be an adequate approach which requires of the previous determination of both minimum and maximum density. These will be calculated in the following sections.

**Table 4.3:** Composition of rubber-soil mixtures

Specimen	$\chi$	$V$	$G_{sRSm}$
0RSm	0	0	2.65
10RSm	0.10	0.21	2.33
15RSm	0.15	0.29	2.2
20RSm	0.20	0.38	2.08
30RSm	0.30	0.51	1.88
45RSm	0.45	0.66	1.64
100RSm	1	1	1.12

*Minimum density*

According to BS 1377-4 (1990), the sample was introduced in a glass cylinder and allowed to fall freely so that the air was entrapped between the soil particle, creating the maximum number of voids. A representative test sample of 1000 g and a 1 l glass cylinder, graduated to 20 ml, were employed for the test. After the sample was introduced in the container, the cylinder was turned in several occasions and then the sample was kept flat to record the volume reading. Ten tests were performed and the maximum volume was recorded. Minimum density of RSm was determined as follows:

$$\rho_{min} = \frac{m}{V} \quad (4.6)$$

Where  $m$  (g) is total mass of the sample, and  $V$  ( $m^3$ ) is the greatest of 10 volume readings recorded to the nearest 10 ml within the glass cylinder.

A similar procedure was adopted to determine RSm minimum density, with the only difference that 2.5% moisture was added to the sample in order to avoid excessive segregation. Ten tests were then performed on each RSm mixture to obtain the maximum volume and thus calculate the minimum density for each RSm. Masses of rubber ( $m_R$ ) and sand ( $m_S$ ) used for each sample are listed in Table 4.4.

Table 4.4 shows the minimum density of RSm samples, calculated using Equation 4.6, and the total masses of each sample. The results show that RSm minimum density ( $\rho_{min}$ ) decreases with the addition of rubber particles until  $\chi = 30\%$  (Fig. 4.7), attributed to their lower specific gravity in comparison with sand specimen.

**Table 4.4:** Minimum density of RSm

Test	$m_S$ (g)	$m_R$ (g)	$\chi$	$V$	$m_t$ (g)	$\rho_{min}$ ( $g/cm^3$ )	$G_{SRSm}$	$e_{maxRSm}$
0RSm	1000	0	0	0	1000	1.47	2.65	0.80
10RSm	879.3	97.7	0.10	0.21	977	0.97	2.33	1.41
20RSm	792	198	0.20	0.38	990	0.78	2.08	1.67
30RSm	695.8	298.2	0.30	0.51	994	0.67	1.88	1.80

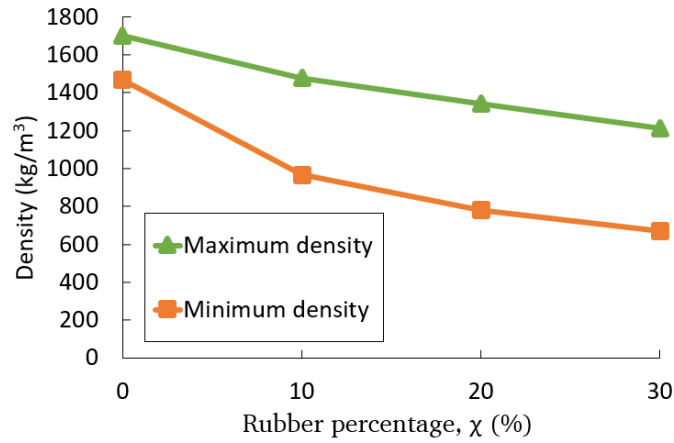


**Figure 4.7:** Maximum and minimum density of RSm

### *Maximum density*

According to BS 1377-4 (1990), RSm maximum density was determined by means of compacting the soil sample with a vibrating hammer. Sand specimens were tested under water. A 4 l mould was introduced within a large container where the water level had to remain at the same level to ensure the correct compaction of the saturated sample. The sample was divided into three equal parts so that the compaction was conducted in various steps. A circular tamper was placed on top of the mould, and the sample was compacted with the vibrating hammer for 2 minutes during each compaction step. A steady downward force equivalent to 400 N was applied to the tamper and to the sample through the vibrating hammer. Once the third compaction step was completed, the surface of the sample was levelled with the mould body. Two samples were tested per material and the greater of the two dry masses was used to determine RSm maximum density ( $\rho_{max}$ ):

$$\rho_{max} = \frac{m}{V} \quad (4.7)$$

Where  $m$  (g) is the greater of the two dry masses of the soil compacted and  $V$  ( $m^3$ ) is total volume of the mould occupied by soil.

The same approach was adopted to determine  $\rho_{max}$  of RSm, with the difference of testing the material in moist conditions to avoid rubber particles to float, given its low specific gravity ( $G_{sR} = 1.15$ ). Two samples were tested per rubber composition resulting

in a total of six RSm compacted. Table 4.5 shows the average value corresponding to every specimen in which the greatest mass, including moisture, of each rubber inclusion was used to calculate RSm maximum density. Figure 4.7 shows that the value of maximum density  $\rho_{max}$  decreases with rubber addition, as seen with  $\rho_{min}$ .

**Table 4.5:** Maximum density of RSm

Test	$m_S$ (g)	$m_R$ (g)	$\chi$	$m_t$ (g)	$V$ (cm <sup>3</sup> )	$\rho_{max}$ (g/cm <sup>3</sup> )	$G_{RSm}$	$e_{minRSm}$
0RSm	3949	0	0	3949	2314	1.71	2.65	0.55
10RSm	3129.17	347.69	0.10	3476.85	2318	1.50	2.33	0.55
20RSm	2477.28	619.32	0.20	3096.6	2318	1.34	2.08	0.56
30RSm	1957.41	838.89	0.30	2796.3	2318	1.21	1.88	0.56

### Relative density

The values of  $e_{min}$  and  $e_{max}$  have been obtained from:

$$e = \frac{G_{SRSm}\gamma_w}{\rho_{RSm}g} - 1 \quad (4.8)$$

where  $G_{SRSm}$  is RSm specific gravity,  $\rho_{RSm}$  is the dry density adopted for each RSm, and  $g$  is gravity.

Figure 4.8 shows the values of  $e_{min}$  and  $e_{max}$  corresponding to RSm. As observed, the maximum void ratio increases at greater rubber inclusions, whereas the minimum void ratio remains almost constant with the addition of rubber.

The term equivalent void ratio  $e_{eq}$  was proposed in previous studies (Zheng-Yi and Sutter, 2000; Anastasiadis et al., 2012a) to calculate the maximum shear modulus and thus reflect on the reduction in soil stiffness of RSm due to the low stiffness of rubber. Compared to the traditional calculation of void ratio,  $e_{eq}$  consider the volume occupied by rubber to be part of total volume of voids, whereas uniquely the volume occupied by sand contributes to the mixture stiffness, calculated as follows:

$$e_{eq} = \frac{V_v + V_r}{V_s} \quad (4.9)$$

As established in previous studies Pistolas et al. (2018), Figure 4.8 shows that  $e_{eq}$  increases as at higher rate than the maximum void ratio. In Chapter 7, Equation 4.9 is used

instead of the traditional calculation of void ratio to analytically calculate the dynamic soil stiffness and compare it with the empirical results obtained in Chapter 5.

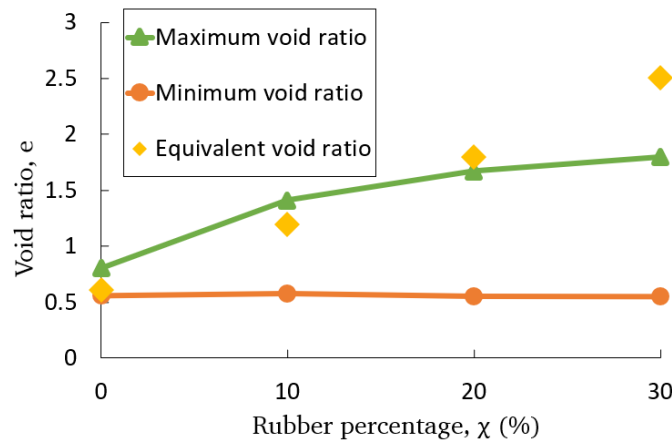


**Figure 4.8:** Maximum, minimum void ratio of RSm

### *RSm material descriptors*

As shown in Figure 4.7, both the maximum and minimum density of RSm decay with the rubber content. From there, the values of  $e_{min}$  and  $e_{max}$  have been obtained (Figure 4.8). This reflects the variability in the number of voids and the compaction state of the specimen with the rubber content. Therefore, these values were used as a reference for the sample preparation of RSm specimens to ensure a relatively similar relative density and thus constitute an objective unit of comparison. Different approaches were, however, adopted depending on the set of experiments and the objective of the programme. Here is a brief summary of the material descriptors used:

- Chapter 4; the main material descriptor is the gravimetric proportion which was achieved at a constant sample volume. Additionally, the sample compaction state was controlled to ensure a similar initial relative density,  $D_R = 57\text{-}64\%$ .

- Chapter 5; the main material descriptors are the gravimetric proportion, at a constant initial volume, and a dense initial relative density, i.e. 65-85%. This was undertaken for samples of both cyclic triaxial and resonant column tests.

- Chapter 6; the material descriptor is the gravimetric proportion reached by keeping a constant initial volume content. This is done to maintain the number of bags included in the soft zones whilst maintaining the rubber/sand mass ratio.



## 4.4 Oedometer tests

A series of compression tests with various unloading-loading cycles were performed using a conventional oedometer on specimens consisting of i) shredded rubber and Leighton Buzzard sand (ShRm), and ii) crumb rubber and Leighton Buzzard sand (CrRm). The objective is to gain a more quantitative understanding about the compressive behaviour of RSm at different gravimetric proportions and particle shapes. The shear stress - shear strain analysis compares the nature of RSm hysteretic behaviour.

### 4.4.1 Equipment, sample preparation and methods

#### *Equipment*

One dimensional compression tests were carried out in a 75 mm diameter by 20 mm height oedometer apparatus on RSm. The apparatus met the requirements established in [BS 1377-5 \(1990\)](#) with a maximum axial load capacity of  $\pm 1440$  kg, reached when the weight hanger is loaded at 10:1 ratio position. The vertical compression of the specimen was recorded using a linear variable differential transformer (LVDT) capable of measuring values with a resolution of 0.001 mm. Data acquisition was done by means of DS72 control software.

#### *Sample preparation*

RSm specimens were formed by adding rubber mass of ShR or CrR to sand depending on the gravimetric proportion as presented in [Table 4.6](#). Particulate soils were mixed under dry conditions and then spooned into the mould of the oedometer. To avoid segregation of RSm particles, a 2.5% moisture content was added to each specimen, being mixed uniformly. The thickness and length of both sand and RSm had a size lesser than 1/5 of the height of the ring in order to avoid the effect of particle size ([Head, 1994](#)). [Figure 4.9](#) shows a representation of the various distances recorded prior and during testing to calculate the initial height of the sample. The main objective of this chapter is to elucidate the effect of rubber content on the compressibility of RSm. Given the

significant increase in rubber volume due to lower specific gravity of rubber (Section 4.9), maintaining a similar height was required to ensure a similar initial sample volume, around  $90 \text{ cm}^3$ . Thus, the mixtures containing different rubber shape could be tested under similar initial conditions. In addition to this, the number of initial voids was also controlled in such a way that the relative density of both ShRm and CrRm was similar for the different rubber contents (Table 4.6). This does not only allow an objective comparison with studies in the literature but maintains the same compaction state to compare the different gravimetric proportions. As shown in Table 4.6, specimens containing either elongated or crumb exhibit a nearly similar initial void ratio ( $e_0$ ). Thus, the sample void ratio, corresponding to the average value of ShRm and CrRm, is plotted in relation to the minimum and maximum void ratio determined for RSm (Figure 4.10). It is observed that the value increases with rubber content as it occurs with the value of  $e_{max}$ . Using the expression of relative density presented in Chapter 2, this relationship is equivalent to an initial relative density of between 55-64% for all mixtures (Lambe and Whitman, 2010). This means that specimens tested with the oedometer apparatus were in a medium initial compaction state, enabling the comparison between the different rubber content and also rubber shape/size.

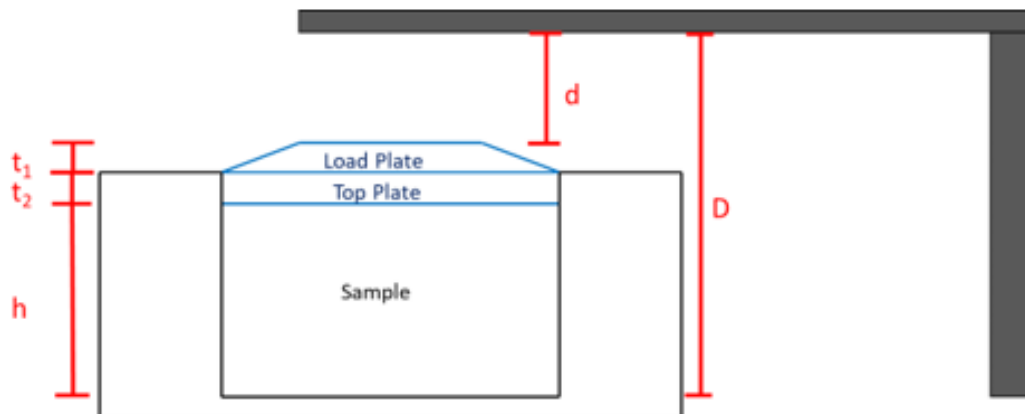


**Figure 4.9:** Conventional oedometer apparatus set-up

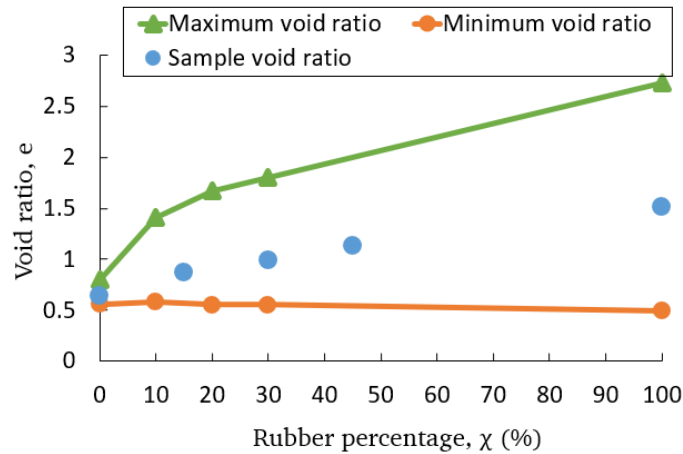


**Figure 4.10:** Sample void ratio for oedometer tests in relation to maximum and minimum void ratio

**Table 4.6:** Classification of specimens for oedometer tests

Test ID	Material	$\chi$ (%)	$e_0$
1-0ShRm	Leighton Buzzard sand	0	0.64
2-15ShRm	ShR:LBS	15	0.87
3-30ShRm	ShR:LBS	30	0.99
4-45ShRm	ShR:LBS	45	1.13
5-100ShRm	ShR	100	1.55
6-15CrRm	CrR:LBS	15	0.84
7-30CrRm	CrR:LBS	30	0.93
8-45CrRm	CrR:LBS	45	1.06
9-100CrRm	CrR	100	1.51

### Methods

The consolidation ring was the lateral confining device once the cell components were assembled after the specimen preparation. The porous plate and loading cap were placed on top of the specimen prior to the consolidation test. A small weight was then added to the beam hanger to maintain the contact between the loading cap and specimen, resulting in a pressure below 2 kPa.

Compression tests were carried out by doubling the increment of vertical stress applied to the sample, meeting the test procedure criteria defined in BS 1377-5 (1990). Samples were subjected to five load-unload cycles in which the vertical stress approximately doubled in each of the cycles from 20kPa up to 2231kPa, with unloading ramping

down to 20kPa. Readings were then noted before every load increment based on the values observed in the LVDT. Due to the rapid and significant deformation of RSm samples, readings were made more frequently, during the first minute, after every load application. Readings were then spaced to the point of taking one reading per minute for a period of five minutes. Table 4.6 presents a summary of oedometric tests performed on RSm. Each test was labelled with a test ID, which was noted as  $\chi$  (%) - and CrRm or ShRm. Whilst ShRm represents mixtures containing shredded rubber, CrRm refers to mixtures containing crumb rubber.

#### 4.4.2 Results and discussion

The effect of the gravimetric proportion ( $\chi$ ), rubber shape (shred or crumb) and vertical effective stress ( $\sigma'_v$ ) on the compressibility of RSm were investigated. The normalised change in void ratio ( $\Delta e/e_0$ ), accumulated plastic strain, compression and swelling indices ( $C_c$ ,  $C_s$ ), constrained modulus (M) and shear stress-shear strain behaviour were evaluated based on the results obtained applying loading-unloading cycles.

##### *Change in void ratio*

Figures 4.11a and 4.11b represent the change in void ratio of i) ShRm and ii) CrRm at  $\chi = 0, 15, 30, 45$  and 100%. Samples were subjected to five load-unload cycles.

The response of sand only sample is unsurprisingly stiffer than that of any RSm. An almost negligible change in void ratio is observed in sand with vertical stress. Given that mineral sand particles are assumed to be incompressible, the change in void ratio is uniquely due to particle rearrangement. Then, change in void ratio is more significant as rubber content increases, going down to  $\Delta e/e_0 = 0.72$  with the application of 20 kPa at  $\chi = 100\%$ . As observed with plane strain visualisations, the change in the void ratio of RSm during a compression test is a result of both particle rearrangement and deformation of rubber. However, and as seen in sand specimens, there is a small reduction in voids caused by particle rearrangement. Therefore, rubber deformability as well as the amount of both ShR and CrR has a significant effect on the compressibility.

Regardless of the rubber type, both figures show a similar behaviour. A near linear reduction in  $\Delta e/e_0$  is revealed with every loading stage. Except, when  $\chi > 45\%$  at high loads, the rate of change in the void ratio decreased. The behaviour is clearly non-linear. Such behaviour is consistent with the idea that RSm start to behave as solid material at very high stresses for any rubber percentage due to the significant particle rearrangement and the resultant reduction in the void ratio. Thus, it can be expected that at high stresses void spaces are negligible and behaviour is dominated by rubber.

The main difference between specimens containing ShR or CrR stems from the absolute change in the void ratio with rubber content and stress level. It is observed that mixtures consisting of ShR presents a greater reduction in number of voids than CrR specimens. The shape effect in the one-dimensional compression behaviour are more marked at  $\chi \geq 30\%$  ShR. These may be due to the greater bending and elongation of ShR in comparison with crumb particles, visually identified during the plane strain visualisations in Figures 4.2b and 4.3b. This result is in accordance with previous studies, e.g. Lee et al. (2010), which stated that the rubber-like behaviour, characterised for presenting lower shear moduli and a greater elasticity, more prominent at  $\chi \geq 30\%$ . At  $\chi = 100\%$  and 2200 kPa, both ShRm and CrRm seem to follow the same trend due to the negligible number of voids as a consequence of rubber deformation.

Although rubber is considered to present a high elasticity, Figures 4.11a - 4.11b show accumulated deformations on all loading cycles, even when it is dominated by rubber ( $\chi = 100\%$ ). This shows evidences of energy storage and dissipation in RSm in every loading-unloading-reloading. The area between each loading-unloading loop is a measure of energy dissipation. Thus, the energy dissipation is higher in the first cycle due to the larger accumulation of plastic deformation experienced by the mixture. The hysteretic behaviour, however, appears to be maintained even at very high stresses which contrasts with the minimum deformation and hence energy dissipation observed in sand only specimens.

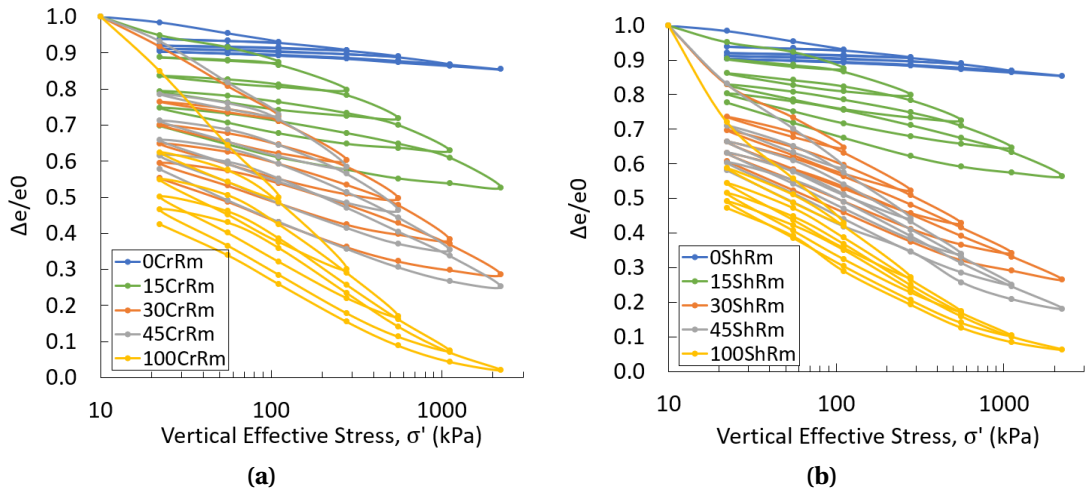


**Figure 4.11:** Change in void ratio with effective vertical stress of RSm with a) crumb rubber particles and (b) shredded rubber particles

### *Plastic strain*

As established in Chapter 2, plastic strain has been calculated by reporting the maximum axial strain recorded for every mixture after every loading/unloading cycle. This is done on the basis to elucidate the evolution in plastic deformation of RSm whilst increasing the normal stress in every loading-unloading-reloading cycles. Results seen in Fig. 4.12 show that sand, as expected, does not suffer from a significant deformation, reaching values of around  $\varepsilon_u = 3.7\%$ . The plastic strain increases with rubber amount and unloading cycles which corresponds to the increment in the vertical stress.

Figure 4.12 shows similar trends in evolution of plastic strain with number of unloading cycles and rubber percentage. Note that, the maximum irrecoverable deformations occur in the first cycle for all RSm. This reveals one of the main limitations in relation to the addition of rubber as part of soil foundations, which is the excessive settlement experienced by RSm (Edil and Bosscher, 1994). Although plastic strain increases after the first unloading cycle, this rise occurs at a much lower rate. For instance, 45% ShRm reaches  $\varepsilon_u = 19\%$  after one cycle and it goes up to  $\varepsilon_u = 24\%$  after five cycles. This increase in plastic strain with number of cycles is less prominent and rubber content decreases, as shown in Figure 4.12. The majority of the plastic deformation could therefore be minimised at any rubber percentage by pre-loading the mixture at stresses of  $\sigma \approx 100$  kPa.

This has been proposed in the literature to reduce the potential settlement of mixtures containing rubber crumbs (Sheikh et al., 2012) or tire shreds (Edil and Bosscher, 1994) by loading the specimens to a normal stress of up to 800 kPa.

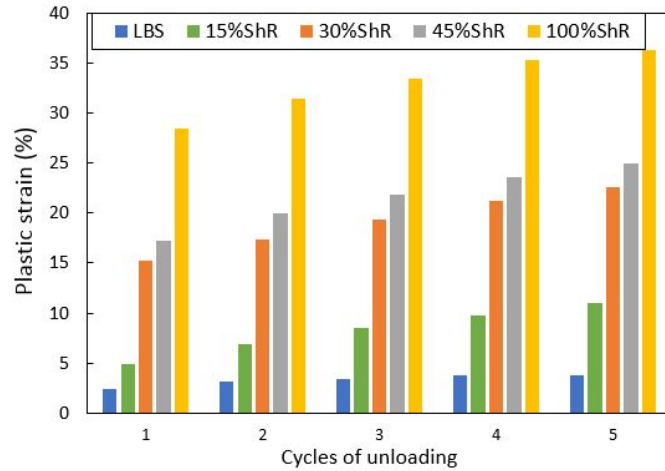


**Figure 4.12:** Plastic strain after each cycle of unloading

### *Compression/swelling indices*

Compression ( $C_c$ ) and swelling ( $C_s$ ) indices have been determined for every RSm specimen, containing either ShR or CrR, for the five loading-unloading sequences. The equations used to calculate these values have been described in the Chapter 2.

Figures 4.13a and 4.13b show the variation in compression index with rubber percentage and vertical effective stress. For both ShRm and CrRm, the value of  $C_c$  increases with the addition of greater rubber inclusions up to 1115 kPa as displayed in Fig. 4.11a. The compressibility of sand remains nearly constant with vertical stress resulting in a  $C_c \approx 0.05$ . This differs from the high compression index shown by any RSm ( $C_c = 0.1-0.9$ ) which suggests the high change in void ratio with every loading.

At  $\chi = 15\%$ , both ShRm and CrRm present a nearly similar behaviour showing an increase in compression index when applying higher vertical stresses. This reveals that the behaviour of the mixture is not influenced by the rubber shape and it is mainly governed by physical properties of sand. There is therefore a definite sand-like behaviour at low rubber percentages as observed in previous studies, e.g. Lee et al. (2007), Kim and Santamarina (2008) and Lee et al. (2010).

At  $\chi \geq 30\%$  and up to  $\sigma = 557$  kPa, ShRm present higher compression index than CrRm which can be related to the greater change in void ratio shown in Figs. 4.11a-4.11b. As seen in plain strain models, this can be linked to the entrapment suffered by shred rubber in-between incompressible mineral particles. This phenomenon, added to the elongated shape of ShR, results in an increase number of contacts causing a greater deformation compared to crumbs. Unlike the way it occurs in conventional mineral soils (sand), there is a significant reduction of  $C_c$  with vertical stress at  $\chi > 30\%$ . This demonstrates the high capacity of both crumbs and shreds to resist shear stresses, leading to an improvement in material stiffness.

At  $\sigma > 557$  kPa, the compression index reduces gradually until it converges to approximately the same value, i.e.  $C_c \approx 0.3$ . This shows the nearly similar stiffer response of both ShRm and CrRm under the action of very high stresses as a result of the negligible number of voids. As stated in previous studies (Platzer et al., 2018), a fraction of the porous spaces is occupied by the deformed rubber particles. This study proposes the existence of a ultimate state at which the compressive behaviour of RSm is controlled by rubber at any rubber percentage as clearly shown in Figures 4.13a and 4.13b.

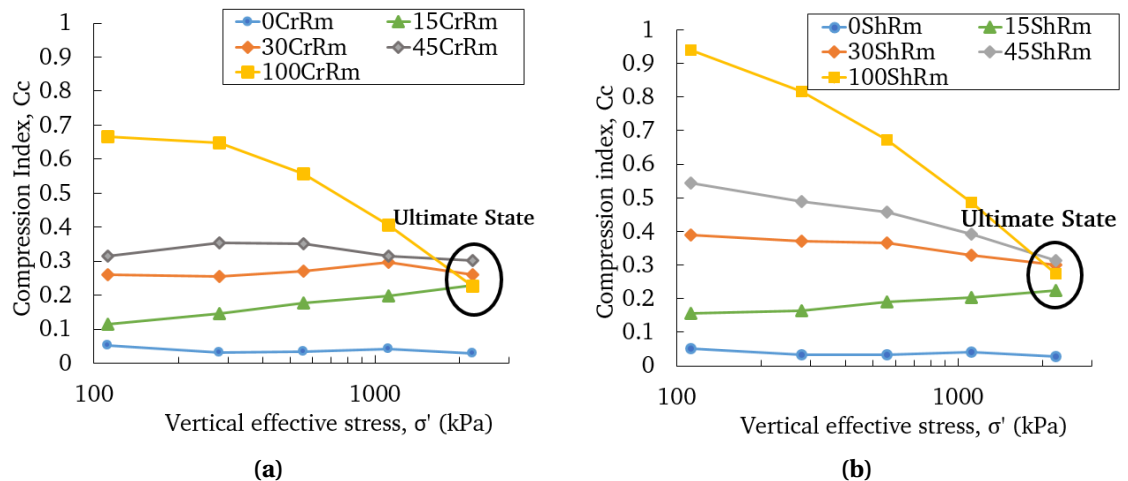


**Figure 4.13:** Compression index versus vertical effective stress of RSm with a) crumb rubber particles and b) shredded rubber particles

Figures 4.14a and 4.14b show the swelling indices of samples containing rubber crumbs and shreds, respectively. Similarly to  $C_c$ , RSm specimens present higher  $C_s$  values than sand only and this is more pronounced with additional rubber content.



The swelling index increases for CrRm at  $\chi = 15-45\%$  when applying higher stresses until  $\sigma = 2231$  kPa. Hence, the ability of crumb particles to recover part of the deformation improves with every loading sequence. On the other hand, this improvement in  $C_s$  is only observed on samples containing ShR at  $\chi = 15\%$ , or at lower vertical stresses  $\sigma = 111-557$  kPa. In other words, mixtures containing shreds develop its maximum capacity to elongate and recover the deformation at smaller stresses than with crumb rubber, which may be due to the initial level of entrapment and high contact area observed in the plain strain visualisations (Figure 4.2b).

By comparing Figure 4.14a and Figure 4.14b, it can be seen that  $C_s$  of samples containing ShR is substantially higher than with CrR. Note that, this study assumes the deformability of ShR and CrR to be the same given that both particles have been extracted from the same rubber tyres and they present a similar poisson ratio ( $\nu = 0.5$ ). The main difference between the two samples lies then in the rubber shape and, in consequence, the aspect ratio between deformable and rigid particles. The higher contact area between rubber shreds and acrylic discs compared to rubber crumbs (Fig. 4.2b) and the consequent higher shear deformation of rubber particles gives rise to a greater compressibility (Fig. 4.2b). The deformation suffered by ShR is then mostly recovered after unloading the material. This helps to explain why the swelling index is much higher with shreds than with rubber crumbs.

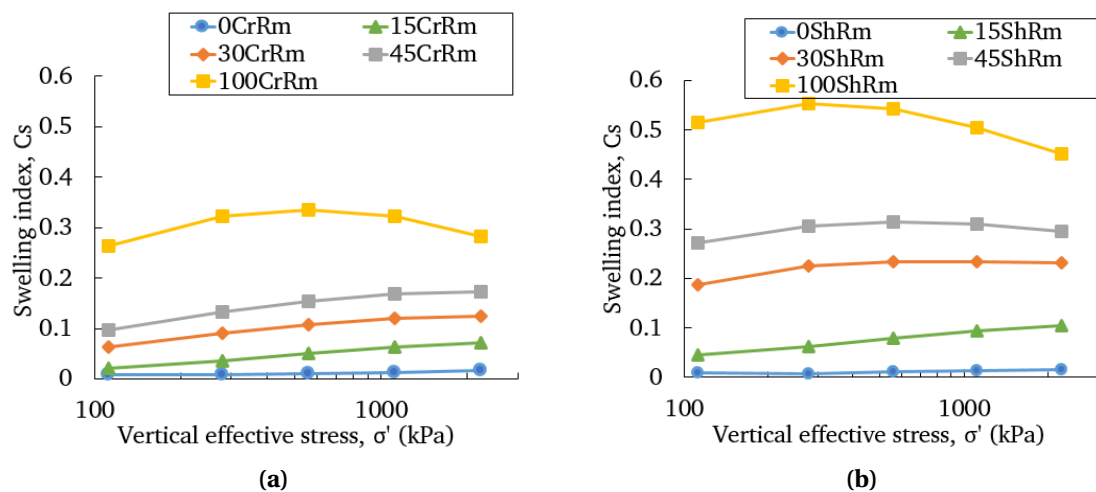


**Figure 4.14:** Swelling index versus vertical effective stress of RSm with a) crumb rubber particles and b) shredded rubber particles

***Constrained modulus***

Constrained modulus ( $M$ ) was obtained from the slope of stress-strain curve at each load increment for specimens containing ShR. Figure 4.15 shows the change in constrained modulus against vertical stress.

$M$  increases with vertical stress and decreases with rubber percentage. In comparison with other rubber contents,  $\chi = 15\%$  presents greater constrained modulus which can be attributed to the higher number of contacts between sand particles, as stated in previous investigations Lee et al. (2010). At higher rubber inclusions, it can be postulated that the primary load-carrying capacity is built between sand particles after the bending and deformation of rubber particles and that is why these samples present a significantly lower constrained modulus. This coincides with Lee et al. (2014) who stated that primary force chains are created between sand while rubber particles deform and fill the interfacial voids due to its lower stiffness.

Two behaviour can be found in the evolution in constrained modulus with vertical stress, i.e. sand-like and rubber-like behaviour. At low stresses ( $\sigma = 100\text{-}200$  kPa) sand-like behaviour is observed at  $\chi = 0\text{-}15\%$ , characterised by a higher constrained modulus whereas rubber-like behaviour, which reveals a lower constrained modulus, is shown at  $\chi = 30\text{-}100\%$ . At higher stresses ( $\sigma > 1115$  kPa), all rubber contents tend to converge in a relatively similar constrained modulus at  $\sigma = 2231$  kPa, lower than the value seen in sand only specimens.

As discussed in Section 4.4.2, the number of voids within specimens containing rubber is almost negligible at high stresses, for both CrR and ShR, and it is the deformation of rubber which leads to a stiffer response. Therefore, it can be stated that at  $\sigma > 1115$  kPa, the compressibility of RSm is fundamentally governed by rubber particles at any rubber percentage, which leads to nearly similar constrained modulus.

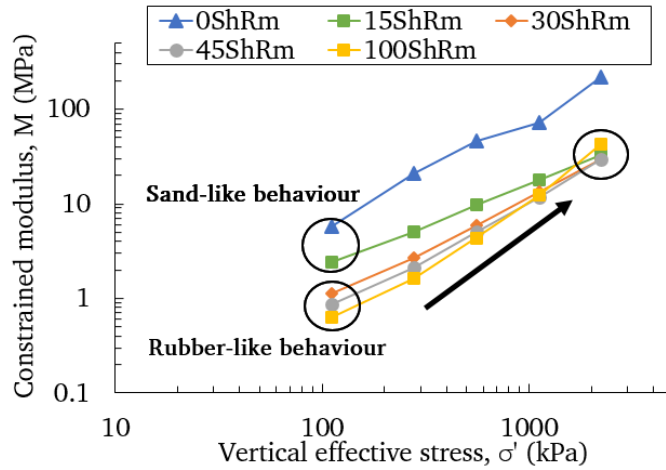


**Figure 4.15:** Constrained modulus with applied vertical stress of RSm

### *Stress-strain behaviour*

In this section, the compression and particle rearrangement of RSm specimens are reported on through the analysis of shear stress vs shear strain loops under one-dimensional loading. Although oedometer tests do not allow for lateral deformation of the material tested, this study has decided to study the hysteretic behaviour of RSm to compare the effect of particle properties, i.e. rubber content and shape, on the compressibility of RSm. Hence, a comparison between bulk rubber and particulate specimen has been undertaken to investigate the nature of particle to particle interactions.

### *Particulate vs bulk behaviour*

A comparison between a bulk rubber, which represents a solid block, and a RSm, which characterises the particle to particle interaction, was undertaken by applying four loading-unloading cycles. Whilst bulk rubber was tested using unconfined compression apparatus, a oedometer was used to perform compression tests on RSm containing  $\chi = 30\%$ . The objective was to understand the evolution in the vertical deformation with the application of vertical stress. Compared to previous sections, constant stress amplitude tests were performed on each material.

This study has transformed vertical loads and deformations into shear stress  $\tau$  and shear strain  $\gamma$  to quantitatively compare the results obtained from every apparatus. Figure 4.16 shows the stress - strain behaviour of the two samples.

Figure 4.16 reveals that RSm experiences an initially pronounced shear strain compared to bulk rubber. This is attributable to (i) the particle rearrangement and (ii) to the deformation and bending of particulate rubber as a consequence of the entrapment between mineral particles. The hysteretic behaviour arises with the permanent deformation in the first cycle but then it remains almost constant. Given the bulk rubber is considered to be a continuous material without voids, the initial plastic deformation and then the continuous recovered deformation is attributable to rubber elasticity. This suggests that the hysteretic behaviour of rubber material is primarily a consequence of its deformability. As observed in Figure 4.16, this behaviour is observed in multiple cycles revealing the capacity of rubber to dissipate energy due to its high deformation and subsequent recovery. This differs from the energy dissipation seen in sand only specimens, consequence of the inter-particle friction due to particle rearrangement.

Regarding the soil shear stiffness, defined as the ratio of  $\tau$  over  $\gamma$ , two phenomena can be distinguished from Figure 4.16. For rubber bulk, shear stiffness remains nearly constant with strain and the same happens on unloading cycle. However, for the case of RSm shear stiffness increases with vertical stress to the ultimate state point where it tends to a similar stiffness as the bulk rubber. In other words, the particulate sample behaves as a bulk rubber at high stresses, attributed to the absence of voids. On unloading, the lower stiffness is regained.

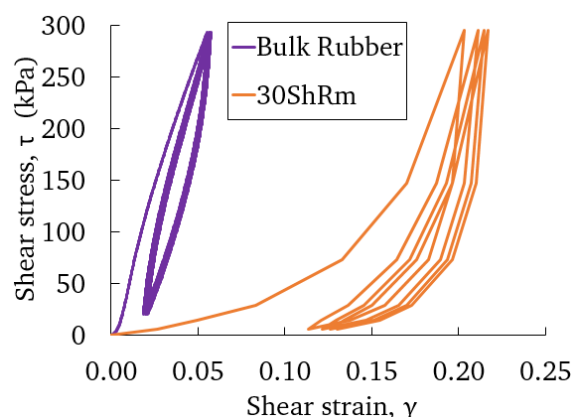


**Figure 4.16:** Shear stress - shear strain of bulk rubber and 30% ShRm

*Rubber content and shape*

Figures 4.17a and 4.17b compare shear stress - shear strain behaviour from the oedometer tests depending on rubber percentage and shape. Both figures include the rubber bulk and RSm presented in Figure 4.16. The fourth unloading-reloading cycle were used for clarity purposes to compare deformation and hysteresis developed.

A series of observations can be made from the unloading-reloading loop of RSm at  $\chi = 0$  - 100%:

1. The magnitude of  $\gamma$  increases with rubber percentage
2. Conventional mineral (sand) particles are relatively stiff with insignificant hysteretic behaviour.
3. Initial shear stiffness increases in every rubber percentage with strain during loading stage and it decreases on unloading.
4. Initial shear stiffness decreases with amount of rubber.
5. Shear stiffness relatively constant in bulk rubber.
6. Stiffer response of RSm with vertical stress, at any rubber percentage, which tends to similar shear stiffness of bulk rubber.
7. Hysteretic behaviour observed in both bulk and particulate rubber.

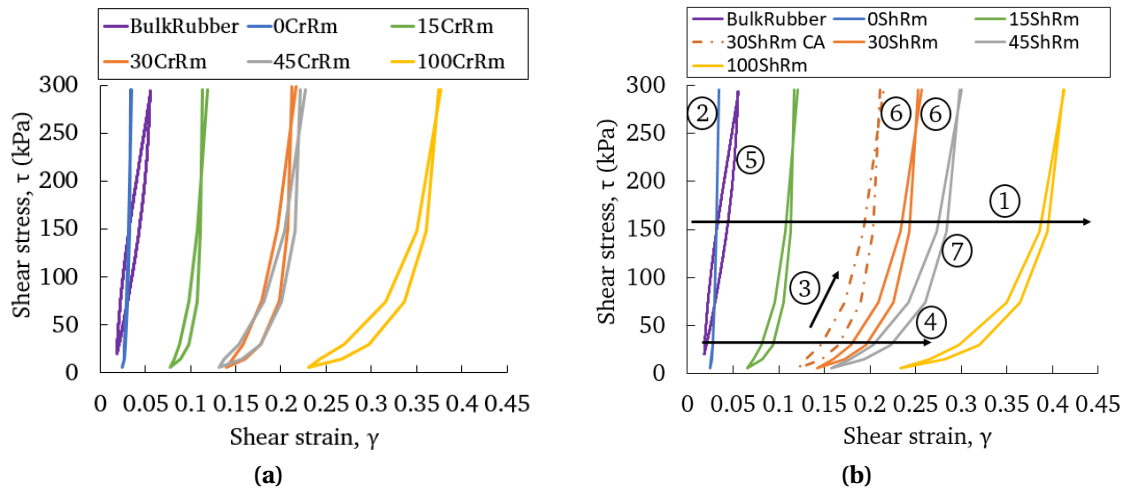


**Figure 4.17:** Shear stress - shear strain curve of RSm with a) crumb rubber particles and b) shredded rubber particles

In both figures, sand only is identified with a narrow almost vertical stress-strain curve which represents the small deformation and hysteresis experienced under one-dimensional unloading-reloading. In contrast, the majority of RSm, including rubber bulk, are characterised by a high material deformation and a hysteretic loop associated with the energy dissipated by the mixture in every loading-unloading sequence. It is evident that  $\gamma$  increases when adding rubber for both CrR and ShR at  $\chi > 15\%$ . At this rubber percentage, the specimen shows a rubber-like behaviour, with lower values of stiffness, due to the rubber deformation. On the other hand, specimens containing either ShR or CrR experience similar stress-strain response at  $\chi = 15\%$ , showing a sand-like behaviour which is mainly controlled by the sand physical properties.

Regarding the rubber shape, Figure 4.17b shows greater deformation in ShR samples compared to CrR as shown in Figure 4.17a. The rubber-like behaviour is seen in both ShR and CrR at  $\chi > 15\%$ , but this is more evident in shred particles which suffer from a greater deformation. The results presented in existing literature (Rao and Dutta, 2006; Lee et al., 2010) establish that RSm experience a greater deformation at greater rubber contents and reducing rubber particle size. However, no research has studied the influence of particle shape on the compressibility of RSm. As presented in Section 4.3.1, mean size ratio of ShR used in this study is slightly higher than CrR and mean thickness of both rubber shapes was limited to 1 mm. On the other hand, the aspect ratio of ShR ranges between 2 and 6 whilst the aspect ratio in specimens containing CrR is around 1. The only factor influencing the particle interaction with sand is uniquely the rubber shape. Consequently, the compressibility of RSm containing particulate rubber is not only influenced by rubber content but also rubber size and shape.

## 4.5 X-ray tomography on RSm

As a continuation of the plain strain visualisations and the stress-strain analysis based on oedometer tests, this study has quantified the particle scale interaction at a microscopic level. The objective is to elucidate the development in both void ratio and contact area of RSm under cyclic loading and thus relate it to its macromechanics in following chapters. Small-oedometer samples containing 30% ShR were placed inside an x-ray tomographic scanner and digitally processed to produce 3D images.

### 4.5.1 Equipment, materials and methods

The system used was a Nikon XTH 225 ST located at the Research Centre at Harwell, Oxfordshire (UK). The experimental set-up consisted of a load cell, a vertical piston, a micrometer and a small oedometer with an internal diameter of 14 mm. The set-up was designed for this particular scanner and was mounted on the rotating table of the scanner, more details on the equipment can be found in [Nadimi and Fonseca \(2018\)](#). Specimen size studied was 14 mm in diameter and a height of 11 mm. The force was exerted by manually screwing the micrometer into the sample until the pre-set load was reached. A high precision micrometer with an axial loading capacity of 450 N was used. The sample container was made of Perspex with 2 mm thickness for which a value of less than 3  $\mu\text{m}$  deflection under the maximum applied force was measured. The lateral friction was minimized by considering a 1 mm gap between the container and the X-ray window. The exerted force was monitored by a low profile 'pancake type' load cell.

The images were acquired at three stages: prior to loading (Stage 0), under a vertical load of 120N (Stage 1) and after unloading to 35N (Stage 2). A total of 3142 projections were collected per scan, with an exposure of 500 ms per projection. The 3D images acquired had a resolution of 9.2  $\mu\text{m}$  (length of voxel edge). In an x-ray scanning, the objects within the sample attenuate different levels of x-ray beam energy, depending on the material composition and density. Denser materials, i.e. sand, attenuate more than less dense materials, i.e. rubber and void space, and this difference in attenuation is

represented by the intensity values of the voxels (3D pixels). The contrast of intensity level allows for differentiation of the three phases within the image, shown in Fig. 4.18. The rubber has intensity values between the void (black) and the sand grains (brighter).

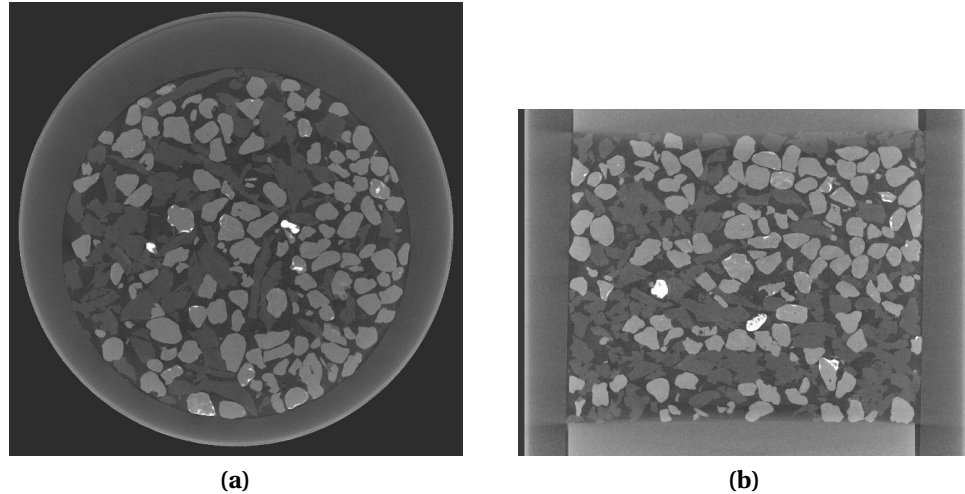


**Figure 4.18:** Tomographic image of the sample prior to loading: a) cross sectional view and b) vertical section

## 4.5.2 Results and discussion

An in-house imaging processing code was developed in Matlab to segment the images by separating them into the three phases. This includes a two-step binarisation using Otsu's thresholding (Otsu, 1979), for which the sand phase was first isolated and secondly the rubber phase was separated from the void space. Cross sections through the 3D segmented images at the three stages of loading are presented in Fig. 4.19. The subsequent step of image processing was to identify the contacts between the sand grains and the rubber (Fonseca et al., 2013). The measurements consisted in counting the number of voxels (volumetric pixel) forming each of the three phases and the contact regions. The volumes of sand, rubber and void space were obtained by multiplying the number of voxels by the voxel size ( $9.233^3 \mu\text{m}^3$ ). For the contact areas the number of voxels was multiplied by  $9.233^2 \mu\text{m}^2$  to obtain the area of surfaces.



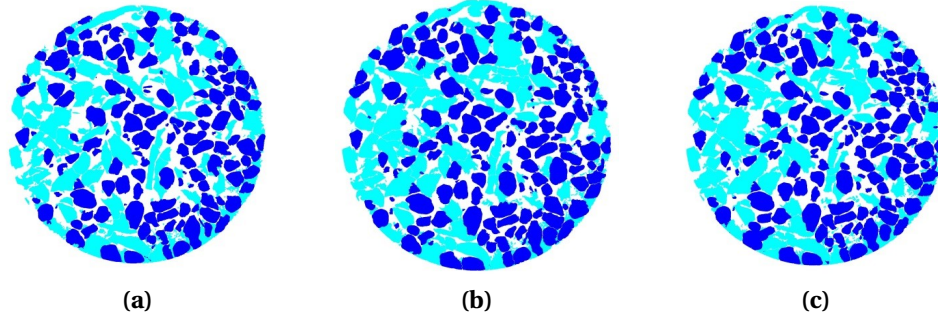


**Figure 4.19:** Cross sectional views through the segmented images with the three phases differentiated: a) Stage 0, b) Stage 1 and c) Stage 2

Table 4.7 shows the height of the sample and void ratios, measured from the 3D images, at the three stages load stages. The void ratio ( $e_{im}$ ) was calculated as:

$$e_{im} = \frac{N_{voxel}^{void}}{N_{voxel}^{sand} + N_{voxel}^{rubber}} \quad (4.10)$$

where,  $N_{voxel}^{void}$  is the number of voxels forming the void space,  $N_{voxel}^{sand}$  are voxels occupied by sand grains and  $N_{voxel}^{rubber}$  are voxels occupied by rubber.

**Table 4.7:** Measurements of sample height and global void ratio of sample at the three stages, obtained from the 3D images

	Stage 0	Stage 1	Stage 2
Load (N)	0	120	35
Sample height (mm)	11.14	10.24	10.51
Void ratio ( $e_{im}$ )	0.441	0.345	0.358

The evolution in rubber volume under loading and unloading is presented in Fig. 4.20a together with the evolution in sample void ratio. It is seen that the rubber undergoes volumetric compression when the loads increases to 120 N, due to rubber's deformation, and on unloading to 35 N almost all the deformation is recoverable as expected. This verifies the assumption made by Platzer et al. (2018) who hypothesised that the volume changes experienced by RSm are consequence of particle re-arrangement but also rubber deformation under loading. Indeed, the evolution in rubber volume shown in Figure 4.20a reveals that there is a temporary change in rubber volume under loading, contrary to the assumption made that rubber is incompressible. However, this change

in volume is postulated in this study to be attributable to the presence of micro-porosity, as well as fissures and cracks, observed within the particulate rubber (Figure 4.21). This will be further discussed in Section 4.5. Interestingly, the void ratio range obtained using the tomography images, i.e. 0.32-0.46, is lower than the minimum void ratio experimentally calculated from the maximum density of RSm (Figure 4.8). This could be attributed to the different set-up and the sample preparation in each apparatus. While the maximum density was calculated in a 4 l mould (Section 4.7), the void ratio calculated via x-ray analysis was obtained from 14 mm by 11 mm samples prepared at an initial dense state to ensure the contacts between particulate rubber and sand. This discrepancy in the magnitude of  $e$  suggests that the analysis to determine the number of voids should not be directly extrapolated between these two sets of experiments.

The evolution of the contact area between sand grains and rubber is presented in Fig. 4.20b. In this case, we can see an increase in the contact area as applied load increases (secondary axis in reverse order) and on unloading only part of the new formed contact areas are lost. This is an interesting finding given that it appears to mimic (qualitatively) the evolution of the void ratio. This reveals that rubber particles remain attached to the surrounding particles, 'locking' the possible contact sliding attributable to the high inter-particle friction in comparison with conventional mineral soils, e.g. [Lopera Perez et al. \(2016\)](#). This finding is in accordance with previous investigations ([Lee et al., 2007](#); [Lee et al., 2014](#)) who found the existence of a contractive behaviour in RSm with adding 20% rubber that inhibited the sliding between sand and rubber particles and prevented the appearance of buckling.

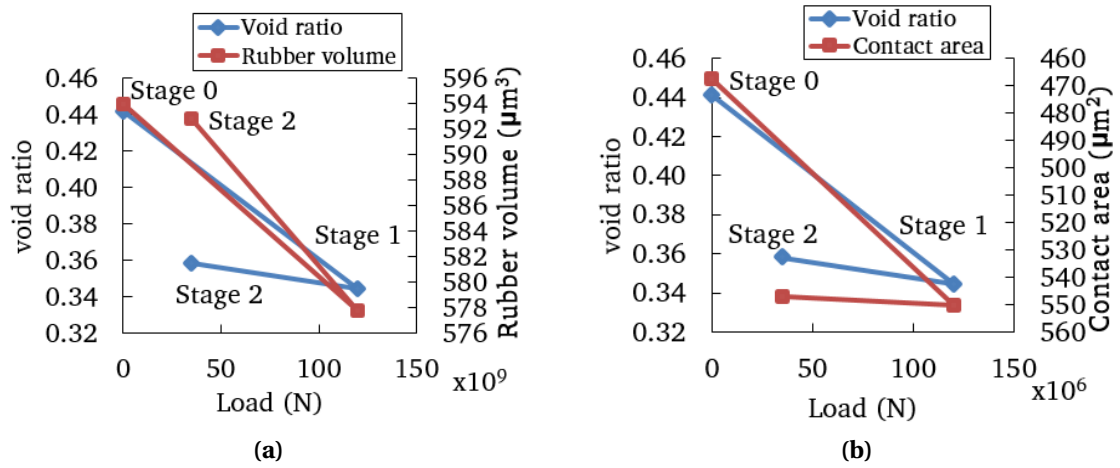


**Figure 4.20:** Evolution in void ratio with a) rubber volume and b) contact area of 30% ShRm from mini oedometer tests

### 4.5.3 Energy dissipation at a particle scale

Energy dissipation in sands is caused by particle re-arrangement and sliding at inter-particle contacts (Zheng-Yi and Sutter, 2000; Anastasiadis et al., 2012b). Results illustrated in Figures 4.20a-4.20b seem to demonstrate that there are other mechanisms at play when particles are deformable (rubber) and/or mixed with rigid particles (sand). It may be postulated that rubber particles dissipate part of the energy by sliding at inter-particle contacts and this can explain the initial (and significantly higher) irrecoverable response during the first loading cycle. This is due to particle arrangement induced by stress increases and voids being filled by (deformed) rubber particles. Hence, it would seem that the dissipation during the first loading-unloading cycle in sands, rubber and RSm is caused by inter-particle contact sliding and density changes associated with particle rearrangement.

On the other hand, the more constant dissipation occurring at subsequent loading-unloading cycles for all RSm can be explained by a different mechanism. Rubber particles "lock" and their deformation takes over the dissipation mode. Results obtained in Figure 4.20a have indicated that the contact area of particulate rubber increases upon loading and only very slightly reduces during unloading. Similar observations were made in terms of void ratio (Fig. 4.20b). This occurs with very high inter-particle friction

at contacts of rubber particles. It may be postulated that dissipation by individual rubber particles is developed similarly as it would occur in (bulk) rubber block, but their collective behaviour and interaction with other particles causes additional non-linearity on the stress-strain response. Hence energy dissipation mechanisms at the macro-level are the result of physical phenomena at the micro-level.

These mechanisms have been postulated based on quantitative image analysis (Section 4.5), but also based on set of standard oedometers tests on RSm comprising sand and ShR/CrR following preliminary analyses on plane strain visualisations of acrylic discs and rubber particles of different shapes (Section 4.2). The results across the three experimental set-ups provide an intuitive explanation of the micro-scale interactions affecting the observed macro-scale behaviour.

## 4.6 RSm compressive behaviour

In the light of the analysis undertaken, this study tries to explain the evolution in the compressive and stress-strain behaviour of RSm, understood as a three phase material, under uniaxial vertical load. A series of assumptions have been made:

- Sand particles are infinitely rigid (non-flexible) and incompressible.
- Rubber in its bulk phase has a Poisson ratio of 0.5 and consequently recovers its volume despite suffering significant deformations (Figure 4.16).
- The reduction in size of voids and, in turn, the volumetric change in RSm is a result of:
  - i) compression; associated with particle rearrangement, and
  - ii) distortion; which accounts for deformation, bending and/or crush of particles at high stresses.

Table 4.8 shows the differences between a solid block and particulate samples of only sand and only rubber materials. The stress-strain and compressive behaviour of RSm can therefore be elucidated at a macro level from the combination of rigid and flexible particles and its individual behaviour at a microlevel.

**Table 4.8:** Conceptual framework to explain the particle shear and compressive behaviour of mineral (sand) and rubber particles

	Bulk Phase		Particle + void phases	
	Compression	Distortion	Compression	Distortion
<b>Sand</b>	No	No	Yes M: increases with $e$	Yes G: decreases with $\gamma$
<b>Rubber</b>	No ( $\nu = 0.5$ )	Yes G: decreases with $\gamma$	Yes M: increases with $e$	Yes G: increases with $\gamma$

***Rigid (mineral) soils***

The first case is mineral (sand) soil in its bulk phase where no compression nor shear deformation is possible due to being an infinitely rigid material. On the other hand, the reduction in the number of voids in conventional particulate soils (sand) points to a rise in constrained modulus with vertical stress under isotropic loading as observed in Figure 4.15. As vertical stress keeps increasing, there is a higher number of contacts between sand particles and in turn significant friction/sliding effects. This results in a compact state where sand particles cannot withstand high loads due to lack of ductility (Sheikh et al., 2012) causing particle breakage as discussed in previous studies, e.g Fu et al. (2014). It can then be postulated that shear stiffness of mineral particles reach a peak before particle's crush and then it decreases with deformation.

***Deformable (rubber) materials***

Rubber in its bulk phase (rubber cylinder) does not experience any compression as a consequence of the change in void ratio given that there are no voids within the solid block. However, the response of the material under high vertical stresses is to deform which, in last instance, leads to a decrease in the material shear stiffness with deformation. Given that rubber is assumed to be incompressible ( $\nu = 0.5$ ), the only explanation to describe the high deformation exhibited by the bulk rubber under loading (Figure 4.16) is the existence of micro-pores within the solid block (Figure 4.21). A high porosity, in addition to numerous fissures and cracks on the rubber surface, were found using microscopic images as can be seen in Figure 4.21. The hysteresis found in the solid rubber is initially attributed to the plastic deformation experienced by the bulk but then,

a constant hysteretic behaviour is observed (Figure 4.16) which can be only associated with its elasticity and capacity to recover its shape.

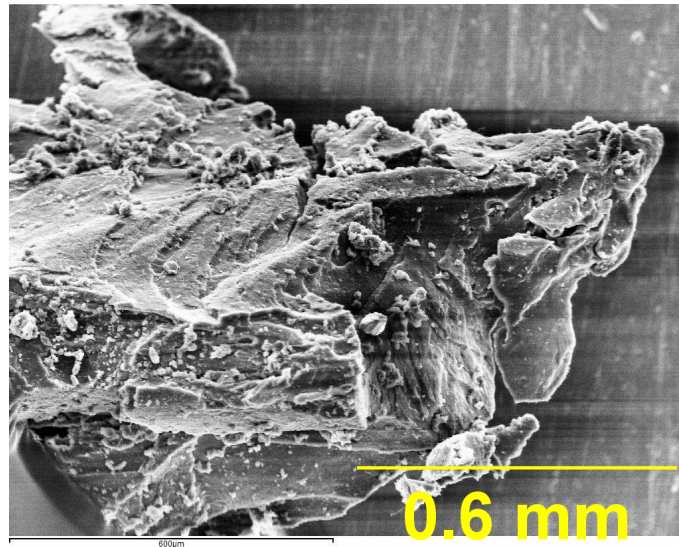


**Figure 4.21:** Microscopic image showing high porosity together with fissures and cracks found on surface of recycled rubber particle

With regards to particulate rubber, an increase in the constrained modulus is also observed with the difference that this occurs at a lower rate than with mineral (sand) specimens. This can be mainly attributed to the low bulk stiffness introduced by rubber particles (Zheng-Yi and Sutter, 2000). On the other hand, the increase in the contact area (Figure 4.20b) and the high inter-particle friction of rubber prevent any slippage between particles. In other words, the movement between rubber particles is "locked" leading to an improvement in the shear stress. This would aid explaining why there is null particle breakage at specimens with  $\chi > 60\%$ , e.g. Fu et al., 2014. In last instance, this gives rise to an improvement in the material stiffness with shear strain. The shear stiffness of particulate rubber tends to that of the bulk rubber at high stresses as shown in Figure 4.17a. However, the anisotropic interaction between particles generates non-symmetric dissipation patterns, reason why solid block and particulate specimens show a different hysteretic behaviour.

***Rigid (sand)- deformable (rubber) particle mixtures***

The particulate behaviour of RSm can then be understood as a combination, in variable extent, of the individual behaviour of sand only and rubber only specimens. In terms of compression, the change in size of voids leads to an increase in constrained modulus. This is more evident when reducing rubber content, attributed to the dominance of physical properties of sand, and the resultant sand-like behaviour. At high stresses, rubber's deformation starts to fill the voids between soft and rigid particles, increasing the contact area (Platzer et al., 2018). This, together with the high-interparticle friction (Lopera Perez et al., 2016), inhibits the particle sliding. In other words, rubber particles adds resistance against shear stresses, postponing any possible slippage and/or particle breakage. Based on the reduction in the crushing of particles as shown in research to date (Fu et al., 2014)), this effect is more significant at greater rubber percentages with the appearance of rubber-like behaviour. The temporary change in rubber volume observed in RSm via x-ray tomographic images (Figure 4.20a) is attributed to the high capacity of particulate rubber to deform (Platzer et al., 2018). The significant deformation exhibited by RSm is, in turn, developed as a result of the porosity, crack and fissures found on the rubber surface, via microscopic images (Figure 4.21), which can help to explain the reported temporary change in volume and its recovery.

## 4.7 Summary

In this chapter, the micro and macro mechanics of RSm containing ShR and CrR have been studied using plain strain visualisations, conventional oedometer tests and 3D x-ray tomographic images on small-oedometer samples.

- A greater change in void ratio as well as higher values of compression and swelling indices have been found in mixtures containing rubber shreds.
- RSm is a three phase material comprising of solid incompressible (sand), solid deformable (ShR/CrR) particles and voids. The change in void ratio is attributable to both i) particle rearrangement and ii) distortion, due to deformation and bending.
- Rubber addition increases the capacity to deform of RSm that leads to an increase in particle-to-particle contacts. This inhibits the particle sliding, attributable to the high inter-particle friction, and increases the resistance to shear stresses.
- 3D x-ray tomographic images have demonstrated that contact area between sand and rubber particles increases upon loading and slightly reduces during unloading. In terms of new understanding, this study has demonstrated that the particle shape, in conjunction with rubber content, has an effect on the evolution of compressibility and the stress-strain behaviour of RSm. This suggests that rubber shape should also be accounted to understand the effect of particle properties on the response of RSm under loading. As a result of the high capacity to deform of rubber, RSm experience an improvement in the shear stiffness. This means that rubber adds an additional resistance against vertical loading which postpones the particle slippage and, in last instance, the possible particle breakage. The hysteretic behaviour experienced by both bulk and particulate rubber is found to be dominated by rubber deformation and void-filling capacity. This aid in explaining the distinction in energy dissipation mechanisms found at a particle scale between sands, where the energy is known to be dissipated through inter-particle sliding, and RSm, where the high inter-particle friction prevents the slippage, and deformation takes over the dissipation.



## *Cyclic behaviour of RSm - Element test*

---

### **5.1 Introduction**

The investigation on the dynamic behaviour of RSm has been primarily focused on the range from very small-to-medium amplitudes (Mashiri, 2014). The impact of previous strong motions has shown how soil deposits can be subject to large deformations with the appearance of prolonged aftershock conditions. Under such deformations, saturated soils are likely to suffer from stiffness and damping degradation. However, research to date fails to acknowledge the effect of test conditions, e.g. cycles, on the dynamic behaviour of mineral soils and, in particular, RSm.

This chapter presents the results corresponding to the cyclic behaviour from tests performed on RSm at small-to-large deformations. First, specimens are tested under saturated, undrained conditions using a cyclic triaxial equipment. This was done to evaluate the evolution in pore water pressure and its effect on the bulk parameters that characterise the dynamic behaviour, i.e. shear modulus and damping ratio, whilst altering rubber content and number of cycles. Second, the low strain range is analysed via torsional resonant column tests on RSm specimens tested under undrained, dry conditions to determine the maximum shear modulus and minimum damping ratio. The bulk parameters experimentally calculated will be used to predict the stiffness and damping degradation curves for RSm containing shredded rubber (Chapter 7).

## 5.2 Cyclic triaxial equipment

The main aim of this investigation is to understand the response of RSm under cyclic loading, identifying those factors that influence the characterisation of its dynamic behaviour. To obtain this information, a cyclic triaxial apparatus was employed in accordance with [ASTM D3999 \(2011\)](#). By doing so, the cyclic behaviour, together with liquefaction potential, of RSm specimens containing shredded rubber (ShR) were determined under isotropically consolidated, undrained, saturated conditions by applying strain controlled cycles.

### 5.2.1 Equipment, materials and methods

#### *Equipment*

Cyclic triaxial experiments were performed using ©Dynatriax Dynamic pneumatic triaxial system at Edinburgh Napier university. The apparatus is a computer controlled servo-pneumatic system capable of performing both static and dynamic triaxial at an operating frequency of up to 10 Hz (Figure 5.1). The double acting pneumatic actuator presents a maximum load capability of  $\pm 5$  kN with an integrated LVDT displacement transducer. The standard triaxial cell of the equipment can manage both cell and back pressures up to 1000 kPa. The Compact Dynamic Controller has 16 transducer input channels using 16 bit ADC and it manages high sensitivity controlled loops, i.e. displacement, cell and back pressure, with a P.I.D. feedback of up to 10 kHz. Values corresponding to the minimum and maximum range as well as the accuracy of all transducers attached to the controller have been presented in Table 5.1.

Data acquisition was carried out by means of the software DYNATRIAX. Recorded data were: time (s), confining pressure ( $\sigma_3$ )(kPa), back pressure (BP)(kPa), axial load (N)(kN), pore water pressure ( $u$ )(kPa), change in pore water pressure ( $\Delta u$ ) and vertical displacement ( $\delta$ )(mm). All these variable readings were recorded every millisecond resulting in a total of 1,000 data points per second.

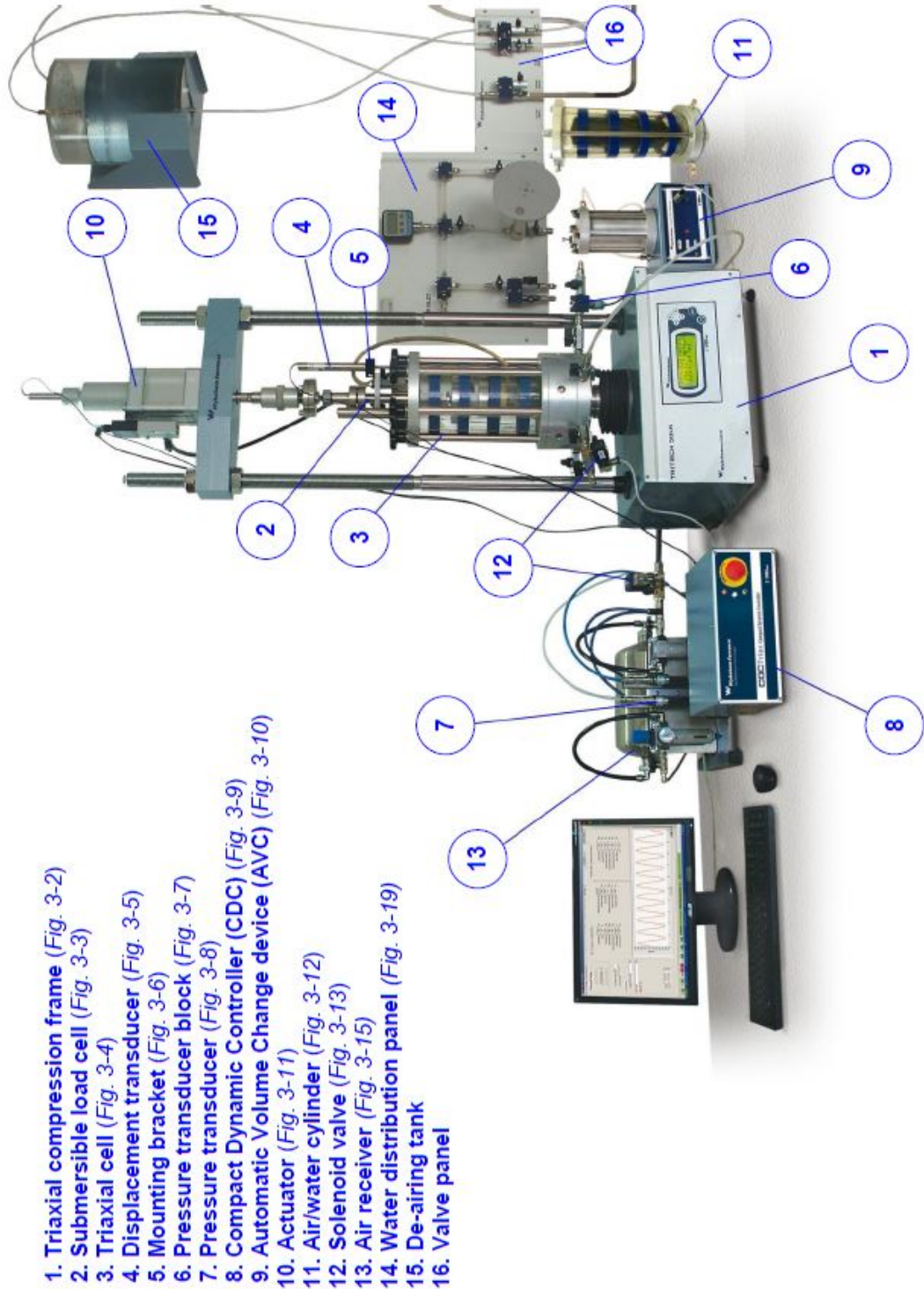


**Figure 5.1:** Cyclic triaxial equipment and set up

**Table 5.1:** Resolution and range for transducers of cyclic triaxial experiments

Transducer	Minumum range	Maximum range	Resolution
Load	-5000 N	5000 N	$\pm 0.1$ N
Integrated LVDT	-1 mm	50 mm	$\pm 0.001$ mm
Actuator	-1 mm	30mm	$\pm 0.01$ mm
Volume change	10cc	90cc	$\pm 0.01$ cc
Cell Pressure	-50 kPa	1000 kPa	$\pm 0.1$ kPa
Back Pressure	-100 kPa	1000 kPa	$\pm 0.1$ kPa
Pore pressure	-100 kPa	1000 kPa	$\pm 0.1$ kPa

### ***Material preparation***

Specimens tested in the cyclic triaxial apparatus were formed in a split cylindrical mould of 50 mm diameter by 100 mm height. RSm samples were prepared at various gravimetric proportions  $\chi = 0, 10, 20$  and 30%. The investigation on the dynamic behaviour of RSm was limited to elongated rubber particles. The terminology RSm is used to refer to mixtures containing sand mixed up with shredded rubber (ShR).

RSm samples were prepared within a 0.2 mm rubber membrane thickness to keep the sample saturated during the test. The membrane was first secured to the equipment base pedestal, followed by the introduction of a porous disc and filter paper, which were held in place by using two O-rings. Porous discs and filter papers were placed at both ends of the sample to restrict any possible movement of loose particles. Each half of the split cylindrical mould was then placed around the rubber membrane and base pedestal to maintain them in place by using fasteners. A vacuum pressure of 20 kPa was then applied to adhere the rubber membrane to the mould.

The procedure followed to pour RSm into the rubber membrane is a modification of the dry deposition method proposed by [Ishihara \(1996\)](#), given that elongated rubber could not be placed through a funnel shaped cone. A minimum of 2.5% moisture was needed during sample preparation to minimise the segregation of sand particles. This is in line with previous authors ([Li et al., 2016](#)) who addressed the segregation of sand whilst preparing the mixture in dry conditions. Adding a small amount of moisture introduces a thin water phase in which pressures are found to be negative. This suction

serves to hold particles in place against any self-weight gravitational forces following pouring. Samples were bagged with moisture content for a period of 24 hours before sample testing. RSm were then poured into the mould with a small scoop able to fit in the specimen dimensions without difficulties.

Homogeneity during sample preparation is necessary to ensure the repeatability of a test. This was achieved by maintaining the specimen relative density, formed prior to evaluating the dynamic properties of RSm. Furthermore, this was adopted as the main material descriptor to compare mixtures with different rubber content. The minimum and maximum density of sand and RSm were determined in Chapter 4 following the standard BS 1377-4 (1990). These values have been used as a reference to determine the value of the relative density for RSm before testing them.

An initial medium-to-dense state ( $D_r = 65-85\%$ ) was achieved for RSm before testing the specimen with either torsional resonant column or cyclic triaxial equipment. For that, the sample void ratio  $e_{sample}$  (Table 5.2), together with sand and rubber quantities, were calculated based on  $e_{min}$  and  $e_{max}$  for every rubber percentage. In line with the sample preparation for the oedometric tests (Chapter 4), both height, i.e. 100 mm, and sample volume, i.e.  $200\text{ cm}^3$ , were set at a similar value for all contents whilst the rubber content increased to maintain the rubber/sand mass ratio as established in the gravimetric proportion. Thus, material was split into equal parts and poured in the mould lined with a latex membrane in four layers. A light tamping was uniformly applied to each sample layer until reaching 25 mm height, and subsequently until reaching 100 mm height. Figure 5.2 shows the compaction state of sand and 30% RSm after preparing the specimens but prior to saturating and consolidating the mixtures. Values corresponding to average sample void ratio ( $e_{sample}$ ) as well as relative density are shown in Table 5.2. As shown in Figure 5.3, the sample density decreases in line with minimum and maximum density while the sample void ratio increases with the maximum void ratio, needed to maintain a similar initial compaction state. Hence, the relative density of RSm varied between 78 - 86%, which reveals that the specimens reached a dense-to-very initial dense state (Lambe and Whitman, 2010).

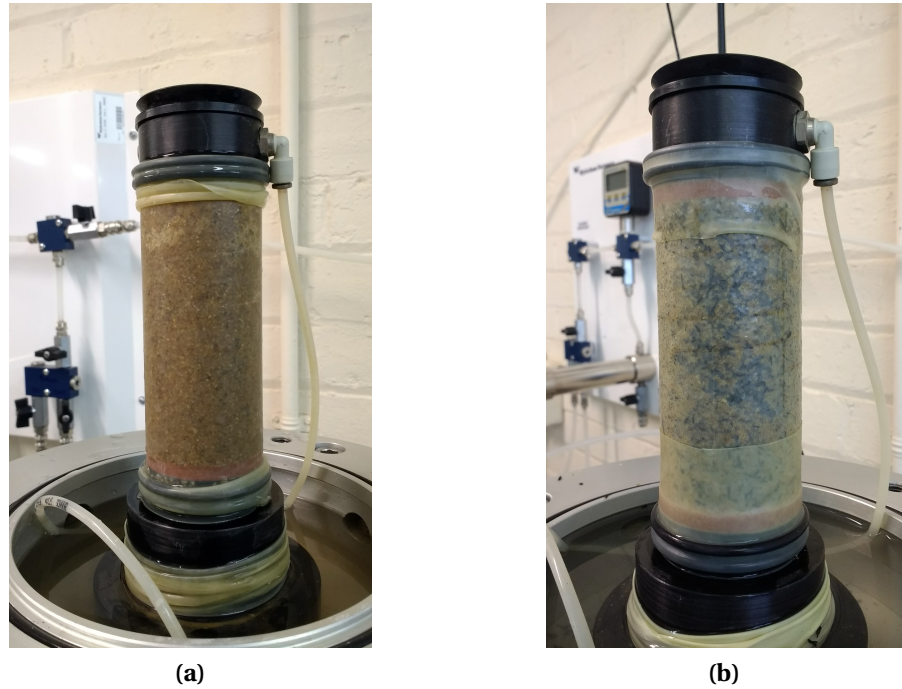


**Figure 5.2:** Sample preparation for cyclic triaxial tests of (a)sand and (b) 30%RSm

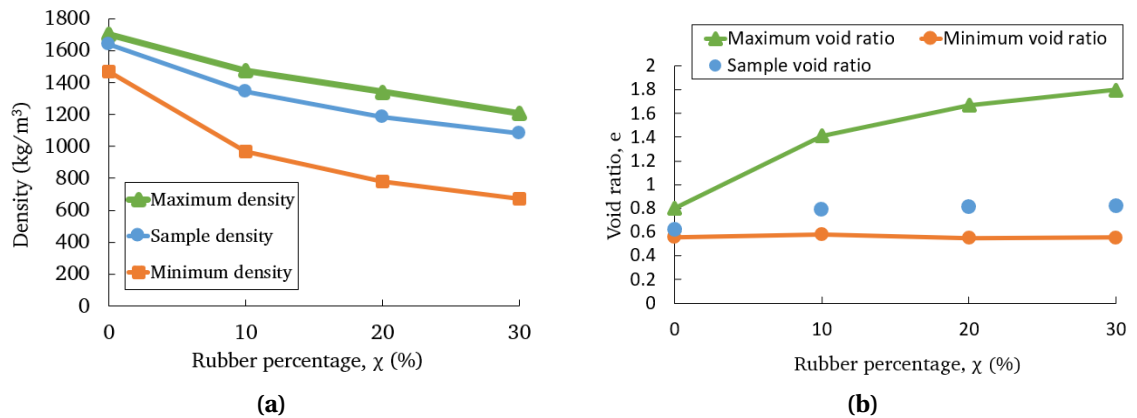


**Figure 5.3:** Maximum, minimum and sample a) density b) void ratio

**Table 5.2:** Relative density obtained for cyclic triaxial tests

Test	$e_{minRSm}$	$e_{maxRSm}$	$e_{sample}$	$D_r$ (%)
0RSm	0.54	0.80	0.61	78.8
10RSm	0.55	1.41	0.73	81.7
20RSm	0.55	1.67	0.74	82.8
30RSm	0.55	1.80	0.73	86.2



### *Saturation*

Cyclic triaxial specimens were saturated according to the back pressure saturation technique as per [ASTM D7181 \(2011\)](#). A saturation  $B$ -value of at least 0.95 was achieved.

The triaxial cell was mounted on the formed sample and slowly filled with water, whilst having the top vent open, to prevent any build-up pressure. The top vent was then closed when water reached the desired level and a cell pressure of 20 kPa was applied. A de-aired water flow was introduced from the pore water pressure valve, circulated through the sample and finally extracted using the back pressure valve, whilst maintaining the 20 kPa cell pressure. This process was carried out for a period of 20-30 minutes, depending on the RSm specimen, until the sample was completely filled with water to remove trapped air. This pre-saturation process was successfully tested to facilitate the specimen saturation. Once the pre-saturation was completed, back and pore water pressure valves were closed, cell pressure was dropped to a nominal 10 kPa and a back pressure equal to 5 kPa was introduced in the sample to initiate the saturation. At this point, the submersible load cell was brought into contact with the specimen top. A external vacuum pressure of 5 kPa was then applied to attach the specimen to the actuator load cell.

The saturation process was performed on RSm specimens by increasing the cell and back pressure at different rates. The difference between cell and back pressure was maintained between 30 and 40 kPa to keep under 20 kPa the total effective stresses applied to the sample. Cell pressure was increased in increments of 40 kPa and kept at that level for intervals of 10 minutes. Back pressure was increased 30 kPa in every interval to be 10 kPa under the cell pressure value. Pore water pressure valve was opened for a duration of 10 minutes until the change in volume was zero. This process was repeated until cell pressure reached 200 kPa. On the other hand, cell and back pressure were increased by 20 kPa in intervals of 20 minutes, until they reached 310 kPa.

The degree of saturation was calculated by using the  $B$ -value, which is defined as the ratio between change in pore water pressure ( $\Delta u$ ) and change in cell confining pressure ( $\Delta\sigma_3$ ), as shown in Equation 5.1. The degree of saturation ( $B$ ) was measured

by increasing cell pressure, maintaining back pressure closed, and reading the change in specimen pore pressure. A  $B$ -value  $\geq 0.95$  was achieved at a cell pressure of 310  $kPa$ :

$$B = \frac{\Delta u}{\Delta \sigma_3} \quad (5.1)$$

### *Consolidation*

Every RSm specimen was isotropically consolidated after the saturation. This was done by applying an effective confining pressure along the sample surface so as to maintain the particle in contact. A back pressure of 300  $kPa$  was kept constant and cell pressure was increased to 400  $kPa$ . Pore water pressure also reached 400  $kPa$  when increasing confining pressure. The valve was then opened, dropping to the back pressure value, for a duration of 30 minutes until the change in volume was less than 1  $cm^3$ . This process triggered the primary consolidation of deformable rubber particles and ensured specimens to be subjected to an effective confining pressure of 100  $kPa$ . Figure 5.4 shows the membrane state after applying a 100  $kPa$  confining pressure to a 20% RSm sample.



**Figure 5.4:** Membrane after consolidation during cyclic triaxial test



### Methods

Cyclic tests were carried out by means of sinusoidal waveforms transmitted through the triaxial actuator. The actuator was attached to the specimen top via an induced vacuum pressure. A series of hysteretic stress-strain loops were then obtained as a result of the medium-to-large deformations applied to the mixture at  $\sigma_m = 100$  kPa.

A summary of the type of test and its attributes are presented in Table 5.3. Each test was labelled with a test ID, which was noted as  $\chi$  (%) - RSm -  $\gamma_{cyc}$ . In this regard,  $\chi$  specifies the percentage of rubber by mass of shredded rubber introduced in the mixture, and  $\gamma_{cyc}$  is the cyclic shear strain amplitude. This last one refers to the single shear strain amplitude. A total of 16 tests with the same deformation amplitude, accounting for  $\gamma_{cyc} = 0.05, 0.1, 0.2$  and  $1\%$ , under strain controlled conditions were undertaken at a frequency rate of 1 Hz. A maximum of four hundred cycles (N) were applied to every specimen in order to determine dynamic properties, as well as liquefaction potential, of RSm in the medium-to-large strain range.

**Table 5.3:** Classification of cyclic triaxial experiments

Test ID	$\chi$ (%)	Single amplitude, $\gamma_{cyc}$ (%)	Cycles, N
1-0RSm0.05	0	0.05	400
2-0RSm0.1	0	0.1	100
3-0RSm0.2	0	0.2	41
4-0RSm1	0	1	14
5-10RSm0.05	10	0.05	400
6-10RSm0.1	10	0.1	400
7-10RSm0.2	10	0.2	240
8-10RSm1	10	1	50
9-20RSm0.05	20	0.05	400
10-20RSm0.1	20	0.1	400
11-20RSm0.2	20	0.2	400
12-20RSm1	20	1	400
13-30RSm0.05	30	0.05	400
14-30RSm0.1	30	0.1	400
15-30RSm0.2	30	0.2	400
16-30RSm1	30	1	400

## 5.2.2 Cyclic behaviour at medium-to-large strains

The cyclic behaviour has been studied for rubber content  $\chi = 0 - 30\%$  by evaluating the change in deviatoric stress ( $q$ ), which gives an indication of soil stiffness, with number of cycles ( $N$ ). The value  $N$  represents the number of strain controlled cycles applied to each sample whilst maintaining a constant cyclic strain amplitude. Stress paths have also been determined by comparing the change in deviatoric stress ( $q$ ) against the effective mean stress ( $p'$ ).

### *Sand*

Figures 5.5-5.6 shows the results of cyclic triaxial tests conducted on sand at  $\gamma_{cyc} = 0.05, 0.1, 0.2$  and  $1\%$ . At  $\gamma_{cyc} = 0.05$ , the stress - strain response experienced by sand is initially linear elastic. This linear elastic behaviour is similar to the stress-strain behaviour observed under one-dimensional compression loading (Chapter 4) where an almost negligible hysteresis was found. However, the dynamic response varies from the elastic initial straight line to an asymmetrical ellipse as the strain amplitude increases, i.e.  $\gamma_{cyc} > 0.05\%$ . This results in a gradual decrease in soil stiffness tending to zero with the number of cycles. As established by previous authors (Li et al., 2016; Wichtmann and Triantafyllidis, 2016), the permanent plastic deformation found in soils under loading leads to a gradual loss in the inter-granular contacts between particles and the subsequent degradation of the soil stiffness. Figure 5.5b reveals hysteretic behaviour attributed to the plastic deformation experienced by the specimen.

In Figures 5.5c-5.5d, the stress-strain response of sand shows a pronounced asymmetry, in which maximum and minimum deviator stresses present greater values in compression than in tension. There is a clear stress-path dependent anisotropic response. Also note that the decay in soil stiffness observed in Figure 5.5b is more evident at larger strains, i.e.  $\gamma_{cyc} = 0.2 - 1\%$ , where the deviator stress becomes zero after  $N=41$  and  $N=14$ , respectively. At this strain amplitude, the dynamic response of sand reveals a predominantly plastic behaviour. As explained in the Chapter 4, the size of voids decreases in RSm under the action of deformations, i.e. particle rearrangement, which

leads to a rise in contact area. However, the inter-particle friction between sand particles cannot withstand the large deformations, also due to the rise in the pore water pressure, which results in a eventual particle slippage and loss of inter-particle contacts.

### ***10% Rubber soil mixture***

Figures 5.7-5.8 illustrate the dynamic response of 10% RSm at  $\gamma_{cyc} = 0.05, 0.1, 0.2$  and 1 %. A similar stress - strain response is observed, as obtained for the case the case of sand at  $\gamma_{cyc} = 0.05$ , which reflects the nearly elastic behaviour of the mixture after 400 cycles. Yet a greater hysteresis is observed in contrast with sand which can be mainly attributed to the ability of rubber to deform and recover its size, as shown in the constant stress-strain analysis of bulk rubber in Section 4.3.2.

There is a change, however, in the cyclic behaviour of RSm at larger strain amplitudes (Figs. 5.7b-5.7d). In contrast to the significant anisotropy found in sand at  $\gamma_{cyc} = 0.2$  and 1%, the cyclic response of 10% RSm exhibits a nearly isotropic response in relation to soil stiffness decay. Referring to findings from Lee et al. (2007) and Lee et al. (2010), this can be interpreted as the transition from sand-like to rubber-like behaviour when adding rubber particles owing to the rubber deformability. Note that, plastic deformation increases with number of cycles that reveals the elastoplastic behaviour of the mixture.

In terms of soil stiffness, Figure 5.8 shows a reduction in maximum and minimum deviator stress at all shear strain levels (i.e.  $\gamma_{cyc} = 0.05-1$  %) compared to sand samples. As with sand specimens, deviator stress decreases with number of strain controlled cycles which reveals the development in plastic deformation. Nevertheless, the cycles required to trigger the specimen liquefaction increased in comparison with sand tests at  $\gamma_{cyc} = 0.2$  and 1%. The results obtained revealed that 10% RSm withstood 240 strain controlled cycles at  $\gamma_{cyc} = 0.2$  % (Figure 5.7b) whereas sand liquefied after  $N = 41$ . Consequently, it can be observed that the inclusion of 10% ShR improves the resilience of sand under the action of cyclic loading at medium-to-large deformations.

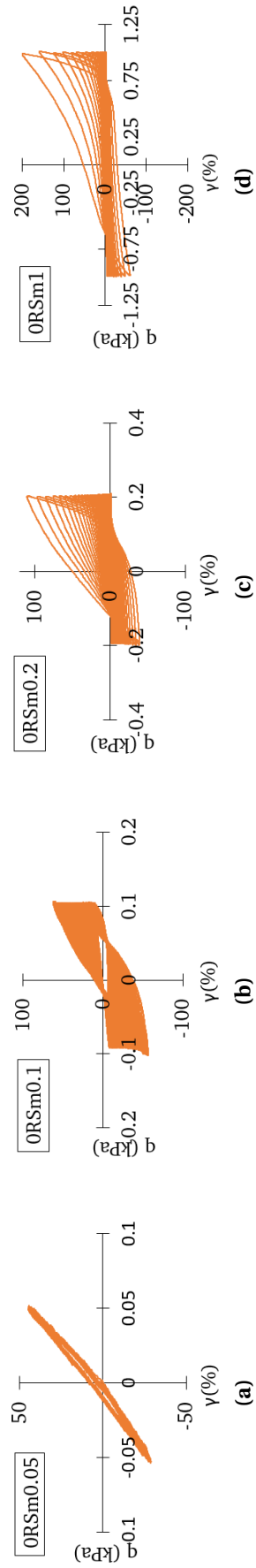


**Figure 5.5:** Cyclic behaviour of ORSm at (a)  $\gamma_{cyc} = 0.05\%$   $N = 400$  (b)  $\gamma_{cyc} = 0.1\%$   $N = 84$  (c)  $\gamma_{cyc} = 0.2\%$   $N = 41$  and (d)  $\gamma_{cyc} = 1\%$   $N = 14$

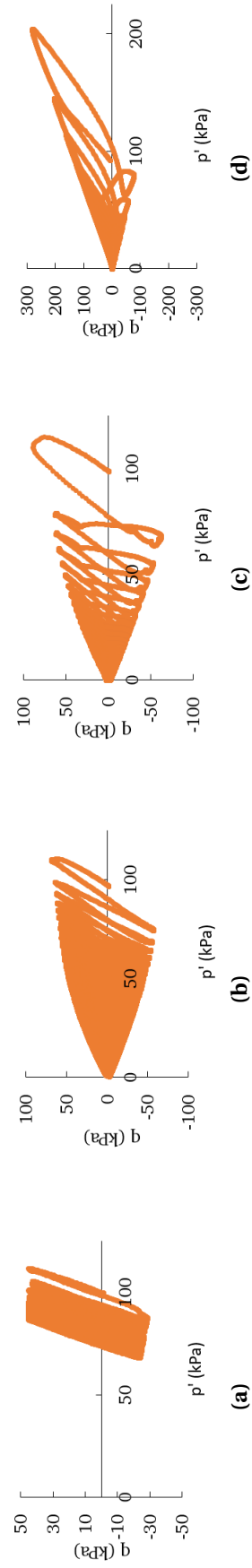


**Figure 5.6:** Stress path of ORSm at (a)  $\gamma_{cyc} = 0.05\%$   $N = 400$  (b)  $\gamma_{cyc} = 0.1\%$   $N = 84$  (c)  $\gamma_{cyc} = 0.2\%$   $N = 41$  and (d)  $\gamma_{cyc} = 1\%$   $N = 14$

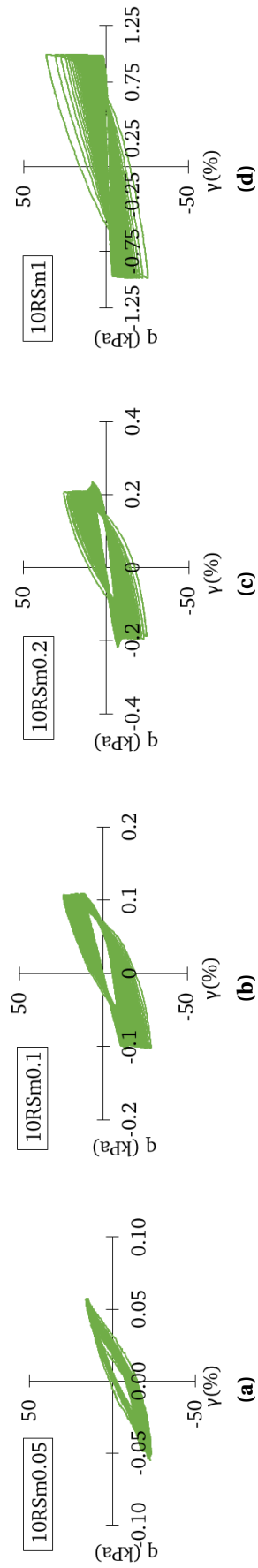


**Figure 5.7:** Cyclic behaviour of 10RSm at (a)  $\gamma_{cyc} = 0.05\%$   $N = 400$  (b)  $\gamma_{cyc} = 0.1\%$   $N = 400$  (c)  $\gamma_{cyc} = 0.2\%$   $N = 240$  and (d)  $\gamma_{cyc} = 1\%$   $N = 50$

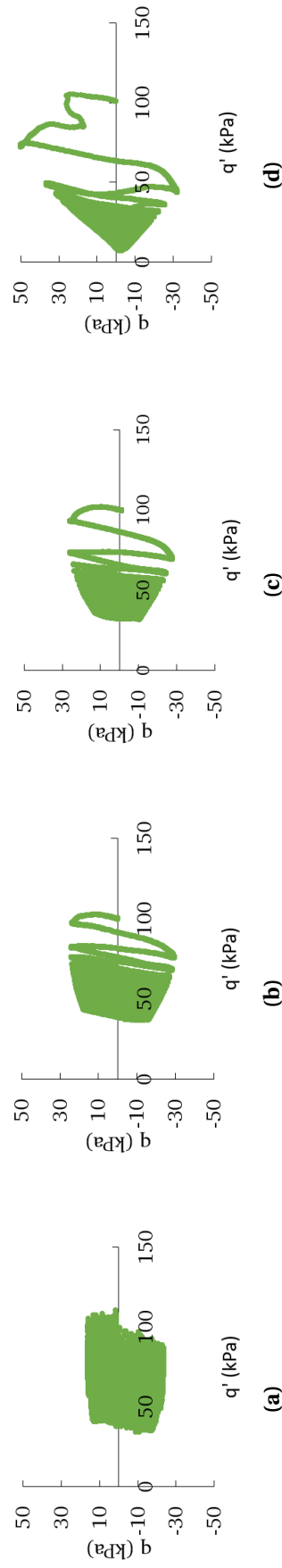


**Figure 5.8:** Stress path of 10RSm at (a)  $\gamma_{cyc} = 0.05\%$   $N = 400$  (b)  $\gamma_{cyc} = 0.1\%$   $N = 400$  (c)  $\gamma_{cyc} = 0.2\%$   $N = 240$  and (d)  $\gamma_{cyc} = 1\%$   $N = 50$

**20% and 30% Rubber soil mixture**

Figures 5.9, 5.10, 5.11, and 5.12 show the results corresponding to 20% RSm and 30% RSm, respectively. A lower maximum and minimum deviator stress, i.e. compression and tension, is observed compared to sand and 10 % RSm. This decay in the deviator stress is attributed to the lower stiffness and higher compressibility added by particulate rubber, as shown in the evolution of constrained modulus (Chapter 4) and demonstrated in previous studies (Kim and Santamarina, 2008; Sheikh et al., 2012).

In terms of the dynamic response, Figures 5.10-5.12 show a moderate decline in soil stiffness with the cycles in contrast with sand specimens. A nearly elastic behaviour is observed in both 20 and 30% RSm at  $\gamma_{cyc} = 0.05-0.2\%$  where evident signs of plastic deformation can only be noticed at very large strain amplitudes ( $\gamma_{cyc} = 1\%$ ). This confirms the transition from sand-like to rubber-like behaviour, characterised by lower stiffness but a higher capacity to deform under loading, more marked at  $\chi = 30\%$ .

As explained in Section 4.5, rubber particles present a high capacity to distort which leads to a substantial reduction in size of voids and fill of voids between rigid soils, e.g. (Platzer et al., 2018). The contact area increases between rigid/compressible particles, and any possible slippage is "locked". This contributes to a development of resistance to shear stress and leads to a decay in stiffness degradation, more pronounced at greater rubber contents, i.e.  $\chi = 20-30\%$ .

Despite the appreciable reduction in deviator stress at  $\gamma_{cyc} = 1\%$  (Figure 5.9d), 20 % RSm did not liquefy when subject to 400 strain controlled cycles. Consequently, adding rubber increased the capacity of the mixture to undergo large deformations without experiencing a significant reduction in soil strength. This can be directly related to the higher compressibility observed in RSm containing both shredded and crumb particles (Chapter 4), and also the minimum change in the contact area of RSm under loading-unloading cycles. Hence, it can be observed that the cyclic behaviour of RSm containing  $\chi \geq 20\%$  is controlled by rubber and its capacity to compress at high strains. This differs from the slippage and loss in particle contacts of sand specimens which led to a rapid decay in soil stiffness (Figure 5.5d).

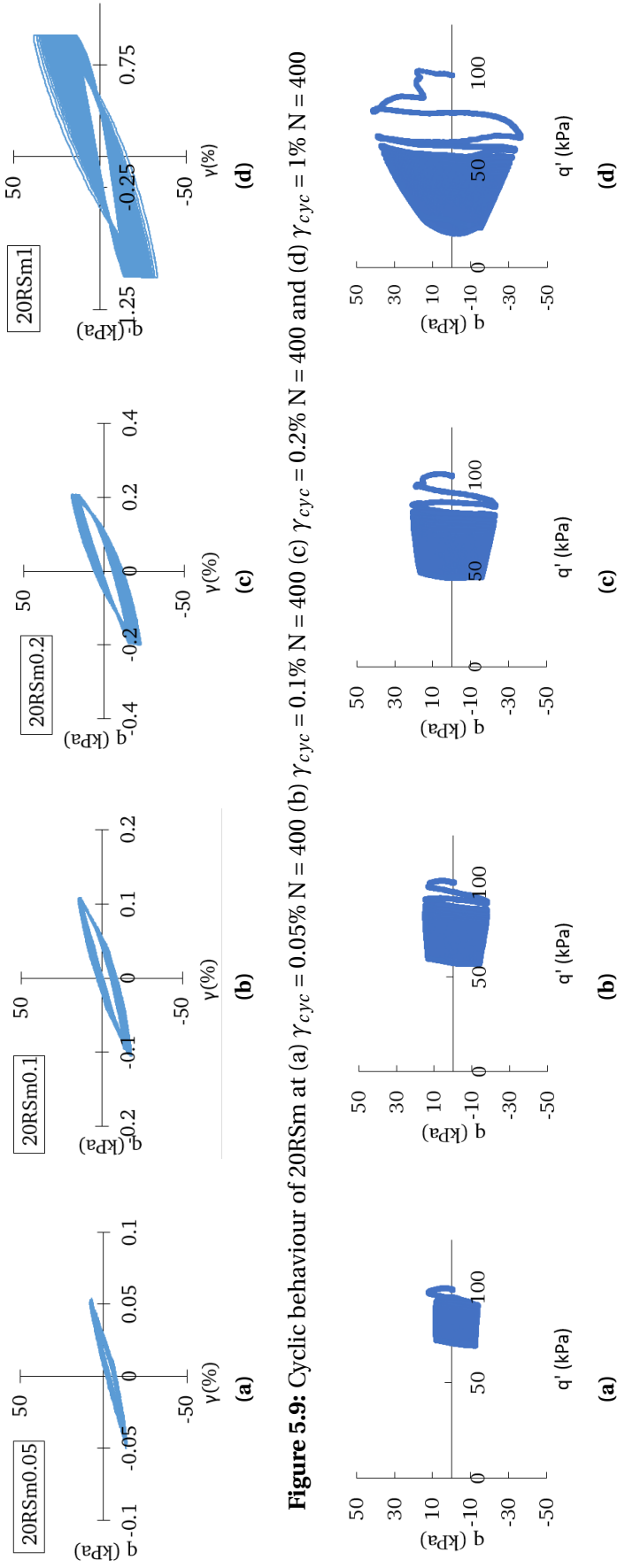


**Figure 5.9:** Cyclic behaviour of 20RSm at (a)  $\gamma_{cyc} = 0.05\%$   $N = 400$  (b)  $\gamma_{cyc} = 0.1\%$   $N = 400$  (c)  $\gamma_{cyc} = 0.2\%$   $N = 400$  and (d)  $\gamma_{cyc} = 1\%$   $N = 400$

**Figure 5.10:** Stress path of 20RSm at (a)  $\gamma_{cyc} = 0.05\%$   $N = 400$  (b)  $\gamma_{cyc} = 0.1\%$   $N = 400$  (c)  $\gamma_{cyc} = 0.2\%$   $N = 400$  and (d)  $\gamma_{cyc} = 1\%$   $N = 400$

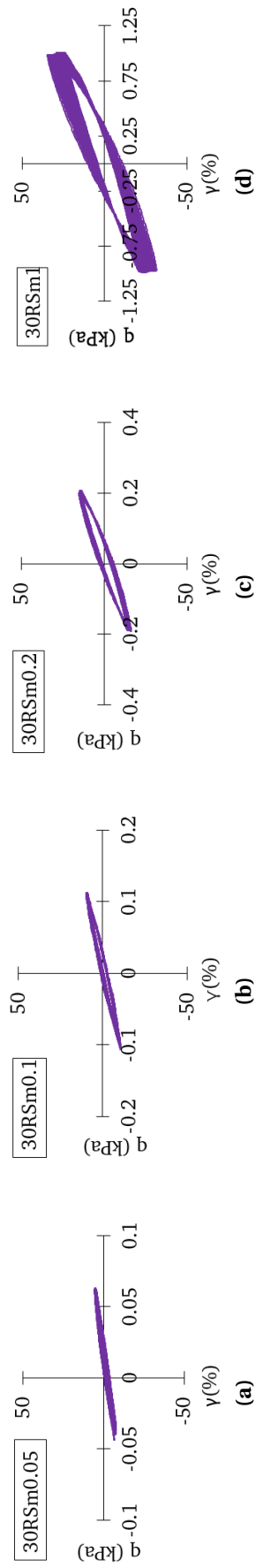


**Figure 5.11:** Cyclic behaviour of 30RSm at (a)  $\gamma_{cyc} = 0.05\%$   $N = 400$  (b)  $\gamma_{cyc} = 0.1\%$   $N = 400$  (c)  $\gamma_{cyc} = 0.2\%$   $N = 400$  and (d)  $\gamma_{cyc} = 1\%$   $N = 400$

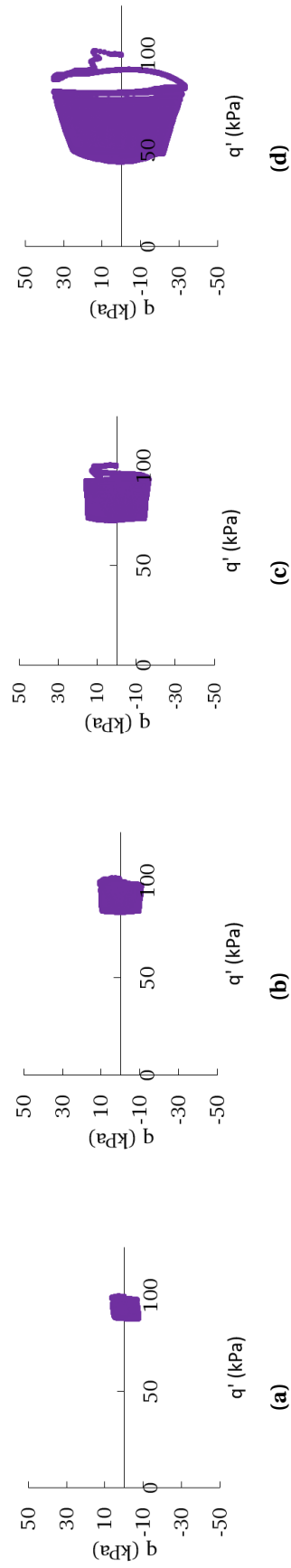


**Figure 5.12:** Stress path of 30RSm at (a)  $\gamma_{cyc} = 0.05\%$   $N = 400$  (b)  $\gamma_{cyc} = 0.1\%$   $N = 400$  (c)  $\gamma_{cyc} = 0.2\%$   $N = 400$  and (d)  $\gamma_{cyc} = 1\%$   $N = 400$



### 5.2.3 Liquefaction potential

Liquefaction potential of RSm has been assessed considering the number of strain controlled cycles required to reach a pore pressure ratio  $r_u = 1$ , i.e. soil liquefies. Pore pressure ratio is obtained from the ratio between the change in pore water pressure and the effective confining pressure (Section 2.3.3). Figure 5.13 shows the change in the pore water pressure and, as a result, the pore pressure ratio  $r_u$  with the number of cycles  $N$  and the strain amplitude for RSm.

A variable behaviour in the generation of pore water pressure can be observed depending on the amount of rubber and strain amplitude. Hence, the accumulation of pore water pressure and the number of cycles to reach liquefaction can be related to the type of mixture. In accordance with previous studies, such as the case of (Tsuha et al., 2012), who identified a pattern in the behaviour of driven piles, i.e. stable, unstable and meta-stable, in offshore foundations in relation to the shaft cyclic amplitude, this investigation distinguishes between two behaviours with regards to the evolution in liquefaction potential: (i) stable, and (ii) unstable. The objective of this section is to classify mixtures within each group to elucidate the effect of cyclic loading on the liquefaction resistance. These two states are defined in this investigation as:

- **Stable zone**, where pore water pressure stabilises or accumulates slowly over hundreds of strain controlled cycles. The specimen does not liquefy whilst it remains here.
- **Unstable zone**, where pore water pressure increases rapidly under the action of strain controlled cycles reaching values of  $r_u > 0.9$ . It is observed that soil liquefaction may occur at  $N < 100$ .

Figure 5.13 depicts the accumulation of  $r_u$  at all RSm under tested shear strain amplitudes. The rise in pore water pressure causes a reduction in inter-particle forces, which leads to the subsequent decrease in effective stress, resulting in the decay of soil strength as established in previous studies (Wichtmann and Triantafyllidis, 2016; Zhang et al., 2016). The permanent deformation experienced by RSm (Section 5.2.2), is then attributable to the loss of contacts between particles. Figure 5.13a shows that sand reaches a value of  $r_u > 0.95$  after 84 cycles, reflecting the rapid accumulation of

pore water pressure that results in the soil liquefaction. Sand is therefore identified to be contained within the unstable zone.

The next trend in Figure 5.13a, which is identified as 10% RSm, shows a lower accumulation of pore water pressure which gives rise to a  $r_u = 0.82$  after  $N = 400$ . Hence, 10% RSm remains within the stable zone at this strain amplitude. By adding 10% ShR, the liquefaction resistance improved passing from the unstable liquefaction threshold, at  $N = 84$ , to withstanding 400 dynamic cycles. The improvement in the liquefaction resistance is even more evident at  $\chi = 20$ -30%. The evolution in pore water pressure results in a pore pressure ratio  $r_u = 0.48$  and  $0.2$ , after  $N = 400$ . Both specimens remained thus, within the stable zone, far from the liquefaction threshold located at  $r_u = 0.90$ .

Figures 5.13b-5.13c reveal the increase in pore pressure ratio and liquefaction potential of RSm at larger strain amplitudes (i.e.  $\gamma_{cyc} > 0.1\%$ ). The gradual accumulation of pore water pressure at these strain levels points to a lower number of cycles prior to liquefying. This seems to be more prominent in sand specimens passing from  $N = 82$  at  $\gamma_{cyc} = 0.1\%$  to  $N = 14$  cycles at  $\gamma_{cyc} = 1\%$ . On the other hand, Figure 5.13b shows that 10% RSm liquefied at  $\gamma_{cyc} = 0.2\%$  after  $N = 284$  with a final  $r_u = 0.94$ , which might be due to the rapid generation of pore water pressure. This sample can be found within the unstable zone. Despite the greater accumulation in  $r_u$  compared to  $\gamma_{cyc} = 0.1\%$ , it is observed in Figure 5.13b that the final pore pressure ratio corresponding to 20 - 30% RSm still remained within the stable zone ( $r_u = 0.6, 0.3$ ).

The increase in pore water pressure is more evident at  $\gamma_{cyc} = 1\%$ , as seen in Figure 5.13c. 10 % RSm liquefied after  $N = 40$ , in contrast to the 14 cycles found with sand. A substantial decrease in the generation of pore water pressure is shown by adding  $\chi = 20\%$ . This is comparable to the decrease in  $r_u$  with the addition of 10% ShR at  $\gamma_{cyc} = 0.1\%$ . On this occasion, 20% RSm stays within the limits of the stable zone due to reaching a  $r_u = 0.88$  after  $N = 400$ . By adding 30% ShR, a decay in pore pressure ratio (i.e.  $r_u = 0.65$ ) was found. Therefore, it is observed that 20 and 30 % RSm can undergo 400 strain controlled cycles at  $\gamma_{cyc} = 1\%$ , remaining within the stable zone.

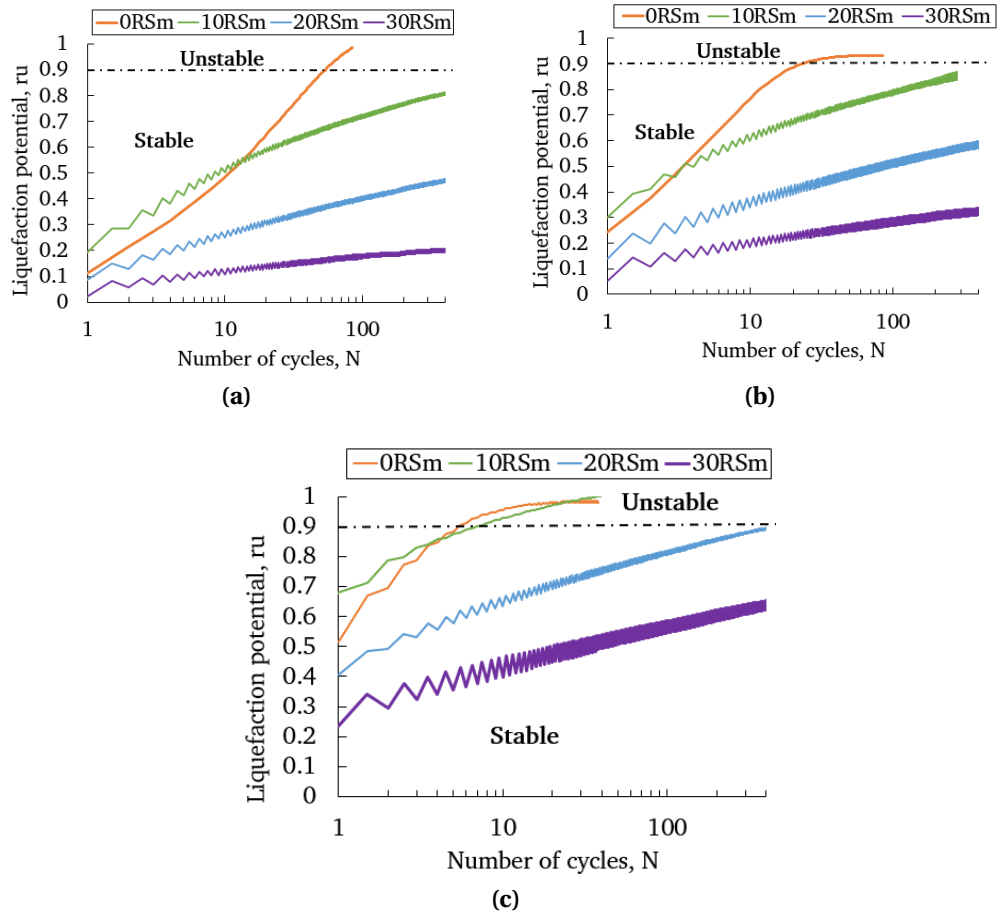


**Figure 5.13:** Liquefaction potential of RSm at (a)  $\gamma_{cyc} = 0.1\%$  (b)  $\gamma_{cyc} = 0.2\%$  and (c)  $\gamma_{cyc} = 1\%$

Figure 5.13 reveals that the liquefaction resistance of the mixture improves when adding shredded rubber and decreases with strain amplitude. At  $\chi = 20\text{-}30\%$ , mixtures withstood 400 loading cycles without liquefying (i.e.  $\gamma_{cyc} = 0.05\text{-}1\%$ ). The tendency shown in previous figures point to rubber deformability as one cause to explain the lower accumulation in pore water pressure. Although both sand and rubber are considered to be incompressible in its bulk state ( $\nu = 0.5$ ), a temporary change in volume is experienced by particulate rubber under loading attributed to its micro-porosity as well as the fissures/cracks found on their surface (Section 4.5). Therefore, whilst in sand specimens the entirety of the applied vertical loading results in the direct increase of pore water pressure, in RSm part of the external loading leads to an increase in pore water pressure and part of it is "directed" to trigger the change in volumetric conditions observed through the x-ray tomographic tests in Chapter 4.

The enhancement in liquefaction resistance is at odds with results found in previous

investigations (Promputthangkoon and Hyde, 2007; Shariatmadari et al., 2018) which showed an increase in liquefaction potential with rubber content. On the other hand, this result is in accordance with other studies which established that by adding big tyre chips (Hazarika et al., 2006; Otsubo et al., 2016; Mashiri et al., 2016), and rubber powder (Bahadori and Manafi, 2015; Bahadori and Farzalizadeh, 2018) a significant attenuation in pore water pressure can be achieved.

To date, only Mashiri et al. (2016) studied RSm liquefaction potential at medium-to-large strains with the application of up to 400 strain controlled cycles. A similar decrease in stiffness degradation with rubber content was reported by Mashiri et al. (2016). However, a maximum of 326 cycles were withstood by these mixtures at  $\gamma_{cyc} = 0.15 - 0.5\%$  in contrast to the 400 cycles shown in this study by applying up to  $\gamma_{cyc} = 1\%$ . This may be attributed to the fact that Mashiri et al. (2016) focused on RSm with tyre chips ( $D_{r50}/D_{s50} = 20$ ) in contrast to the smaller particulate rubber (ShR) used in this investigation. This would also concur with the work on rubber powder (Bahadori and Manafi, 2015; Bahadori and Farzalizadeh, 2018) which established that the use of smaller rubber particles help in the development of the liquefaction resistance as a consequence of the greater rubber-to-rubber particle contacts.

#### 5.2.4 Shear modulus at medium-to-large strains

Shear modulus of RSm has been determined based on the stress-strain analysis shown in Section 5.2.2 and following the expressions presented in Chapter 2. The effect of particle properties, i.e. rubber content and size, on  $G$  is discussed as a function of the volumetric state variable ( $\gamma$ ). The initial results correspond to the value of the bulk parameters after two cycles ( $N = 2$ ) given that the initial results are commonly discarded because of the commonly observed overshooting (Nakhaei et al., 2012; Ehsani et al., 2015). The soil stiffness is then calculated as a function of  $N$  to evaluate the cyclic effect on saturated RSm.

***Effect of rubber content***

Figure 5.14a shows the variation in shear modulus of RSm at various strain amplitudes,  $\gamma_{cyc} = 0.05, 0.10, 0.20, 1\%$ , and rubber contents,  $\chi = 0, 10, 20$  and  $30\%$ . It is observed that shear modulus decreases with rubber content in the strain range studied. The decay in  $G$  is most pronounced with the addition of  $10\%$  ShR, and then the rate of reduction decreases with greater rubber contents, i.e.  $\chi = 20-30\%$ .

At  $\gamma_{cyc} = 0.2 - 1\%$ , it can be observed that the differences in shear modulus decrease between  $10, 20$  and  $30\%$  RSm, exhibiting a nearly identical shear modulus at  $\gamma_{cyc} = 1\%$ . Hence, the stiffness degradation in sand and  $10\%$  RSm occurs at a higher rate than in  $20-30\%$  RSm. These results support the argument that the addition of rubber reduces the stiffness degradation in the medium-to-large deformation range as a consequence of the elasticity added by rubber, as confirmed in the literature (Anastasiadis et al., 2012b; Pistas et al., 2018).

Figure 5.14a depicts the reduction in shear modulus with the application of larger strain amplitudes for all RSm. This decay in  $G$  is more significant in sand specimen, passing from  $G = 48.5$  MPa, at  $\gamma_{cyc} = 0.05\%$ , to  $G = 4.8$  MPa, at  $\gamma_{cyc} = 1\%$ . On the other hand, the effect of strain amplitude on the stiffness degradation of  $30\%$  RSm is lesser than on sand particles moving from  $G = 5.1$  MPa, at  $\gamma_{cyc} = 0.05\%$ , to  $G = 1.1$  MPa, at  $\gamma_{cyc} = 1\%$ . As previously mentioned, this is attributable to the higher compressibility with rubber, making the mixture less susceptible to experience stiffness degradation.

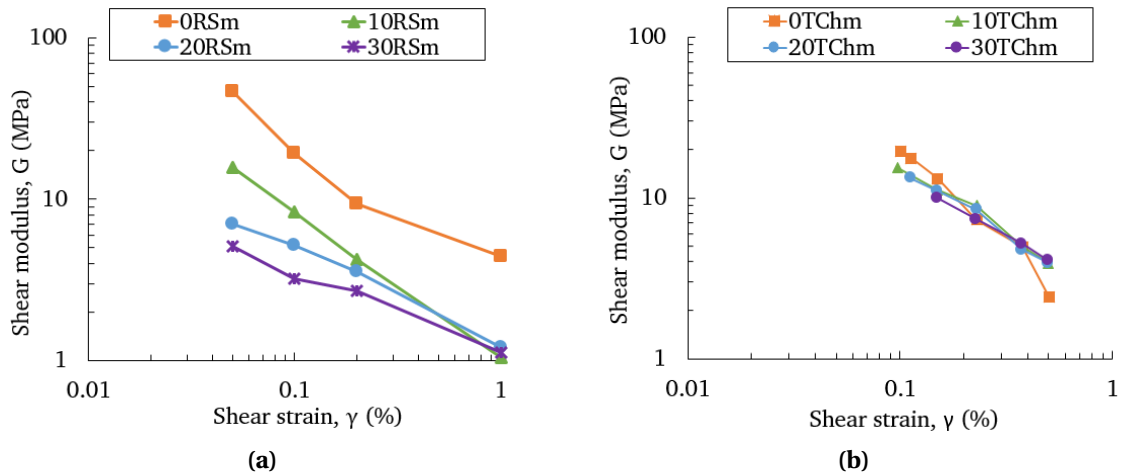


**Figure 5.14:** Shear modulus - shear strain at  $N = 2$  from a) this study, and b) Mashiri (2014)

### *Effect of rubber size*

The effect of size ratio between sand and rubber particles is discussed in this section by comparing the empirical results from this study with previous investigations.

Results obtained by Mashiri (2014) are shown in Figure 5.14b, which illustrate the variation in shear modulus with shear strain of sand-tyre chips mixtures (STCh). There are common features between this and Mashiri's investigation (Figures 5.14a-5.14b) such as adopted rubber contents and shear strain amplitudes, i.e.  $\gamma_{cyc} = 0.1-0.5\%$ . The main difference between the two studies come from the use of different particle sizes, where Mashiri (2014) used big rectangular tyre chips which exhibit a greater size compared to sand particles ( $d_{R50}/d_{S50} > 20$ ). This differs from the smaller size ratio ( $d_{R50}/d_{S50} \approx 1.8$ ) adopted in this investigation.

It is noticed in Figure 5.14b that soil stiffness decreases when adding rubber, and the difference in shear modulus between TChm drops steadily at large strains, as occurs in Fig. 5.14a. In this regard, all TChm exhibit a decay in shear modulus with strain amplitude up to  $\gamma = 0.4\%$ , where 30% TChm exhibits the greatest soil stiffness. This result contrasts with the trend seen in this study (Figure 5.14a), where sand exhibits the greatest stiffness. However, the main discrepancy is found in the higher soil stiffness exhibited by TChm compared to all RSm shown in Figure 5.14a at the strain range  $\gamma = 0.1-0.5\%$ . The difference in the soil stiffness of the mixture is more than double between

both investigations at  $\gamma = 0.2\%$ . e.g., 10% and 20% RSm exhibit  $G = 4.2$  MPa and 3.6 MPa in contrast to 10% and 20% TChm which show  $G = 9$  MPa and 8.5 MPa (Figure 5.14b).

As discussed in the literature (Lee et al., 2010; Pistolas et al., 2018) the rubber-like behaviour is more prominent when adding higher content of smaller particulate rubber, as a result of the rise in rubber-to-rubber contacts ( $S_R < 1$ ). The reported results supports the basis that adding bigger rubber particles, e.g. tyre chips, and thus, the increase in size ratio ( $S_R > 10$ ), points to an increase in mixture shear modulus and the contrary occurs with smaller rubber particles.

### ***Effect of cycle number***

Previous strong motions have shown that soil deposits can be subjected to large deformations which can be accentuated with the appearance of prolonged aftermath conditions (Nazari et al., 2014; Towhata, 2014). Under such deformations, saturated soils (Okur and Ansal, 2007; Brennan et al., 2005; Wichtmann and Triantafyllidis, 2016) might experience a significant stiffness and damping degradation. So far, only Mashiri et al. (2016) has investigated the cyclic effect on saturated sand-tyre chips mixtures up to 20 cycles. This study seeks to address this gap in the literature by evaluating the change in soil stiffness and damping ratio of RSm by applying a total of 400 strain controlled cycles. Figure 5.15 shows the change in  $G$  with  $N$  at  $\gamma_{cyc} = 0.05, 0.1, 0.2, 1\%$  at  $N = 400$ .

At medium strain amplitudes ( $\gamma_{cyc} = 0.1\%$ ), shear stiffness of mixtures containing rubber is not altered by the number of cycles and only sand appears to be affected by  $N$ , moving from  $G = 19.2$  MPa, at  $N = 2$ , to  $G = 14$  MPa, at  $N = 20$ . This seems to be in consonance with trends observed in the stress paths in Section 5.2.2, where an appreciable plastic deformation was observed in sand only specimens. At higher cycles, Figure 5.15a shows the gradual decrease in  $G$  of sand moving from  $G = 19.2$  MPa, at  $N = 2$ , to  $G = 1.14$  MPa, after 130 cycles when the sample liquefied (Figure 5.13a).

The evolution in shear modulus at high cycles of sand contrasts with the low change in soil stiffness after 10 cycles, where the specimen did not experience a significant stiffness degradation. However, at higher cycles and large amplitudes, the rise in pore water pressure led to a loss in surface contacts and a consequent stiffness degradation.

For  $\chi = 10\%$ , the stiffness degradation occurs at a lower rate, whereas for  $\chi = 20\text{-}30\%$ , the reduction in shear modulus is almost negligible as a consequence of the small accumulation in pore water pressure shown in Figure 5.13a. As observed in Figure 5.15, adding 10% rubber changes the predominately plastic behaviour of sand specimens to elasto-plastic and to a nearly elastic cyclic behaviour at  $\chi > 10\%$ .

Figure 5.15b and 5.15c show the marked reduction in soil stiffness of sand and 10% RSm at strain amplitudes  $\gamma_{cyc} = 0.2$  and 1%. The minimum shear modulus depicted in the graph correspond to the point when the specimens liquefied. Despite the initial high stiffness exhibited by sand at all strain amplitudes, sand stiffness decreases at a much higher rate than any RSm attributable to the higher increase in pore water pressure. Hence, 20% and 30% RSm exhibit higher soil stiffness than lower rubber contents after  $N = 80$  at  $\gamma_{cyc} = 0.1\%$ ,  $N = 15$  at  $\gamma_{cyc} = 0.2\%$  and  $N = 10$  at  $\gamma_{cyc} = 1\%$ . Based on the results with x-ray tomographic tests (Chapter 4), the compressibility and the induced contact area under loading increases the resistance against shear stresses of RSm and minimise the slippage between particles. As a result, the rubber deformability controls the behaviour of RSm under cyclic loading, being able to bend and deform under large deformations without experiencing significant stiffness degradation.



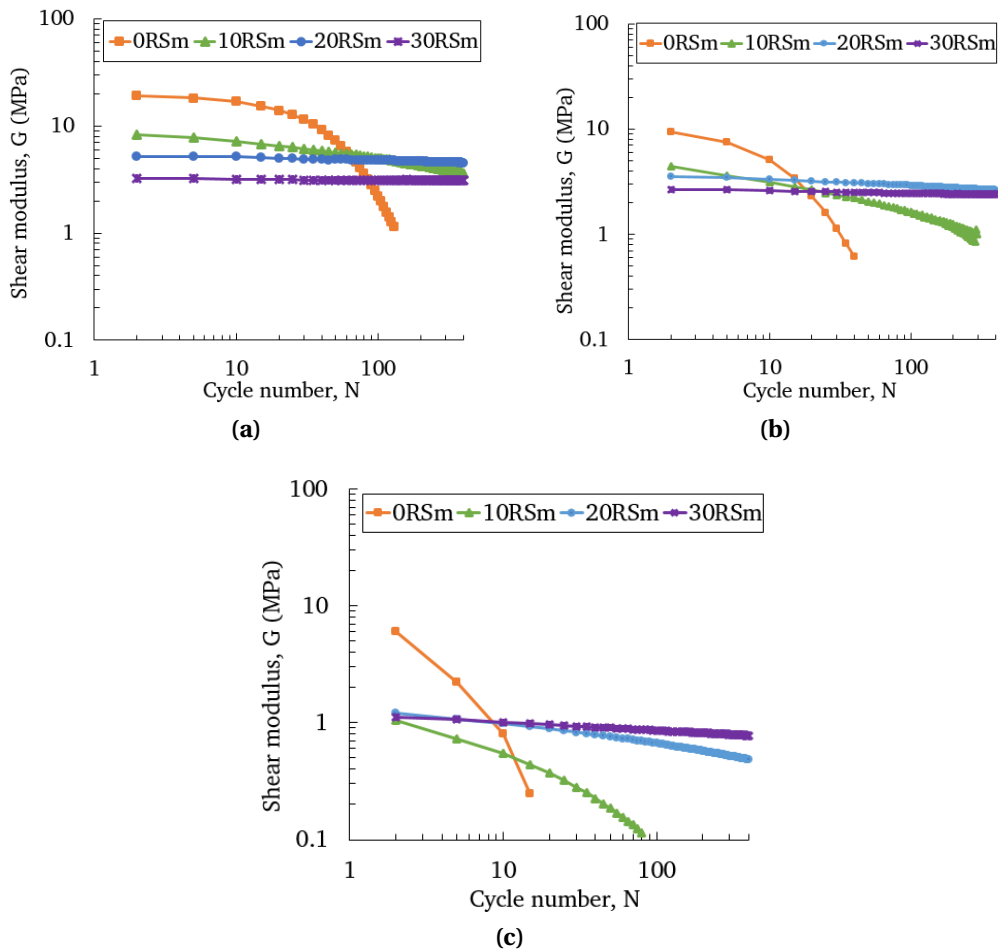


**Figure 5.15:** Shear modulus - number of cycles up to  $N = 400$ , at (a)  $\gamma_{cyc} = 0.1\%$ , (b)  $\gamma_{cyc} = 0.2\%$  and (c)  $\gamma_{cyc} = 1\%$

### 5.2.5 Damping ratio at medium-to-large strains

The hysteretic material (non-linear) damping has been evaluated in this section from the stress-strain analysis obtained from RSm specimens tested under undrained conditions. The damping ratio herein discussed corresponds to the material damping of a soil at an element scale and it is correlated to the energy dissipation mechanisms elucidated from the particle interaction in RSm (Chapter 4).

#### *Effect of rubber content*

The effect of rubber content on the hysteretic damping ratio when subjected to medium-to-large strains is displayed in Figure 5.16a. It is observed that 10% RSm exhibits greater damping than any rubber percentage at all strain amplitudes. This finding confirms

the improvement in the capacity to dissipate energy of RSm with the addition of rubber. This coincides with previous studies on the dynamic behaviour of RSm (Ehsani et al., 2015; Li et al., 2016; Pistolas et al., 2018) which stated that there is an improvement in the damping capacity by adding up to  $\chi = 20\%$ .

This can be explained on the basis that damping in rubber-soil mixtures is the product of both i) friction between particles contacts, but mainly ii) deformation of rubber, as established by Zheng-Yi and Sutter (2000). This is in consonance with the results obtained from the oedometer and x-ray tests in Chapter 4. The initial energy dissipation found in RSm is caused by the particle re-arrangement and sliding at inter-particle contacts. This is revealed via the initial irrecoverable deformation of the mixtures. However, the constant dissipation at subsequent cycles is explained by a different mechanism. The high inter-particle friction and rubber compressibility induces an increase in contact area and, consequently, a prevention of particle sliding. Therefore, the deformation of rubber dominates the dissipation mode.

The high damping ratio exhibited by 10% RSm can then be associated with the damping obtained from the predominant friction between mineral (sand) particles, i.e. friction damping, added to the rubber deformation. The combination of the two appears to contribute more to the overall damping than the hysteretic damping shown by sand specimens. Nevertheless, it is found in Figure 5.16a that additional rubber content ( $\chi = 20\text{-}30\%$ ) causes a decay in damping capacity at all strain amplitudes. As stated in section 5.2.2 and shown in previous studies (Lee et al., 2010), RSm exhibit a predominant rubber-like behaviour at  $\chi > 10\%$ , and an increase in rubber-to-rubber contacts. Thus, damping developed by RSm can be attributable to the predominant deformation of rubber, i.e. deformation damping. Hence, material damping generated by 20 and 30% RSm points to a lower damping capacity than at lower rubber contents. This confirms the hypothesis that there exists an optimum rubber percentage ( $\chi = 10\text{-}30\%$ ) at which the damping capacity is maximum (Senetakis et al., 2012a).

In terms of shear strain, Figure 5.16a depicts the increase in damping ratio of sand under the action of larger strains. It is observed that  $\xi$  reaches a peak at  $\gamma_{cyc} = 0.2\%$ , and then the value drops at  $\gamma_{cyc} = 1\%$ . As established by Pistolas et al. (2018), this is

due to the existence of a limiting shear strain  $\gamma_{lim}$ , defined as the strain at which the higher damping ratio is observed in soils, which appears to increase with the addition of rubber. Although a reduction in the damping capacity is seen at  $\chi > 10\%$  (Anbazhagan and Manohar, 2016), the limiting shear strain is found earlier in sand specimens which differs from the increasing trend observed in the damping ratio of 20-30% RSm. This suggests that the maximum damping ratio has not arisen yet and it increase at larger strain amplitudes.

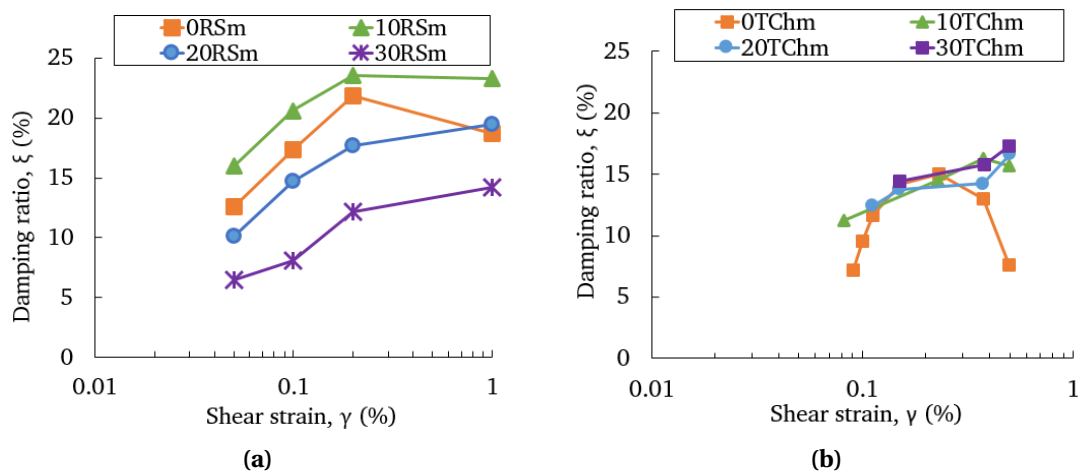


**Figure 5.16:** Damping ratio - shear strain curve at  $N = 2$  from a) this study, and b) Mashiri (2014)

### Effect of rubber size

The change in size ratio between sand and rubber particles has been assessed by comparing the results of this study with the empirical investigation conducted by Mashiri (2014). Figure 5.16b shows the variation in damping capacity with strain amplitude by adding big rubber tyre chips, which present a size ratio  $d_{R50}/d_{S50} > 20$  (Mashiri, 2014). A decrease in damping ratio with the addition of  $\chi = 20-30\%$ , displayed in Figure 5.16a ( $d_{R50}/d_{S50} \approx 1.5$ ), differs from the generalised improvement in the damping capacity of tyre chip mixtures (TChm) for all rubber inclusions depicted in Figure 5.16b.

It can be observed that all TChm follow a similar trend with a positive increase in damping ratio with rubber. Damping improvement is achieved adding 10% TCh whereas the inclusion of additional rubber generates a marginal increase in damping ratio, showing slight differences in  $\xi$  between 10-30% TChm. However, the damping

ratio exhibited in this study with 10% RSm present greater values in Figure 5.16a than all TChm illustrated in Figure 5.16b. This discrepancy in damping capacity can then be attributed to the different size ratio of both mixtures. The primary load-carrying chains created within soil matrix depend on the amount and size of rubber/sand and this will define the transition between sand-like behaviour and rubber-like behaviour as stated by Kim and Santamarina (2008) and Lee et al. (2010).

Consequently, adding larger rubber particles in the mixture leads to a stiffer soil matrix than with smaller particulate rubber, showing a predominant sand-like behaviour. On the other hand, a clear rubber-like behaviour is observed in RSm at higher rubber contents in this study ( $\chi > 10\%$ ), as revealed in Figures 5.14a and 5.16a. This is also consistent with previous studies (Li et al., 2016; Pistolas et al., 2018) which stated that there is an improvement in the damping capacity of RSm at low confining pressures ( $\sigma_m < 200$  kPa) and when adding particulate rubber.

### ***Effect of cycle number***

The evolution in damping ratio has been depicted in Figure 5.17 as a function of cycle number and strain amplitudes at  $\gamma_{cyc} = 0.1-1\%$ . With the exception of sand at  $\gamma_{cyc} = 0.1\%$ , all RSm exhibit a marked negative tendency in evolution of damping ratio.

At  $\gamma_{cyc} = 0.1\%$ , it is noted that  $\xi$  decreases gradually with N, regardless of rubber percentage, until N = 20. After this, damping capacity continues dropping but the rate of degradation is observed to be lower. On the other hand, the trend depicted by sand reveals that  $\xi$  is slightly affected by the number of cycles until N = 10, but then it starts to gradually increase until N = 100. The friction damping developed by particulate sand is thus greater than the combination of particle sliding and rubber deformation developed by RSm at N = 100. However, whilst all RSm maintain a similar damping capacity, the value shown by sand drops due to liquefying. The same phenomenon is seen at  $\gamma_{cyc} = 0.2\%$  in Figure 5.17b. Sand exhibits a greater damping capacity than the rest of RSm at N = 20 but then it liquefies resulting in a significant decay of damping ratio. On this occasion, all RSm present a greater capacity to dissipate energy due to being subjected to more deformation. The main difference between the two strain amplitudes stems

from the fact that RSm experience a lower stiffness degradation at  $\gamma_{cyc} = 0.2\%$ , and this is less significant with the addition of rubber.

Albeit sand exhibits an initial higher damping, the addition of rubber results in greater damping capacity after 20 strain controlled cycles at  $\gamma_{cyc} > 0.2\%$ . The explanation for this behaviour is on the basis that particle sliding is ineffective in mineral (sand) specimens after several cycles due to the rise in pore water pressure and once particles have been re-arranged. Thus, the contribution of the damping developed by sliding of sand particles to the total damping capacity is attenuated as the specimen is subjected to more cycles, whereas energy dissipation generated by rubber deformation remains in the long-term. This phenomenon is more evident in sand and 10% RSm at  $\gamma_{cyc} = 0.2 - 1\%$  (Figs. 5.17b-5.17c). The energy dissipated in RSm is thus controlled by rubber deformation as rubber content increases.

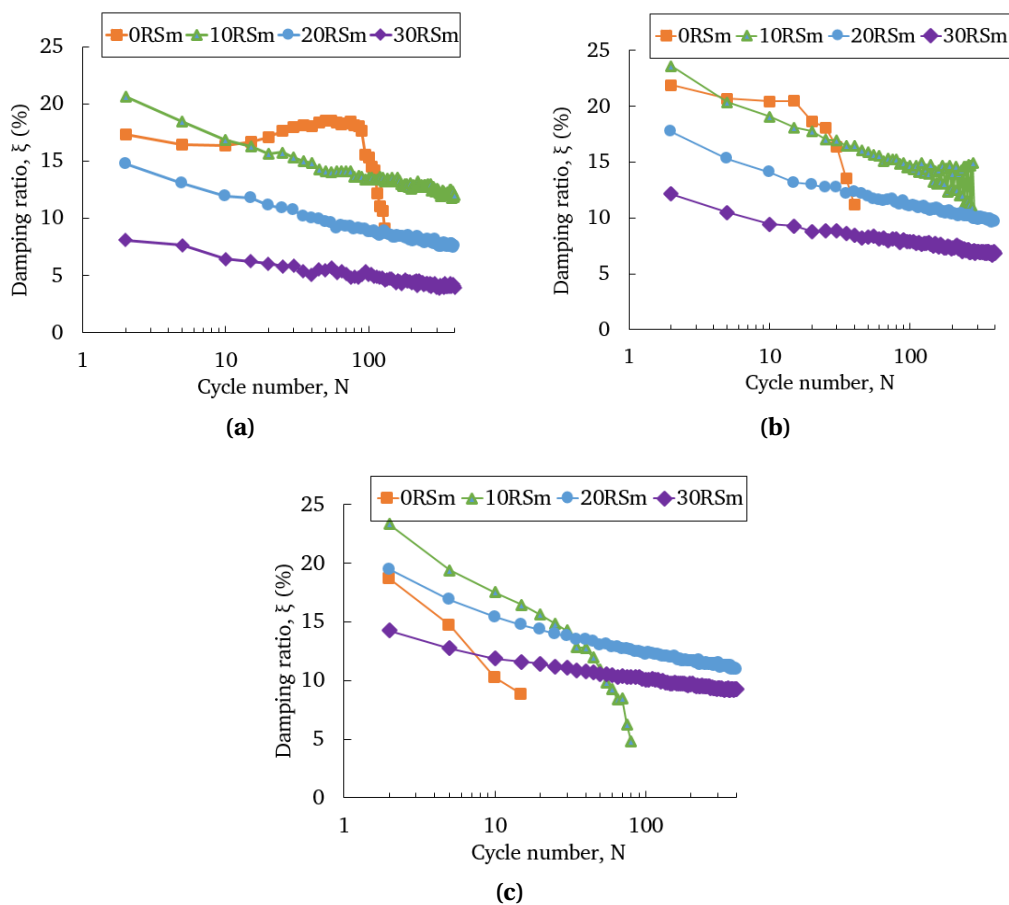


**Figure 5.17:** Damping ratio - number of cycles up to  $N = 400$  at (a)  $\gamma_{cyc} = 0.1\%$ , (b)  $\gamma_{cyc} = 0.2\%$  and (c)  $\gamma_{cyc} = 1\%$

## 5.3 Torsional resonant column equipment

To fully characterise the dynamic behaviour of RSm, both shear modulus and damping ratio have been calculated from very small-to-medium strain amplitudes via torsional resonant column experiments. The expressions adopted to calculate maximum shear strain as well as maximum soil stiffness ( $G_0$ ) have been discussed in Chapter 2. The evaluation of minimum damping ratio ( $\xi_0$ ) is herein discussed in accordance with the calculation of the material viscous (linear) damping ratio. Equipment, specimen preparation and test set-up carried out are covered as follows:

### 5.3.1 Equipment, materials and methods

#### *Equipment*

Resonant column tests were performed using a ©GCTS TSH-200 Resonant Torsional column shear testing system at the Department of Soil Mechanics at the Indian Institute of Science, Bangalore. This research was part of a three months placement funded under the Newton Bhabha PhD Placement Programme 2018. [ASTM D4015 \(2015\)](#) was adopted to perform these experiments.

The equipment used can vibrate the top of the soil specimen to frequencies up to 250 Hz by means of a torsional device which is connected to a rotational sensor and a torque transducer. All of them are attached to the top platen shown in Figure 5.18. This equipment accepts specimens with diameters from 50 mm to 100 mm. The standard motor of the system has a 2.3 Nm torque capacity and weighs 1.8 kg. It was pressurised by using pneumatic pressure fluid. The Computer Aided Testing System (CATS) available offered an advanced digitalised servo control over the sensors and transducers of the system. Experimental data recording was completed via GCTS control software installed in the equipment. Recorded data were: time (s), torque (T)(Nm), back pressure (BP)(kPa), confining pressure ( $\sigma_m$ )(kPa), acceleration (a)(g) and phase shift (rad). One thousand data points per second per variable were stored, as previously done with cyclic triaxial experiments. Table 5.4 shows the minimum and maximum range as well as resolution

of torque, cell/back/pore pressure and volume change are in Table 5.4.

**Table 5.4:** Resolution and range for transducers of resonant column experiments

Transducer	Minimum range	Maximum range	Resolution
Torsional load	0	2.3 Nm	$\pm 0.00001$ Nm
Rotational angle	0	360 degrees	$\pm 0.1$ degree
Volume change	0 cc	90 cc	$\pm 0.001$ cc
Cell Pressure	-50 kPa	1000 kPa	$\pm 0.1$ kPa
Back Pressure	-100 kPa	1000 kPa	$\pm 0.1$ kPa
Pore pressure	-100 kPa	1000 kPa	$\pm 0.1$ kPa

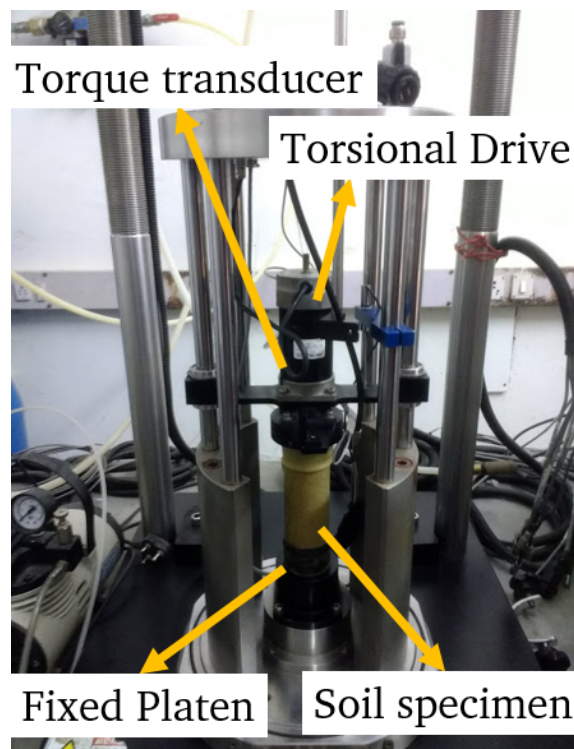


**Figure 5.18:** Resonant column equipment and set-up

There are sources of error that can affect the interpretation of the output data. A general assumption is that the soil only experiences torsional deformation under the action of the torsional single-degree of freedom oscillation under resonance. However, there are a series of factors which can have an effect on the resultant resonant frequency (Kumar and Clayton, 2007; Clayton et al., 2009) as herein described:

- Different patterns of soil distortion, i.e. flexure, torsion, axial shortening, due to the incorrect connection between the top cap and the specimen, inaccurate alignment of drive coils, or the fact that the specimen top is not perfectly horizontal.

- Additional distortions, result of bending of apparatus components, which would lead to a softer response of the specimen. These additional distortions might be associated with the compliance between different elements of the apparatus including; i) compliance between specimen and apparatus, i.e. slippage and bedding, ii) compliance between drive system and platen, i.e. connections of coils and drive head, or iii) support compliance, i.e. lack of base fixity.
- Additional degrees of freedom. This can occur due to the compliance between the drive head and base platen or the slippage between different components of the system. All these factors can result in a shear wave velocity of between 6.7% and 27.5% higher than the value of the specimen (Kumar and Clayton, 2007) with a subsequent increase in the shear modulus which magnitude can be a 41% higher (Clayton et al., 2009). The literature establishes the issues related to the data interpretation are more likely to arise in specimens with a high torsional stiffness or strongly cemented materials. Hence, the calculated shear modulus and damping ratio determined from resonant column tests are considered to remain acceptable for resonant frequencies up to 175 Hz. This is for instance the case of this investigation, with a maximum 130 Hz of resonant frequency and 111.8 MPa corresponding to the maximum shear modulus of sand.

### ***Material preparation***

Resonant column tests were conducted on 50 x 100 mm samples of RSm containing shredded rubber at various gravimetric proportions  $\chi = 0, 10, 20$  and 30%. Figure 5.18 shows a sand specimen before consolidation. RSm specimens were prepared following the procedures explained in Section 5.2.1. A 2.5% minimum moisture was added to minimise the segregation of particulate sand. RSm specimens were prepared in the apparatus to reduce the specimen disturbance. To ensure consistency and repeatability of resonant column experiments, an initial relative density was adopted as the main material descriptor for every RSm. In line with the sample preparation for the cyclic triaxial tests (Section 5.2.1), both height, i.e. 100 mm, and sample volume, i.e. 200  $cm^3$ , were set at a similar value for all contents whilst the rubber content increased to maintain the rubber/sand mass ratio. Then, the number of voids in the specimen was



controlled in such a way that sample void ratio remained proportionally at the same distance from the values of  $e_{min}$  and  $e_{max}$  for each gravimetric proportion (Figure 5.5). Hence, four layers of 25 mm were formed by adding the required amount of rubber and sand to maintain the gravimetric proportion. As shown in Table 5.5, all RSm specimens remained within the aimed dense relative density, i.e.  $D_r = 65-85\%$ . Although small differences can be found in terms of relative density between cyclic triaxial and resonant column tests, an objective comparison has been undertaken in this study to understand the dynamic behaviour of RSm from small-to-large deformations, as later analysed and discussed in Chapter 7.

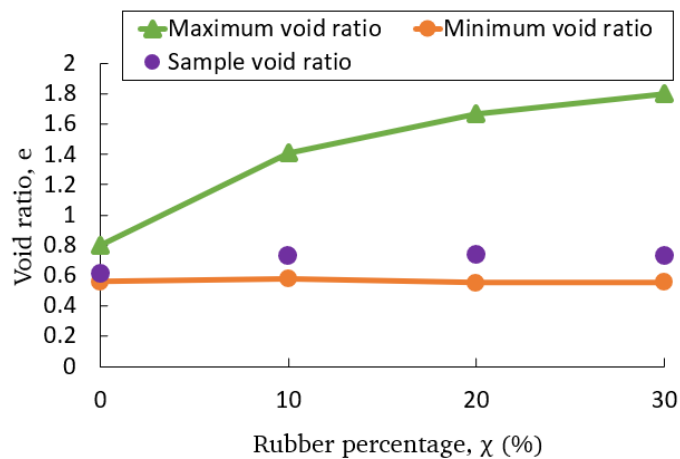


**Figure 5.19:** Maximum, minimum and sample void ratio

**Table 5.5:** Relative density obtained for resonant column experiments

Test	$e_{minRSm}$	$e_{maxRSm}$	$e_{sample}$	$D_r$ (%)
0RSm	0.54	0.80	0.62	74.8
10RSm	0.55	1.41	0.79	74.6
20RSm	0.55	1.67	0.81	74.9
30RSm	0.55	1.80	0.82	78.6

Whilst specimens tested in cyclic triaxial apparatus were prepared under undrained, saturated conditions, samples prepared in torsional resonant column were tested under dry conditions. This was done on the basis that the degree of saturation does not have a significant effect on the evaluation of soil dynamic properties at small-to-medium strain amplitudes (Anastasiadis et al., 2012a; Senetakis et al., 2012b).

### ***Methods***

Once the sample was prepared in place, the end platen and the vibration excitation device (motor) were attached to the specimen. A vacuum pressure of 20 kPa was applied during sample preparation and maintained for the test setup. This was done to prevent any specimen disturbance as a consequence of the extra weight placed on top of the specimen containing deformable rubber.

The vibration excitation device was connected to the sine wave generator and the power supply. The readout instruments required to measure acceleration and shear strain were also connected. Isotropic stresses up to 100 kPa were applied to RSm specimens, enclosed by the rubber membrane, introducing an air-confining media through the pneumatic pressure system.

To proceed with the determination of shear stiffness and damping, a torsional load was externally applied to the top of the specimen (Figure 5.18) whilst the bottom platen, which represents the passive-end, was fixed. Excitation frequency was increased by applying the same torque, until reaching the system resonance. At this point, the soil undergoes the maximum response, in terms of strain amplitude, known as the soil fundamental frequency.

Torque amplitude was increased from 0.01 Nm up to 0.9 Nm for every RSm to obtain representative values of shear stiffness and damping along the range of small-to-medium strain levels. All samples were isotropically consolidated under the same pressure ( $\sigma_m = 100$  kPa). A summary with the resonant column experiments is presented in Table 5.6. A test ID classifies each sample identifying rubber amount as well as strain amplitude tested in every experiment.

Resonant column tests were performed under dry, undrained conditions to evaluate both shear modulus and damping ratio of RSm at small strain amplitudes (i.e.  $\gamma_{cyc} = 1 \times 10^{-4} - 1 \times 10^{-1}$  %). Based on the literature review, cyclic effect is not considered for the evaluation of  $G$  and  $\xi$  at small-to-medium strains. This is on the basis that soil elements experience a relatively small deformation when predominately tested in the linear elastic zone. For this reason, this is not part of the scope of this study.

**Table 5.6:** Classification of resonant column experiments

Test ID	$\chi$ (%)	Cyclic shear strain amplitude, $\gamma$ (%)
1-0RSm	0	$1.8 \times 10^{-4}$ - $5.3 \times 10^{-2}$
2-10RSm	10	$2.5 \times 10^{-4}$ - $4.7 \times 10^{-2}$
3-20RSm	20	$3.9 \times 10^{-4}$ - $5.6 \times 10^{-2}$
4-30RSm	30	$5.3 \times 10^{-4}$ - $6 \times 10^{-2}$

### 5.3.2 Shear modulus at small-to-medium strains

#### *Effect of rubber content*

The variation in shear modulus - shear strain curve is illustrated in Figure 5.20a for all RSm. It is noticed that the overall soil stiffness decreases with the addition of rubber. As already stated, this is due to the low stiffness introduced by the presence of rubber as a result of its high capacity to deform under load. This coincides with previous studies (Senetakis et al., 2012a; Pistolas et al., 2018; Zheng-Yi and Sutter, 2000), all of which found a significant reduction in the mixture stiffness at  $\chi > 20\%$  (Figure 5.20b). Shear modulus at very small strains corresponds to the maximum shear stiffness  $G_0$  of an undisturbed soil. From Figure 5.20a, it is shown that  $G_0 = 111.8$  MPa, 52.3 MPa, 20.2 MPa, and 7.9 MPa for  $\chi = 0, 10, 20$  and 30%, respectively. All RSm exhibit a relatively constant shear modulus at medium strains, i.e.  $\gamma = 0.01\%$ , from which the mixture stiffness gradually decreases. This phenomenon is observed to be more pronounced at  $\chi = 0\%$  and 10%, as one would expect for a sand dominated mixture, i.e. sand-like behaviour (Lee et al., 2010). On the other hand, the decay in soil stiffness with strain amplitude is lower with rubber content ( $\chi = 20, 30\%$ ). Therefore, stiffness degradation is also attenuated with rubber content at small-to-medium strain amplitudes, in consonance with the results reported in the medium-to-large strain range (Figure 5.15).

### Effect of rubber size

Senetakis et al. (2012a) investigated the dynamic behaviour of RSm containing crumb particles. Figure 5.20b shows the results on RSm containing crumb rubber with a  $d_{R50}/d_{S50} > 5$  in contrast with the mixture, containing shredded rubber, evaluated in this study with a  $S_R \approx 1.8$ . It can be observed that there is a greater reduction in shear modulus of RSm containing ShR (Figure 5.20a) in contrast with mixtures containing CrR (Figure 5.20b), which is more evident at  $\chi > 10\%$ . This is for instance the case of 30% RSm which presents a value of around 7.9 MPa, whilst 35% RSm presented by Senetakis et al. (2012a) shows  $G = 19$  MPa. Following the discussion from Chapter 4, this could be attributed to the greater size of crumb rubber investigated by Senetakis et al. (2012a) which would result in a higher number of contacts between sand particles, i.e. sand-like behaviour. On the other hand, a greater number of rubber-to-rubber contacts would be the cause of the higher reduction in the mixture stiffness, as demonstrated by Anastasiadis et al. (2012b).

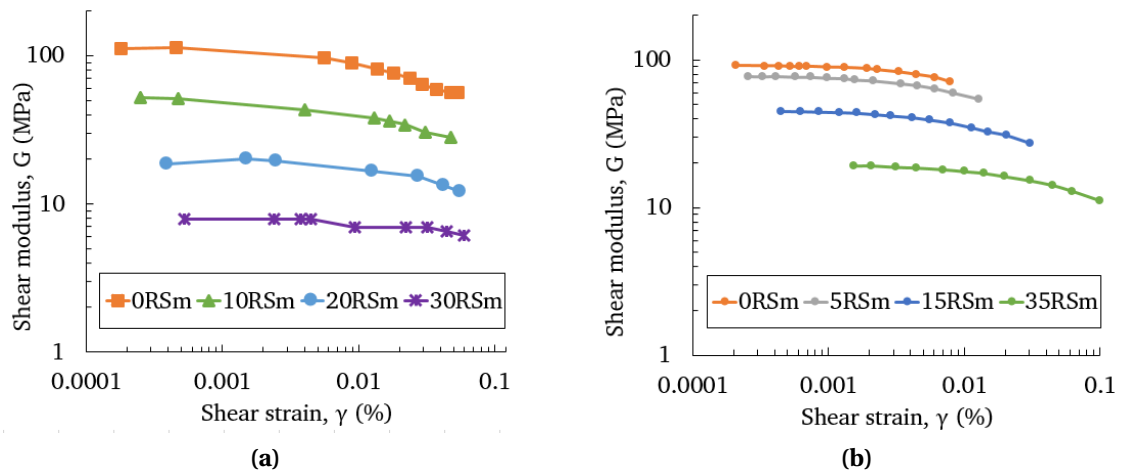


**Figure 5.20:** Shear modulus - shear strain from a) this study, and b) Senetakis et al. (2012a)

### 5.3.3 Damping ratio at small-to-medium strains

#### *Effect of rubber content*

Damping ratio has been studied as a function of shear strain for RSm at small deformations as seen in Figure 5.21a. Compared to the hysteretic (non-linear) damping ratio (Figure 5.16a), viscous (linear) damping ratio increases steadily at all rubber contents with the application of higher deformations. At very small strains ( $\gamma = 0.0001\%$ ), it is noted an improvement in the minimum damping ratio with rubber addition. Minimum damping ratio  $\xi_0 = 0.52\%$ ,  $1.52\%$ ,  $2.51\%$ ,  $2.44\%$  is exhibited for each rubber content  $\chi = 0\%$ ,  $10\%$ ,  $20\%$ , and  $30\%$ .

As established by [Zheng-Yi and Sutter \(2000\)](#), energy dissipation mechanisms in RSm at an element scale are attributed to the combined development of the friction damping through particle sliding of rigid soils in addition to damping generated via rubber deformation. Damping ratio of RSm increases in this study with the rubber content up to  $\chi = 20\text{-}30\%$ . This is in consonance with existing research ([Zheng-Yi and Sutter, 2000](#); [Anastasiadis et al., 2012a](#)), which established that the evolution in damping capacity is favoured by the inclusion of rubber.

It is then observed that the evolution in damping ratio with shear strain exhibits a more linear shape when increasing the amount of rubber, as occurred with the stiffness degradation curve. This can be related to the high flexibility added by rubber material. All mixtures seem to convey in a nearly similar damping ratio at around  $\gamma_{cyc} = 0.015\%$ , which is in the line with the results presented by [Senetakis et al. \(2012a\)](#) and [Pistolas et al. \(2018\)](#). After this, the damping ratio increases at a higher rate in sand than the rest of RSm, exhibiting greater damping ratio than 20-30% RSm.

**Effect of rubber size**

Figure 5.21b shows the evolution in viscous damping ratio versus shear strain of RSm containing particulate crumb (Senetakis et al., 2012a) with a  $S_R > 5$ . It can be observed that the minimum damping ratio increases with rubber content, reaching a value  $\xi_0 = 2\%$  at  $\chi = 30\%$ . By comparing Figures 5.21a and 5.21b, a similar tendency is noted in the evolution of viscous (linear) damping of RSm in relation to the rubber amount. Whilst mixtures containing low rubber contents exhibit a lower minimum damping ratio, all mixtures seem to convey in a similar damping ratio at  $\gamma_{cyc} = 0.01-0.015\%$  regardless of the rubber size. Consequently, rubber shape does not appear to have a significant effect on the evolution of viscous damping at small-to-medium strains.

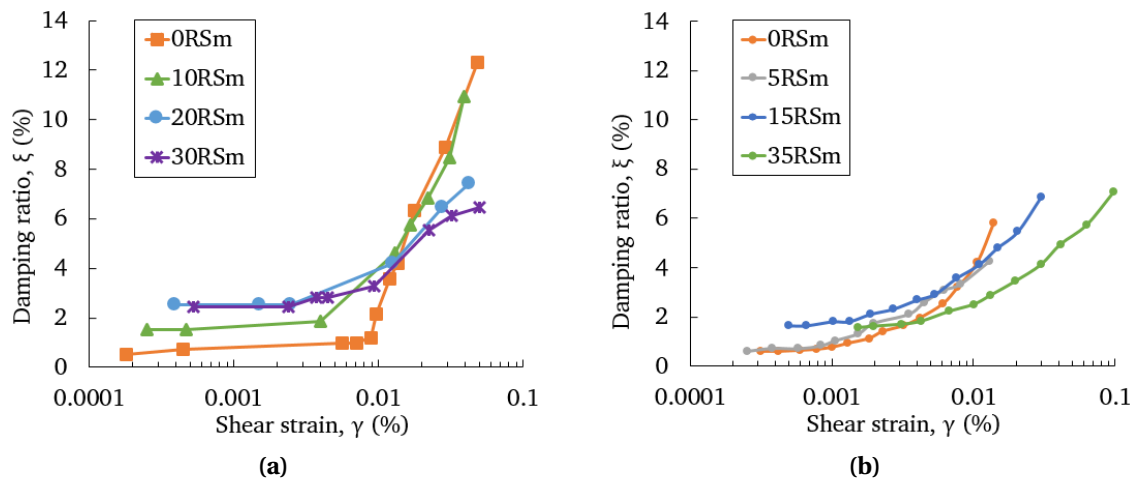


**Figure 5.21:** Damping ratio - shear strain curve from a) this study, and b) Senetakis et al., 2012a

## 5.4 Summary

Dynamic behaviour of RSm has been evaluated in the small-to-large strain range through a series of cyclic triaxial and resonant column tests.

- Liquefaction resistance of RSm increased when adding rubber. A conceptual model was adopted to distinguish between stable zone; where RSm samples did not liquefy, and unstable zone; where liquefaction was observed. All sand specimens remained within the unstable zone due to liquefying at  $N < 100$ . Adding  $\chi = 20\text{-}30\%$  enabled the mixture to withstand 400 strain controlled cycles up to  $\gamma_{cyc} = 1\%$ .

- Soil stiffness decreased with strain amplitude and number of cycles at every rubber percentage. Adding rubber to the mixture led to a reduction in the overall soil stiffness which was attributed to the lower stiffness and capacity to deform of rubber. By contrast, adding more rubber ameliorated the cyclic effect on soil stiffness degradation.

- Material hysteretic damping of RSm increased when adding  $\chi = 10\%$  and then decayed at higher rubber contents at medium-to-large strains.

- Whilst rubber shape did not appear to have an effect on the evolution of viscous damping ratio at small-to-medium strains, the results pointed to an improvement in viscous material damping with rubber content up to  $\chi = 30\%$ .

In terms of new understanding, this study has found that the energy dissipated through particle friction in addition to the deformation of rubber results in a higher damping capacity of RSm at small-to-large strains. This study has also demonstrated that mixing small shredded rubber and sand results in a mixture which exhibits a high resilience against the action of medium-to-large deformations, induced via multi-cyclic loading. This is attributed to the high deformability added by rubber which leads to a lower accumulation of pore water pressure and a higher liquefaction resistance. Whilst sand-like soils liquefy and experience a significant loss in soil stiffness and material damping, rubber-like soils can withstand up to 400 strain controlled cycles without liquefying. This means that RSm, which contain at least 20% rubber mass, can continue dissipating energy in the long-term whilst experiencing a minimum soil stiffness degradation.

# *Cyclic behaviour of a small scale RSm foundation*

---

## **6.1 Introduction**

The literature review of this study has focused on the fundamental dynamic behaviour of RSm in the context of an element test. Indeed this is the main focus of this thesis, having analysed the effect of particle properties and test conditions on the mixture stiffness and damping capacity (Chapter 5).

A review of the literature on the cyclic performance of geotechnical seismic isolation systems, concretely using RSm, has also been discussed in Chapter 3. The findings in this field argue that the isolation efficiency of soft zones improves when altering its geometrical conditions. However, the issues around implementation are significant. Consider, for example, RSm installed as discrete zones, e.g. as columns or layers, contiguous with the host soil. Questions about the geometry and interaction of RSm with the host soil must be addressed if RSm is to enhance seismic protection. A rigorous investigation is beyond the scope of this thesis but it seemed worthwhile to take the opportunity to devise a number of simple small-scale shaking table tests to gain some insight into the way in which zones of RSm influence a host soil system. Thus this chapter presents an account of the development, execution and findings of small-scale shaking table tests.



## 6.2 Equipment, materials and methods

This chapter presents the results of an initial experimental exploration of the influence of soft zones, specifically vertical installations of rubber-soil mixtures, on the dynamic behaviour of a small-scale foundation-soil system subject to cyclic loading.

A shaking table was used to apply a sequence of sinusoidal excitations to the foundation-modified soil system. The soil model was devised to allow zones of RSm to be packed adjacent to, and to support, a 'foundation'. The stiffness of the modified RSm zone was de facto controlled by the RSm composition. The aim of these tests is to reveal the natural frequency, amplification, and damping properties of the foundation system, and any shifts, due to the presence of vertical soft zones. The objectives are:

- To reveal amplification, natural frequency, and damping capabilities of a foundation-modified soil system altered by the installation of soft zones.
- To determine the damping capacity of the foundation-modified soft zone.
- To identify the optimum rubber percentage of RSm to attenuate the dynamic response of the foundation-modified soil system.
- To relate shaking table findings to pre-existing work on soft zones.

### *Overview of the experimental set-up*

The foundation system is represented by a box containing a lumped mass located atop a central foundation pillar of silicon rubber of similar plan dimension as the box (Figure 6.1). The foundation column is secured at its base inside a rigid shake box. A mass of 3 kg was fixed inside the box to control the natural frequency of the silicon foundation. The dynamic oscillation of the unsupported lumped mass and foundation column has been designed to mimic that of a SDOF lumped mass system.

The space between the foundation column and inside walls of the shake box in the direction of oscillation was packed with small bags containing RSm at  $\chi = 0 - 40\%$ . In this way, the oscillation of the foundation column is supported laterally by soft zones, but has a consistent, i.e. fixed for all test, set of properties (Figure 6.1). The soft zones are

installed to absorb and dissipate the transfer of energy from shake box to the foundation column and, in turn, to the top of the lumped mass. The narrower spaces between the foundation column and shake box normal to the direction of oscillation were not packed to avoid frictional contact and hence to remove one source of unaccountable energy losses.

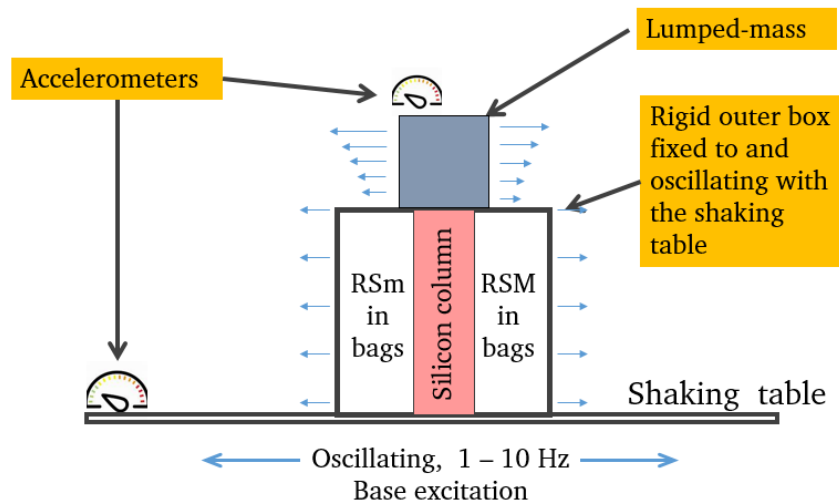


**Figure 6.1:** Experimental set-up for shaking table test

### ***Equipment***

The experimental testing was performed on a custom-built 0.5 m by 0.5 m shaking table. The table was shaken sinusoidally in one horizontal direction using an Electromechanical Cylinder (EMC) 80-32 manufactured by Rexroth (Figure 6.2). The EMC had a piston diameter equivalent to 80 mm and a built-in Rexroth ball screw assembly with a diameter of 32 mm according to the ISO 15552 standard cylinder. A 180 mm long by 40 mm diameter steel craft shank was employed to connect the EMC to the base plate of the shaking table. The uniaxial horizontal movement was thus ensured by screwing the end of the rod to a fixed metallic section on the table. The EMC can apply a maximum force of 21.6 kN and a velocity of 1.6 m/s, which is the equivalent to a payload capacity of 2200 kg and  $50 \text{ m/s}^2$ . Resolution and range for transducers are in Table 6.1.

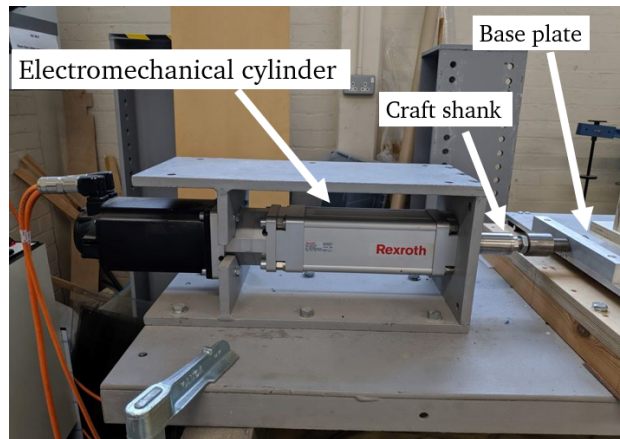


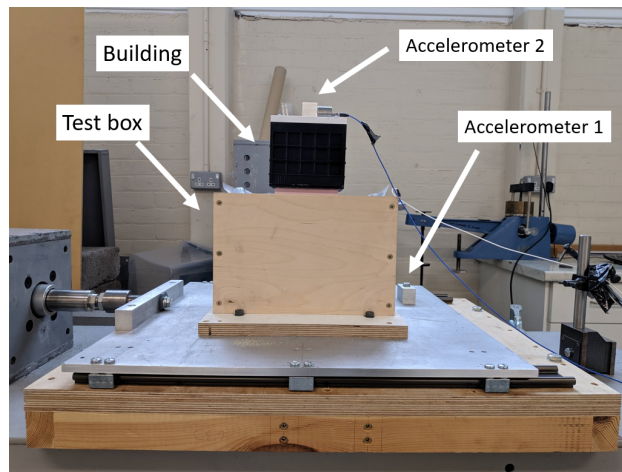
**Figure 6.2:** Electromechanical Cylinder

The tests were performed inside a 0.285m x 0.185m x 0.185m timber box with rectangular shape using 15 mm thickness walls (Figure 6.3). The walls of the box were rigidly fixed. The base plate was placed and fitted on top of two parallel rails which ensured the horizontal movement of the shaking table. The rails were attached to a timber base which was screwed to the top of a 1.5 m x 1.5 m x 1 m box filled up with sand. The sand within the container served to minimize extraneous vibration.

The horizontal response was measured with accelerometers mounted on the outer part of the rigid box ( $A_1$ ), and atop the lumped-mass ( $A_2$ ) as seen in Figure 6.3.  $A_1$  is a DYTRAN 3055B1 whereas  $A_2$  is a PCB 393B04 manufactured by piezometrics (Table 6.1). Vertical accelerations were not expected and have not been measured in this thesis. Data sampling was undertaken using Labview software linked to a compact data acquisition system (cDAQ) 9178 fitted with a 9234 accelerometer module at a rate of sampling rate of 0.2 ms. A series of calibration tests were performed to check the performance of the accelerometers by comparing experimental and theoretical values, based on the evolution of harmonic sinusoidal motions. This was done to ensure that the horizontal accelerations recorded by the carriage mimicked that of the applied input motion, via the EMC, and thus verify the boundary effects of the rigid walls.

**Table 6.1:** Resolution and range for transducers of EMC

Equipment	Minumum range	Maximum range	Resolution
EMC Velocity	0	1.6 m/s	$\pm 0.01$ m/s
EMC Load	0	21600 N	$\pm 0.1$ N
EMC Stroke	11 mm	94.5 mm	$\pm 0.01$ mm
Accelerometer 1	-50 g	50 g	$\pm 0.000005$ g
Accelerometer 2	-5 g	5 g	$\pm 0.000005$ g

**Figure 6.3:** Front view of the rigid box

### *Scaling laws*

The mechanics of model tests on soil-structure systems are well known which comprise of two main principles (Iai et al., 2005). The first focuses on the material behaviour of soil, and it states that the stress-strain behaviour of the soil in the model should represent that of the prototype by a series of scaling relationships, i.e. scaling relationships. The soil behaviour, characterised by its shear strength and stiffness, is stress-dependent and thus the stress-strain behaviour should be studied in order to reach the same conditions with the model. The second principle related to the mechanics of soil-structure systems. Hence, the fundamental laws of mechanics, i.e. mass balance and equilibrium, should be achieved in both the prototype and the model.

Adequate similitude relationships are required for the design of small scaled-model tests, e.g. shaking table tests, so that the experimental results can be extrapolated to full-scale conditions. In line with the most widely 1g similitude relationships (Iai,

1989), there are three independent scaling factors: geometry scaling factor ( $\lambda$ ), which is applied to the scale model design, density scaling factor ( $\lambda_\rho$ ), assumed to be equal to 1 for the same soil, and strain scaling factor ( $\lambda_\epsilon$ ), determined using shear wave velocity measurements and also assumed to be 1. The value  $\lambda$  is also known as the scaling factor and it represents the number of times a full-size prototype is scaled down; i.e.  $\lambda = \text{size prototype} / \text{size of model}$ .

Scaling laws are the relationships that enable the comparison between the scaled-models and the real prototypes. As shown in Table 6.2, there are different scaling laws depending whether the scale model is tested under dynamic centrifuge or 1g shaking table tests. The differences are found in the stress condition, acceleration and time. 1g model tests reflect the stress field associated with a 1g field, which is the case of the shaking table experiments discussed in this Chapter. On the other hand, centrifuge model tests experience the stress field consistent with the prototype due to applying centrifugal accelerations, while the acceleration needs to be accordingly scaled.

**Table 6.2:** Scaling laws for dynamic centrifuge tests and 1g shake table test (Park and Kim, 2013)

Quantities	Dynamic centrifuge	1g shake table test
Displacement, length	$\lambda$	$\lambda$
Acceleration, gravity	$\lambda^{-1}$	1
Mass	$\lambda^3$	$\lambda^3$
Density	1	1
Stress	1	$\lambda$
Strain	1	1
Time (Dynamic)	$\lambda$	$\lambda^{0.5}$

The scaling relationships can be applied to soil models when the deformations are relatively low, such as the case of this study, prior to the failure (Park and Kim, 2013). This is one of the main limitations found when using 1g models. Significant discrepancies are commonly found between the stress ratio recorded in the model and the prototype, due to the non-linear effects of confining stress on the evolution of shear strength and shear modulus under large deformations. Hence, a direct relationship cannot be established between a prototype and its model under the ultimate state of stability due

to the presence of large deformations or loss of soil contact (Iai et al., 2005).

Based on the scaling relationships (Table 6.2), the acceleration recorded on a 1g model test would be the same as applied to the full scale prototype. On the other hand, geometry and mass of the model box, stress and time should be scaled. The objective of this Chapter is to explore the evolution in the acceleration histories of a single degree of freedom system whilst modifying the lateral conditions. Hence, the idea is not to directly extrapolate the results to a full-scale prototype but to compare the different configurations so as to elucidate the influence of adding rubber on the cyclic performance of the system. Therefore, the values herein presented should not be directly related to any full-size condition test. As for future work, a scaling factor ( $\lambda$ ) could be created between a prototype and this model to scale the stress conditions and thus simulate more realistically the seismic behaviour of the soft zones on a reduced scale model.

### ***Material preparation***

The vertical installation of the soft zones predetermined the specimen preparation. The homogeneity of the mixture was at risk as a consequence of the expected segregation of smaller particulate sand, as established by previous studies on RSm (Pistolas et al., 2018). The solution consisted of bagging a constant RSm volume. RSm was placed into small plastic bags of 140 mm by 90 mm which in turn were packed into each side of the shake box. Water was also added to the bags (2.5% moisture) to reduce the segregation.

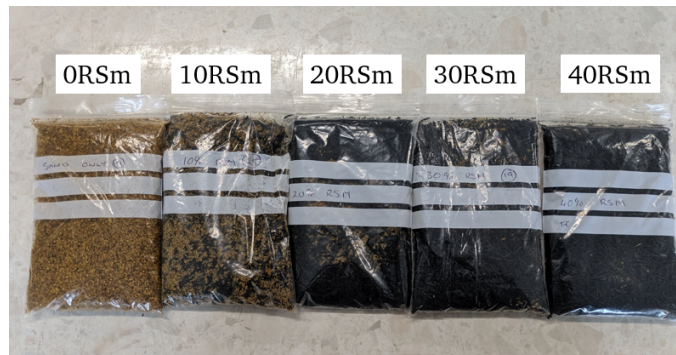
A fixed volume was adopted to ensure the homogeneity in the installation of the modified adjacent soil. Each bag contained hence a common volume of RSm ( $140 \text{ cm}^3$ ) regardless of the mixture ratio, which was controlled by adjusting the corresponding mass of a known volume to the prescribed volume. The equations used for the determination of gravimetric proportions needed for every RSm percentage are expressed in Section 2.3.2. Masses, phase volumes and void ratios calculated are given for each mixture in Table 6.3.

**Table 6.3:** Mass solids, volume solids, voids and void ratio per bag

Specimen	Mass solids (g)	Volume solids ( $cm^3$ )	Volume voids ( $cm^3$ )	Void ratio
0RSm	217	81.89	58.11	0.71
10RSm	169.71	72.79	67.21	0.92
20RSm	146.09	70.19	69.81	0.99
30RSm	123.13	65.51	74.49	1.14
40RSm	105.25	61.42	78.58	1.28

It is important to note that the presence of gaps in the mixture bags together with the gaps that inevitably form between bags means that volumetric state measures, such as void ratio, are of limited validity. Attempts to define the volumetric state are necessarily indicative and should be treated accordingly. This is because volume measures are definable at three different scales (Figures 6.4-6.5):

- At particle scale; interparticle voids, i.e. conventional interpretation.
- At bag scale; void volume within RSm bags = interparticle voids + intrabag voids.
- At shake box scale; void volume within shake box = bag voids + interbag voids.

**Figure 6.4:** Mixture bags with RSm at  $\chi = 0-40\%$ 

Bags were packed in the large spaces (Figure 6.5) on opposing faces of the foundation column. The large spaces were adjacent to those column faces that lie normal to the direction of horizontal oscillation. Bags were manually compacted and they were installed adjacent to the silicon foundation column acting as vertical soft zones or walls. Fourteen bags were required to pack the large spaces up to a height of 185 mm, that is 55 mm below the top of the shake box rim. The effect of the plastic bags on the response of the system has not been considered. Further work is needed in this regard



to evaluate the influence of the embedding materials in the dynamic behaviour such as the additional energy losses due to the friction developed intra plastic bags.

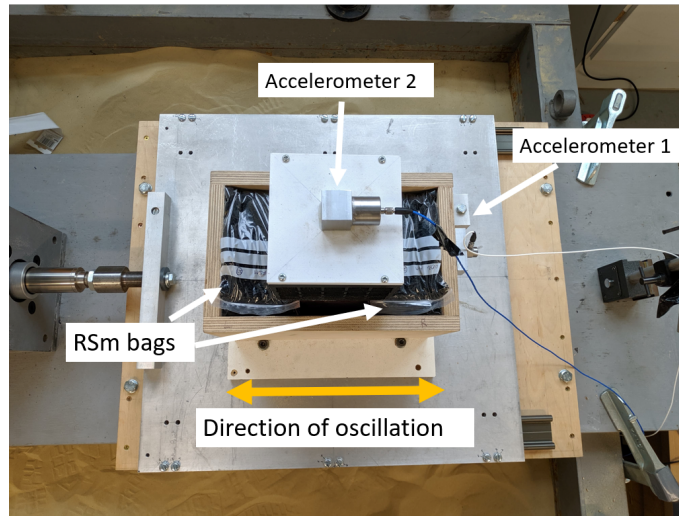


**Figure 6.5:** Plan view of rigid box

### *Methods*

The shake table tests 'sweep' for the natural frequency of the foundation-modified soil system for each RSm mixture. Sweeps were performed at integer frequency intervals from 1 to 10 Hz and lasted for 5 seconds. Oscillation displacement in each test, and hence foundation column resistance was kept constant throughout the sweep, by control of velocity. For example, a test at 1 Hz as part of a sweep with a single amplitude displacement of 2.5 mm has a peak control velocity  $5\pi$  mm/s, whereas to maintain the displacement amplitude at 2.5 mm in a 2 Hz test, the peak control velocity has to be  $10\pi$  mm/s. Peak displacement, velocity and acceleration are calculated in accordance with the expressions which define the sinusoidal motion over time (Section 2.5.3).

Table 6.4 shows displacement, velocity and peak acceleration transferred from the EMC to the base plate and the box model. As it is shown, the peak input acceleration increases with the input frequency so as to maintain a 2.5 mm single displacement.



**Table 6.4:** Determination of velocity, displacement and acceleration for experimental programme

Frequency	Displacement (mm)	Velocity (mm/s)	Acceleration (g)
1	2.5	15.71	0.01
3	2.5	47.12	0.09
5	2.5	78.54	0.25
7	2.5	109.96	0.49
9	2.5	141.37	0.81

Notwithstanding earlier remarks about the definition of mixture densities, the test procedure had three stages, the first two of which go some way to ameliorate the influence of an intractable density calculation:

- Stage 1 is as indicated above, a sequence of 10 tests at increasing integer frequency (1-10 Hz) and appropriate velocity adjustments.
- Stage 2 is a sequence of tests at decreasing integer frequency (9-1 Hz) and appropriate velocity adjustments.

The reason for the up-down frequency sequences was that it was anticipated that the initial up sequence tests would serve to densify and further cyclic loading would not result in further volumetric change in the soft zones. Indeed that appeared to be the case as the down-frequency amplification ratio curves followed closely the higher up-frequency amplification, only deviating at around the natural frequency. Bear in mind the foundation soil column, being silicon, will not densify. This deviation was read to be evidence of densification as amplification increased when moving along the down-frequency sequences.

- Stage 3 was a limited range fine sweep at frequency intervals of 0.25 Hz centred on the peak amplitude frequency. This served to improve the resolution around what had been revealed to be the resonant frequency.

Time and frequency domain analysis was applied to every sweep analysis, as discussed in Section 2.4.3, as a means of evaluating the maximum response of the studied structure. Energy dissipation and vibration isolation efficacy by means of installing vertical soft zones are evaluated in relation to rubber content and input frequency.

## 6.3 Results and discussion

### 6.3.1 Acceleration response

#### *Sand only condition*

Figure 6.6 presents a typical set of acceleration histories for the shaking table and the top of the foundation at three different control frequencies: 3 Hz, 5.5 Hz and 9 Hz. The first analysis was adding sand only to the vertical installations.

At  $f = 3$  Hz (Figure 6.6a), oscillation of the lumped mass follows closely that of the excitation reaching a maximum acceleration of approximately  $\pm 0.1$  g. There is little amplification of the input motion at this frequency and no phase lag is observed between the output and the input motion.

At  $f = 5.5$  Hz, the lumped-mass response shows an amplification that increases with the number of cycles. A steady state is reached in which the peak acceleration is about  $\pm 2.85$  g, significantly higher than at  $f = 3$  Hz. Figure 6.6b also reveals that the phase lag between the input motion and the top of the lumped-mass is around 90 degrees which according to conventional analysis (Chopra, 2011) is indicative of resonance when the input frequency matches the system natural frequency.

It can be noted when the modified vertical installation contained sand only, peak amplification occurs at  $f = 5.5$  Hz. This is considered to be the reference used for comparison with other RSm mixtures. Figure 6.6c shows the response of the lumped-mass at higher frequencies ( $f = 9$  Hz). It is observed that the lumped-mass slightly amplifies the input motion compared to relatively low frequencies, but it does not reach the response observed at the resonant frequency ( $f = 5.5$  Hz).

This is also confirmed by the lag between the atop building and the box which reveals a value close to 180 degrees, far from triggering resonance. The increase in the output acceleration can be attributed to the rise in the frequency and the associated control velocity as shown in Table 6.4.

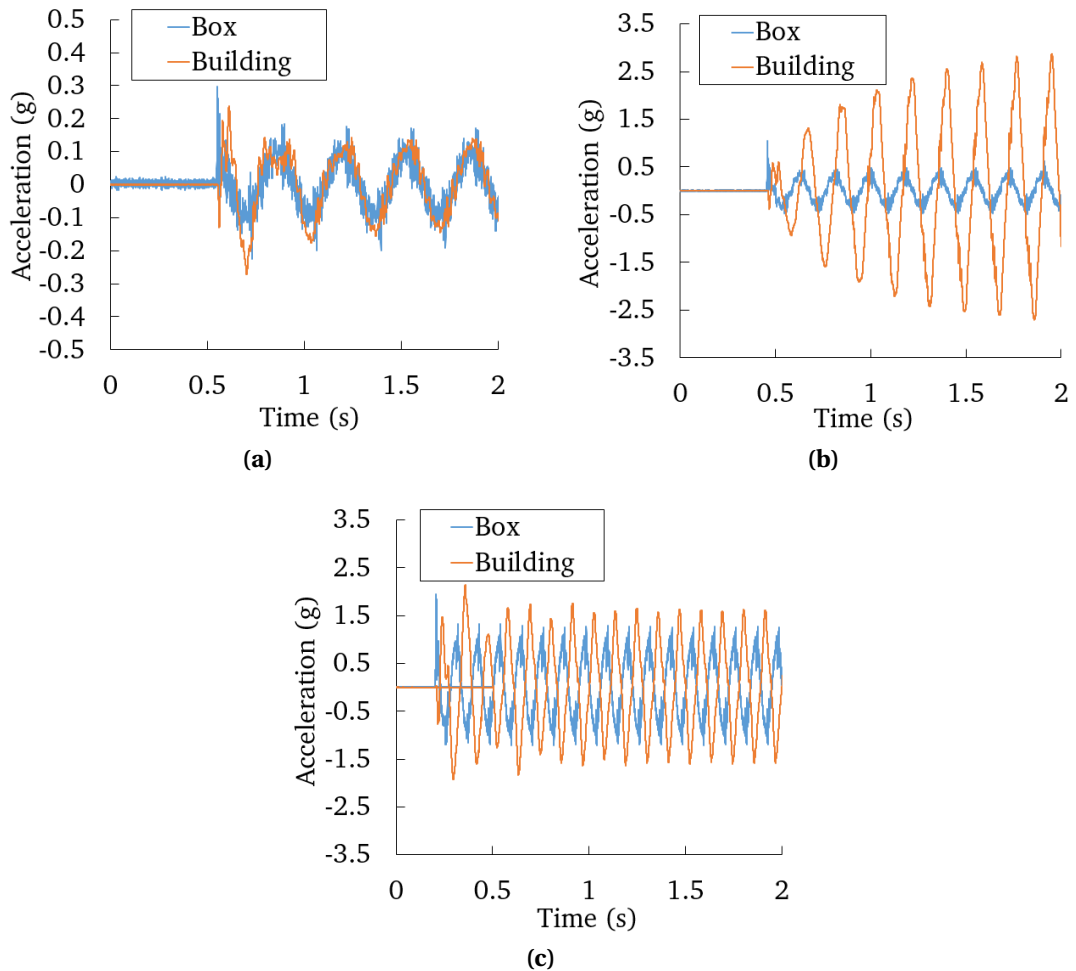


**Figure 6.6:** Transmitted accelerations on building and box at a)  $f = 3$  Hz b)  $f = 5.5$  Hz and c)  $f = 9$  Hz

***Rubber-sand mixtures***

Figure 6.7 presents a set of acceleration histories for the lumped-mass at two frequencies: 5.5 and 5 Hz. The acceleration time series reveal the results obtained when modifying the content of the vertical soft zones for  $\chi = 0$  to 40%. A total of three cycles are depicted once the system reaches the steady state condition, between 2 and 2.6 s.

Figure 6.7a shows a systematic decrease in acceleration amplitude with the addition of rubber; the peak acceleration moves from  $\pm 2.85$  g with sand only to  $\pm 1.5$  g at  $\chi = 10 - 20$  % and then to  $\pm 0.77$  g with  $\chi = 30 - 40$ %. When moving down from the resonant frequency of sand only configuration ( $f = 5$  Hz), the acceleration amplitude increases with the addition of  $\chi = 10 - 20$  % or slightly decreases at greater gravimetric proportions  $\chi = 30 - 40$  %. The increase in horizontal acceleration with rubber can be attributed

to the fact that the input frequency approaches the natural frequency of the modified soil with RSm hence, the system approaches resonance. Indeed, the phase lag between input and output motion was around 90 degrees when adding  $\chi = 10$ , whereas the phase lag decreases at greater rubber contents. This finding reveals that the response of the building-foundation system is influenced by the fundamental frequency of the motion and the natural frequency of the system, which is altered by the rubber content. Consequently, typical multi-storey buildings, characterised by a lower fundamental frequency, or areas prone to suffer from low-frequency earthquakes, could potentially see an increase in the transmitted accelerations if the soft zone was implemented around the soil foundation. This suggests that a more comprehensive study of the cyclic performance of a structural system is required to determine if the inclusion of rubber would result in an effective seismic isolation (Figure 6.7a), or in an amplification of the input motion (Figure 6.7b).

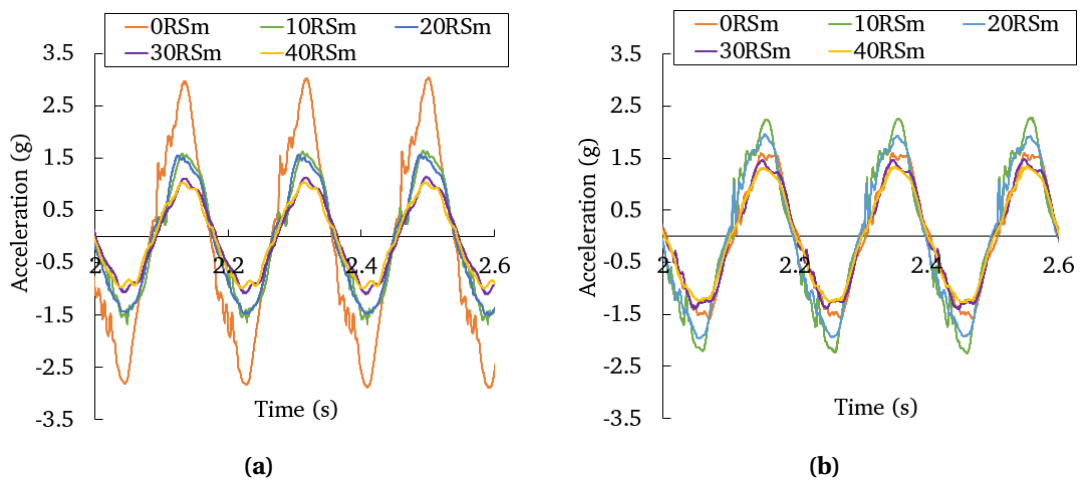


**Figure 6.7:** Transmitted accelerations on building and box at a)  $f = 5.5$  Hz and b)  $f = 5$  Hz

### 6.3.2 Amplification ratio

The cyclic response of a building-foundation system can be evaluated by calculating the ratio between the displacement, velocity, or acceleration at some location on the building and the base motion, also known as amplification ratio (Chopra, 2011).

The amplification ratio (AR) has been obtained in this study from acceleration histories, ratio of the peak steady state values from the building top and the shake box.

Figure 6.8 shows the amplification ratio for different rubber contents both when (a) increasing and (b) decreasing input frequency. This is to ensure that the foundation-modified soil reached its densest state as discussed before in the test methods.

Figures 6.8a-6.8b follow similar trends when increasing and decreasing the input frequency. However, higher peaks are obtained in Figure 6.8b, which combines the acceleration series when decreasing the input frequency (Stage 2) and the fine sweep performed around the fundamental frequency (Stage 3) for different rubber contents. This is more evident with bags containing sand only and  $\chi = 10$ -20% revealing the greater amplification of the peak acceleration attributed to the denser state of the soil.

Figure 6.8b reveals how the presence of soft rubber zones affected the amplification conditions in the shake table box for the four different RSm. In general, there is a reduction in the amplification and natural frequency of the foundation-modified soil system with the addition of rubber. From a high value of AR = 8 at about 5.5 Hz in the sand only tests, to values of AR = 5.6 at about 4.25 Hz when adding 40% rubber. This is in line with previous studies (Kaneko et al., 2013; Nappa, 2014) that showed a lengthening of the system period, or shortening of frequency, with the implementation of soft zones, causing a shifting in the dynamic response of the modified system.

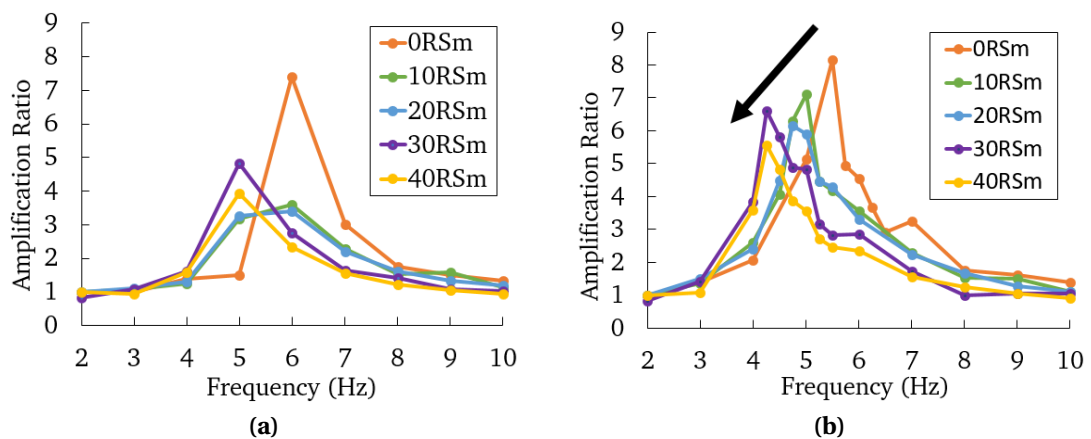


**Figure 6.8:** Amplification ratio versus input frequency during a) stage 1 and b) stage 2-3

The evolution in the resonant or peak frequency and amplification ratio with rubber content is shown in Figure 6.9a. A gradual decay in the peak frequency of the foundation-soil system is revealed in Figure 6.9a with the addition of rubber, passing from 5.5 Hz

with sand only to 4.25 Hz at  $\chi = 40\%$ . Considering that the peak frequency reveals the frequency at which resonance is reached, hence when the input and the system frequency match up, Figure 6.9a shows that the natural frequency of the foundation-modified soil decreases with rubber content.

This could be related to the transition in the material behaviour of RSm discussed in Chapter 4. Whilst sand-like behaviour was observed at low rubber contents, characterised by a greater constrained modulus, rubber-like behaviour was observed at  $\chi > 10\%$  which suffered from a greater compressibility due to rubber deformability. As established by previous authors (Mahdavisefat et al., 2017) and discussed in Chapters 5 and 7, the low rubber stiffness results in a decay of the mixture shear modulus with the addition of rubber. This can aid explaining why the sand only configuration presents a higher natural frequency which decreases as more rubber is added.

Figure 6.9b presents the change in the amplification ratio at peak frequencies and at the fundamental frequency of sand only ( $f = 5.5$  Hz) for the different rubber contents. AR values reveal a decrease in the peak steady state of the foundation-soft zone system with the addition of rubber, which follows the trend shown for the peak frequencies (Figure 6.9a). The reduction in amplification is more significant at 5.5 Hz which passes from  $AR = 8$  with sand only to  $AR = 2.5$  at  $\chi = 40\%$ . These results reveal the shift in the amplification conditions and subsequently the effective offset of incident vibrations with the addition of soft zones, more prominent at greater rubber contents.

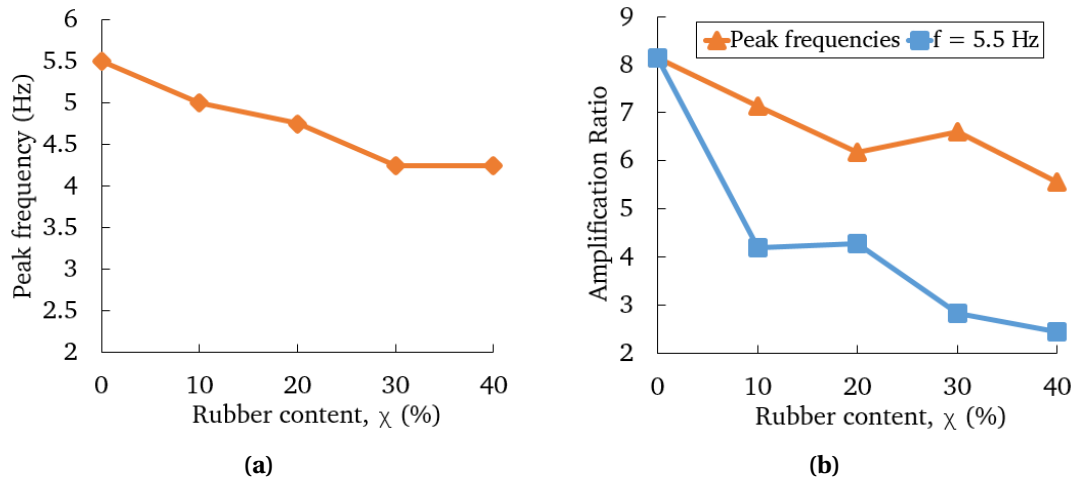


**Figure 6.9:** a) Frequency, and b) amplification ratio at resonant frequency and  $f = 5.5$  Hz, with rubber content

## 6.4 Analysis

### 6.4.1 Energy dissipation at lab scale

Figure 6.10 shows the amplification ratio sweeps for  $\chi = 0$  and 40% from which the damping ratios for the lumped-mass-foundation system can be calculated using the half-power bandwidth. As explained in Section 2.5.3, the half-power bandwidth is determined at a lab scale from the resonant frequency and the maximum response of the system. This is the reason why a fine sweep at frequency intervals of 0.25 Hz around the peak frequency was performed.

In Figure 6.10, it is evident that the addition of rubber content to the vertical installations leads to a reduction in both peak frequency and maximum amplification ratio. Moreover, a narrower band can be visually found in the half-power bandwidth for sand only configuration, revealing at first instance a lower damping capacity in comparison with 40% RSm. The same approach has been applied to all rubber mixtures to compare the damping capacity of the foundation-modified soil system by altering the properties of the lateral supports.

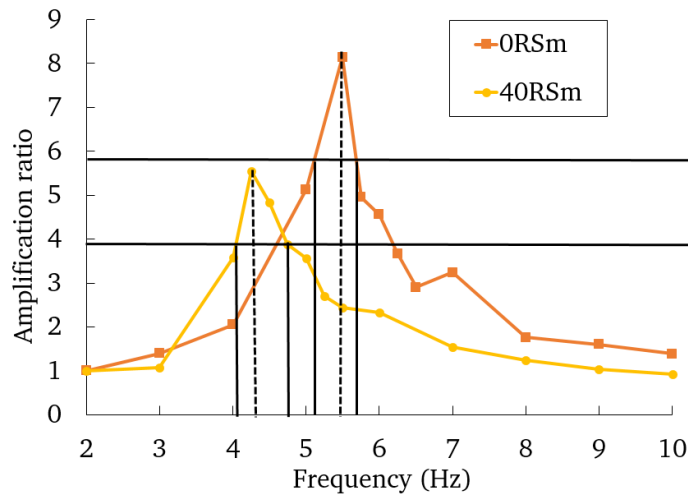


**Figure 6.10:** Half power bandwidth for the foundation-soil system at  $\chi = 0$  and 40%

Figure 6.11 shows the evolution in damping ratio with rubber content of the foundation-soft zones. The results point to an improvement in damping capacity with rubber content, doubling the damping ratio when adding  $\chi = 30\%$ . This provides a basis for explaining the decay in the system amplification ratio (Figure 6.9b) with rubber content. Hence, adding rubber increases the capacity to dissipate energy of the entire system which results in a reduction of the horizontal accelerations at the peak frequency.

As discussed in Section 2.5, the attenuation in transmission of body waves and, in turn, horizontal accelerations is attributed to two main causes; (i) mechanical properties of the soil throughout the wave is transmitted (material damping) and (ii) geometrical characteristics of the medium (geometrical damping). Due its greater dimensions, the damping ratio calculated at a lab or field scale is combination of the two forms of damping. Consequently, the results shown in Figure 6.11 account for both material and geometrical damping of the foundation-modified soil system. In order to elucidate the origin of each form of damping, the material damping of RSm will be analysed in Chapter 7 from very small to large deformations. Hence, the energy dissipation mechanisms found in RSm will be discussed by comparing the results obtained at a particle (Chapter 4), element scale (Chapter 5), and 1g model scale (Chapter 6).



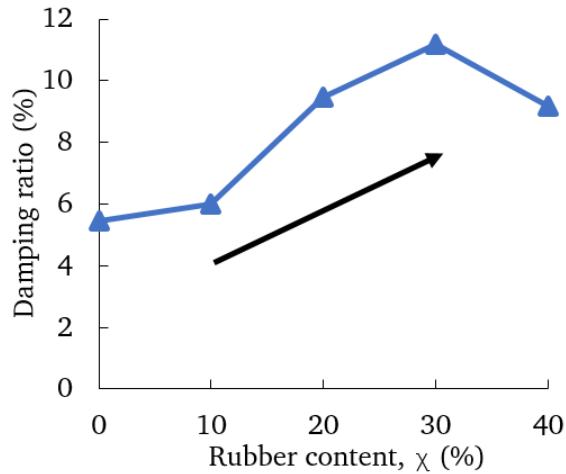


**Figure 6.11:** Damping ratio at lab scale with RSm varying rubber content

### 6.4.2 Vibration isolation efficacy

The influence of vertical soft zones in isolating vibrations has been assessed by determining the change in amplification ratio with rubber using as reference the sand only soil. Whilst not pretending to be a precise/quantitative analysis of the results, this section discusses the trend in AR shown when varying the input frequency (Figure 6.12).

Two frequency bands can be observed in relation to the alteration in AR; (i) frequencies before and (ii) after the resonant frequency of sand only. For the former, there is a greater amplification of the input motion in contrast with sand only scenario. This amplification is more significant at  $\chi = 30-40\%$  due to the shifting in the natural frequency of the system, as shown in Figure 6.8b. This has also been addressed in the literature (Bandyopadhyay et al., 2015; Brennan et al., 2019) demonstrating that the shifted response causes a detrimental effect around the natural frequency of the modified soil. The practical implication of this finding implies that modifying the soil with RSm can lead to an amplification of accelerations. This would be more evident with the appearance of predominately low-frequency earthquakes or around slender buildings, i.e. low fundamental frequency.

The addition of rubber points to, however, a decrease in amplification ratio at frequencies higher than 5 Hz. This phenomenon is more significant as the rubber content increases with reductions of up to 70% in amplification ratio adding  $\chi = 30-$

40%. On top of the shifting in the foundation-soft zone natural frequency when adding rubber, the results reveal an attenuation in the horizontal accelerations recorded on top of the building. The inclusion of vertical RSm soft zones can thus mitigate part of the incident vibrations, seen to be more effective at higher rubber contents. In practice, this could be more effective for low-storey buildings, with higher fundamental frequency, or in areas where predominately high-frequency earthquakes are expected.

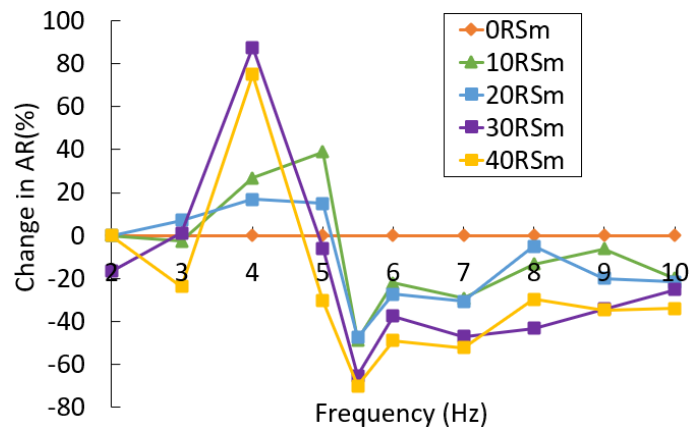


**Figure 6.12:** Change in amplification ratio with rubber content versus sand only configuration

### 6.4.3 Comparison with literature review

This study has undertaken an initial experimental exploration of soft zones by adding vertical installations of packed RSm bags, adjacent to the soil foundation. The objective was to study the alteration in the dynamic performance and determine the damping capacity of the soil foundation-modified soil system subject to cyclic loading.

Prior to this, only [Mahdavisefat et al. \(2017\)](#) had studied the structural response of a foundation-modified soil system with vertical RSm columns to prevent the transmission of ground vibrations, i.e. frequency = 10-400 Hz. The study revealed an attenuation of between 60 and 70% of incoming surface waves with  $\chi = 30\%$ . The efficient vibration mitigation was attributed to the excellent energy absorption properties of RSm.

As depicted in [Figure 6.8b](#), the decay in amplification with rubber is due to both (i) the shift in the natural frequency and (ii) the attenuation of the peak values. The alteration observed in the natural frequency ([7.7](#)) can be related to the reduction in stiffness of the modified soil with rubber, as demonstrated in existing research [Anastasiadis](#)

et al. (2012b), and shown via cyclic triaxial and resonant column testing in Chapter 5. Adding rubber to the vertical installations alters the amplification conditions and thus, offset incident vibrations at frequencies higher than the fundamental frequency of the foundation-modified soil. This has been shown in Figure 6.12 by depicting the negative change in amplification ratio of RSm installations with respect to sand only.

This is in accordance with literature review (Hazarika et al., 2006; Tsang et al., 2012; Kaneko et al., 2013) which proposed the inclusion of rubber to mitigate the action of strong motions. In those studies, the system was proven more efficient with content ( $\chi = 30\text{-}50\%$ ), and by increasing geometrical aspects such as thickness or depth of the isolating layer. The justification to explain the enhancement of seismic performance relied, however, on the apparent increase in hysteretic damping, devised from triaxial tests performed at an element scale. Therefore, no previous study on RSm has attempted to evaluate damping of a lab scaled system, nor provided sufficient evidences to explain the origin of the energy dissipated in a foundation with vertical soft inclusions.

The results corresponding to damping at a lab scale (Section 6.4) revealed an improvement in the capacity to dissipate energy of the foundation-modified soil system. This supports the argument postulated in existing research (Tsang et al., 2012; Kaneko et al., 2013) which state that the decay in peak amplifications is attributable to the increase in damping ratio. However, damping at a larger scale includes other forms of damping, i.e. geometrical damping, which are not commonly addressed in the literature. For that, the concept of wave screening, extensively studied by previous authors (e.g. Woods (1968) and Lombardi (2012)) to justify the reduction in ground-borne vibrations, should be considered. Indeed, investigations focused on the design of wave barriers to enhance seismic protection (Kirtas et al., 2009; Nappa, 2014; Brennan et al., 2019) showed that the inclusion of soft zones can significantly reduce the amplification of seismic disturbances. This is due to the dynamic impedance between soils and, in turn, the filtering effect by reflecting incident waves. It could be thus hypothesized that the increase in damping with soft zones is result of combining material and geometrical damping. This will be covered in Chapter 7 by comparing the energy dissipation mechanisms reported in a particle, element and lab scale context in this investigation.

To conclude, this chapter should be seen as an initial experimental study that explores the feasibility of an alternative design to improve the structural response against cyclic loading. Despite the high isolation efficiency shown in previous studies by implementing RSm isolating layers (Xiong and Li, 2013; Bandyopadhyay et al., 2015), a unique design configuration has been proposed whereby horizontal layers are installed before the superstructure. Hence, the vertical disposition of the soft zones herein proposed would allow its application to any existing and new infrastructure whilst minimizing the limitation associated with foundation settlement. As a continuation of this study and previous investigations on vertical soft zones (Mahdavisefat et al., 2017; Lombardi, 2012), the use of RSm columns should be considered the next step to prove the effectiveness of the system as a geotechnical seismic isolation system. Further research is required to consider alternative design aspects in relation to the installation and geometrical conditions.

## 6.5 Summary

An initial experimental exploration of the influence of vertical installations of RSm on the dynamic behaviour of a lumped mass-foundation system has been undertaken in this chapter. The fundamental frequency, amplification and damping capacity of the system have been evaluated by subjecting a soil model to small scale shaking table tests:

- The presence of vertical soft zones affect the amplification conditions. A shift in the fundamental frequency of the system is observed with the addition of rubber. The decay in natural frequency together with the improvement in damping ratio at higher rubber contents leads to a reduction in amplification ratio.

- A detrimental effect on the structural response is found at frequencies close to the fundamental frequency of the modified soil. On the other hand, soft zones containing RSm can mitigate part of the peak accelerations at frequencies above its natural frequency, which is more evident at higher rubber contents.

- This feasibility study reveals that implementing vertical installation of RSm soft zones can enhance the protection of a system against cyclic loading. This is the first step to prove its effectiveness as a seismic isolation system and allow its application to both new and existing buildings in order to enhance their seismic protection.

In terms of new understanding, this study has shown that the cyclic response of a small-scaled model with a complex geometry, i.e. containing soft zones, can be idealised to mimic that of a single-degree of freedom. Also, the attenuation in peak horizontal accelerations has been attributed to the increase in damping capacity of the system, which reflects that the energy dissipated is the result of combining the material damping and the dynamic impedance, due to filtering the incident waves. The results from this study suggest that the implementation of soft vertical installations can result in an increase in the amplification of accelerations at lower frequencies, hence in earthquake prone regions with predominately low-frequency seismic motions or around slender buildings. The system is effective in attenuating disturbances at higher frequencies, e.g. around low-storey buildings or in areas with high-frequency earthquakes.

# *Characterisation of dynamic properties in RSm*

---

## **7.1 Introduction**

In Chapter 6, the installation of vertical soft zones containing RSm resulted in an enhancement of damping capacity and structural response to cyclic loading. Experimenting with full-size prototypes and scaled models can be, however, time and resource intensive. Alternative forms of studying the response of a ground soil with a complex geometry, such as the case of vertical RSm installations, is required including the use of 2D and 3D numerical simulations. Prior to this stage, a rigorous investigation is yet required to fully understand the dynamic behaviour of RSm and thus elucidate the correlation between the micro and macro behaviour of the mixture.

Stiffness and damping relationship curves are presented as a function of particle properties and test conditions to elucidate their extent of influence on RSm dynamic behaviour. Material damping is discussed in relation to the dissipation mechanisms observed in the particle (Chapter 4), element (Chapter 5) model scale (Chapter 6).

Soil stiffness - shear strain relationship curves are studied by calculating the reference strain and adjusting normalised shear modulus - shear strain curves to the experimental results. Damping ratio - shear strain relationships are adjusted to the models proposed by [Darendeli \(2001\)](#) and [Phillips and Hashash \(2009\)](#).

## 7.2 Dynamic behaviour of RSm

An accurate approximation of both stiffness and damping relationships is needed to characterise the dynamic behaviour of RSm and thus, simulate the ground response of the mixture when subject to excitations in numerical simulations.

Previous studies (Nakhaei et al., 2012; Ehsani et al., 2015; Pistolas et al., 2018) have proposed stiffness and damping strain curves to predict the variation in the dynamic properties of RSm containing granulated rubber. This study has investigated, on the other hand, the evolution in shear modulus and damping ratio of mixtures containing elongated shredded rubber (ShR). A comparison is undertaken to elucidate the upper and lower boundaries in relation to the evolution in the bulk parameters:

### 7.2.1 Effect of particle properties

#### *Shear modulus*

Shear modulus - shear strain curves for RSm are illustrated in Figure 7.1a based on the results collected from the cyclic triaxial tests, at medium-to-large strains, and the torsional resonant column tests, from small-to-medium strains, in Chapter 5. Figure 7.1b shows the normalised shear modulus  $G/G_0$  which represents the stiffness degradation as a result of the strain amplitude undergone by the specimen.

It is observed in Figure 7.1b that sand and 10% RSm exhibit a similar stiffness degradation at the entire strain amplitude. Adding more rubber ( $\chi = 20-30\%$ ) points to a more linear normalised shear modulus curve in the range from small-to-large deformations. This result supports the basis that RSm exhibit a sand-like behaviour at low rubber percentages ( $\chi = 10\%$ ), where the loss of inter-particle contacts is more significant under loading (Kim and Santamarina, 2008). On the contrary, the inclusion of rubber creates additional rubber-to-rubber particle contacts, i.e. rubber-like behaviour. In other words, adding rubber increases the capacity to deform of the mixture, inducing greater contacts between particles. As discussed in Chapter 4, rubber particles add

resistance against shear stresses postponing any possible slippage. This reduces the stiffness degradation of RSm which is more pronounced as rubber content increases.

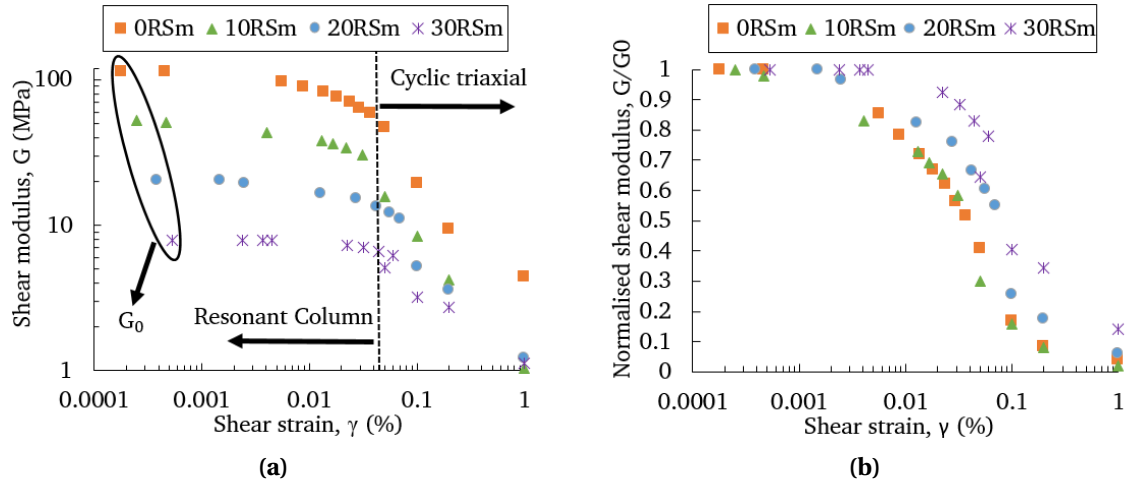


**Figure 7.1:** a) Shear modulus and b) normalised shear modulus versus shear strain

Figures 7.2a-7.2b depict the normalised shear modulus as a function of the volumetric state variable from existing literature. These graphs show the stiffness degradation curve of mixtures containing  $\chi = 10\%$  and  $30\%$ .

At  $\chi = 10\%$ , the stiffness relationship from this study follows those curves proposed in existing research at very small-to-medium strains, but then it experiences a greater degradation at higher strains. This discrepancy can be attributable to the variance in particle properties and test conditions. That said, confining pressure adopted in previous studies range between 69 kPa and 100 kPa whilst size ratio varies between  $S_R = 1 - 20$ . Only Kaneko et al. (2013), Mashiri et al. (2016), and this study have studied the evolution in bulk parameters adding elongated rubber particles. As established in Chapter 4, these elongated particles would experience a greater deformation compared to granulated rubber as a result of the entrapment between mineral particles and also due to the higher number of sand-to-sand particle contacts. This might explain why the mixtures studied by Mashiri et al. (2016), with big rubber tyres and  $S_R > 20$ , or this study, with shredded rubber, i.e.  $A_R > 6$ , exhibit a greater stiffness degradation at small rubber percentages than in other studies.

At  $\chi = 30\%$ , the trend of the normalised shear modulus from this study exhibit higher values than previous studies at small-to-medium strains. Then it falls within the lower



and upper boundaries at larger deformations. By comparing Figure 7.2a and Figure 7.2b, it can be observed that the reference strain ( $\gamma_{ref}$ ), which corresponds to the shear strain at which  $G/G_0 = 0.5$ , associated with 30% RSm is higher than that of 10% RSm. This is in line with previous investigations (Anastasiadis et al., 2012b; Senetakis et al., 2012b), in which mixtures containing higher rubber contents exhibited a more linear dynamic behaviour and, as a consequence, the stiffness degradation suffered by RSm was lower as more rubber was added. This is attributed to the greater number of rubber-to-rubber contacts and the increase in resistance against shear stresses.

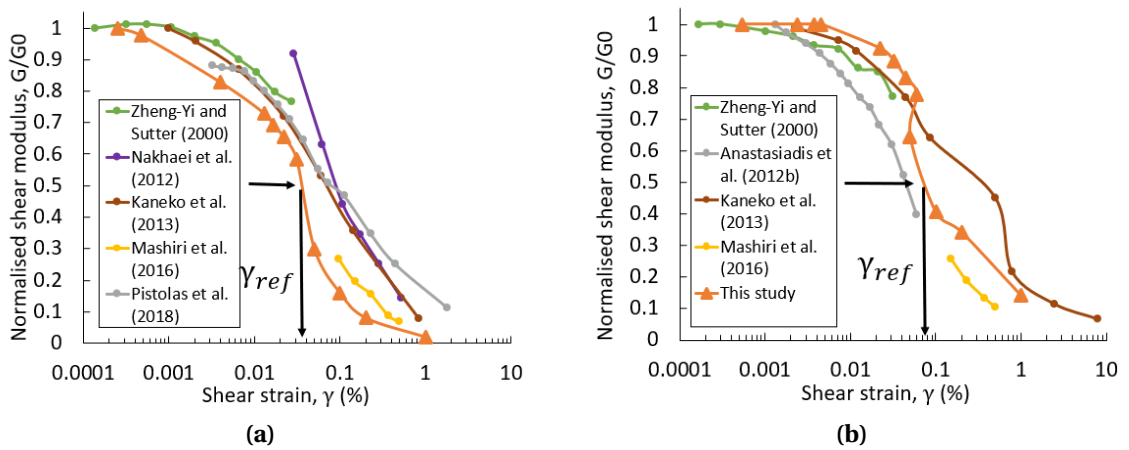


**Figure 7.2:** Normalised shear modulus versus shear strain of RSm at a)  $\chi = 10\%$ , and b)  $\chi = 30\%$

### Damping ratio

Figure 7.3 depicts the damping ratio - shear strain curve from experimental results gathered in Chapter 5. As occurred with the normalised shear modulus - shear strain (Figure 7.1b) relationship, adding rubber leads to a more linear behaviour under loading, which is identified by a sustained evolution in the damping capacity.

Figure 7.3 shows that adding  $\chi \geq 10\%$  contributes to a greater energy dissipation capacity at small strains, in consonance with Senetakis et al. (2012a) and Li et al. (2016). This tendency changes, however, at greater deformations where sand and 10% RSm exhibit greater hysteretic damping at larger deformations. That said, it is difficult to distinguish between sand and 10% RSm. Beyond  $\gamma_{cyc} = 0.1$  or  $0.2\%$ , the linear relationship breaks down. Indeed sand and 10% RSm point to an upper limit, even

a reduction in damping, at high shear strains. As established by Pistolas et al. (2018), this is due to the existence of a limiting shear strain  $\gamma_{lim}$ , defined as the strain at which the higher damping ratio is observed for mixtures, which appears to increase with the addition of rubber. Despite the reduction in material damping at  $\chi > 10\%$  (Anbazhagan and Manohar, 2016), the upper limit in damping found in sand-like specimens contrasts with the increasing trend observed in the material damping of 20-30% RSm. In accordance with Pistolas et al. (2018), this may be attributed to the dislocation of rubber and sand particles, hence, both limiting strain and upper damping ratio are not yet revealed for mixtures containing higher rubber contents. Further experimental work is required to understand the influence of deformable (rubber) particles on the limiting strain of RSm at larger deformations.

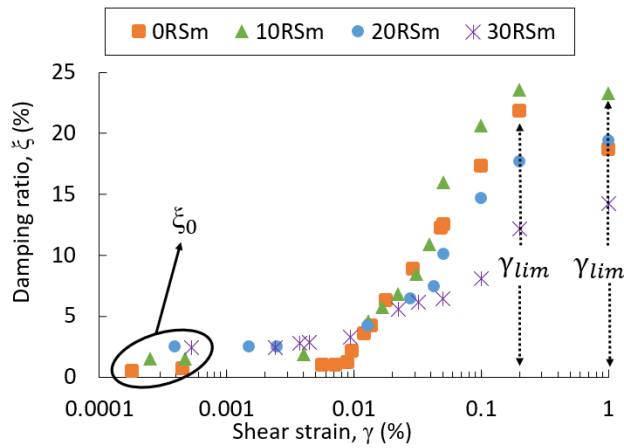


**Figure 7.3:** Damping ratio - shear strain of RSm

The evolution in damping ratio with shear strain of previous experimental studies is shown in Figures 7.4a-7.4b including the results of this study at  $\chi = 10\%$  and 30%. Minimum damping ratio for RSm, observed at  $\gamma = 0.0001\%$ , evaluated in this study exhibit similar values than mixtures studied in previous investigations.

At  $\chi = 10\%$ , the trend shown in damping ratio is similar to existing research at small strains, but then it increases at a higher rate from  $\gamma = 0.02\%$ , corresponding to the higher stiffness degradation suffered by the mixture at this strain amplitude (Figure 7.2a). It is also observed that the limiting shear strain ( $\gamma_{lim}$ ) associated with 10% RSm occurs at lower deformations when compared to existing research (Kaneko et al., 2013; Pistolas

et al., 2018). This leads to greater values in material damping at around  $\gamma = 0.05 - 0.2\%$ , which is maintained at larger deformations.

At  $\chi = 30\%$ , as observed with the normalised shear modulus, the evolution in damping ratio falls within the boundaries shown by previous studies. The reduction in damping is significant when compared to results shown at  $\chi = 10\%$  (Figure 7.4a). This reduction in material damping has been shown by other authors (Ehsani et al., 2015; Li et al., 2016) who revealed an optimum damping ratio in RSm by adding up to  $\chi = 10\%$ , which decreases when the rubber-like behaviour arises, i.e.  $\chi > 20\%$ . It is evident in Figure 7.4b that the limiting shear strain is not reached by most of the reviewed studies, including this investigation, suggesting that the upper damping is yet to arise and it will occur at larger deformations, i.e.  $\gamma > 1\%$ . This newly supports the high capacity of rubber to deform and dislocate (Pistolas et al., 2018), which results in a more linear dynamic behaviour as rubber content increases.

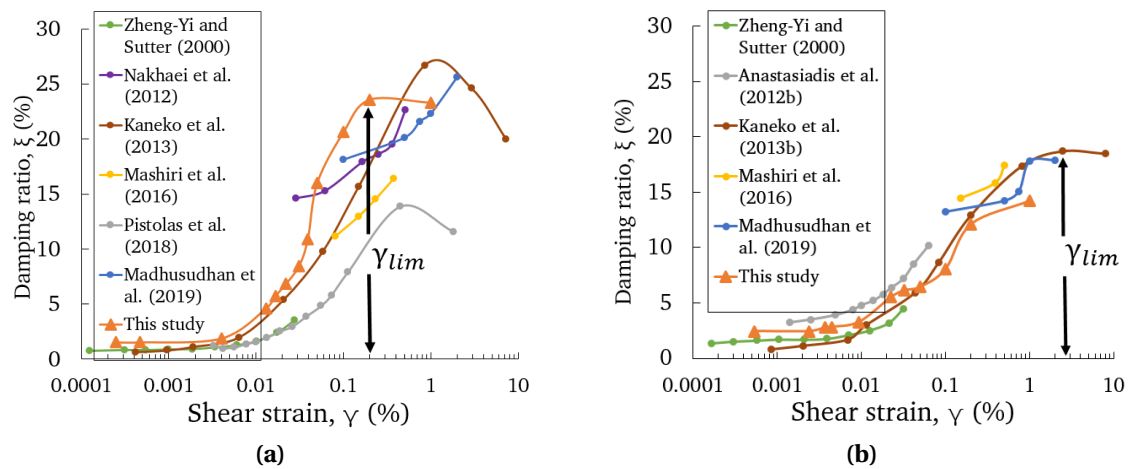


**Figure 7.4:** Damping ratio - shear strain of RSm at a)  $\chi = 10\%$ , and b)  $\chi = 30\%$

## 7.2.2 Cyclic effect on dynamic behaviour

Most of the studies on RSm have focused on evaluating the dynamic properties of the mixture whilst altering particle properties. Only a few studies (Mashiri et al., 2016; Madhusudhan et al., 2019), have also studied the effect of cycles on the dynamic behaviour of RSm when subject to cyclic loading. Given the evident stiffness and damping degradation of saturated RSm specimens shown in Chapter 5, this study proposes the

creation of a new approach to assist in explaining the evolution in stiffness and damping as a function of both particle properties and test conditions.

### ***Shear modulus and liquefaction potential***

Using the conceptual model adopted for liquefaction potential in Section 5.2.3 and following the framework established by Tsuha et al. (2012), two zones can be identified in Figures 7.5a and 7.5b: (i) unstable and (ii) stable regions. The unstable region groups all specimens which liquefied after a certain number of cycles (in parentheses). This is differentiated from the stable region, which encapsulates the samples containing higher rubber contents and capable of withstanding 400 strain controlled cycles. This way of representing shear modulus versus rubber content can aid in visualising the existence of a threshold which distinguishes between i) "safe" stable and ii) "unsafe" unstable zones. This could then be applied to saturated RSm to understand the evolution in mixture stiffness in relation to its initial shear modulus and the rubber amount.

The stiffness degradation of RSm is shown in Figure 7.5a in the context of strain level, rubber percentage, and number of cycles to liquefaction. Referring to previous sections, soil stiffness decreases with rubber content and shear strain amplitude, except for  $\gamma_{cyc} = 1\%$ , where all RSm presents a relatively similar shear modulus. Figure 7.5b shows the value corresponding to the liquefaction potential ( $r_u$ ) prior to liquefaction for sand-like soils or after 400 strain controlled cycles for rubber-like soils.

It can be clearly observed that the number of cycles to liquefy increases at lower strain amplitudes and with additional rubber. Whilst sand and 10% RSm liquefied after a certain number of cycles, 20% and 30% RSm undergo a lesser decay in soil stiffness, i.e. stiffness degradation. This supports the argument presented in this study that rubber-like soils ( $\chi > 10\%$ ) are more resilient against cyclic loading.

The improvement in the resilience against cyclic loading with rubber can be relevant in circumstances where a high number of cycles are expected, e.g. prolonged aftershocks (Nazari et al., 2014) or vibrations from railways (Signes et al., 2017). Moreover, these results prove that the change in the dynamic soil stiffness can be highly influenced by the number of cycles in the medium-to-large strain range. Contrary to assumptions

made in the literature (Nakhaei et al., 2012; Madhusudhan et al., 2019; Kokusho, 1980), the decay in soil stiffness of specimens here studied continues after 20 cycles, which reveals the need to evaluate the cyclic effect on saturated soils at large strains.

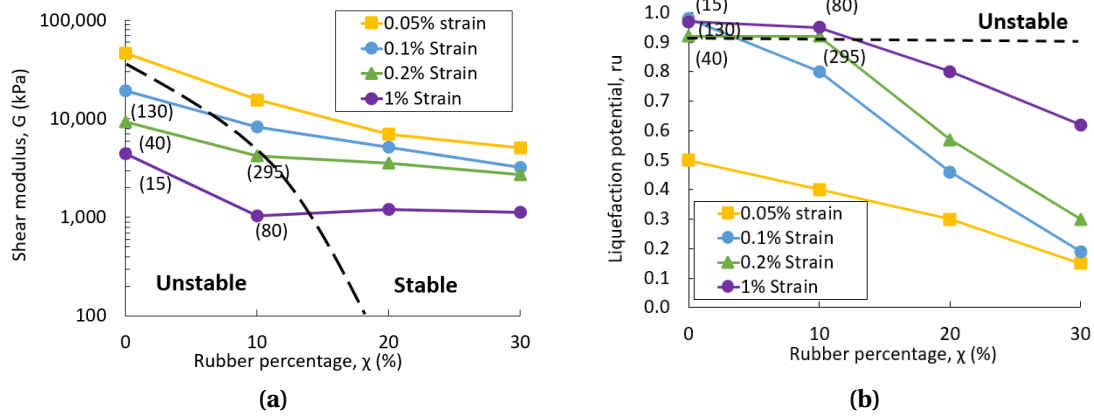


**Figure 7.5:** a) stiffness degradation and b) liquefaction potential versus shear strain, rubber percentage and cycles to liquefaction

### Damping ratio

The evolution in damping ratio is presented in Figure 7.6 as a function of rubber percentage, strain amplitude and number of cycles to liquefaction.

At  $N = 2$ , damping capacity of RSm improves adding  $\chi = 10\%$ , then it decreases with additional rubber as observed in Figure 5.16a. Damping ratio is traced for all RSm when  $\gamma_{cyc} = 1\%$  ( $N = 15$ ),  $\gamma_{cyc} = 0.2\%$  ( $N = 40$ ), and  $\gamma_{cyc} = 0.1\%$  ( $N = 130$ ). These cycles correspond to the last reported value of damping ratio in each strain amplitude prior to liquefaction of sand specimen. The change in damping capacity can thus be evaluated in a simplified form by knowing the initial damping ratio, the rubber percentage and the strain amplitude applied to the specimen.

For  $\gamma_{cyc} = 0.1\%$ , damping ratio exhibited by sand and 10% RSm decrease to half of its initial value, whilst the rate of degradation decays as the rubber content increases. As occurred at  $N = 2$  for all strain levels, damping improves uniquely when adding  $\chi = 10\%$ . However, this tendency changes at greater strain amplitudes. At  $\gamma_{cyc} = 0.2\%$  and  $N = 40$ , there is an important loss in soil stiffness of sand owing to the accumulation in pore water pressure and consequent reduction in particle contacts. Therefore, the damping

generated by rubber deformation continues at greater deformations. As a result, 10% and 20% RSm exhibit greater damping capacity than lower rubber contents.

The negative trend in the evolution of damping ratio with cycles is more evident at  $\gamma_{cyc} = 1\%$ , where all RSm present a greater dissipation capacity compared to sand only configuration. The decay in damping capacity occurs at a lower rate with the addition of rubber and the application of higher  $\gamma_{cyc}$ . For instance, sand changes from  $\xi = 19\%$  ( $N = 2$ ) to  $\xi = 9\%$  ( $N = 15$ ), whereas 30% RSm passes from  $\xi = 14\%$  to  $\xi = 12\%$  in the same cyclic range. Although sand-like soils ( $\chi < 20\%$ ) exhibit an initial higher capacity to dissipate energy, rubber-like soils experience a lesser decay in damping.

Prior to this investigation, only Mashiri et al. (2016), with tyre chips under saturated conditions, and Madhusudhan et al. (2019), with granulated rubber and dry conditions, studied the cyclic effect up to 20 strain controlled cycles. Whilst Madhusudhan et al. (2019) showed no decay in material damping with the number cycles, Mashiri et al. (2016) revealed the reduction in damping, which was ameliorated by adding more rubber. The latter was, however, limited to a lower strain amplitude range  $\gamma_{cyc} = 0.1 - 0.5\%$ . The results reported in this study support the basis that saturated (mineral) soil experience a significant stiffness and damping degradation, more evident as strain amplitude increases. In practice, adding small elongated rubber in the mixture could be seen as a solution to ameliorate the foreseeable decay in energy dissipation shown by mineral soils when subject to cyclic loading.

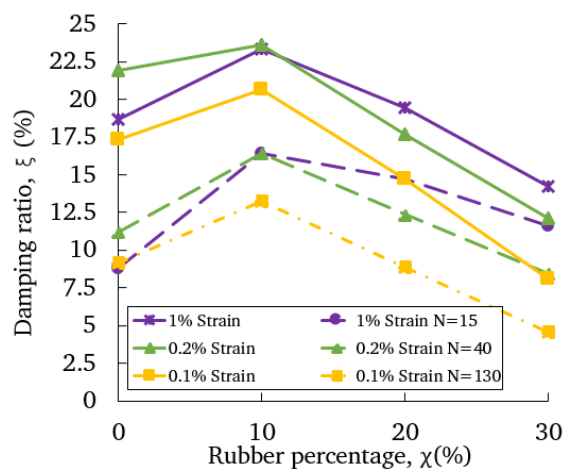


**Figure 7.6:** Damping degradation versus shear strain, rubber percentage and cycles to liquefaction

Table 7.1 shows a conceptual framework created in this investigation based on the experimental results in conjunction with studies reviewed in the literature (Section 3.5.3) to elucidate the effect of particle properties and test conditions on RSm dynamic behaviour. The framework classifies the extent of influence associated with each parameter in the evolution of stiffness and material relationship curves, as a function of the deformation undergone, with respect to a sand specimen ranging from "significant decrease" to "significant increase". In other words, it describes the overall tendency in the evolution of the two bulk parameters when comparing a mixture containing rubber to a sand specimen. Thus, whilst the significant increase refers to a rise in the value of either the normalised stiffness or damping ratio when compared to sand, the significant decrease describes a decay in the value of the bulk parameter.

As discussed in this chapter, rubber content, size ratio and number of cycles appear to have a direct effect in the evolution of shear modulus and damping ratio. In general terms, it can be established that a more linear dynamic behaviour, and reduced rate of stiffness degradation, is observed with rubber under cyclic loading. This coincides with the transition in the behaviour of the mixture from sand-like to rubber-like behaviour. The particle effect is accentuated when the size ratio is lower than 1, i.e. rubber particle size < sand particle size, and at higher confining pressures (< 200 kPa) as a consequence of the increase in the rubber-to-rubber particle contacts.

In accordance with previous studies, the addition of rubber points to an optimum damping capacity at around  $\chi = 10\%$  from which the material damping decays, hence its tendency is to decrease at higher rubber contents. At small-to-medium strains, the particle effect is more accentuated as the size of rubber decreases ( $S_R < 1$ ), whereas at medium-to-large strains, the effect is more pronounced as the size of sand decreases ( $S_R > 1$ ) due to the higher sand-to-sand particle contacts. In the entire strain amplitude range, the increase in confining pressure results in a reduction of material damping, more pronounced at  $\sigma_m > 200$  kPa.

On the other hand, the nearly similar size of particulate rubber and sand studied in this investigation leads to results which slightly differs from existing research. In this regard, higher stiffness degradation, but also higher damping ratio, has been found in

RSm of this investigation at low rubber contents ( $\chi = 10\%$ ), more observed in samples with a  $S_R > 1$ . This could be attributable to the elongated rubber shape ( $A_R = 6$ ) of this investigation, which would result in an increase of contacts between sand. At higher rubber contents, the stiffness and damping - shear strain curves follow those of previous studies, exhibiting the behaviour of rubber-like soils.

The cyclic effect has been studied in this investigation from medium-to-large deformations. As previously discussed, its influence in both soil stiffness and damping leads to a significant decay in their values as sand content increases. By contrast, the mixture exhibits a higher capacity to deform as more rubber is added (Chapter 4). Hence, the decay in damping capacity and, more importantly, soil stiffness is ameliorated at  $\chi = 20\text{-}30\%$ . Table 7.1 could be used as a framework for future studies to investigate the effect of additional particle properties, i.e. aspect ratio or material stiffness, as well as bulk particle properties including particle size distribution or relative density, on the dynamic behaviour of RSm.

**Table 7.1:** Effect of particle properties and test conditions on the dynamic behaviour of RSm

Parameter	Small to medium strains		Medium to high strains	
	$G/G_0$	$\xi$	$G/G_0$	$\xi$
Rubber content	⊕	⊕	⊕	≤ 10% ⊕ > 10% ⊖
Size ratio, $D_{50r}/D_{50s} > 1$	⊕ ⊕	⊕	⊕	≤ 200kPa ⊕ >200kPa ⊖
Size ratio, $D_{50r}/D_{50s} < 1$	⊕	⊕ ⊕	⊕ ⊕	≤ 200kPa ⊕ >200kPa ⊖
Effective confining pressure	⊕	⊖	⊕	⊖
Number of cycles	NE	NE	< $\chi = 20\%$ ⊖ ⊖ ≥ $\chi = 20\%$ NE	< $\chi = 20\%$ ⊖ ⊖ ≥ $\chi = 20\%$ ⊖

Note: ⊕ Increase; ⊕ ⊕ Significant increase;  
⊖ Decrease; ⊖ ⊖ Significant decrease; NE = No Effect

### 7.2.3 Energy dissipation mechanisms in RSm

The energy dissipation mechanisms found in RSm are discussed by comparing the results obtained at a particle (Chapter 4), element (Chapter 5) and lab scale (Chapter 6).



### ***Particle and element scale***

The experimental testing discussed in Chapters 4 and 5 evaluated the energy dissipation mechanisms associated with the mechanical properties of the soil, also known as material damping (Section 2.5.1). This is on the basis that RSm specimens subjected to oedometer, resonant column and triaxial tests were studied under isolated conditions where the geometrical characteristics have a negligible effect on the dynamic properties.

The results obtained in Section 4.4.3 evidenced the energy dissipation mechanisms associated with material damping at a particle scale. On one side, the dissipation in sands was caused by inter-particle contact sliding and due to particle re-arrangements. On the other hand, the addition of rubber inhibited the particle sliding and the energy dissipation was controlled by rubber deformability.

At an element scale (Figure 7.3), the material damping was quantified revealing the high damping ratio of sand at medium-to-large deformations. By adding  $\chi = 10\%$ , an improvement in the material damping was observed from combining the dissipation due to particle re-arrangements and rubber deformability. By contrast, adding more rubber ( $\chi = 20\text{-}30\%$ ) led to a decay in the material damping at medium-to-large deformations, which has been attributed in existing research (Li et al., 2016) to the increase in the rubber-to-rubber contacts, i.e. rubber-like behaviour. This result is opposite to the trend found at small strains ( $\gamma < 0.01\%$ ), where viscous damping increased with rubber.

### ***Lab scale system***

From the results discussed in this thesis, discrepancies in the evolution of damping ratio have been observed at an element and lab scale. Interestingly, the evolution in the material damping is at odds with the trend shown for the damping ratio evaluated during the shaking table tests in Chapter 6 (Figure 7.7a). Whilst the material damping decreases at  $\chi > 10\%$  in the medium-to-large strain range, the damping ratio reported in the lab scale context increases, almost doubling the value by adding  $\chi = 30\%$ . Although RSm containing  $\chi = 0\%$  and  $10\%$  show a higher material damping, the results from the shaking table reveal that soft zones with  $\chi > 10\%$  experience a lower amplification

ratio hence, they are more effective in mitigating the incident horizontal accelerations. Therefore, results from this study support the view that incident vibrations are more attenuated as damping increases, as established in existing research (Xiong and Li, 2013; Bandyopadhyay et al., 2015). The main discrepancy between this and previous studies stems from the basis to explain energy dissipation at lab/field scale.

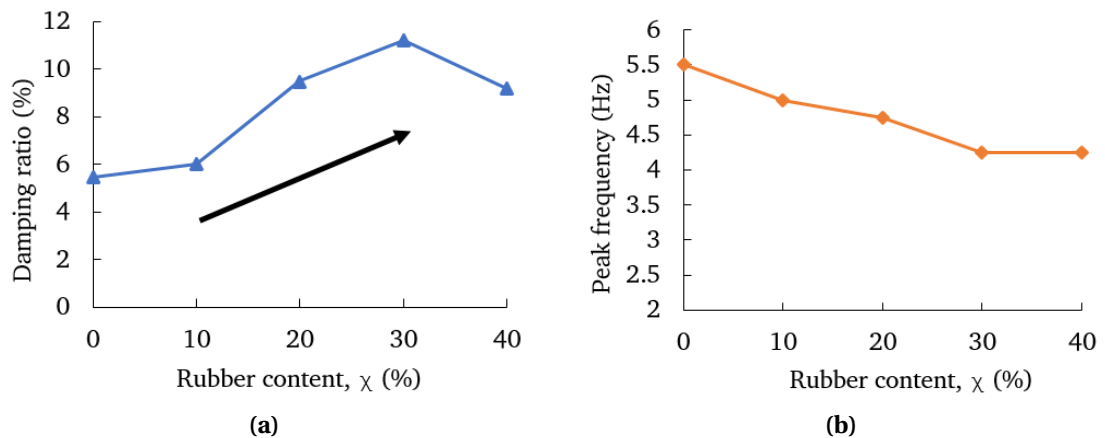


**Figure 7.7:** a) Peak frequency, and b) damping ratio at lab scale

To aid in understanding the energy dissipation evaluated in the foundation-modified soil system, this study discussed in Section 2.5.2 the concept of wave screening, adopted by previous studies to mitigate ground-borne vibrations (Woods, 1968; Alzawi, 2011; Mahdavisefat et al., 2017). This mechanism relies on the basis that introducing soft barriers increases the dynamic impedance with the surrounding soil, reflecting part of the incident waves and attenuating the energy, denoted as geometrical damping.

The dynamic impedance can be accentuated with the inclusion of materials characterised by a lower shear stiffness such as super absorbent polymer (Nappa, 2014; Flora et al., 2018), dessert jelly (Brennan et al., 2019) or RSm (Mahdavisefat et al., 2017). This was the argument adopted by Lombardi et al. (2015) to explain the attenuation in the boundary effects of a shaking table with foam layers, characterised by a low stiffness and high dynamic impedance.

The same view could thus be applied to this study and the incorporation of rubber within the vertical installations given that it reduces the overall soil stiffness (Figure 7.4) and, subsequently, the natural frequency of the foundation-soil system (Figure

7.7b). The reduction in the soil stiffness of the vertical soft zones would lead to an increase in the dynamic impedance between the outer rigid (timber) walls and the less stiff retrofitted walls with RSm. As a result, part of the waves generated by means of the shaking table, and transmitted through the rigid walls, would be reflected and this would be more pronounced as the dynamic impedance increases.

The reflection of parts of the incident energy, due to the wave scattering, opens an alternative explanation to justify the increase in damping capacity and decay in peak accelerations registered on the building. Most of the studies in the literature (Hazarika et al., 2006; Tsang et al., 2012) rely on the apparent increase in material damping by adding rubber to justify the attenuation in the structural response. However, the damping ratio calculated by these studies is devised from resonant column and triaxial tests at an element scale, not considering additional factors such as the influence of geometrical aspects on the dynamic properties. Apart from this, no previous study has compared the damping capacity at various scales.

Given that the negative trend shown in the evolution of material damping (Figure 7.3), this study introduces the argument that part of the incident stress waves are reflected as consequence of the increase in dynamic impedance with the addition of rubber. In other words, the increase in the overall damping capacity observed at a lab scale with RSm could be attributable to not only the hysteretic material damping, consequence of the non-linear behaviour of RSm with the addition of deformable particles, but other aspects such as wave reflection due to the interaction between the soft zone and the host soil. Based on these observations, the determination of material damping would be insufficient to justify the energy dissipation mechanisms and, in turn, the seismic performance of soft zones under cyclic loading.

The results from shaking table tests (Chapter 6) and the arguments herein discussed are part of an initial exploration to test the influence of soft zones. Thus, these cannot be considered to be a fully developed basis. A more comprehensive investigation would be required to validate the hypothesis that two forms of damping, i.e. material and geometrical, are acting on the attenuation of sinusoidal motions with the installation of vertical RSm installations and thereafter quantify its contribution.

### 7.3 Determination of $G_0$ and $\xi_0$ for RSm

Maximum shear modulus and initial damping ratio calculated via torsional resonant column tests are compared with analytical expressions proposed in the literature. The calculation of  $G_0$  and  $\xi_0$  for a range of rubber contents is undertaken using different expressions. To determine maximum shear modulus, particle and bulk properties as well as test conditions are considered. For the calculation of minimum damping ratio, expressions proposed by [Anastasiadis et al. \(2012b\)](#) and [Senetakis et al. \(2012a\)](#) are employed which also consider size ratio and equivalent void ratio.

#### 7.3.1 Sand

Table 7.2 presents expressions proposed in previous investigations to determine the maximum shear modulus of sands, as a function of sample void ratio. The variation in maximum shear modulus is shown by comparing the results obtained with the resonant column test and the expressions herein shown.

All the proposed expressions show a relatively similar shear modulus compared to the experimental result of this study, except for the case of [Iwasaki et al. \(1979\)](#), which shows a smaller value. Equations 7.2 and 7.3 ([Hardin and Richart, 1963](#)) provide a better approximation which results in a lower variation with respect to the experimental results, i.e. -5.4 and +2%.

**Table 7.2:** Calculation of  $G_0$  for sand

References	F(e)	$A_G$	$n_G$	$G_0$ (MPa)	Variation(%)	Equation No.
This study	-	-	-	111.8	-	(7.1)
<a href="#">Hardin and Richart (1963)</a>	$\frac{(2.17-e)^2}{1+e}$	7000	0.5	105.8	-5.4	(7.2)
<a href="#">Hardin and Richart (1963)</a>	$\frac{(2.97-e)^2}{1+e}$	3300	0.5	114.2	+2	(7.3)
<a href="#">Iwasaki et al. (1979)</a>	$\frac{(2.17-e)^2}{1+e}$	9000	0.38	78.3	-30	(7.4)
<a href="#">Kokusho (1980)</a>	$\frac{(2.17-e)^2}{1+e}$	8400	0.5	126.9	13.5	(7.5)

Note:  $G_0 = A_G F(e) (\sigma_3)^{n_G}$

In terms of damping, the expression proposed by [Menq \(2003\)](#) has been compared with the experimental results obtained on RSm at very small strains. To calculate the minimum damping ratio of sand, Equation 7.6 includes mean effective size  $D_{50}$ , confining pressure  $\sigma_3$ , and curvature coefficient  $C_u$ :

$$\xi_0(\%) = 0.55(C_u)^{0.1} D_{50} \left( \frac{\sigma_3}{P_a} \right)^{-0.08} \quad (7.6)$$

Where  $C_u = 1.25$ ,  $D_{50} = 0.85$  are mechanical properties corresponding to Leighton Buzzard sand investigated in this study (Chapter 4),  $\sigma_3 = 100$  kPa, and  $P_a = 101.325$  kPa. From Equation 7.6, the minimum damping ratio calculated for sand is  $\xi_0 = 0.59\%$ , similar to the value obtained through resonant column test ( $\xi_0 = 0.52\%$ ), revealing the high correlation between analytical and experimental results.

### 7.3.2 Rubber-soil mixtures

For the determination of maximum soil stiffness in RSm, two approaches are adopted in this study. First, [Pistolos et al. \(2018\)](#) proposed to adjust the equation to calculate the maximum soils stiffness in mineral soils created by [Menq \(2003\)](#) for RSm . This new expression includes the mixture equivalent void ratio ( $e_{eq}$ ) (as determined in Chapter 4), rubber percentage  $r$ , and mean effective size of sand  $D_{50s}$ :

$$G_{0RSm} = 67.1(C_{uSand})^{-0.2} e_{eq}^f \left( \frac{\sigma_3}{P_a} \right)^{n_G} r_G \quad (7.7)$$

$$e_{eq} = \frac{V_v + V_r}{V_s} \quad (7.8)$$

$$f = -1.3 - \left( \frac{D_{50s}}{12} \right)^{0.82} \quad (7.9)$$

$$n_G = 0.48(C_{uSand})^{0.09} - 0.0009r \quad (7.10)$$

$$r_G = 1.025^r \quad (7.11)$$

Where  $r$  is the rubber percentage,  $V_v$  is the volume of voids,  $V_r$  is the volume of rubber, and  $V_s$  is the volume of sand.

An alternative expressions was created by [Anastasiadis et al. \(2012b\)](#) to calculate the maximum shear modulus of RSm containing particulate rubber, which mainly depends on size ratio between sand and rubber particles ( $D_{50s}/D_{50r}$ ). Equation 7.12 was established for mixtures with uniform soils:

$$G_{0RSm} = G_{0sand} F_{eeq} A_G \quad (7.12)$$

$$F_{eeq} = \frac{1}{e_{eq}^{X_e}} \quad (7.13)$$

$$X_e = 2.1365 \left( \frac{D_{50s}}{D_{50r}} \right)^{0.22} \quad (7.14)$$

$$A_G = 0.3919 \left( \frac{D_{50s}}{D_{50r}} \right)^{-0.1602} \quad (7.15)$$

Where,  $G_{0soil}$  is maximum shear modulus of sand added to the mixture,  $D_{50s}$  is sand mean effective size, and  $D_{50r}$  is rubber mean effective size.

Table 7.3 shows the results corresponding to the maximum shear modulus for each rubber percentage. This includes Equation 7.7, according to [Pistolas et al. \(2018\)](#), Equation 7.12, based on [Anastasiadis et al. \(2012a\)](#), and the variation in the value of the experimental results with respect to the analytical expressions.

The two proposed equations provide a better fit to the empirical results as rubber content increases. In other words, the expressions used appear to underestimate the value of soil stiffness at low rubber percentages ( $\chi = 10\text{-}20\%$ ). An explanation for this discrepancy might be attributed to the fact that previous studies used granular rubber instead of elongated shredded rubber particles as used in this study. Hence, only the size ratio but not rubber shape, i.e. aspect ratio, is considered for the determination of soil stiffness. Further investigation is required to include the effect of this particle property on the variation of the soil stiffness with rubber content.

**Table 7.3:** Calculation of  $G_0$  for RSm

References	$G_0$ exp.(MPa)	$G_0$ Menq (MPa)	Var.(%)	$G_0$ Anastasiadis (MPa)	Var.(%)
10RSm	52.3	38.66	-34.2	34.41	-26.1
20RSm	22.2	16.77	-22.1	15.71	-16.8
30RSm	7.9	8.3	+5.72	8.4	+4.7

In terms of damping capacity, [Senetakis et al. \(2012a\)](#) proposed an equation to calculate the minimum damping ratio of RSm with granulated rubber. The value of viscous damping capacity is calculated as a function of mineral soil (sand) damping added to the mixture  $\xi_{0soil}$  and the constants A and B which, in turn, depend on the size ratio between rubber and sand particles. The expression proposed by [Senetakis et al. \(2012a\)](#) states as follows:

$$\xi_{0RSm}(\%) = \xi_{0sand}F(r_\xi) \quad (7.16)$$

$$F(r_\xi) = Ar + B \quad (7.17)$$

Where,  $r$  is rubber content and  $A = 0.1487$  and  $B = 1$  when  $D_{50s} \approx D_{50r}$ .

The minimum damping ratio has been calculated in Table 7.4 for RSm by using Equation 7.16, based on the expression established by [Senetakis et al. \(2012a\)](#), obtaining  $\xi_0 = 1.47\%$ ,  $2.34\%$ , and  $3.22\%$  for  $\chi = 10\%$ ,  $20\%$  and  $30\%$ . As established for the calculation of damping ratio for sand (Equation 7.6), Equation 7.16 captures the improvement in the damping capacity with rubber addition and do not differ significantly from the experimental results obtained from cyclic triaxial tests, i.e.  $\xi_0$  experimental. Only 30% RSm exhibits a lower minimum damping capacity than the estimated by Equation 7.16 on the basis that the optimum damping capacity found in this study occurs when adding  $\chi = 20\%$ . This coincides with the findings shown in the literature ([Zheng-Yi and Sutter, 2000](#); [Senetakis et al., 2012a](#)), in which an increasing trend was found in terms of non-linear viscous damping as the rubber content increased (Figure 7.8b).

**Table 7.4:** Calculation of  $\xi_0$  for RSm

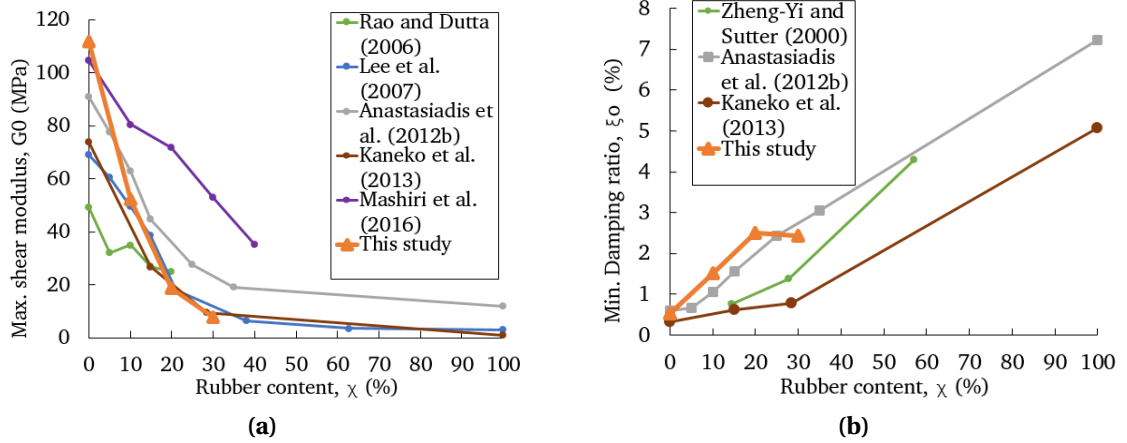
References	$\xi_0$ exp. (%)	$\xi_0$ (%) Senetakis2012	Var.(%)
10RSm	1.52	1.47	-3.5
20RSm	2.51	2.34	-6.6
30RSm	2.44	3.22	+32

Figure 7.8 show both maximum shear modulus and minimum damping ratio in order to compare the results from this study with existing research.

It can be observed that sand used in this investigation exhibits a maximum shear modulus greater than the average (Figure 7.8a). A reduction in the overall soil stiffness is found with rubber content as a consequence of low rubber stiffness. However, the negative trend shown in this study is more pronounced than in previous investigations which might be due to the rubber particle shape and size. In this regard, the introduction of big tyre chips (Mashiri et al., 2016), with a size ratio  $S_R > 20$ , result in a higher number of contacts between sand particles and therefore an increase in the overall soil stiffness as observed in Figure 7.8a. By contrast, Anastasiadis et al. (2012a) and Kaneko et al. (2013) tested particulate rubber with a mean size ratio similar to the sandy material. This results in a higher number of contacts between rubber and, in turn, a decay in the overall soil stiffness.

With regards to the evolution in  $\xi_0$  (Figure 7.8b), most of the studies show an improvement in the minimum damping capacity with rubber content up to  $\chi = 100\%$ . According to the experimental results analysed in Chapter 5, this study has also proven the development in the damping capacity of mixture containing rubber up to  $\chi = 20\%$ , point at which the value remains . As established by Zheng-Yi and Sutter (2000) and Anastasiadis et al. (2012b), these results demonstrate that there is an improvement in the damping capacity at small strains by combining the friction between particles and rubber deformation.





**Figure 7.8:** Maximum shear modulus and minimum damping ratio of RSM

## 7.4 Stiffness relationship of RSM

Hyperbolic models have been previously proposed to predict the non-linear dynamic behaviour of soils via shear modulus - shear strain curves. [Hardin and Drnevich \(1972\)](#) created a hyperbolic asymptotic model capable of relating stress and strain in a soil to predict the evolution in the dynamic properties. This model, however, presents certain limitations due to only considering one curve-fitting variable, denoted as reference strain ( $\gamma_r$ ) ([Zhang et al., 2005](#)), not able to fully capture the evolution in soil stiffness of plastic soils. Alternatively, [Darendeli \(2001\)](#) proposed a normalised shear modulus shear strain relationship modifying the equation initially established by [Hardin and Drnevich \(1972\)](#). Equation 7.18 introduces the coefficient of curvature ( $a$ ), which depends on the number of cycles and the frequency loading, to adjust the original hyperbolic model:

$$\frac{G}{G_0} = \frac{1}{1 + \left(\frac{\gamma}{\gamma_r}\right)^a} \quad (7.18)$$

Where,  $\gamma$  is the current strain value,  $\gamma_r$  is the reference strain, and  $a$  is a coefficient which depend on loading frequency, number of cycles and type of soil.

### 7.4.1 Reference strain

According to Equation 7.18, the value of reference strain needs to be calculated. Reference strain ( $\gamma_r$ ) refers to the shear strain at which  $G/G_0 = 0.5$ . This variable is required to define the curve which depicts the variation in soil shear modulus with strain amplitude of a soil. For this study, reference strain has been calculated based on normalised curves traced from the experimental results shown in Figure 7.4 for every rubber content. To corroborate the empirical results, these values have been compared with the analytical expression proposed by Senetakis et al. (2012a) (Table 7.5). Equation 7.19 is used to calculate the reference strain for RSm containing granulated rubber (Senetakis et al., 2012a), determined using the reference strain corresponding to sand ( $\gamma_{sand}$ ):

$$\gamma_{RSm} = \gamma_{sand} F(r_\gamma) \quad (7.19)$$

$$F(r_\gamma) = a_1 r^2 + a_2 r + a_3 \quad (7.20)$$

Where,  $r$  is the rubber percentage (%),  $a_1 = 0.003$ ,  $a_2 = -0.01$ , and  $a_3 = 1$  are the values for RSm when rubber and sand present similar size ratio, i.e.  $D_{50s} \approx D_{50r}$ .

As shown in Table 7.5, reference strain is similar for sand and 10% RSm but then this value increases with rubber content. This indicates that the response of the mixture presents a more linear shape at  $\chi > 10\%$ , as discussed in Section 7.1b. On the other hand, no clear effect of rubber content on curvature coefficient is observed, ranging between 1.31 and 1.42 for all RSm. Table 7.5 also shows slight differences between empirical and analytical results, obtained via Equation 7.19, which corroborates the high correlation with the expressions proposed by Senetakis et al. (2012a).

**Table 7.5:** Calculation of reference strain  $\gamma_{RSm}$  for RSm

References	Exp. $\gamma_{RSm}$ (%)	$\gamma_{RSm}$ by Senetakis2012	Var.(%)	Curvature (a)	$R^2$
0RSm	0.035	-	-	1.17	0.992
10RSm	0.034	0.042	+23.5	1.37	0.984
20RSm	0.067	0.07	+4.5	1.42	0.977
30RSm	0.106	0.12	+12.3	1.31	0.951

### 7.4.2 Normalised shear modulus curve based on Darendeli (2001)

Equation 7.18 has been adopted to predict the variation in normalised  $G/G_0$  with strain amplitude. For that, experimental values of  $\gamma_r$  and  $a$  have been taken from Table 7.5 and used to calculate  $G/G_0$  for every rubber content.

Adding  $\chi \pm 10\%$  increases the resilience of the mixture, which results in a lower stiffness degradation, more evident at medium-to-large strains as observed in Figure 7.9. Although Darendeli (2001) created his expression based on 200 dynamic tests performed on granular soils, the results shown in Figure 7.9 reveal a high correlation between the experimental data and the proposed expression, where  $R^2$  is in excess of 0.95 for all RSm. However, Equation 7.18 does not seem to provide a good fit at large strain amplitudes ( $\gamma > 0.1\%$ ) where there is a rapid decay in normalised shear modulus curve. This is mainly noted in Figure 7.9 at high rubber contents, i.e.  $\chi = 20-30\%$ .

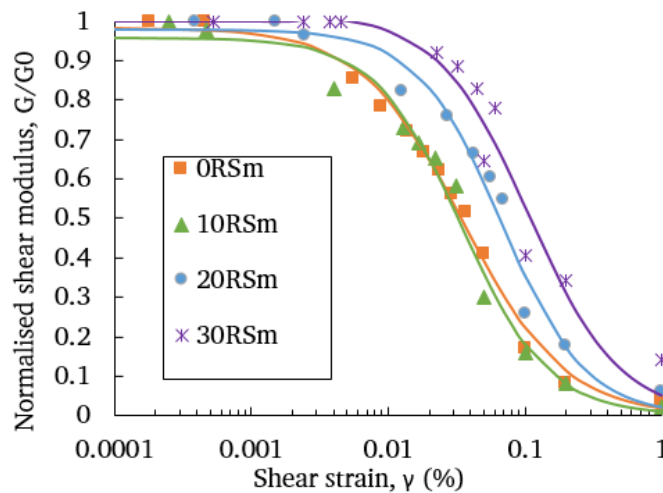


**Figure 7.9:** Normalised shear modulus - shear strain of RSm based on Darendeli (2001)

### 7.4.3 Normalised shear modulus curve based on MMF model

Alternatively, this study proposes the use of a different modified hyperbolic model to determine the variation in normalised shear modulus with strain amplitude, known as the Morgan-Morgan-Finney (MMF) non-linear sigmoidal model. Equation 7.21 describes the MMF model to the normalised  $G/G_0$  curve as follows:

$$\frac{G}{G_0} = \frac{ab + c\gamma^d}{b + \gamma^d} \quad (7.21)$$

Where,  $a$ ,  $b$ ,  $c$  and  $d$  are function parameters and  $\gamma$  is the current value of shear strain. Equation 7.21 can be re-written as:

$$\frac{G}{G_0} = \frac{ab\gamma^d + c}{b\gamma^d + 1} \quad (7.22)$$

When the value of  $c = 1$ , and  $\gamma \approx 0$ , the value of  $G = G_0$ , which occurs for any soil specimen at very small strains. Thus, Equation 7.22 can be reduced to:

$$\frac{G}{G_0} = \frac{ab\gamma^c + 1}{b\gamma^c + 1} \quad (7.23)$$

Equation 7.23, with three function parameters, has been adopted instead of the original MMF expression (Equation 7.21), to determine the value of normalised shear modulus of RSm. Table 7.6 shows each of the function parameters ( $a$ ,  $b$ ,  $c$ ) obtained to adapt the model to the empirical results for every RSm. In general, it can be observed that values of function parameters follow an increasing trend with rubber amount. The parameter  $a$  represents the magnitude of the normalised shear modulus at the maximum recorded strain, i.e.  $\gamma = 1\%$ . It is shown that this value is just above 0 for the case of  $\chi = 0-10\%$ , whilst the magnitude of the value reaches 0.16 at  $\chi = 30\%$ . This reflects the lower stiffness degradation at large deformations with the addition of rubber, inaccurately captured with the expression proposed by Darendeli (Figure 7.9). Parameter  $c$  plays the same role as the curvature coefficient  $a$  in Darendeli's expression (Equation 7.18), hence the increase in the magnitude of this parameter results in an increase of the reference strain, and the subsequent translation of the curve, which reflects a more linear dynamic behaviour, as shown in Figure 7.10.

The standard error and  $R^2$  have been calculated to demonstrate the goodness-of-fit using the MMF model. It is noticed that  $R^2$  increases for 20-30% RSm compared to the non-linear hyperbolic model proposed by Darendeli (2001). With the MMF model, the evolution in the normalised shear modulus is less abrupt and the model predicts with better accuracy the change in soil stiffness at medium-to-large deformations ( $\gamma >$

0.1%). This model provides then an alternative expression to predict the non-linearity exhibited by RSm due to the addition of the highly deformable rubber.

**Table 7.6:** Function parameters of MMF (Equation 7.23) for RSm

References	a	b	c	Standard error	$R^2$
0RSm	0.002	42.942	1.133	0.031	0.992
10RSm	0.002	95.958	1.357	0.054	0.982
20RSm	0.028	60.019	1.506	0.057	0.977
30RSm	0.161	125.225	1.890	0.060	0.967

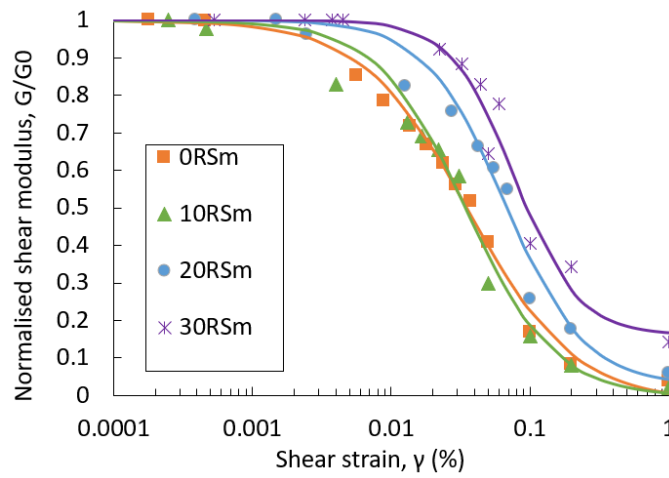


**Figure 7.10:** Normalised shear modulus - shear strain using MMF model

## 7.5 Damping ratio relationship of RSm

The variation in damping ratio with strain amplitude is discussed in this section by adopting various non-linear models proposed in previous studies (Darendeli, 2001; Phillips and Hashash, 2009; Senetakis et al., 2012a). One of the first expressions to predict the hyperbolic non-linear material damping with respect to shear strain curve was established by Masing (1926), and it is based on the known Masing rules. Equation 7.24 is used to determine damping ratio following Masing rules that includes the value of current and reference strain:

$$\xi_{Masing,a=1}(\%) = \frac{100}{\pi} \left( 4 \frac{\gamma - \gamma_r \ln\left(\frac{\gamma + \gamma_r}{\gamma_r}\right)}{\frac{\gamma^2}{\gamma + \gamma_r}} - 2 \right) \quad (7.24)$$

The material damping curve is scaled and shifted based on the value of the curvature coefficient  $a$ . This value adopted to adjust the curvature of the hyperbolic normalised shear modulus to the experimental results, which depends on the loading frequency and number of cycles. The expression proposed by [Masing \(1926\)](#) to determine the material damping curve stays as:

$$\xi_{Masing} = c_1 \xi_{M,a=1} + c_2 \xi_{M,a=1}^2 + c_3 \xi_{M,a=1}^3 \quad (7.25)$$

$$c_1 = -1.1143a^2 + 1.8618a + 0.2523 \quad (7.26)$$

$$c_2 = 0.0805a^2 - 0.071a - 0.0095 \quad (7.27)$$

$$c_3 = -0.0005a^2 + 0.0002a + 0.0003 \quad (7.28)$$

Despite the good approximations obtained with the expressions established by [Masing \(1926\)](#), previous studies ([Phillips and Hashash, 2009](#)) address the discrepancy between empirical and analytical results in the medium-to-large strain range. A solution was proposed by [Darendeli \(2001\)](#), who established an alternative expression to match both shear modulus and damping ratio at the same time by developing an empirically based modified hyperbolic model. Hence, [Darendeli \(2001\)](#) included in the expression the minimum damping ratio, empirically determined, to overcome the underestimation observed in damping at small-to-medium strains. A reduction factor  $DF(\gamma)$  is applied to the original Masing equation to adjust the evolution in damping degradation based on stiffness reduction, via normalised shear modulus - shear strain curve, at medium-to-large strains. Equation 7.29 shows the modified expression for determining damping strain relationship as a function of the number of cycles and the normalised shear modulus ( $G/G_0$ ):

$$\xi_{Darendeli} = DF(\gamma) \xi_{Masing} + \xi_0 \quad (7.29)$$

$$DF(\gamma) = b_1 \left( \frac{G_\gamma}{G_0} \right)^{0.1} \quad (7.30)$$

$$b_1 = 0.6329 - 0.0057 \ln N \quad (7.31)$$

Figure 7.11 shows the evolution in damping ratio versus shear strain for RSm of this investigation by adjusting shear modulus to damping ratio using Equation 7.29. It is noted that the expression provided by Darendeli provides a good fit at small-to-medium strains, i.e.  $\gamma_{cyc} = 0.0001$ -0.05%. However, a different behaviour is observed between sand-like and rubber-like specimens at larger strains ( $\gamma_{cyc} > 0.05\%$ ). In this regard, the expression appears to overestimate the damping ratio for high rubber contents ( $\chi = 20$ -30%), whereas the opposite trend occurs at low rubber contents, which is in line with the observations made by Phillips and Hashash (2009) about mineral soils.

Darendeli (2001) created this expression based on the results from dynamic tests performed on partially saturated granular soils. This might be one reason to explain the discrepancy between experimental and analytical results at large deformations. However, the tests performed in this study were undertaken in fully saturated conditions via cyclic triaxial experiments. Moreover, whilst Darendeli approximated his expression of experimental results on sands and clays, the material studied is a combination of a deformable particle (rubber) and a rigid mineral (sand) soil.

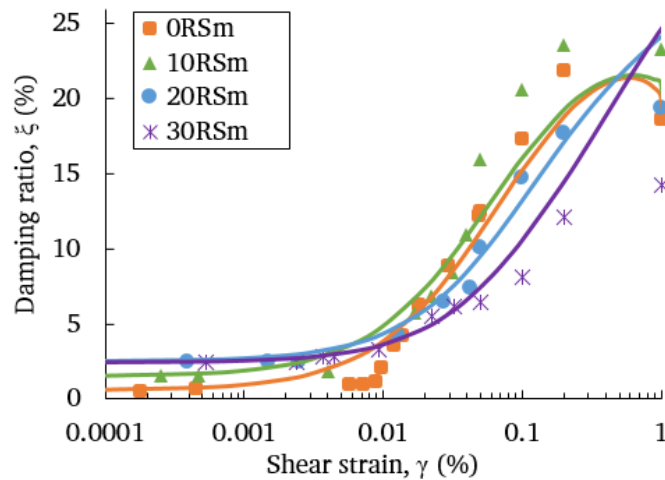


**Figure 7.11:** Normalised damping ratio - shear strain based on Darendeli (2001)

### 7.5.1 Damping ratio curve based on Senetakis et al. (2012a)

An alternative expression was proposed by Senetakis et al. (2012a) for estimating the damping ratio shear strain curve of RSm containing particulate rubber from very small-to-large deformations. Equation 7.32 identifies the correlation between normalised damping ratio, expressed by subtracting the effect of minimum damping ratio from the overall damping capacity ( $\xi - \xi_0$ ), and the normalised shear modulus associated with the material, obtained from the proposed MMF model (Section 7.4.3):

$$\xi_{Senetakis} - \xi_0 = a_6 \left( \frac{G}{G_0} \right)^2 + a_7 \left( \frac{G}{G_0} \right) + a_8 \quad (7.32)$$

Where,  $a_6$ ,  $a_7$  and  $a_8$  are function parameters.

By normalising  $\xi - \xi_0$ , it eliminates the effect of small-strain damping ratio and the possible effect of rubber on the damping capacity of the mixture at small deformations. Parameters  $a_6$ ,  $a_7$  and  $a_8$  were determined by calculating the second order polynomial equation from the correlation between normalised damping ratio and normalised shear modulus of all RSm (Figure 7.12). It is noticed in Figure 7.12 that the correlation between damping and stiffness is accurate in the small-to-medium strain range. However, the correlation is more scattered as the soil degradation increases, i.e. at higher strain amplitudes. This might be explained on the basis that Senetakis et al. (2012a) created this expression on empirical results of RSm at small-to-medium strain and was extrapolated to mixtures at larger deformations, being less accurate.



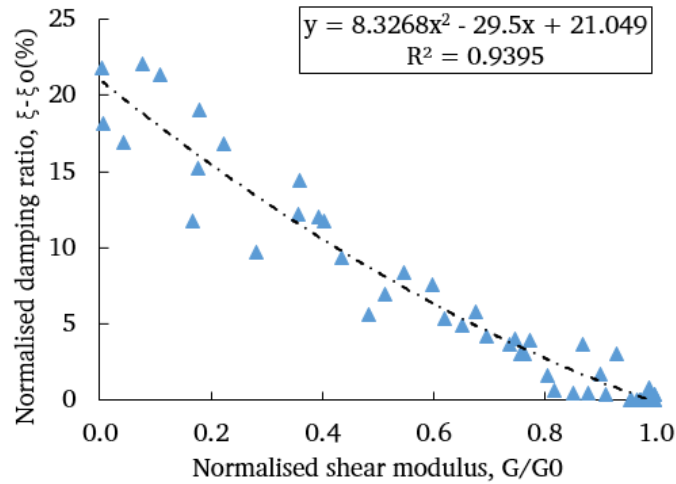


**Figure 7.12:** Correlation between  $\xi - \xi_0$  and  $G/G_0$  of RSm based on Senetakis et al. (2012a)

In light of the results shown in Figure 7.12, this study decided to individually apply the second order polynomial equation to the normalised damping curve corresponding to every rubber content ( $\chi = 0\%$ ,  $10\%$ ,  $20\%$ , and  $30\%$ ) (Figs 7.13). Function parameters  $a_6$ ,  $a_7$  and  $a_8$  have been calculated for each RSm, as shown in Table 7.7, and adjust more accurately to each one of the parameters depending on rubber content. The correlation function ( $R^2$ ) is represented next to the function parameters of every RSm in Table 7.13, showing values higher than 0.951, which indicates the good fit of the expression.

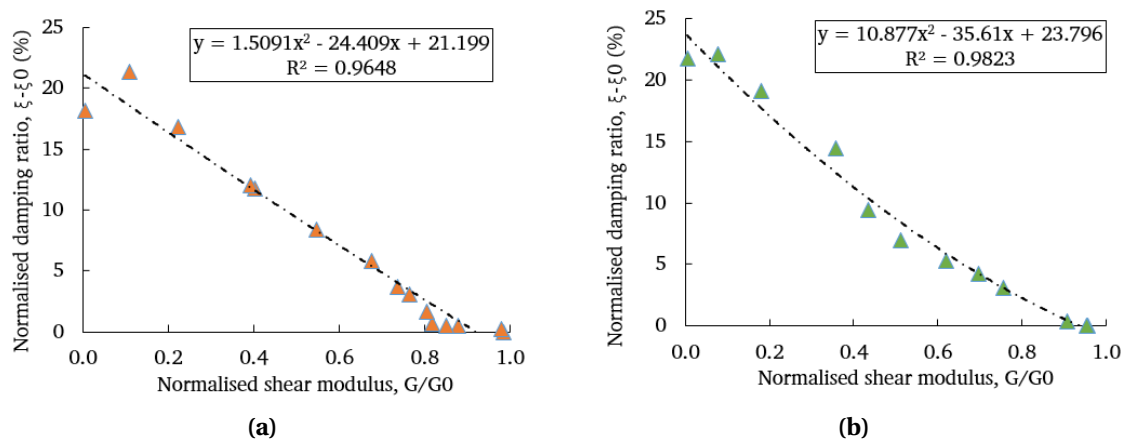


**Figure 7.13:** Correlation between  $\xi - \xi_0$  and  $G/G_0$  of a) 0RSm and b) 10RSm

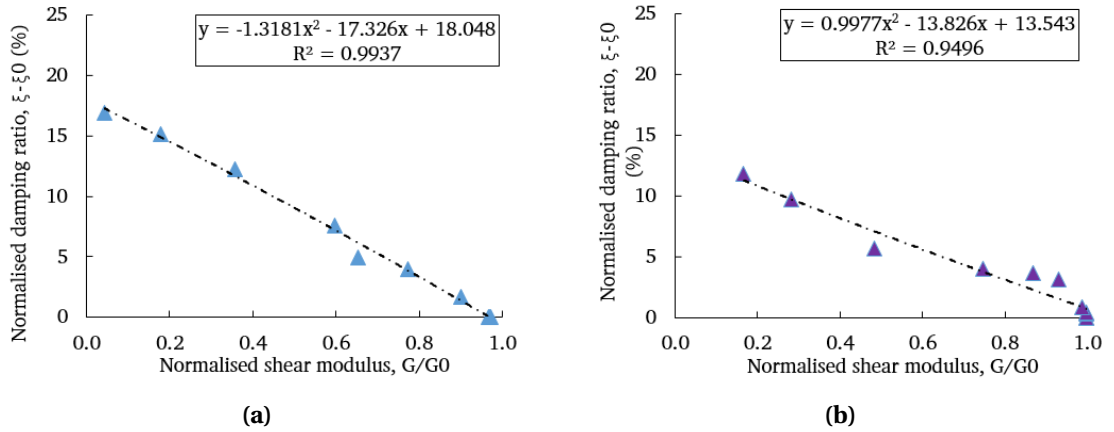


**Figure 7.14:** Correlation between  $\xi - \xi_0$  and  $G/G_0$  of a) 20RSm and d) 30RSm

**Table 7.7:** Function parameters to adjust damping based on Senetakis et al. (2012a)

References	$a_6$	$a_7$	$a_8$	$\xi_0$	$R^2$
ORSm	1.51	-24.41	21.2	0.59	0.965
10RSm	10.88	-35.61	23.8	1.52	0.982
20RSm	-1.32	-17.33	18.05	2.51	0.994
30RSm	0.97	-13.76	13.53	2.44	0.951

Figure 7.15 shows the evolution in damping ratio in accordance with the experimental results on RSm and the trend in the analytical expression by adjusting the function parameters obtained in Table 7.7 to the expression proposed by Senetakis (Equation 7.32). A high correlation is observed between measured and estimated damping values which corroborates the use of the expression proposed by Senetakis et al. (2012a) to simulate the damping ratio relationship of RSm. However, some discrepancies can be found between the analytical and experimental values in the medium-to-large strain range amplitude, i.e.  $\gamma_{cyc} = 0.2-1\%$ . This can be attributed to two factors: (i) the expression was created for RSm specimens in dry state, and did not consider the rise in pore water pressure, and (ii) the expression was established based on results obtained at small-to-medium deformations. The latter is of importance when evaluating the evolution in damping capacity at large deformations due to the appearance of a limiting shear strain, strain at which the maximum damping capacity arises, from which damping ratio decays (Pistolas et al., 2018). As observed in Figure 7.15, the expression created by

Senetakis et al. (2012a) does not capture this decay in hysteretic damping, observed in sand and 10% RSm, at large deformations.

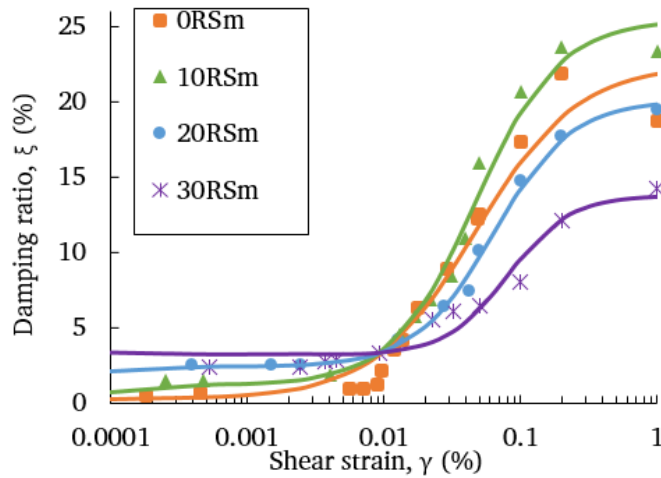


Figure 7.15: Normalised damping ratio - shear strain based on Senetakis et al. (2012a)

## 7.5.2 Damping ratio curve based on Phillips and Hashash (2009)

Albeit the model proposed by Senetakis et al. (2012a) presents a high correlation between estimated and empirical results, the proposed damping curve keeps increasing at large strains for every mixture. This finding differs from the trend shown with the experimental results in Figure 7.15. An explanation for this is that previous expressions (Senetakis et al., 2012a; Pistas et al., 2018) were applied to the dynamic properties obtained from soils in dry conditions. However, as explained for the analysis of the liquefaction potential (Figure 7.5b), the rise in pore pressure ratio leads to a reduction in inter-particle contacts and, as a result, a significant stiffness and damping degradation, more evident at large deformations.

An alternative approach is herein proposed to describe the increase in material damping for saturated RSm from small-to-large amplitudes. For that, this study introduces the use of the expression proposed by Phillips and Hashash (2009) using a different reduction factor. This model is a function of the normalised shear modulus and three function parameters. The model is commonly known as the Pressure-Dependent Hyperbolic model or Modulus Reduction and Damping curve fitting (MRDF). This model is commonly adopted in 1D ground response analysis, such as Deepsoil, as an

alternative non-Masing unload-reload rule after the backbone curve to predict the non-linear behaviour of mineral soils at medium-to-large deformations. In practice, this expression provides a better fit than previous equations by matching the empirical results with the original damping proposed by Masing (1926), by means of using an alternative reduction factor  $F(\gamma_m)$ :

$$\xi_{Hashash} = F(\gamma_m)\xi_{Masing} + \xi_0 \quad (7.33)$$

$$F(\gamma_m) = p_1 - p_2\left(1 - \frac{G_\gamma}{G_0}\right)^{p_3} \quad (7.34)$$

Where,  $G_{\gamma_m}/G_0$  is the normalised shear modulus and  $p_1$ ,  $p_2$  and  $p_3$  are non-dimensional parameters to obtain the best possible fit with the target damping curve.

Table 7.8 shows the parameters estimated for each rubber content to depict the damping curves traced in Figure 7.16. It can be observed that the curve fitting parameters ( $p_1, p_2, p_3$ ) are nearly similar for 0RSm and 10RSm. At  $\chi > 10\%$ , the evolution in the values of  $p_1$  and  $p_3$  follow a decreasing trend, whereas  $p_2$  increases.

**Table 7.8:** Function parameters to adjust damping based on Phillips and Hashash (2009)

References	$p_1$	$p_2$	$p_3$	$\gamma_r$ (%)	<b>a</b>	$\xi_0$
0RSm	0.65	0.32	15.71	0.035	1.17	0.59
10RSm	0.67	0.28	17	0.034	1.37	1.52
20RSm	0.6	0.38	11	0.067	1.42	2.51
30RSm	0.5	0.7	6.5	0.106	1.31	2.44

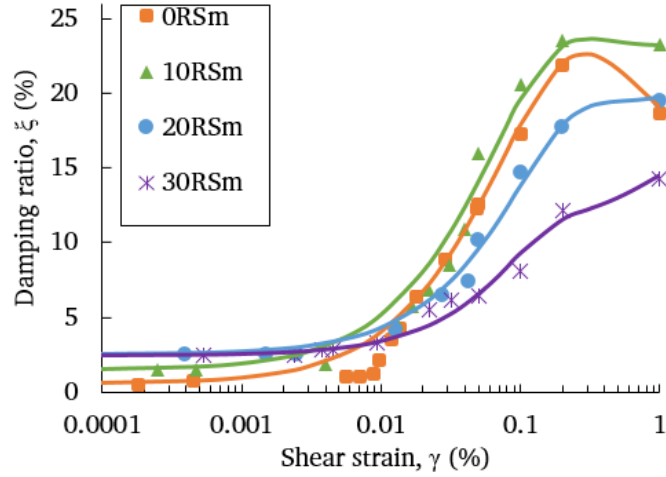


**Figure 7.16:** Normalised damping ratio - shear strain based on Phillips and Hashash (2009)

Equations 7.35-7.36-7.37 have been proposed in this study to determine the value of  $p_1$ ,  $p_2$ ,  $p_3$  and apply to Equation 7.34 depending on the rubber content:

$$p_1 = -0.0003\chi^2 + 0.0038\chi + 0.653 \quad (7.35)$$

$$p_2 = 0.0009\chi^2 - 0.0146\chi + 0.324 \quad (7.36)$$

$$p_3 = -0.0145\chi^2 + 0.0979\chi + 16.15 \quad (7.37)$$

The reduction factor ( $F(\gamma_m)$ ) adjusts the damping curve to the empirical values providing a better fit than the damping curves adjusted using Equation 7.29 (Darendeli, 2001). Therefore, it can be observed that the new expression identifies the decay in damping for sand and 10RSm, whereas a gradual increase in the damping ratio is predicted at  $\chi = 20-30\%$  for very large strains. The total  $R^2$  associated with the goodness of fit of this expression is equal to 0.983 and provides a better approximation than the damping strain curves created by Senetakis et al. (2012a) ( $R^2 = 0.943$ ). Thus, this study suggests the use of this analytical approach to alternatively predict the variation in material damping of saturated mixtures containing elongated particulate rubber.

## 7.6 Summary

In this chapter, the dynamic behaviour of RSm has been studied in the small-to-large strain range comparing the experimental results with existing research:

- Although adding rubber attenuated the cyclic effect, stiffness and damping degradation were yet observed to be significant up to 100 strain controlled cycles. This observation differs from the statement that dynamic properties remain constant beyond the 10th cycle ([Kokusho, 1980](#)). This suggests that the number of cycles should be accounted when dealing with saturated soils, subject to large deformations.

- Adding rubber points to an improvement in the damping capacity in the lab scale context, unlike the evolution in material damping. This suggests the presence of other forms of stress wave attenuation, i.e. wave scattering.

- Although a high correlation was found between the normalised  $G/G_0$  - shear strain curve and the empirical results using the expression established by [Darendeli \(2001\)](#), an alternative expression has been adopted to provide a better fit at medium-to-large strains by using the Morgan-Morgan-Finney model.

- The expression proposed by [Senetakis et al. \(2012a\)](#) for mixtures with granulated rubber provides a better fit than original damping curves ([Masing, 1926](#); [Darendeli, 2001](#)). However, this approach does not appear to be as accurate for saturated specimens, using alternatively the expression proposed by [Phillips and Hashash \(2009\)](#).

In terms of new understanding, this study has proposed a conceptual framework to elucidate the effect of particle properties and test conditions on the dynamic behaviour of RSm. It shows that the number of cycles has a detrimental effect on the evolution of shear modulus and damping ratio of saturated sands. This is proven to be ameliorated with the addition of small elongated rubber, which use could be adopted as a solution to prevent the stiffness and damping degradation due to the action of strong earthquakes. This study has also proposed the use of different expressions to predict the non-linear behaviour of RSm so that they can accurately simulate, with the use of numerical simulations, the ground response analysis of soils containing rubber.

## *Conclusions*

---

### **8.1 Introduction**

The disposal of scrap tyres has become a major environmental problem around the world. For its recovery, a geomaterial has been used as part of civil constructions, commonly known as Rubber-Soil mixture (RSm). Existing literature shows that adding rubber particles into sandy soil reduce the soil stiffness and can increase its damping capacity. The use of RSm has the potential to be used as a geotechnical seismic isolation system and hence provide protection against earthquakes. However, the static and dynamic behaviour of the mixture is still not well understood due to the various bulk and particle properties as well as test conditions that affect its characterisation. Limitations are also encountered in relation to the implementation of the system, questioning its use for existing long-term permanent constructions.

To address these gaps, the aim of this study was to understand the response of RSm under cyclic loading and evaluate its effectiveness in attenuating accelerations when used to retrofit a soil foundation. A review of the research approach, findings, conclusions and limitations incurred is presented in the following sections.

## 8.2 Summary of findings

Three research questions facilitated in addressing the aim and objectives of this study:

*1. What is the relationship between the micro and macro-structure of RSm and how does this correlate to the mechanics of RSm during particle shear and compression?*

Objective i) of this study was to define the mechanics of rigid-deformable mixtures, concretely RSm, establishing the inter-correlation between the bulk parameters with its micro and macro-structure. This has been undertaken based on the the background information (Chapter 2) and the literature review (Chapter 3) of this investigation with the following key findings:

- A variable-parameter-property scheme is introduced to explicitly define the distinction between system variables, test conditions, material (micro) properties, and bulk (macro), and thus interpret the behaviour of soils, and concretely RSm.
- The complexity of the framework increases when adding a deformable particle in the soil skeleton, with additional particle properties such as rubber mass, size, shape, stiffness and its interaction with stiffer (sand) particles.
- The shear strength of the mixture increases with the addition of tyre derived aggregates whereas the opposite trend is found with rounded tyre crumbs.
- The rubber-like behaviour is primarily found at high rubber contents and when the sand particles have a higher size due to the increase in the number of rubber-to-rubber particle contacts. A sand-like behaviour, characterised by a higher stiffness and lower deformation, is observed at low rubber contents and with big rubber chips.
- A common trend is found in the evolution of shear modulus where the overall soil stiffness decays whilst damping capacity increases at small-to-medium strains in the transition from sand-like to rubber-like behaviour. There is, however, insufficient experimental data to characterise the dynamic behaviour of RSm



from small-to-large deformations attributable to the various material properties and test conditions involved.

- The addition of tyre derived aggregates and rubber powder points to an increase in the liquefaction resistance when mixed up with liquefiable soils. However, a gap in the literature exists in relation to the cyclic effect on the evolution of stiffness and damping of saturated RSm at medium-to-large strains.
- Implementing RSm horizontal layers under the soil foundation can potentially mitigate vertical and horizontal accelerations. The main inconvenient of this design is that can only be implemented prior to the construction of new buildings, with a limiting vertical load to prevent excessive settlement.

Objective ii) was to characterise the compressibility of RSm whilst assessing the effect of rubber shape. Plain strain models and oedometer test results were performed in Chapter 4 on samples containing Leighton Buzzard sand (LBS) with either shredded (ShR) or crumb (CrR) rubber at  $\chi = 0, 15, 30, 45$  and  $100\%$ . 3D tomographic images were also taken from mini-oedometer tests under loading. The main results are:

- A greater change in void ratio as well as higher values in compression and swelling indices were found in specimens containing ShR. This was attributed to the entrapment and the increase in contact area as a consequence of its shape.
- At high stresses, the two rubber shapes revealed a nearly similar stiffer response as a result of the negligible number of voids. This led to an ultimate state at which the compressible behaviour was entirely controlled by rubber.
- The evolution in the one-dimensional compression of RSm is found to be the result of both i) particle re-arrangement and ii) distortion of rubber. As rubber is assumed to be incompressible, the temporary change in volume is attributable to the high micro porosity, in addition to the fissures/cracks, found on its surface.

In terms of new understanding, this study has demonstrated that the particle shape, in conjunction with rubber content, has an effect on the evolution of compressibility and the stress-strain behaviour of RSm. Hence, the bulk (macro) parameters that characterise the response of RSm under static/dynamic loading are influenced by the particle (micro) properties, including rubber shape, size, stiffness and its interaction with particulate sand. The rubber-like behaviour is found at high rubber contents and with smaller particulate rubber. Consequently, the particle-to-particle contacts affects the evolution in compressibility of RSm, which increases with rubber content and elongated rubber shape. This is attributed to both particle re-arrangement and rubber deformation as a result of the microporosity as well as fissures/cracks found in particulate rubber. Due to the high capacity of rubber to distort, RSm experience an improvement in the distortional stiffness. This means that rubber adds an additional resistance against vertical loading which postpones the particle slippage and breakage.

*2. How do the particle properties and test conditions influence the response and energy dissipation mechanisms of rubber-soil mixtures under cyclic loading?*

Objective iii) of this thesis was to study the evolution of bulk parameters ( $G$ ,  $\xi$ ) that define the dynamic behaviour of RSm. Cyclic triaxial and resonant column experiments were conducted on saturated RSm containing shredded particulate rubber at  $\chi = 0 - 30\%$  (Chapter 5). Stiffness and damping relationship characterisation were studied as a function of both particle properties and test conditions. Modified hyperbolic models were adapted to the experimental results (Chapter 7). These are the main findings:

- The liquefaction resistance of sand improved by adding rubber and decreased with the strain amplitude. Sand-like specimens liquefied before reaching 100 cycles. The inclusion of  $\chi = 20-30\%$  enabled the mixture to withstand 400 strain controlled cycles at  $\gamma = 1\%$ , remaining within the stable zone. The addition of smaller rubber particles points to an improvement in the liquefaction resistance, due to the higher number of contacts between rubber particles.
- The overall soil stiffness decreased with an increase in the strain amplitude and number of cycles at every rubber percentage. The low stiffness added by rubber

resulted in a reduction of shear modulus as rubber content increased. Adding rubber reduced the cyclic effect on the stiffness degradation. A greater reduction in soil stiffness was found by adding smaller rubber particulate.

- At medium to large strains, adding  $\chi = 10\%$  improved the hysteretic damping and, subsequently, decreased at greater rubber contents. Higher values in damping were found with smaller rubber particles. At small-to-medium strains, material damping improved with rubber whilst the rubber shape did not have an impact. Albeit sand exhibits an initial higher damping, the addition of rubber results in greater damping capacity after 20 strain controlled cycles at  $\gamma_{cyc} > 0.2\%$ .
- Prior to this investigation, only [Mashiri et al. \(2016\)](#) had examined the cyclic effect on the dynamic behaviour of RSm. The results reported in this study support the basis that saturated soils experience a significant stiffness and damping degradation, more evident as strain amplitude increases.
- The maximum shear modulus and minimum damping ratio calculated via the analytical expressions proposed by [Senetakis et al. \(2012a\)](#) revealed similar values than the experimental results of this study, with shredded rubber.
- A high correlation was found between empirical results and the normalised shear modulus - shear strain curves proposed by [Darendeli \(2001\)](#). An alternative approach was applied to the results of this study using the non-linear sigmoidal model (MMF) which provided a better fit at medium-to-large strains.
- Expressions established by [Senetakis et al. \(2012a\)](#) showed a better fit than the original damping curves established by [Darendeli \(2001\)](#) and [Masing \(1926\)](#). The empirical results were alternatively adjusted to the Modulus Reduction and Damping Fitting curves (MRDF) created by [Phillips and Hashash \(2009\)](#), hence the limiting strain and the decay in hysteretic non-linear damping was predicted.

---

Objective iv) was to elucidate the energy dissipation mechanisms developed in RSm from a particulate level, using 3D x-ray tomographic images, and its correlation to an element, with resonant and cyclic triaxial tests, and a 1g model scale, through shaking table experiments. These are the main conclusions extracted:

- 3D x-ray tomographic images revealed a reduction in rubber volume under loading which was subsequently recovered. However, the contact area between sand and rubber remained constant as a consequence of the locking effect.
- The energy dissipation occurring in sands and during the first loading-unloading cycle of RSm is caused by contact sliding and particle re-arrangement. At subsequent cycles, rubber restricts the friction between particles and the dissipation mechanism is controlled by the rubber deformation.
- Hysteretic damping associated with sand only specimens revealed high values at medium-to-large strains. However, the value of damping significantly decayed until it liquefied as a consequence of the loss in inter-particle contacts.
- Material damping evaluated in RSm was presented as a combination of both friction and deformation damping, which helped to explain the higher hysteretic damping when adding  $\chi = 10\%$ . The energy dissipation was controlled by rubber deformation as the rubber content increased resulting in a decrease in damping but also a lower damping degradation under cyclic loading.
- At a 1g model scale, i.e. shaking table, the damping capacity increased with rubber. However, this trend is at odds with the material damping evaluated at an element scale. The damping capacity of the foundation-soft zone is then hypothesised to be result of combining material and geometrical damping, result of the wave scattering due to the inclusion of soft vertical installations with RSm.

In terms of new understanding, the study has shown that the increase in the number of rubber-to-rubber contacts leads to a decay in shear modulus of RSm. On the other hand, an improvement in liquefaction resistance is found by adding shredded rubber. Hence, a conceptual framework has been proposed to elucidate the effect of particle properties and test conditions on the dynamic behaviour of RSm. It is proven that the number of cycles has a detrimental effect on the evolution of shear modulus and damping ratio of saturated sands. Thus, this study has demonstrated that mixing small shredded rubber and sand results in a mixture which exhibits a higher resilience against the action of medium-to-large deformations, via multi-cyclic loading. Adding 20 % rubber mass could be a solution to prevent foreseeable stiffness and damping degradation due to the action of strong earthquakes. This study has also proposed the use of different expressions to predict the non-linear behaviour of RSm so that they can accurately simulate, with numerical simulations, the ground response analysis of soft zones.

With regards to the energy dissipation mechanisms in RSm, the rubber deformation controls the dissipation mode after several cycles, and this is more evident as rubber content increases. This leads to an improvement in hysteretic material damping by adding  $\chi = 10\%$ . At a 1g model scale, an increase in the overall damping capacity of a foundation-modified soil is exhibited by adding up to  $\chi = 40\%$ . This was argued to be the result of combining the energy dissipation by the material and the geometrical characteristics of the medium, due to the reflection of incident waves.

*3. Can the introduction of vertical soft zones comprising particulate rubber to the ground enhance the resistance of soil foundations against dynamic loading?*

Objective v) of this research was focused on understanding the response of a foundation-modified soil system under cyclic loading. This study proposed to laterally support the foundation zone by adding vertical installations with RSm. A sweep analysis was performed on the system via shaking table tests at various frequencies (1-10 Hz) and rubber contents ( $\chi = 0 - 40\%$ ) to evaluate the structural response (Chapter 6). The vibration isolation efficacy was evaluated by comparing the amplification ratio of modified RSm soft zone with the sand only configuration. These are the main findings:

- The denser state of the vertical installations revealed a greater amplification of the input motion, observed with the application of a sweep analysis around the fundamental frequency of the system.
- The system response amplified as the input frequency approached the natural frequency, also influenced by the presence of soft zones. A shift in the amplification conditions was found with the addition of rubber due to the decay in shear modulus, as previously demonstrated by means of cyclic triaxial and resonant column tests (Chapter 5).
- The attenuation in the amplification ratio is associated with both the (i) shift in the structural response and the (ii) increase in system damping capacity.
- The vertical installation of soft zones, by means of bagging a constant RSm volume and placing it around the host soil, arises as an alternative route to overcome issues related to the installation of continuous horizontal layers.

In terms of new understanding, this study has shown that the cyclic response of a small-scaled model with a complex geometry, i.e. containing soft zones, can be idealised to mimic that of a single-degree of freedom. The installation of vertical RSm soft zones can attenuate peak horizontal accelerations, otherwise observed on a soil foundation comprising a stiffer (sand) initial configuration. An amplification of the input motion is, however, found at lower frequencies, as it could be the case of earthquake prone regions with predominately low-frequency seismic motions or around slender buildings. A comprehensive study is therefore required to evaluate the applicability of the system at different frequency ranges. The effectiveness of the system to isolate disturbances appears to be more significant when adding more rubber and at frequencies higher than the natural frequency of the modified system. This could be used to protect low-storey buildings or in areas where high-frequency earthquakes are expected. Consequently, this thesis proposes an alternative design whereby RSm soft zones can be implemented to enhance the resistance of soil foundations against dynamic loading in both existing and new constructions.

### 8.3 Limitations and recommendations for future work

Based on the limitations identified in the previous section, there are various recommendations for future research:

- Further testing, including resonant column and cyclic triaxial tests, could be undertaken to analyse the dynamic behaviour of RSm with the addition of more realistic soil gradings and hence gain further insights into the stiff-deformable particle interaction.
- This investigation has been focused on studying the dynamic behaviour of RSm with different particle (micro) properties, i.e. size, shape and content. More research is required to evaluate the effect of additional test conditions and bulk (macro) properties on the dynamic behaviour of mixtures containing ShR, particularly the effect of confining pressure and relative density.
- 3D tomographic images were taken in this study from mixtures under one-dimensional vertical loading. Future studies should attempt to examine the evolution in contact area and volume of the rubber whilst performing static (monotonic) or cyclic triaxial testing. This will provide with a basis to better understand the energy dissipation mechanisms in the element scale context.
- MMF/MRDF models were successfully adjusted to predict the evolution in soil stiffness and damping of RSm with shredded rubber. Additional analysis can be done to extend its use to predict the behaviour of RSm containing other particulate rubber types, e.g. tyre or chopped tyres.
- Further testing is needed in the lab scale, via shaking table or centrifuge modelling, to better understand the influence of the input amplitude and also the packaging of materials on the cyclic response of the vertical soft zones. The vertical/horizontal displacement should be recorded to address the effect of the densification on the cyclic response and how this can be minimised.

- This investigation has been limited to the study of the cyclic performance of a scaled foundation-modified soil by applying harmonic sinusoidal motions. Future research should consider the application of realistic but complex seismic motions and thus, explore the efficacy in isolating both vertical and horizontal accelerations by implementing vertical soft zones with RSm.
- This study has considered a unique thickness and depth for the vertical soft zones. More shaking table testing is needed to assess the influence of geometrical characteristics and the distribution of RSm columns on the structural response, with the adequate consideration of scaling laws to extrapolate the results.
- This study had argued that the increase in damping capacity of the modified soil with RSm could be attributed to both material and geometrical damping. Although the different forms of stress wave attenuation have been identified in Geotechnical Earthquake Engineering, these are still not well understood when discrete elements, with different material properties, are added to the ground soil. A better understanding of the energy dissipation mechanisms occurring around soft zones, mainly at the interface with adjacent soil layers, is required and thus elucidate the correlation between the particle, element and in-situ scale.

Most of the investigations in the field are limited to testing RSm in the element scale context with certain studies looking at 1g stress field conditions via shaking table experiments. Finite element models is a feasible route to simulate the cyclic behaviour of the mixture when implemented at larger scale, alternative to time and resource intensive full-scale models. The deformability of rubber appears to play a critical role in the cyclic response of a soil containing RSm. However, this highly deformable behaviour has not been properly captured by the current non-linear soil models when simulating the implementation of the mixture in 2D and 3D. A better understanding of the ground response of highly deformable soils is required to translate the known dynamic behaviour of RSm, studied via cyclic triaxial/resonant column testing, to more realistic models. The cyclic response of RSm could thus be studied under the action of simple (harmonic sinusoidal) or complex (seismic events) motions.



## References

---

- Alzawi, A. (2011). “Vibration Isolation Using In-filled Geofom Trench Barriers”. In: *Configurations* September, pp. 1–220.
- Anastasiadis, A., K. Senetakis and K. Pitilakis (2012a). “Small-Strain Shear Modulus and Damping Ratio of Sand-Rubber and Gravel-Rubber Mixtures”. In: *Geotechnical and Geological Engineering* 30.2, pp. 363–382. DOI: 10.1007/s10706-011-9473-2.
- Anastasiadis, A., K. Senetakis, K. Pitilakis, C. Gargala, I. Karakasi, T. Edil and S.W. Dean (2012b). “Dynamic Behavior of Sand/Rubber Mixtures. Part I: Effect of Rubber Content and Duration of Confinement on Small-Strain Shear Modulus and Damping Ratio”. In: *Journal of ASTM international* 9.2. DOI: 10.1520/JAI103680.
- Anbazhagan, P. and D.R. Manohar (2016). “Small-to-Large Strain Shear Modulus and Damping Ratio of Sand-Tyre Crumb Mixtures”. In: *GeoChicago 2016*, pp. 305–315. DOI: 10.1061/9780784480151.031.
- Ashmawy, A.K., R. Salgado, S. Guha and V.P. Drnevich (1995). “Soil Damping and Its Use in Dynamic Analyses”. In: *Third International Conference on Recent Advances in Geotechnical Earthquake Engineering and Soil Dynamics*, pp. 35–41.
- ASTM C136 (2006). “Standard Test Method for Sieve Analysis of Fine and Coarse Aggregates”. In: *ASTM International Standard Methods*.
- ASTM D3999 (2011). “Test Methods for the Determination of the Modulus and Damping Properties of Soils Using the Cyclic Triaxial Apparatus”. In: *ASTM International Standard Methods*.

- 
- ASTM D4015 (2015). “Standard Test Methods for Modulus and Damping of Soils by Fixed-Base Resonant Column Devices”. In: *ASTM International Standard Methods*, pp. 1–22. DOI: 10.1520/D4015-15E01.1.4.
- ASTM D6270 (2017). “Standard Practice for Use of Scrap Tires in Civil Engineering Applications”. In: *ASTM International Standard Methods*.
- ASTM D7181 (2011). “Standard Test Method for Consolidated Drained Triaxial Compression Test for Soils”. In: *ASTM International Standard Methods*.
- ASTM D854 (2014). “Standard Test Methods for Specific Gravity of Soil Solids by Water Pycnometer”. In: *ASTM International Standard Methods*.
- Attom, M.F. (2006). “The Use of Shredded Waste Tires to Improve the Geotechnical Engineering Properties of Sands”. In: *Environmental Geology* 49.4, pp. 497–503. DOI: 10.1007/s00254-005-0003-5.
- Babu, G.L., A. Sivakumar, K.S. Rao and S. Venkatesha (2011). “Analysis and Design of Vibration Isolation System Using Open Trenches”. In: *International Journal of Geomechanics* 11.October, pp. 364–369. DOI: 10.1061/(ASCE)GM.1943-5622.0000103..
- Bahadori, H. and R. Farzalizadeh (2018). “Dynamic Properties of Saturated Sands Mixed with Tyre Powders and Tyre Shreds”. In: *International Journal of Civil Engineering* 16.4, pp. 395–408. DOI: 10.1007/s40999-016-0136-9.
- Bahadori, H. and S. Manafi (2015). “Effect of tyre chips on dynamic properties of saturated sands”. In: *International Journal of Physical Modelling in Geotechnics* 15.3, pp. 116–128. DOI: 10.1680/ijpmg.13.00014.
- Balunaini, U., V.K. Mohan, M. Prezzi and R. Salgado (2014). “Shear Strength of Tyre Chip–Sand and Tyre Shred–Sand Mixtures”. In: *Proceedings of the Institution of Civil Engineers - Geotechnical Engineering* 167.6, pp. 585–595. DOI: 10.1680/geng.13.00097.
- Bandyopadhyay, S., A. Sengupta and G.R. Reddy (2015). “Performance of Sand and Shredded Rubber Tire Mixture as a Natural Base Isolator for Earthquake Protection”. In: *Earthquake Engineering and Engineering Vibration* 14.4, pp. 683–693. DOI: 10.1007/s11803-015-0053-y.
-

- 
- Bo, Q., L. Ali and D.M. Irini (2014). “Numerical Study of Wave Barrier and its Optimization design”. In: *Finite Elements in Analysis and Design* 84, pp. 1–13. DOI: 10.1016/j.finel.2014.02.002.
- Brara, A., A. Brara, A. Daouadji, A. Bali and E. Mostafa Daya (2016). “Dynamic Properties of Dense Sand-Rubber Mixtures with Small Particles Size Ratio”. In: *European Journal of Environmental and Civil Engineering*, pp. 1–15. DOI: 10.1080/19648189.2016.1139509.
- Brennan, A.J., A. Klar and S. Madabhushi (2019). “Mitigation of Seismic Accelerations by Soft Materials Embedded in the Ground”. In: *Proceedings of the Institution of Civil Engineers - Ground Improvement* 3, pp. 117–140.
- Brennan, A.J., N.I. Thusyanthan and S.P. Madabhushi (2005). “Evaluation of Shear Modulus and Damping in Dynamic Centrifuge Tests”. In: *Journal of Geotechnical and Geoenvironmental Engineering* 131.12, pp. 1488–1497. DOI: 10.1061/(ASCE)1090-0241(2005)131:12(1488).
- Brunet, S., J.C. De La Llera and E. Kausel (2016). “Non-Linear Modeling of Seismic Isolation Systems Made of Recycled Tire-Rubber”. In: *Soil Dynamics and Earthquake Engineering* 85, pp. 134–145.
- BS 1377-4 (1990). *Methods of Test for Soils for Civil Engineering Purposes - Part 4: Compaction-Related Tests*. Vol. 3. 1. British Standard Institution.
- BS 1377-5 (1990). *Methods of Test for Soils for Civil Engineering Purposes*. Vol. 3. 1. British Standard Institution.
- Cho, G., J. Dodds and J. C. Santamarina (2006). “Particle Shape Effects on Packing Density, Stiffness, and Strength: Natural and Crushed Sands”. In: *Journal of Geotechnical and Geoenvironmental Engineering*.
- Chopra, A.K. (2011). *Dynamics of structures : theory and applications to earthquake engineering*. 5th ed. Hoboken: Pearson Education.
- Clayton, C.R.I., J. A. Priest, M. Bui, A. Zervos and S. G. Kim (2009). “The Stokoe Resonant Column Apparatus: Effects of Stiffness, Mass and Specimen Fixity”. In: *Geotechnique* 59.5, pp. 429–437.
-

- 
- Craig, R.F. (2013). *Craig's Soil Mechanics*. 3rd ed. London: Spon. DOI: 10.1017/CBO9781107415324.004.
- Craig, R.F. and J.a. Knappett (2012). *Craig's Soil Mechanics*, p. 570. ISBN: 9780415561259.
- Danon, B. and J. Görgens (2015). "Determining Rubber Composition of Waste Tyres Using Devolatilisation Kinetics". In: *Thermochimica Acta* 621, pp. 56–60. DOI: 10.1016/j.tca.2015.10.008.
- Darendeli, M.B. (2001). "Development of a New Family of Normalized Modulus". In: *CEUR Workshop Proceedings* 1542.9, pp. 33–36. DOI: 10.1017/CBO9781107415324.004.
- Dolce, M., D. Cardone and R. Marnetto (2000). "Implementation and Testing of Passive Control Devices Based on Shape Memory Alloys". In: *Earthquake Engineering and Structural Dynamics* 29.1, pp. 945–968.
- Edil, T.B. and P.J. Bosscher (1994). "Engineering Properties of Tire Chips and Soil Mixtures". In: *Geotechnical Testing Journal* 17.4, p. 453. DOI: 10.1520/GTJ10306J.
- Edinçliler, A., G. Baykal and A. Saygılı (2010). "Influence of Different Processing Techniques on the Mechanical Properties of Used Tires in Embankment Construction". In: *Waste management (New York, N.Y.)* 30, pp. 1073–80.
- Ehsani, M., N. Shariatmadari and S.M. Mirhosseini (2015). "Shear m Modulus and Damping Ratio of Sand-Granulated Rubber Mixtures". In: *Journal of Central South University* 22.8, pp. 3159–3167. DOI: 10.1007/s11771-015-2853-7.
- ETRMA (2015). *End of Life Tyres - Report 2015*. <https://www.etrma.org/wp-content/uploads/2019/09/elt-report-v9a-final.pdf>, last visited on 28/01/2020.
- European Communities (2006). "Implementation of the Landfill Directive at Regional and Local Level". In: *Office for Official Publications of the European Communities*. <https://op.europa.eu/en/publication-detail/-/publication/9c61bcd6-9740-4f1c-9b6d-d2055a2adf04>, last visited on 28/01/2020.
- Flora, A., D. Lombardi, V. Nappa and E. Bilotta (2018). "Numerical Analyses of the Effectiveness of Soft Barriers into the Soil for the Mitigation of Seismic Risk". In: *Journal of Earthquake Engineering* 22.1, pp. 63–93.
-

- Fonseca, J., J. Bernal-Sanchez, A. Riaz, D. Barreto, J. McDougall, M. Miranda-Manzanares, A. Marinelli and V. Dimitriadi (2019). “Particle–Scale Interactions and Energy Dissipation Mechanisms in Sand–Rubber Mixtures”. In: *Géotechnique Letters* 9.4, pp. 1–6. DOI: 10.1680/jgele.18.00221.
- Fonseca, J., C.O. Sullivan and P.D. Lee (2013). “Quantifying the Evolution of Soil Fabric During Shearing Using Scalar Parameters”. In: *Geotechnique* 63.10, pp. 818–829. DOI: 10.1680/geot.11.P.150.
- Foose, G.J., C.H. Benson and P.J. Bosscher (1996). “Sand Reinforced with Shredded Waste Tires”. In: *Journal of Geotechnical Engineering* 122.9, pp. 760–767. DOI: 10.1061/(ASCE)0733-9410(1996)122:9(760).
- Fu, R., M.R. Coop and X.Q. Li (2014). “The Mechanics of a Compressive Sand Mixed with Tyre Rubber”. In: *Geotechnique Letters* 4.3, pp. 238–243. DOI: 10.1680/geolett.14.00027.
- Fu, R., M.R. Coop and X.Q. Li (2017). “Influence of Particle Type on the Mechanics of Sand–Rubber Mixtures”. In: *Journal of Geotechnical and Geoenvironmental Engineering* 143.9. DOI: 10.1061/(asce)gt.1943-5606.0001680.
- Gao, G.Y., Z.Y. Li, C. Qiu and Z.Q. Yue (2006). “Three-Dimensional Analysis of Rows of Piles as Passive Barriers for Ground Vibration Isolation”. In: *Soil Dynamics and Earthquake Engineering* 26.11, pp. 1015–1027. DOI: 10.1016/j.soildyn.2006.02.005.
- Ghazavi, M. (2004). “Shear Strength Characteristics of Sand-Mixed with Granular Rubber”. In: *Geotechnical and Geological Engineering* 22.3, pp. 401–416. DOI: 10.1023/B:GEGE.0000025035.74092.6c.
- Ghazavi, M. and M.A. Sakhi (2005). “Influence of Optimized Tire Shreds on Shear Strength Parameters of Sand”. In: *International Journal of Geomechanics* 5.1, pp. 58–65. DOI: 10.1061/(ASCE)1532-3641(2005)5:1(58).
- Guha-Sapir, D., P. Hoyois, P. Wallemacq and R. Below (2016). “Annual Disaster Statistical Review 2016 - The numbers and trends”. In: *Centre for Research on the Epidemiology of Disasters (CRED)*.
- Hardin, B.O. (1978). “The Nature of Stress-Strain Behaviour for Soils”. In: *Proceeding of the Specialy Conference on Earthquake Engineering and Soil Dynamics*, pp. 3–90.

- 
- Hardin, B.O. and V.P. Drnevich (1972). "Shear Modulus and Damping in Soils: Design Equations and Curves". In: *Soil Mechanics and Foundations Division* 98.7, pp. 667–692.
- Hardin, O. and F.E. Richart (1963). "Elastic Wave Velocities in Granular Soils". In: *Soil Mechanics and Foundations Division* 89.1, pp. 33–66.
- Hazarika, H., E. Kohama and T. Sugano (2008a). "Underwater Shake Table Tests on Waterfront Structures Protected with Tire Chips Cushion". In: *Journal of Geotechnical and Geoenvironmental Engineering* 134.12, pp. 1706–1719. DOI: 10.1061/(ASCE)1090-0241(2008)134:12(1706).
- Hazarika, H., T. Sugano, Y. Kikuchi, K. Yasuhara, S. Murakami, H. Takeichi, A. K. Karmokar, T. Kishida and Y. Mitarai (2006). "Flexibility and Stability Using Enhancement of Structures During Earthquakes Using a Novel Geosynthetic Material". In: *Soils and Foundations* 21.1, pp. 125–130.
- Hazarika, H., K. Yasuhara, M. Hyodo, A.K. Karmokar and Y. Mitarai (2008b). "Mitigation of Earthquake Induced Geotechnical Disasters Using a Smart and Novel Geomaterial". In: *14 World Conference on Earthquake Engineering, WCEE*.
- Head, K.H. (1994). *Manual of Soil Laboratory Testing; Volume 2: Permeability, Shear Strength and Compressibility Tests*. 3rd ed. Boca Raton, FL: CRC Press. ISBN: 0-470-23362-1.
- Humphrey, D.N., T.C. Sandford, M.M. Cribbs and W.P. Manion (1993). "Shear Strength and Compressibility of Tire chips for Use as Retaining Wall Backfill". In: *Transportation Research Record* 1422, pp. 29–35.
- Hyodo, M., S. Yamada, R. Orense, M. Okamoto and H. Hazarika (2007). "Undrained Cyclic Shear Properties of Tire Chip-Sand Mixtures". In: *Proceedings of the International Workshop on Scrap Tire Derived Geomaterials - Opportunities and Challenges*, pp. 187–196.
- Iai, S. (1989). "Similitude for Shaking Table Tests on Soil-Structure-Fluid Model in 1g Gravitational Field". In: *Geotechnique* 29.1, pp. 105–118.
- Iai, S., T. Tobita and T. Nakahara (2005). "Generalised Scaling Relations for Dynamic Centrifuge Tests". In: *Geotechnique* 55.5, pp. 355–362.
-

- 
- Ishihara, K. (1996). *Soil Behaviour in Earthquake Geotechnics*. 1st ed. Oxford: Clarendon Press.
- Iwasaki, T., F. Tatsuoka and Y. Takagi (1979). “Shear Moduli of Sands Under Cyclic Torsional Shear Loading”. In: *Soil and Foundations* 18, pp. 39–56.
- Jangid, R.S. and T.K. Datta (1995). “Seismic Behaviour of Base-Isolated Buildings: A State-of-the-Art Review”. In: *Proceedings ICE: Structures & Buildings* 110.2, pp. 186–203. ISSN: 15452921.
- Kaneko, T., M. Orense P. Hyodo and N. Yoshimoto (2013). “Seismic Response Characteristics of Saturated Sand Deposits Mixed with Tire Chips”. In: *Journal of Geotechnical and Geoenvironmental Engineering* 139.4, pp. 633–643. DOI: 10.1061/(ASCE)GT.1943-5606.0000752.
- Kim, D.S. and K. Konagai (2001). “Key Parameters Governing the Performance of Soft Tunnel Coating for Seismic Isolation”. In: *Earthquake Engineering and Structural Dynamics* 30.9, pp. 1333–1343. DOI: 10.1002/eqe.65.
- Kim, H.K and J.C. Santamarina (2008). “Sand–Rubber Mixtures (Large Rubber Chips)”. In: *Canadian Geotechnical Journal* 45.10, pp. 1457–1466. DOI: 10.1139/T08-070.
- Kirtas, E. and K. Pitilakis (2009). “Subsoil Interventions Effect on Structural Seismic Response. Part II: Parametric Investigation”. In: *Journal of Earthquake Engineering* 13.3, pp. 328–344.
- Kirtas, E., E. Rovithis and K. Pitilakis (2009). “Subsoil Interventions Effect on Structural Seismic Response. Part I: Validation of Numerical Simulations”. In: *Journal of Earthquake Engineering* 13.2, pp. 155–169.
- Kobori, T., M. Takahashi and K. Ogasawara (1993). “Seismic Response Controlled Structure With Active Variable Stiffness System”. In: *Earthquake Engineering and Structural Dynamics* 22.July 1992, pp. 925–941.
- Kokusho, T. (1980). “Cyclic Triaxial Test of Dynamic Soil Properties for Wide Strain Range”. In: *Soils and foundations* 20, pp. 45–60.
- Kramer, S.L. (1996). *Geotechnical Earthquake Engineering*. 1st ed. Upper Saddle River, N.J: Prentice-Hall. ISBN: 0-13-374943-6.

- 
- Kumar, J. and C.R.I. Clayton (2007). "Effect of Sample Torsional Stiffness on Resonant Column Test Results". In: *Canadian Geotechnical Journal* 44.2, pp. 221–230.
- Kumar, S.S., A. M. Krishna and A. Dey (2017). "Evaluation of Dynamic Properties of Sandy Soil at High Cyclic Strains". In: *Soil Dynamics and Earthquake Engineering* 99, pp. 157–167. DOI: 10.1016/j.soildyn.2017.05.016.
- Kurata, N., T. Kobori, M. Takahashi, N. Niwa and H. Midorikawa (1999). "Actual Seismic Response Controlled Building with Semi-Active Damper System". In: *Earthquake Engineering and Structural Dynamics* 28.11, pp. 1427–1447.
- Lambe, T.W. and R.V. Whitman (2010). *Soil Mechanics*. 2nd ed. New York: Wiley.
- Lee, C., H. Shin and J.S. Lee (2014). "Behavior of Sand-Rubber Particle Mixtures: Experimental Observations and Numerical Simulations". In: *International Journal for Numerical and Analytical Methods in Geomechanics* 38.16, pp. 1651–1663. DOI: 10.1002/nag.2264.
- Lee, C., Q.H. Truong, W. Lee and J.S. Lee (2010). "Characteristics of Rubber-Sand Particle Mixtures according to Size Ratio". In: *Journal of Materials in Civil Engineering* 22.4, pp. 323–331. DOI: 10.1061/(ASCE)MT.1943-5533.0000027.
- Lee, J.S., J. Dodds and J.C. Santamarina (2007). "Behavior of Rigid-Soft Particle Mixtures". In: *Journal of Materials in Civil Engineering* 19.2, pp. 179–184. DOI: 10.1061/(ASCE)0899-1561(2007)19:2(179).
- Li, B., M. Huang and X. Zeng (2016). "Dynamic Behavior and Liquefaction Analysis of Recycled-Rubber Sand Mixtures". In: *Journal of Materials in Civil Engineering* 28.11. DOI: 10.1061/(ASCE)MT.1943-5533.0001629.
- Lombardi, D. (2012). "An Innovative Ground Treatment Approach for Seismic Risk Mitigation of Existing Structures". PhD thesis. Naples, Italy.
- Lombardi, D., S. Bhattacharya, F. Scarpa and M. Bianchi (2015). "Dynamic Response of a Geotechnical Rigid Model Container with Absorbing Boundaries". In: *Soil Dynamics and Earthquake Engineering*. DOI: 10.1016/j.soildyn.2014.09.008.
- Lombardi, D., A. Flora, S. Lirer and F. Silvestri (2014). "Soil Grouting for the Seismic Protection of Existing Buildings". In: *Proceedings of the Institution of Civil Engineers - Ground Improvement* 167.3, pp. 206–218.
-



- 
- Lopera Perez, J.C., C.Y. Kwok and K. Senetakis (2016). “Effect of Rubber Size on the Behaviour of Sand-Rubber Mixtures: A Numerical Investigation”. In: *Computers and Geotechnics*. DOI: 10.1016/j.compgeo.2016.07.005.
- Madhusudhan, A., B.R. Boominathan and S. Banerjee (2019). “Factors Affecting Strength and Stiffness of Dry Sand- Rubber Tire Shred Mixtures”. In: *Geotechnical and Geological Engineering*. DOI: 10.1007/s10706-018-00792-y.
- Mahdavisefat, E., H. Salehzadeh and A.A. Heshmati (2017). “Full-scale Experimental Study on Screening Effectiveness of SRM-Filled Trench Barriers”. In: *Géotechnique* January, pp. 1–14. DOI: 10.1680/jgeot.17.P007.
- Masad, E., R. Taha, C. Ho and T. Papagiannakis (1996). “Engineering Properties of Tire/Soil Mixtures as a Lightweight Fill Material”. In: *Geotechnical Testing Journal* 19.3, pp. 297–304. DOI: 10.1520/GTJ10355J.
- Mashiri, M.S. (2014). “Monotonic and Cyclic Behaviour of Sand-Tyre Chip (STCh) Mixtures”. In: p. 290. DOI: 10.1534/genetics.108.093047.
- Mashiri, M.S., M.N. Sheikh, J. Vinod and H.H. Tsang (2013). “Dynamic Properties of Sand-Tyre Chip Mixtures”. In: *ATasmania: Australian Earthquake Engineering Society*, pp. 1–8.
- Mashiri, M.S., J.S. Vinod and M.N. Sheikh (2015a). “Constitutive Model for Sand–Tire Chip Mixture”. In: *International Journal of Geomechanics*. DOI: 10.1061/(ASCE)GM.1943-5622.0000472.
- Mashiri, M.S., J.S. Vinod and M.N. Sheikh (2016). “Liquefaction Potential and Dynamic Properties of Sand-Tyre Chip (STCh) Mixtures”. In: *Geotechnical Testing Journal*. ISSN: 01496115. DOI: 10.1520/GTJ20150031.
- Mashiri, M.S., J.S. Vinod, M.N. Sheikh and J.A. Carraro (2017). “Shear Modulus of Sand–Tyre Chip Mixtures”. In: *Environmental Geotechnics*, pp. 1–9. DOI: 10.1680/jenge.16.00016.
- Mashiri, M.S., J.S. Vinod, M.N. Sheikh and H.H. Tsang (2015b). “Shear Strength and Dilatancy Behaviour of Sand-Tyre Chip Mixtures”. In: *Soils and Foundations* 55.3, pp. 517–528. DOI: 10.1016/j.sandf.2015.04.004.
-

- 
- Masing, G. (1926). "Genspannung und Verfestigung Beim Masing". In: *Second International Congress of Applied Mechanics* 7, pp. 332–335.
- Matsagar, V.A and R.S. Jangid (2008). "Base Isolation for Seismic Retrofitting of Structures". In: *Practice Periodical on Structural Design and Construction* May 2010, pp. 175–185.
- Menq, F.Y. (2003). "Dynamic Properties of Sandy and Gravelly Soils". PhD thesis. Austin, USA: University of Texas.
- Moghaddas, S.N. and A.H. Norouzi (2012). "Bearing capacity of a square Model Footing on Sand Reinforced with Shredded Tire - An Experimental Investigation". In: *Construction and Building Materials* 35, pp. 547–556. DOI: 10.1016/j.conbuildmat.2012.04.092.
- Murillo, C., L. Thorel and B. Caicedo (2009). "Ground Vibration Isolation with Geofom Barriers: Centrifuge Modeling". In: *Geotextiles and Geomembranes* 27.6, pp. 423–434. DOI: 10.1016/j.geotexmem.2009.03.006.
- Nadimi, S. and J. Fonseca (2018). "Image Based Simulation of One-Dimensional Compression Tests on Carbonate Sand". In: *Meccanica*.
- Naeim, F and J.M. Kelly (1999). "Design of Seismic Isolated Structures: From Theory to Practice". In: *John Wiley & Sons* 16.3, pp. 709–710. DOI: 10.1193/1.1586135.
- Nakhaei, A., S.M. Marandi, S.S. Kermani and M.H. Bagheripour (2012). "Dynamic Properties of Granular Soils Mixed with Granulated Rubber". In: *Soil Dynamics and Earthquake Engineering* 43, pp. 124–132. DOI: 10.1016/j.soildyn.2012.07.026.
- Nappa, V. (2014). "Soft Grouting For Sesimic Isolation: Numerical and Physical modelling". PhD thesis. Naples, Italy.
- Nappa, V., E. Bilotta, A. Flora and S. Madabhushi (2016). "Centrifuge Modelling of the Seismic Performance of Soft Buried Barriers". In: *Bulletin of Earthquake Engineering* 14.10, pp. 2881–2901.
- Nazari, N., J.W. Lindt and Y. Li (2014). "Effect of Aftershock Intensity on Seismic Collapse Fragilities". In: *International Journal of Reliability and Safety* 8, p. 174. DOI: 10.1504/IJRS.2014.069526.
-

- 
- Okur, D.V. and A. Ansal (2007). “Stiffness Degradation of Natural Fine Grained Soils During Cyclic Loading”. In: *Soil Dynamics and Earthquake Engineering*.
- Otsu, N. (1979). “A Threshold Selection Method from Gray-Level Histograms”. In: C.1, pp. 62–66.
- Otsubo, M., I. Towhata, T. Hayashida, B. Liu and S. Goto (2016). “Shaking Table Tests on Liquefaction Mitigation of Embedded Lifelines by Backfilling with Recycled Materials”. In: *Soils and Foundations* 56.3, pp. 365–378.
- Pamukcu, S. and S. Akbulut (2006). “Thermoelastic Enhancement of Damping of Sand Using Synthetic Ground Rubber”. In: *Journal of Geotechnical and Geoenvironmental Engineering* 132.4, pp. 501–510. DOI: 10.1061/(ASCE)1090-0241(2006)132:4(501).
- Papagiannopoulos, G.A. and G.D. Hatzigeorgiou (2011). “On the Use of the Half-Power Bandwidth Method to Estimate Damping in Building Structures”. In: *Soil Dynamics and Earthquake Engineering* 31.7, pp. 1075–1079. DOI: 10.1016/j.soildyn.2011.02.007.
- Park, H.J. and D.S. Kim (2013). “Centrifuge Modelling for Evaluation of Seismic Behaviour of Stone Masonry Structure”. In: *Soil Dynamics and Earthquake Engineering* 53, pp. 187–195.
- Phillips, C. and Y.M. Hashash (2009). “Damping Formulation For Nonlinear 1D Site Response Analyses”. In: *Soil Dynamics and Earthquake Engineering* 29.7, pp. 1143–1158. DOI: 10.1016/j.soildyn.2009.01.004.
- Pistolas, G.A., A. Anastasiadis and K. Pitilakis (2018). “Dynamic Behaviour of Granular Soil Materials Mixed with Granulated Rubber: Effect of Rubber Content and Granularity on the Small-Strain Shear Modulus and Damping Ratio”. In: *Geotechnical and Geological Engineering* 36.2, pp. 1267–1281. DOI: 10.1007/s10706-017-0391-9.
- Platzer, A., S. Rouhanifar, P. Richard, B. Cazacliu and E. Ibraim (2018). “Sand–Rubber Mixtures Undergoing Isotropic Loading: Derivation and Experimental Probing of a Physical Model”. In: *Granular Matter* 20.4, pp. 1–10. DOI: 10.1007/s10035-018-0853-7.

- Promptthangkoon, P. and A.F.L. Hyde (2007). "Compressibility and Liquefaction Potential of Rubber Composite Soils". In: *Proceedings of the International Workshop IW-TDGM2007*, pp. 161–170.
- Rao, G.V. and R.K. Dutta (2006). "Compressibility and Strength Behaviour of Sand-Tyre Chip Mixtures". In: *Geotechnical and Geological Engineering* 24.3, pp. 711–724. DOI: 10.1007/s10706-004-4006-x.
- Read, B.E. and G.D. Dean (1998). "The determination of Dynamic Properties of Polymers and Composites". In: *Journal of Sound and Vibration* 211.2, pp. 265–272. DOI: 10.1006/jsvi.1997.1387.
- Robinson, W.H. (2000). "Seismic Isolation of Civil Buildings in New Zealand". In: *Progress in Structural Engineering and Materials* October 1994, pp. 328–334.
- Senetakis, K., A. Anastasiadis and K. Pitilakis (2012a). "Dynamic Properties of Dry Sand/Rubber (SRM) and Gravel/Rubber (GRM) Mixtures in a Wide Range of Shearing Strain Amplitudes". In: 33.1, pp. 38–53. DOI: 10.1016/j.soildyn.2011.10.003.
- Senetakis, K., A. Anastasiadis, K. Pitilakis, A. Souli, T. Edil and S.W. Dean (2012b). "Dynamic Behavior of Sand/Rubber Mixtures, Part II: Effect of Rubber Content on G/GO- $\gamma$ -DT Curves and Volumetric Threshold Strain". In: *Journal of ASTM international* 9, p. 103711. DOI: 10.1520/JAI103711.
- Senetakis, K., M. R. Coop and M. C. Todisco (2013). "The Inter-particle Coefficient of Friction at the Contacts of Leighton Buzzard Sand Quartz Minerals". In: *Soils and Foundations* 53.5, pp. 746–755. ISSN: 0038-0806.
- Shamy, U.E. and C. Denissen (2012). "Microscale Energy Dissipation Mechanisms in Cyclically-Loaded Granular Soils". In: *Geotechnical and Geological Engineering* 30.2, pp. 343–361. DOI: 10.1007/s10706-011-9472-3.
- Shariatmadari, N., M. Karimpour-Fard and A. Shargh (2018). "Undrained Monotonic and Cyclic Behavior of Sand-Ground Rubber Mixtures". In: *Earthquake Engineering and Engineering Vibration* 17.3, pp. 541–553. DOI: 10.1007/s11803-018-0461-x.
- Sheikh, M.N., M.S. Mashiri, J.S. Vinod and H.H. Tsang (2012). "Shear and Compressibility Behaviours of Sand-Tyre Crumb Mixtures". In: *Journal of Materials in Civil Engineering* 25.10. DOI: 10.1061/(ASCE)MT.1943-5533.0000696.

- 
- Signes, C. H., J. Garzon-Roca, J.M. Grima-Palop and R. Insa-Franco (2017). "Use of Rubber Shreds to Enhance Attenuation of Railway Sub-Ballast Layers Made of Unbound Aggregates". In: *Materiales de Construccion* 67.326, pp. 1–10.
- Skinner, R.I., W.H. Robinson and G.H. McVerry (1993). *An Introduction to Seismic Isolation*. 1st ed. John Wiley & Sons.
- Soong, T.T. (1990). *Active Structural Control: Theory and Practice*. 1st ed. New York: Wiley.
- Soong, T.T. and B.F. Spencer (2000). "Active, Semi-Active and Hybrid Control of Structures". In: *Bulletin of the New Zealand Society for Earthquake Engineering* 33.3, pp. 387–402.
- South, J. T., K. L. Reifsnider, S. W. Case, J. J. Lesko, H. Marand and B. J. Love (2001). "Mechanical Properties And Durability Of Natural Rubber Compounds And Composites". In: <http://hdl.handle.net/10919/26306>, last visited on 28/01/2020.
- Takahashi, N., T. Kishishita, Y. Yamamoto, M. Hyodo, F. Miura and N. Yoshimoto (2006). "Shaking Table Testing of Liquefiable Ground Improved By Multi-Layer Soil Improvement". In: *13th World Conference on Earthquake Engineering* 62.2, pp. 502–518. DOI: 10.2208/jscej.62.502.
- Tatliso, N., T.B. Edil and C.H. Benson (1998). "Interaction Between Reinforcing Geosynthetics and Soil-Tire Chip Mixtures". In: *Journal of Geotechnical and Geoenvironmental Engineering* 124.11, pp. 1109–1119. DOI: 10.1061/(asce)1090-0241(1998)124:11(1109).
- Thorby, D. (2008). *Structural Dynamics and Vibration in Practice*. 1st ed. Amsterdam: Elsevier/Butterworth-Heinemann. DOI: 10.1016/B978-0-7506-8002-8.X0001-6.
- Towhata, I. (2014). *Geotechnical Earthquake Engineering*. 1st ed. London: Springer Series in Geomechanics and Geoengineering.
- Tsang, H.H. (2008). "Seismic Isolation by Rubber-Soil Mixtures for Developing Countries". In: *Earthquake Engineering and Structural Dynamics* 37.2, pp. 283–303. DOI: 10.1002/eqe.756.
- Tsang, H.H. (2009). "Geotechnical Seismic Isolation". In: *Earthquake Engineering: New Research*, pp. 55–87.
-

- Tsang, H.H., S.H. Lo, X. Xu and M. Neaz Sheikh (2012). “Seismic Isolation for Low-to-Medium Rise Buildings Using Granulated Rubber-Soil Mixtures: Numerical Study”. In: *Earthquake Engineering and Structural Dynamics* 41.14, pp. 2009–2024. DOI: 10.1002/eqe.2171.
- Tsang, H.H. and K. Pitilakis (2019). “Mechanism of Geotechnical Seismic Isolation System : Analytical modeling”. In: *Soil Dynamics and Earthquake Engineering* 122, pp. 171–184.
- Tsuha, C. H. C., P. Y. Foray, R. J. Jardine, Z. X. Yang, M. Silva and S. Rimoy (2012). “Behaviour of Displacement Piles in Sand Under Cyclic Axial Loading”. In: *Soils and Foundations* 52.3, pp. 393–410.
- Ulgen, D. and O. Toygar (2015). “Screening Effectiveness of Open and In-Filled Wave Barriers: A Full-Scale Experimental Study”. In: *Construction and Building Materials* 86, pp. 12–20. DOI: 10.1016/j.conbuildmat.2015.03.098.
- Valdes, J.R. and T. M. Evans (2008). “Sand–Rubber Mixtures: Experiments and Numerical Simulations”. In: *Canadian Geotechnical Journal* 45, pp. 588–595. DOI: 10.1139/T08-002.
- Verruijt, A. (2010). *An Introduction to Soil Dynamics*. 1st ed. Dordrecht: Springer Netherlands. DOI: 10.1007/978-90-481-3441-0.
- Wang, J.G., W. Sun and S. Anand (2009). “Numerical Investigation on Active Isolation of Ground Shock by Soft Porous Layers”. In: *Journal of Sound and Vibration* 321.3-5, pp. 492–509. DOI: 10.1016/j.jsv.2008.09.047.
- Wichtmann, T. and T. Triantafyllidis (2016). “An Experimental Database for the Development, Calibration and Verification of Constitutive Models for Sand with Focus to Cyclic Loading: Part II—Tests with Strain Cycles and Combined Loading”. In: *Acta Geotechnica* 11.4, pp. 763–774. DOI: 10.1007/s11440-015-0412-x.
- Woods, R.D. (1968). “Screening of Surface Waves in Soils”. In: *Journal of the Soil Mechanics and Foundations Division: Proceedings of the American Society of Civil Engineers* 94, pp. 951–979.
- Woods, R.D., N.E. Barnett and R. Sagesser (1974). “Holography, a New Tool for Soil Dynamics”. In: *Journal Geotechnical Engineering*.

- 
- Wu, W.Y., C.C. Benda and R.F. Cauley (2002). “Triaxial Determination of Shear Strength of Tire Chips”. In: *Journal of Geotechnical and Geoenvironmental Engineering* 123.5, pp. 479–482. DOI: 10.1061/(asce)1090-0241(1997)123:5(479).
- Xiong, W. and Y. Li (2013). “Seismic Isolation Using Granulated Tire-Soil Mixtures for Less-Developed Regions: Experimental Validation”. In: *Earthquake Engineering and Structural Dynamics* 42.14, pp. 2187–2193. DOI: 10.1002/eqe.2315.
- Xu, X. (2009). “Earthquake Protection for Low-to-Medium Rise Buildings Using Rubber-Soil Mixtures”. <http://hdl.handle.net/10722/56991>, last visited on 28/01/2020. PhD thesis. Pokfulam, Hong Kong SAR.
- Yegian, M. and M. Catan (2004). “Soil Isolation for Seismic Protection Using a Smooth Synthetic Liner”. In: *Journal of Geotechnical and Geoenvironmental Engineering* 130.11, pp. 1131–1139. DOI: 10.1061/(ASCE)1090-0241(2004)130:11(1121).
- Yegian, M. and U. Kadakal (2004). “Foundation Isolation for Seismic Protection Using a Smooth Synthetic Liner”. In: *Journal of Geotechnical and Geoenvironmental Engineering* 130.11, pp. 1121–1130.
- Yoshida, N. (2015). *Seismic Ground Response Analysis*. 1st ed. Vol. 36. Springer. DOI: 10.1007/978-94-017-9460-2.
- Youwai, S. and D.T. Bergado (2003). “Strength and Deformation Characteristics of Shredded Rubber Tire - Sand Mixtures”. In: *Canadian Geotechnical Journal* 40.2, pp. 254–264. DOI: 10.1139/t02-104.
- Zhang, B., K.K. Muraleetharan, F. Asce, C. Liu and M. Asce (2016). “Liquefaction of Unsaturated Sands”. In: *International Journal of Geomechanics* 3, pp. 1–9. DOI: 10.1061/(ASCE)GM.1943-5622.0000605..
- Zhang, J., R.D. Andrus and H.C. Juang (2005). “Normalised Shear Modulus and Material Damping Ratio Relationships”. In: *Journal of Geotechnical and Geoenvironmental Engineering* 131.4, pp. 667–692.
- Zheng-Yi, F. and K.G. Sutter (2000). “Dynamic Properties of Granulated Rubber/Sand Mixtures”. In: *Geotechnical Testing Journal* 23.3, pp. 338–344.

Zornberg, J.G., A.R. Cabral and C. Viratjandr (2004). "Behaviour of Tire Shred-Sand Mixtures". In: *Canadian Geotechnical Journal* 41.2, pp. 227–241. DOI: 10.1139/t03-086.